UNIVERSITY OF SOUTHAMPTON

THE SURFACE ORGANOMETALLIC CHEMISTRY OF RHODIUM AND PALLADIUM SUPPORTED ON INORGANIC OXIDES

DARYL BURNABY

A thesis submitted for the Degree of Doctor of Philosophy

Department of Chemistry

December 2000

UNIVERSITY OF SOUTHAMPTON

ABSTRACT

FACULTY OF SCIENCE
CHEMISTRY

Doctor of Philosophy

THE SURFACE ORGANOMETALLIC CHEMISTRY OF RHODIUM AND PALLADIUM SUPPORTED ON INORGANIC OXIDES

By Daryl Burnaby

Extended X-ray Absorption Fine Structure (EXAFS), Energy Dispersive EXAFS (EDE), Diffuse Reflectance Infrared Fourier Transform Spectroscopy (DRIFTS) and Temperature Programmed Desorption (TPD) have been employed to investigate the surface organometallic chemistry of rhodium and palladium supported on high area alumina and titania surfaces.

All the supported organometallic systems in this study have been prepared by Metallo-Organic Chemical Vapour Deposition (MOCVD). Metal loadings of between 2% and 5% were used.

DRIFTS and EDE data suggest that the $[Rh(CO)_2Cl]_2$ dimer is chemisorbed onto both the TiO_2 and Al_2O_3 surfaces as a $[O]Rh(CO)_2(Cl)$ unit. DRIFTS, EDE and TPD studies show that the carbonyl ligands are removed by heating the system under an inert atmosphere up to 220°C, or under a hydrogen atmosphere up to 90°C. This results in the formation of small rhodium clusters on the oxide surface, shown by EDE spectroscopy. The *gem*-dicarbonyl species can be regenerated by exposure of the thermolysed sample to CO at room temperature. Reaction with NO results in substitution with the CO ligands to form a $[O]_2Rh(NO)(Cl)$ species which exhibits greater thermal stability than the *gem*-dicarbonyl species, requiring temperatures of 300°C to remove the ligands and cluster the rhodium. The pre-treatment of the titania and alumina surfaces has been shown to affect the nature of nitrosyl species generated. The *gem*-dicarbonyl species is regenerated by exposure to CO.

$Rh(CO)_2(acac)$ has been shown to be physisorbed intact on the surfaces of titania and alumina. Thermolysis under helium and hydrogen results in evolution of firstly the carbonyl and then the acac ligands. Regeneration of the *gem*- dicarbonyl ligands occurs with exposure to CO at room temperature. Reaction with NO results in the formation of a $Rh(NO)$ species, with *gem*-dicarbonyl regeneration occurring after exposure to CO.

$Pd(acac)_2$ has been shown to be physisorbed intact on the surface of titania by DRIFTS and EXAFS spectroscopies. Thermolysis under helium and hydrogen atmospheres results in the removal of the acac ligands, and the formation of palladium clusters on the titania surface. Re-exposure to CO results in the formation of a mixture of palladium carbonyl species. Reaction with NO results in the formation of a $Pd(NO)$ species.

The surface organometallic chemistry of Rh(sulphos)(cod) and $Rh(sulphos)(CO)_2$ supported on silica, was investigated by DRIFTS and solid state NMR spectroscopy. Reaction with H_2 was shown to result in substitution with the (cod) ligand. Subsequent reaction with C_2H_4 was shown to result in insertion of a variety of alkyl ligands.

Contents

Chapter 2- Experimental Methods

Chapter 3- The Surface Organometallic Chemistry of $[Rh(CO)_2Cl]_2$ Supported on TiO_2 and Al_2O_3

Chapter 4- The Reactions of $[Rh(CO)_2Cl]_2$ Supported on TiO_2 and Al_2O_3 with NO

Chapter 5- The Surface Organometallic Chemistry of $Rh(CO)_2(acac)$ Supported on TiO_2 and Al_2O_3

Chapter 6- The Surface Organometallic Chemistry of $Pd(acac)_2$ Supported on TiO_2

Chapter 7- The Surface Organometallic Chemistry of Rh(sulphos)(cod) and $Rh(sulphos)(CO)_2$ Supported on Silica

Acknowledgements

I would like firstly to thank my supervisor Professor John Evans for all his support, advice and guidance during my time in Southampton. I would also especially like to thank Dr Mark Newton for all his assistance and guidance during my PhD. Without his experience and inspiration (?!), much of the content of this thesis would not have come to fruition. I would like to thank Dave and Bruce in the departmental workshops for their assistance with the construction and maintenance of the EXAFS and DRIFTS cells. Thanks are due to Fred at Daresbury for his assistance with EXAFS experiments, and to Andy, Thomas and Sophia at the ESRF in Grenoble, for their assistance with EDE experiments.

I thank the EPSRC for a studentship during my three years in Southampton, to the CCLRC for the use of the facilities at Daresbury, and the ESRF for use of EDE facilities.

Of my labmates over the three years I would like especially to thank Sandra and Steve, as well as Mark for accompanying me on trips to Daresbury and Grenoble, and for their assistance and time whilst on these visits (and in Southampton). Thanks are also due to my other lab mates and fellow group members Tom, Ship, Peter and Graham, who have helped out and been good company during the course of my PhD.

I would like to acknowledge the following people who have been good friends of mine whilst at Southampton: Sarah, Kenny, Sandra, Peter, Graham, Ship, Nick, Melanie, Jon Joy, Basya, Steve, Simon, John Davies and Vin.

I would also like to thank all my housemates over the three years for being a good bunch of people to have lived with, and all the people who I have played football, cricket and done karate with. I am also grateful for GlaxoWellcome for giving me a job to do after the end of my life as a student.

I would finally like to thank my parents for their support and encouragement over the years.

Abbreviations

DRIFTS	Diffuse Reflectance Infrared Fourier Transform Spectroscopy
EXAFS	Extended X-Ray Absorption Fine Structure
EDE	Energy Dispersive EXAFS
FT	Fourier Transform
IR	Infrared
MOCVD	Metallo Organic Chemical Vapour Deposition
SMSI	Strong Metal Support Interaction
TPD	Temperature Programmed Desorption
UHV	Ultra High Vacuum
XAS	X-ray Absorption Spectroscopy
acac	acetylacetonate
CN	EXAFS derived coordination number
R / Å	EXAFS derived distance from central atom

Chapter 1

Introduction

1.1 Introduction

This thesis comprises of an investigation of the surface organometallic chemistry of selected organorhodium and organopalladium compounds. These compounds are supported on high area titania and alumina by means of Metallo-Organic Chemical Vapour Deposition (MOCVD). The nature of the surface species has been studied, as has the thermal chemistry and reaction with small molecules of catalytic interest. The methods of investigation employed are Extended X-ray Absorption Fine Structure (EXAFS) spectroscopy, Energy Dispersive EXAFS (EDE), Diffuse Reflectance Infrared Fourier Transform Spectroscopy (DRIFTS), and Temperature Programmed Desorption (TPD). This chapter relates this work to the field of heterogeneous catalysis, and serves as an introduction to the subject of surface organometallic chemistry.

1.2 Catalysis

A catalyst increases the rate at which a chemical reaction reaches equilibrium, by lowering its activation energy, without itself being consumed in the process. If several reaction pathways are possible, the catalyst may selectively lower the activation energy for just one of them, producing a greater proportion of the desired product. Nearly 70% of all industrial chemical processes use a catalyst at some stage of their manufacture[1]. There are two main types of catalyst, homogeneous and heterogeneous. Homogeneous catalysts involve the reactants and catalyst being in the same phase. Heterogeneous catalysts involve the reactants and catalyst being in a different phase.

1.2.1 Heterogeneous catalysis

Heterogeneous catalysts are the most employed of all catalyst types in industrial processes. This is due mainly to the stability of such catalysts under extreme conditions of

pressure and temperature, resulting in fast reaction rates and ease of separation of the catalyst from the products. Heterogeneous catalysis requires the chemisorption of reactant molecules, resulting in an alteration in the electronic or geometric nature of the molecule, which results in the lowering of the activation energy of the desired reaction[2]. The strength of chemisorption is often closely related to the catalytic activity. If the molecule is very strongly adsorbed, the chemisorption bond will be difficult to break and the reaction rate will be reduced. If the bond is very weak, the coverage of reactant molecules will be minimal, hence little reaction. Therefore optimal catalytic performance requires intermediate bond strengths. For many important industrial reactions, such as ammonia synthesis, carbon monoxide hydrogenation and hydrocarbon conversion, this criterion is met by Group VIII metals[3,4].

The most common type of heterogeneous catalyst is a transition metal supported on a solid, normally an inorganic oxide (most commonly in industrial processes) or a polymer. This helps to stabilize the metal in a highly dispersed state, in order to maximise the fraction of molecules of the active material at the surface. As the reaction rate is often proportional to the surface area of the active phase, this is an important consideration. The objective of high dispersion is particularly important when Group VIII metals such as palladium, rhodium and platinum are employed, as it is desirable to maximise the usage of these expensive materials. High dispersion can also reduce the degree of sintering at elevated temperature and increase the longevity of the catalyst. This is not always the case, however, as some catalysts show inverse relationships to area for small particles when catalysis occurs on large faces. In this form, the metal will usually consist of small particles, 20-60 Å in diameter, while the extent of metal loading on the support is typically 1-10% by weight.

Conventional methods for the preparation of such supported catalysts include impregnation, deposition, co-precipitation and ion exchange[2]. Impregnation is a particularly widely used method and involves treating a porous oxide with a solution of transition metal ions. Initially the pores are filled with the solution. This is followed by evaporation to remove all the solvent, leaving microcrystals of the salt on the walls of the pores. These salt particles are converted into metal particles by calcination to form an oxidic species, and subsequent reduction under hydrogen at elevated temperatures. Deposition involves sublimation of the organometallic complex onto the surface of the support. This is discussed in greater detail at a

later stage. Co-precipitation requires two reagents, which on combination react to cause coprecipitation of the support and a metal moiety. Ion exchange involves the exchange of protons of acidic hydroxyl groups with cations such as the ammine complexes of platinum and ruthenium; drying and reduction of the resultant species results in highly dispersed catalysts.

A disadvantage of heterogeneous catalysts is a lack of selectivity. This is attributed to the variety of particle shapes and sizes. The different crystal faces exposed give rise to a variety of corner and edge sites. The nature and relative numbers of these adsorption sites will vary with the particle size and morphology, giving rise to sites of different activity and selectivity. The nature of the catalyst can be controlled by modification of preparation procedures. This, however, alters the macroscopic properties of the catalyst, and the problem of particle size variation remains. The inhomogeneity of the catalyst causes problems with reproducibility, characterisation of intermediates, and elucidation of mechanisms. A technique, which allows greater control over the dispersion of metal atoms, is therefore required.

1.2.2 Homogeneous Catalysis

A homogeneous catalyst exists in the same phase as the reactants, commonly in solution. A homogeneous system usually consists of a sequence of linked chemical reactions, which form a closed catalytic cycle involving several different intermediate metal species derived from a well-characterised starting complex. The species in the cycle are normally discrete, soluble transition metal complexes, which can often be characterised by standard spectroscopic techniques, although intermediates may be short lived, and exist in low concentrations. The active species usually contains single metal atom. The reaction sequence can usually be explained in terms of standard organometallic mechanisms, such as oxidative addition, reductive elimination, nucleophilic and electrophilic attack on coordinated ligands and substitution reactions. A homogeneous catalyst typically has only one active metal centre, allowing a high degree of selectivity. As the active species is closely related to the starting molecule, catalysis is reproducible, and controlled design is possible. For example, a

simple ligand change can alter the product ratio by imposing steric or electronic constraints[4]. There are two major disadvantages of homogeneous catalysts. The first is that they are often unstable under the conditions of elevated pressure and temperature, which may need to be employed in industrial processes. Secondly, recovery of the catalyst from the reaction product can be extremely difficult. The high costs of replenishing the catalysts thus often render their industrial application uneconomical.

1.2.3 Hybrid Catalysts

There has recently been much interest in finding a method for combining the practical benefits of heterogeneous catalysts with the advantages of homogeneous catalysts[5]. These 'hybrid' catalysts would therefore be selective, efficient, and reproducible both in their production and the results obtained from them, while their design could be controlled. Hybrid catalysts usually consist of transition metal compounds supported on a surface without a significant change in their structure[6]. Under ideal conditions this would produce single metal centres in a separate phase to the reactants. Anchoring to a surface may result in increased stability of the catalyst.

1.3 Surface Organometallic Chemistry

1.3.1. Introduction

Over the last twenty-five years there has been an increasing interest in the study of the reactivity of organometallic compounds supported on amorphous inorganic oxides[7]. The study of these surface immobilised organometallic fragments has shown similarity to both homogeneous and heterogeneous catalytic systems. Heterogeneous reaction systems are likely to involve surface organometallic fragments as reaction intermediates. An improved understanding of the basic steps of heterogeneous reaction mechanisms and hence catalytic

reactivity can hopefully be gained from the study of the reactivity of well-defined surface organometallic species[8].

The chief advantage of surface supported catalysts over their homogeneous analogues is that the readily formed unsaturated intermediates are stabilised by the surface, which acts as a large, rigid ligand to trap them[9]. The reactivity, distribution of the support material and the relatively uniform structure of supported organometallics may be considered to make them homogeneous in nature, despite the similarities with heterogeneous systems[10]. Studies have shown similarities between the chemistry of surface organometallic complexes of rhodium and that of homogeneous analogues. For these reasons, supported organometallic systems can be considered as hybrid catalysts. The selectivity of the catalyst is improved since isolation of the active sites can help prevent some undesirable side reactions. Some supported organometallic complexes have been shown to be highly effective low temperature catalysts. This is not always possible with conventional homogeneous and heterogeneous analogues[9].

1.3.2 Preparation of Surface Supported Organometallic Systems

The most commonly used method of catalyst preparation is that of impregnation. A disadvantage of this technique is that a solvent is required, and this is very difficult to completely remove from the surface. The presence of solvent on the surface can alter the properties of the catalyst and complicate spectroscopic characterisation of the catalyst. The technique of MOCVD (Metallo-Organic Chemical Vapour Deposition) (section 2.4) involves subliming an organometallic precursor onto the surface of the support and removes the need for any solvent. MOCVD is only suitable for volatile precursors however. MOCVD is ideally suited for the preparation of single crystal supported organometallics, which are studied under UHV conditions. The use of a common preparation technique for surface supported organometallic compounds, on both high surface area and single crystal oxide substrates, allows for better comparison of the results obtained from the two systems. In this study, all supported organometallic systems have been prepared by MOCVD.

1.3.3 Supported Organometallics as Precursors for Highly Dispersed Metal Particles

The production of highly dispersed metal centres with a narrow particle size distribution can be achieved by MOCVD, followed by thermolysis under an inert atmosphere. The presence of ligands, which may only require mild conditions for their removal can prevent the agglomeration of metal atoms into large particles. Treatment with a reducing gas such as hydrogen can have a similar effect on promoting small metal particle formation. An understanding of the mechanisms involved in the transformation from supported organometallic species to small metal particle would aid the understanding of catalytic systems.

1.3.4 Reactions of Organometallic Compounds with Oxide Surfaces

The terminology used in surface organometallic chemistry is the same as that in organometallic chemistry. Oxidative addition, reductive elimination, electrophilic and nucleophilic attack at the metal or ligand centre, and substitution reactions are common mechanisms for the reactions for surface bound organometallics. The various types of surface functionalities involved include hydroxyl groups, protons, redox centres and acid-base centres[11].

The anchoring procedure generally consists of a reaction between the transition metal complex and the surface hydroxyl groups of the oxide to form a bond between the metal centre and a surface oxygen atom. One of the most well studied systems is that obtained by reacting $Rh(\eta^3\text{-}C_3H_5)_3$ with oxide surfaces[12,13,14]. The reaction with high area silica is believed to occur as follows: (see next page)

$[Si]\text{-}OH + Rh(\eta^3\text{-}C_3H_5)_3 \rightarrow [Si]\text{-}O\text{-}Rh(\eta^3\text{-}C_3H_5)_2 + C_3H_6$ (below, propene not shown)

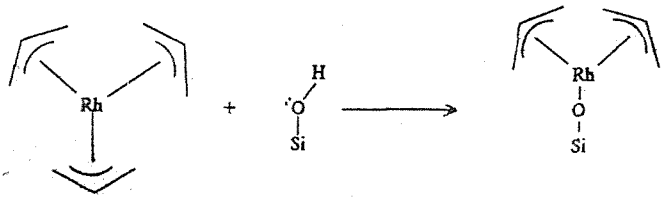

Mass spectroscopy indicates that one equivalent of propene is evolved, and infrared spectroscopy shows that the π allyl character is maintained. However, there are disagreements about the stoichiometry of the reaction, but the utilization of a range of *in situ* experimental techniques should enable more conclusive characterisation[2,10-12].

There has been extensive investigation into the chemistry of Group VIII metal clusters supported on oxide surfaces. Basset *et al*[15,16] and Evans *et al*[17,18] have suggested the following reaction between $Ru_3(CO)_{12}$ and hydroxylated SiO_2. The reaction that is believed to take place is shown below: (2 CO evolved during the reaction)

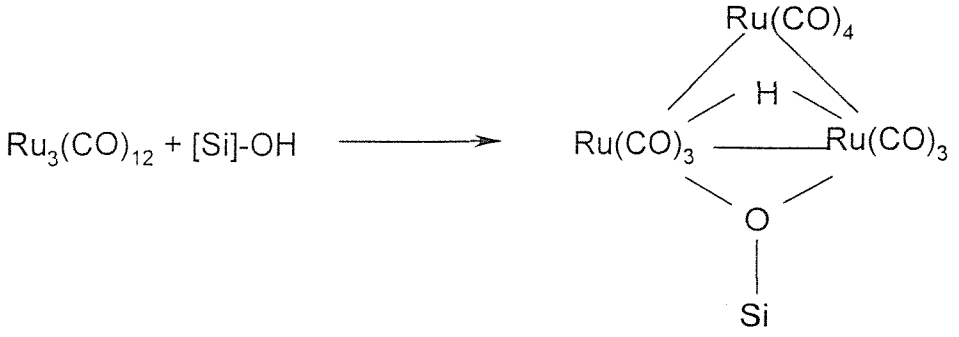

This species was characterised by a combination of IR, Raman and EXAFS spectroscopy. Webb and Robertson, Kuznetsov *et al*[19,20] and Wells et al[21], observed that $Ru_3(CO)_{12}$ was physisorbed on SiO_2. The reported difference in behaviour is probably due to varying oxide pretreatment and preparation methods[4]. Similar variation has been reported for TiO_2 and Al_2O_3.

Other types of interactions with the surfaces are possible, such as Lewis acid interaction. Basset *et al*[22] claimed the formation of an anionic cluster $[HFe_3(CO)_{11}]^-$ when $Fe_3(CO)_{12}$ is adsorbed on Al_2O_3, which is bound to the surface via a Lewis acid interaction between a bridging CO and Al^{3+} site.

The reaction that is believed to take place is shown below:

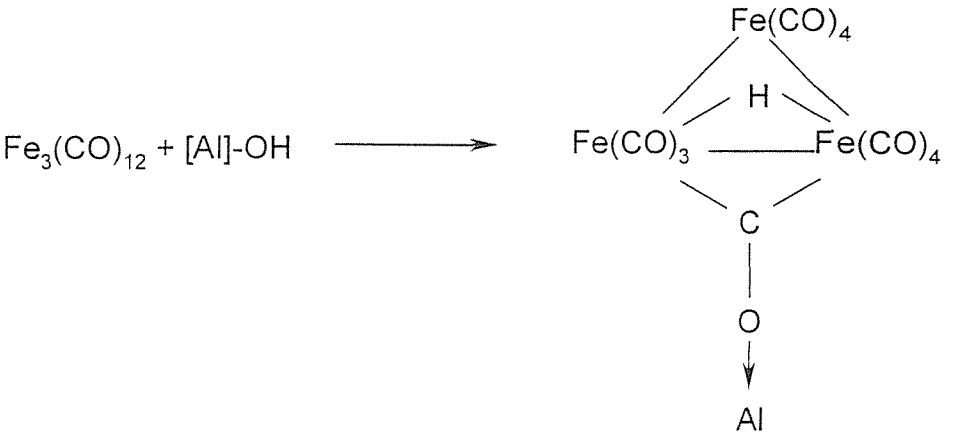

1.3.5 Transformations of Surface Organometallic Species

The reaction procedure in a homogeneous catalytic system can usually be deduced from the known steps of stoichiometric organometallic reactions[9]. The reaction procedure in a heterogeneous catalytic system is far less well understood. The complex reaction mechanisms involved render assignment of the reactions of well-characterised adsorbed molecules difficult. A surface supported organometallic fragment may represent an intermediate species in a particular mechanism if its stepwise conversion into the products can be demonstrated. The reactivity of surface supported organometallic species has been shown on occasions, to follow that of molecular analogues[6]. However, in an instance where a surface supported species bears close structural resemblance to the organometallic, reactivity may be expected to be reduced, due to the bond between the metal centre and the surface. In other instances, reactivity is increased due to coordinative unsaturation, and support induced steric and electronic changes[4]. An insight into the reactivity of heterogeneous systems may be achieved

through an understanding of the chemistry of surface supported organometallics. The mechanism and selectivity of C-C and C-O bond formation is considered particularly important since supported rhodium catalysts are used for converting synthesis gas into C_2-oxygenates[8,23].

An example of a system where surface organometallic species catalyse C-C bond formation, is the reductive coupling of two η^3-allyl ligands coordinated to surface supported Rh^{III}, which occurs upon exposure to CO[6,9].

$$(\equiv Si\text{-}O)Rh^{III}(C_3H_5)_2 + 2CO \rightarrow (\equiv Si\text{-}O)Rh^{I}(CO)_2 + CH_2{=}CH(CH_2)_2CH{=}CH_2$$

This reaction is initiated by the addition of CO to the surface species, causing the η^3-allyl ligands to become η^1 bound. 1,5-hexadiene is evolved as the product after the subsequent reductive elimination.

Metal-carbon bond cleavage by hydrogen on electrophilic early transition metal centres can occur via σ-bond metathesis[24]. The reaction is assumed to proceed via a concerted mechanism involving a 4-centre transition state, though the reaction pathway is described as heterolytic because of the highly electropositive nature of the metal and the substantial negative charge on the alkyl group. The reaction of $Zr[CH_2C(CH_3)_3]_4$ with partially dehydroxylated silica gives $(\equiv SiO)Zr[CH_2C(CH_3)_3]_3$ and one equivalent of neopentane[25]. This surface supported tris(neopentyl)zirconium species undergoes heterolytic Zr-C bond cleavage in the presence of hydrogen to give silica supported Zr^{IV} hydrides[24].

$$(\equiv SiO)Zr[CH_2C(CH_3)_3]_3 + H_2 \rightarrow (\equiv SiO)Zr[CH_2C(CH_3)_3]_2(H) + (CH_3)_4C \rightarrow (\equiv SiO)Zr(H)_3 + 3(CH_3)_4C$$

The high oxophilicity of Zr^{IV} also results in hydrogen transfer from the zirconium to the silica, yielding non-exchangable silicon hydrides[26].

$$(\equiv SiO)Zr(H)_3 + 2(\equiv Si\text{-}O\text{-}Si\equiv) \rightarrow (\equiv SiO)_3ZrH + 2\equiv Si\text{-}H$$

This zirconium hydride species is highly electrophilic as it formally has only 8 metal valence electrons, though coordination of a fourth oxygen atom has been observed from EXAFS spectroscopy, which would result in a 10 electron system[27]. Such strongly electrophilic early transition metal complexes can be used for the activation of C-H bonds, with the formation of stable alkyl complexes. The mechanism of C-H bond activation employing these systems is σ-bond metathesis, with a 4-centre transition state, which is obtained by coordination of the C-H bond to the electrophilic centre. The $(\equiv SiO)_3ZrH$ complex will react stoichiometrically with methane (at 150°C) and cyclooctane (at 25°C) to give the corresponding alkylzirconium species[28]. Reaction of this silica supported cyclooctylzirconium with CO gives insertion into the metal-carbon bond to form the acylzirconium. Cyclooctanal is obtained via protolytic extraction of the product[29].

1.3.6 Catalytic Activity of Surface Organometallic Species

An improved understanding of the catalytic behaviour of a surface organometallic system can only be achieved if the stoichiometries of the elementary steps are well characterised.

The hydrogenolysis of neopentane, isobutane and propane at 50°C is catalysed by the silica supported zirconium^{IV} hydride species, in the presence of hydrogen[26,28]. This is the first reported case of the low temperature catalytic activation of C-H and C-C bonds of alkanes[24]. Conventional heterogeneous systems required much higher temperatures to perform this reaction, and molecular, homogeneous analogues were unable to perform the catalytic cycle. Neopentane is catalytically converted into isobutane and methane[30]. Isobutene, though not observed, is assumed to be a primary product, which is rapidly hydrogenated to isobutane before subsequent conversion into propane and methane. The mechanism involves formation of an alkylzirconium complex via a four-centre exchange reaction[24]. No hydrogenolysis of ethane occurs, which suggests that a crucial elementary step in the decomposition of the alkyl Zr^{IV} intermediate is β-methyl transfer to give a CH_3Zr^{IV} fragment and the corresponding alkene.The reaction scheme is illustrated in figure 1.1.

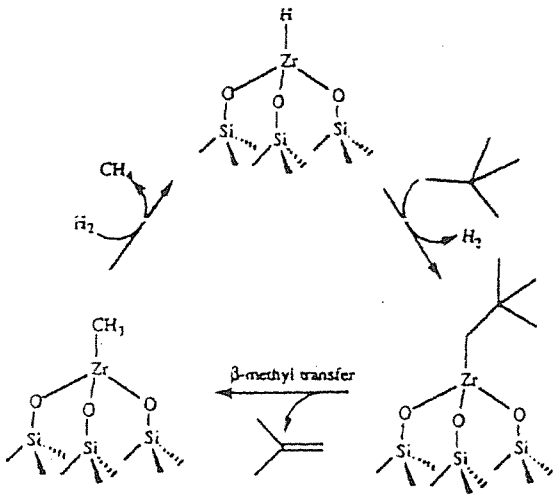

Figure 1.1 Possible Mechanism for the Low Temperature Catalytic Hydrogenation of Alkanes by ($\equiv SiO_3$)ZrH. (ref. 24)

The surface organometallic species formed upon chemisorption of $Rh_6(CO)_{16}$ or $[Rh(CO)_2Cl]_2$ on alumina is an active catalyst for the water gas shift reaction[31,32,33]. The reaction scheme is illustrated in figure 1.2. One of the surface species present during the reaction is the rhodium *gem* dicarbonyl, $Rh^I(CO)_2$ which has been characterised by both EXAFS and infrared spectroscopies[31,34]. The nuclearity of the precursor does not affect the activity of the catalyst, which has one of the highest turnover numbers of any low temperature rhodium based water shift catalysts at 130 mol H_2/ Rh atom/ hour at 50°C under 50 atmospheres of CO[32]. The first stage in the formation of the catalyst is the chemisorption of $Rh_6(CO)_{16}$ onto the alumina surface, with the formation of $Rh^0(CO)_n$ and monodentate surface $Rh^0(CO)_n$ by surface hydroxyl formate. The proposed mechanism for the water gas shift reaction involves oxidation of $Rh^0(CO)_n$ by surface hydroxyl groups or water, to produce $Rh^I(CO)_2$ and $Rh^{III}(H)_2$ complexes. Though $Rh^{III}(H)_2$ is not observed directly, the ready oxidation of propene to propane by the oxidised catalyst is considered evidence for its existence. The dihydride complex will eliminate H_2 in the presence of CO to produce $Rh^I(CO)_2$, which will again undergo nucleophilic attack to H_2O. The hydroxycarbonyl intermediate releases CO_2 by decarboxylation. The yields of CO_2 and H_2 are equal, as expected for the water gas shift reaction. Though the proposed reaction scheme shows the $Rh^0(CO)_n$ species to have more than 1 CO group coordinated to each Rh[24], such a structure is extremely unlikely given the relative size of the CO group and the metal atom. A mixture of

linear and bridging CO sites would be more likely than a combination of both on each metal atom.

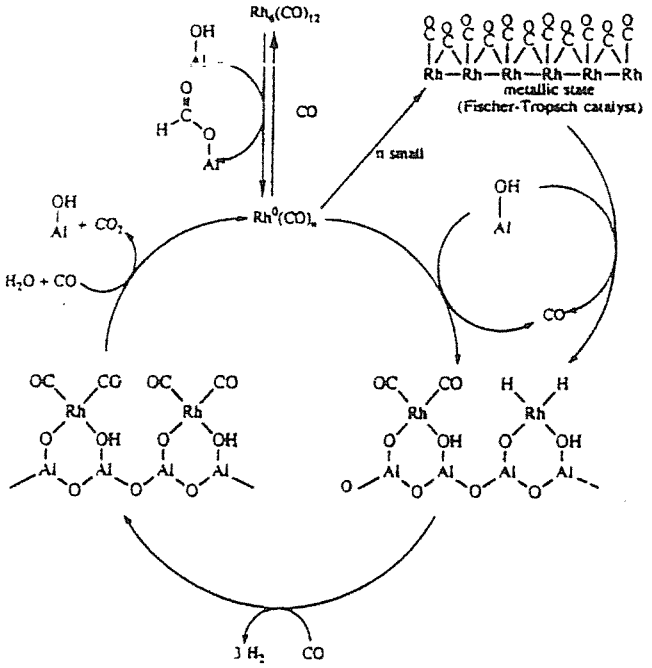

Figure 1.2 Proposed Mechanism for the Catalysis of the Water Gas Shift Reaction by $Rh^{I}(CO)_2$ Supported on Alumina[31-33].

1.4 The Surface Chemistry of Titania

1.4.1 Surface Sites

Titania has three normal crystallographic forms: rutile, anatase and brookite. The most widely used surface area titania, both industrially and in this study is Degussa P25 which is a mixture of anatase (85%) and rutile (15%). Degussa P25 has a surface area of 55 ± 1 m^2g^{-1}, a total pore volume (<500Å) of 0.11 ± 0.01 cm^2g^{-1} and a mean pore diameter of 98Å.[35] Rutile is the thermodynamically stable structure, the transformation from anatase to rutile taking place at approximately 1300K. In both forms, the bulk Ti cations are surrounded by six oxygen neighbours in an octahedral coordination[36]. At the surface of a powder, each of the anatase

and rutile particles will have several different crystallographic planes exposed, in a disordered manner, giving a variety of different hydroxyl groups. In order to exert a degree of control over the resultant surface organometallic species, knowledge of these hydroxyl groups is needed in order to control their distribution.

The nature of the complex formed on reaction between an organometallic compound and an oxide surface will depend both upon the labile ligands on the compound and the concentration of surface hydroxide groups and any other reactive surface functionalities. The resulting surface species may therefore lack homogeneity due to the presence of hydroxyl groups of differing reactivities, a non-uniform distribution of hydroxyl groups on the surface after various intermolecular interactions[4]. Characterisation of the surface properties of titania have been performed by infrared spectroscopy and adsorption studies. Titania is covered with physisorbed water under atmospheric conditions. This is removed by heating under vacuum at 525K prior to any studies[37]. Infrared studies have determined the presence of isolated hydroxyl groups on the (001) plane of anatase and the (110) plane of rutile[37]. Two bands assigned to hydrogen bonded hydroxyl groups are found for the rutile surface as against just one for the anatase. The variation in infrared stretching frequencies for these hydroxyl groups between 3715cm^{-1} and 3410cm^{-1} shows the variation in bond strength, a useful factor when considering reactions[4]. It has been determined that heating at 423K would reduce the concentration of OH groups on the anatase (001) surface from 7.0 OH/nm^2 to 2.0 OH/nm^2 [10,38]. This would result in an average (H)O-O(H) separation of 10Å[10], meaning that only one hydroxyl group is likely to be available for coordination to a metal centre, assuming an even distribution of the hydroxyl groups. Dehydroxylation of titania can create Lewis acid sites, the nature of which has been probed by CO absorption studies. These studies have shown that a very small number of strong acid sites are created on dehydroxylation, along with a large number of weak Lewis acid sites created by removal of molecular water[39].

1.4.2 The Strong Metal Support Interaction (SMSI) Effect

Titania is a reducible support in that high temperature reduction or very high temperature thermal treatment will greatly reduce the capacity of supported metal particles to

adsorb CO or H_2. Tauster *et al* attributed this effect to bonding between the supported metal and the titanium of the support[40]. The term SMSI was initially used to refer to an effect between the support and metal particles, it has since been applied to a range of effects that a support may have on chemisorption and catalytic activity[36,41]. Models proposed for explanation of the SMSI effect on titania supported rhodium have included alloy formation[42], an electronic effect of titanium suboxide beneath the rhodium[43], or rhodium becoming covered by the titanium suboxide species after reduction and blocking the adsorption sites[44,45]. Similar suppression of CO adsorption has been observed for rhodium on alumina after heating to 1100K[46]. It has been proposed that under high temperature oxidising conditions, rhodium is encapsulated by mobile oxide or sub-oxide phases of TiO_2, demonstrated using STM for the Pd/TiO_2 [110] system[47].

The effect on the catalytic properties of titania upon doping with W^{6+} ions has been studied by Verykios *et al*[48,49,50]. An increase in adsorption capacity for both CO and H_2 onto rhodium supported on this system was observed, and the modes of adsorption for the two molecules altered as a result of modifications to the electronic properties of the titania. This increase in adsorption capacity is the opposite effect to that observed with the SMSI, though they are not considered to be related[50]. The variations in the chemisorptive properties of the rhodium crystallites supported on W^{6+} doped titania are considered to be due to electronic interactions at the metal support interface which alter the electronic structure of the supported rhodium particles and the catalyst surface[48,50]. It is proposed that these changes serve to weaken the Rh-CO bond, and therefore strengthen the C-O bond.

1.5 The Surface Chemistry of Alumina

1.5.1 Introduction

Stoichiometrically there is only one oxide of aluminium, namely, alumina (Al_2O_3). There are, however, various polymorphs and hydrated species, the formation of which depends on the conditions of preparation[51]. There are two forms of anhydrous Al_2O_3, namely,

α Al_2O_3 and γAl_2O_3. In αAl_2O_3, the oxide ions form a hexagonal close-packed array and the aluminium ions are distributed symmetrically along the octahedral interstices. The γAl_2O_3 structure is sometimes referred to as a 'defect' spinel structure, meaning a spinel structure with a deficit of cations. αAl_2O_3 occurs naturally as *corundum*, or may be prepared by heating γAl_2O_3 or any hydrous oxide above 1000°C. γAl_2O_3 is obtained by dehydration of hydrous oxides at low temperatures (~450°C).

$$2AlO(OH) \rightarrow \gamma Al_2O_3 + H_2O$$

1.5.2 Surface Acidic and Basic Sites

When exposed to atmospheric moisture, the surface of γAl_2O_3 is covered with adsorbed water molecules. Dehydration at 100 to 150°C leads to the desorption of water, but surface OH groups remain and act as weak Brønsted acids:

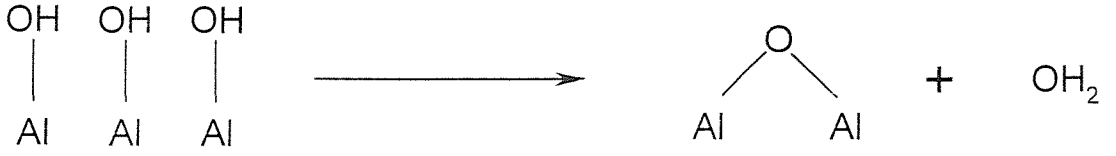

At even higher temperatures adjacent OH groups condense to liberate more H_2O and generate exposed Al^{3+} Lewis acid sites as well as O^{2-} Lewis base sites. The rigidity of the surface permits the co-existance of these strong Lewis acid and base sites, which would otherwise immediately combine to form Lewis acid-base complexes. Surface acids and bases are highly active for catalytic reactions such as the dehydration of alcohols and isomerisation of alkenes[52].

1.5.3 Surface Metal Sites

Metal particles are often deposited on supports to provide a catalyst. For example, finely divided platinum-rhenium alloys distributed through the pore space of γAl_2O_3 are used to interconvert hydrocarbons, and finely divided platinum-rhodium alloy particles supported on γAl_2O_3 are employed in automobile catalytic converters to promote the combination of O_2 with CO and hydrocarbons to form CO_2, and reduction of nitrogen oxides to nitrogen[52]. A supported metal particle has about 40% of its atoms on the surface (although this varies with particle size and morphology), and the particles are protected from fusing together into bulk metal by their separation. The high proportion of exposed atoms is a great advantage for these small supported particles, particularly for metals such as platinum and even more expensive rhodium.

1.6 Surface Rhodium Carbonyl Species

1.6.1 Introduction

Surface rhodium carbonyl species are encountered extensively in this thesis. They have been prepared by a variety of methods, including: reaction of rhodium carbonyl complexes with partially dehydroxylated titania, exchange of hydrocarbon ligands of titania supported rhodium organometallics with CO, and by the adsorption of CO onto titania supported rhodium metal particles. The complex chemistry of such species has been subject to numerous investigations[53,54,55,56], employing infrared spectroscopy, NMR, temperature programmed desorption (TPD), and EXAFS spectroscopy. Infrared spectroscopy is particularly useful, as the vibrational frequency of the ν(C-O) mode is very sensitive to the amount of back donation from occupied metal d orbitals to the π^* orbital of the CO molecule, and intermolecular interactions[4]. Hence useful information about the electronic characteristics of the metal and the bonding of the CO can be obtained. Other advantages include the fact that the ν(C-O) bands are intense, allowing the detection of species in small concentrations, and that particular adsorbed species can be identified in comparison with model systems, such

as rhodium carbonyl clusters and CO absorbed on single crystals. The above mentioned frequency sensitivity results in CO being widely used as a probe molecule, to study metal particle morphology[57].

There is almost universal agreement that there are three principal carbonyl species formed by adsorption of CO on alumina-supported rhodium[55,56]. They consist of:

i) A linear rhodium carbonyl species, whose frequency shifts to a higher wavenumber on increasing coverage from 2050cm^{-1} to 2080cm^{-1}.

ii) A CO molecule bridging two rhodium atoms with a frequency of ca 1850cm^{-1}.

iii) A *gem* dicarbonyl species, where two CO molecules are bound to a single rhodium atom[58]. This species displays two infrared bands due to the coupled symmetric (2095cm^{-1}) and antisymmetric (2030cm^{-1}) stretches.

The first two species are associated with metallic rhodium. The shift in frequency for the linear carbonyl site is indicative of rhodium particles greater than 20Å in size. Such shifts are frequently observed for CO on transition metals and are thought to arise for a variety of reasons[59]:

i) Due to the synergic bonding between CO and rhodium, as coverage increases, so does competition between CO molecules for metal d electrons. This can result in a reduction of the back bonding. Hence the frequency increases as the C-O bond strength has increased. Such a chemical effect is also seen for CO adsorbed on palladium.

ii) Dipole interaction between adjacent CO molecules results in the vibration of one molecule affecting the potential energy of a neighboring molecule. Dipole-dipole coupling could also involve the conduction electrons of the metal[4]. The shifts seen on platinum have been shown to be due to coupling interactions by elegant decoupling NMR experiments.

HREELS studies[60] of CO adsorbed on the Rh(111) crystal face give support to these assignments, as they reveal a band which shifts from 2050cm^{-1} to 2070cm^{-1} on increasing

coverage and a band at 1870cm^{-1} due to a bridging carbonyl. No *gem* dicarbonyl species were identified. The relative distributions of the three species on oxide supported rhodium has been shown to be dependant on metal loading[61], reduction conditions[62], rhodium precursors[63,64], and the supports[65,66]. Yates[67] showed that for a 0.2% weight Rh sample, $Rh(CO)_2$ units predominated and had a CO/Rh ratio of 1.9, whereas a 10% weight sample had a CO/Rh ratio of 0.5, with the monocarbonyl species predominating.

1.6.2 The Rhodium *gem* Dicarbonyl Species

The rhodium *gem* dicarbonyl species is characterised by the fact that it displays no shift in frequency with increasing coverage and is thought to exist as an isolated Rh^I site[68,69,70]. The species is characterised by two infrared bands at ≈2100cm^{-1} and 2030cm^{-1}.[4,56,70,71]. However, it has recently been shown that a small shift in wavenumber for this species up to 9cm^{-1} may be observed with increasing coverage[71,72]. Isotopic substitution studies[73] have confirmed it to be a non linear C_{2v} species, as the expected number of bands were observed and their frequencies matched the calculated values within experimental error. It was noted that isotopic substitution was faster than CO desorption under vacuum at 295K.

Investigations of the formation of the gem dicarbonyl species have traditionally involved treatment of a surface supported rhodium catalyst with carbon monoxide. Initial proposals suggested that the $Rh^I(CO)_2$ was formed via the dissociation of CO, resulting in the oxidation of Rh^0 to Rh^I by oxygen adatoms[56,74]. Subsequent studies, however, have shown that the *gem* dicarbonyl species is formed at temperatures lower than that required for CO dissociation[75,76]. An alternative model proposed that electrons were transferred from the rhodium to the alumina support[77], though this could not account for the formation of the said species on titania and silica. The theory that the reduction of OH^- groups of the support may be responsible for Rh^I formation has received much support[71,78,79], including results which have shown that a reduction in hydroxyl groups is associated with the development of the *gem* dicarbonyl[80]. Recent work by Evans *et al* has not supported the previous theory, but proposed that the reaction converting Rh^0 to Rh^I on the TiO_2 (110) surface is more likely to be associated with a small concentration of surface defects (oxygen vacancies) which provides

sites of variable local stoichiometry[55]. It should be noted, however, that this study refers to regeneration of the $Rh^{I}(CO)_2$ after thermal desorption of the original species formed by MOCVD of $[Rh(CO)_2Cl]_2$, instead of a supported metal system prepared by wet impregnation, and is conducted on a rutile single crystal rather than a high surface area powder system. Verykios *et al*[22] have found hydroxyl group signals to be enhanced during CO adsorption onto titania, contrary to results on silica and alumina. They have concluded that the interaction of CO with Rh/TiO_2 causes changes both in the state of dispersion of the crystallites and the surface structure of the support. The structural changes in the titania during CO chemisorption led the authors to suggest that the support can also participate to some extent in the interaction with the adsorbent, and this type of metal support interaction may be related to the high catalytic activity of Rh/TiO_2 in CO hydrogenation.

Formation of $Rh^{I}(CO)_2$ on single crystal rutile (110) under UHV conditions, was first reported by Evans *et al*[55]. The MOCVD of $[Rh(CO)_2Cl]_2$ was employed instead of treatment of the supported metal with CO in order to avoid the high pressures likely to be required for such a system. The *gem* dicarbonyl bands were observed by FT-RAIRS at $2112cm^{-1}$ and $2028cm^{-1}$, with XPS showing that chlorine from the precursor remains on the surface remains with a different binding energy to that observed for the parent molecule. Thermolysis of the surface species shows that desorption of CO occurs between 450 and 500K, resulting in the formation of small particles of metallic rhodium. Regeneration of the *gem* dicarbonyl species occurred upon re-exposure to CO at room temperature. Heating to temperatures of 500K or more meant that the *gem* dicarbonyl species could only be partially regenerated upon exposure to CO, accompanied by the adsorption of linearly bound CO on the metal particles, indicated by an infrared band at $2064cm^{-1}$. Heating to 800K resulted in the formation of large metal clusters, from which the *gem* dicarbonyl species could not be regenerated. Exposure to CO resulted in the appearance of a linear carbonyl band at $2060cm^{-1}$ and a broad bridging band at $1870cm^{-1}$.

Further studies of this system found the frequency of the band associated with the symmetric stretch of the *gem* dicarbonyl to shift with increasing coverage from $2104cm^{-1}$ to $2113cm^{-1}$.[81]. This shift may arise from dynamic dipole and chemical interactions between CO

atoms in adjacent $Rh^{I}(CO)_2$ species, which are less significant than those observed in CO adsorption studies on Rh single crystal surfaces[82].

Other workers have reported a shift in the gem carbonyl frequency with increasing coverage. The bands shifted from 2097cm^{-1} to 2100cm^{-1} and 2030cm^{-1} to 2034cm^{-1} with increased exposure to CO of 0.5% weight Rh on TiO_2[71]. It has been suggested that as the rhodium loading is increased, more strongly oxidised surface hydroxyl groups are occupied, resulting in a shift to higher frequencies[4]. These signals were accompanied by a broad, weak absorption due to bridging carbonyl at 1830cm^{-1}.[71].

The *gem* dicarbonyl species has been observed to be dominant on highly dispersed metal systems, with the linear and bridging species predominating with higher metal loading, or increased metal particle size caused by thermal treatment[71,81]. For catalysts with identical metal loading, the nature of the support has been shown to influence the particle size distribution and hence the nature of the rhodium carbonyl surface species[70]. The nature of the support has also been shown to influence the rate of decomposition of surface carbonyl systems, as well as reactivity with CO and H_2[66,83].

Zhang and Verykios studied CO adsorption on 0.5% weight Rh/TiO_2 and observed that *gem* dicarbonyl species accounted for 90% of the carbonyl species present[56]. This study identified bands at 2105cm^{-1} and 2087cm^{-1} arising from the decarbonylation of $Rh^{I}(CO)_2$ and were assigned to $Rh^{I}_2(CO)$ and $Rh^{I}(CO)$ respectivly, which are thought to exist as intermediate species. The following mechanism has therefore been proposed for the decarbonylation of $Rh^{I}(CO)_2$ at temperatures above 400K:

$$Rh^{I}(CO)_2 \rightarrow Rh^{I}(CO) + CO$$

$$Rh^{I}(CO) \rightarrow Rh^{I} + CO$$

Only a small proportion is was identified as being converted into the linearly adsorbed species on rhodium metal $Rh^{O}(CO)$, which the authors consider to have arisen from reduction of the $Rh^{I}(CO)$ species.

Rh K-edge EXAFS spectroscopy has also been used to observe the disruption of small rhodium crystallites to form rhodium *gem* dicarbonyl species upon adsorption of CO, by Koningsberger *et al*[84]. On a 1% weight Rh sample, admission of CO reduced the rhodium neighbour coordination from 5 to 1.3. This was accompanied by the presence of an average 1.7 carbonyl groups per rhodium atom, and coordination to a surface oxygen atom at 2.06Å. With CO adsorption on a 0.5% weight sample, complete disruption of the rhodium particles was indicated by the absence of any rhodium neighbours[76]. This disruption of alumina supported metal particles was also observed by Joyner et al. However, the rhodium particles had been prepared by wet impregnation of $RhCl_3.xH_2O$, and reduced under H_2 at 473K, and the rhodium atoms were still bound to chlorine from the precursor[85,86].

Dictor and Roberts have proposed the presence of more than one type of dicarbonyl state, with differing mobilities and adsorption properties, as an explanation for the non-first order kinetics for CO desorption from dicarbonyl sites[87]. Such a situation would have important catalytic implications and has been supported by NMR spectroscopy due to the lack of discrimination provided by infrared spectroscopy.

NMR spectroscopy, even in the solid state, is useful in differentiating between adsorbed states of adsorbed CO[88]. Early studies of CO adsorbed on Rh/Al_2O_3 had suggested that the three commonly recognized rhodium carbonyl species were observed, with the dicarbonyl species being motionally averaged to produce a narrow peak[89]. Further studies have shown the spectra to be more complex, and that the relative proportions of CO species in the various sites determined by line shape integration does not necessarily equal that from CO uptake measurements[90]. Further problems with recording these spectra have included the absence of sharp features in the powder patterns[91,92], or of narrow bands in spectra recorded with magic angle spinning[93]. Studies were therefore conducted upon a sample with a very high proportion of dicarbonyl species in order to simplify the problem[94]. One of these showed a rapid mutual exchange of CO molecules, while another showed the CO molecules to be rigid within the NMR timescale. The low percentage of CO molecules present on a supported sample, and the long acquisition times required because of the long ^{13}C relaxation times in the absence of any protons, have presented major problems in the solid state NMR study of supported rhodium carbonyl species.

1.7 The 3-Way Automotive Exhaust Catalyst System

1.7.1 Introduction

A 'three way catalyst' simultaneously promotes the removal of each of the three major pollutants in automotive exhaust gases, namely CO, NO and hydrocarbons[95,96]. Platinum, which in 1992 found 34% of its total usage in such automotive catalysts[97,98], serves as an effective catalyst for the oxidation of CO and hydrocarbons[96,97]. Rhodium, which in the same year, found 87% of its usage in automotive catalysts[97,98], is superior for reduction of NO to N_2[99]. A summary of the main reactions performed by these catalysts is shown:

$2NO + 2CO \rightarrow N_2 + 2CO_2$

$2NO + 2H_2 \rightarrow N_2 + 2H_2O$

1.7.2 Composition of the Catalyst

A catalytic converter is made from a honeycombed ceramic monolith composed of corderite ($2MgO.2Al_2O_3.5SiO_2$)[95], covered with a thin layer of alumina, 30-50μm thick, which acts as a support for the metals. The metals are applied to the stabilised alumina coated monolith as dilute solutions of salts. There is a precise control of the noble metal uptake to ensure that performance requirements will be met and that metal wastage is minimised. The noble metal loadings on the alumina are typically 0.15-0.27g of rhodium and 1.5-2.4g of platinum. Other additives such as ceria are contained in the catalyst, which increase the durability, and contribute to the performance of the catalyst.

Ceria has been shown to perform several functions[95,100]. One of these is to store and subsequently release oxygen derived from NO_x decomposition during net oxidising conditions (fuel lean air/ fuel ratios) and therefore enhance the conversion of NO_x to N_2[101]. The interconversion of CeO_2 with Ce_2O_3 is likely during this process. The stored oxygen in the CeO_2 is then available for reaction with CO and hydrocarbons during subsequent fuel rich/ fuel ratio conditions. Due to oxygen spillover from the metal to the reduced ceria, the

Rh/CeO_2 system is deactivated more slowly than the Rh/Al_2O_3 system, thus enhancing NO decomposition activity by extending the lifetime of the catalyst prior to deactivation from the accumulation of surface oxygen produced from NO reduction[95,102].

The most important effect of the ceria is its alteration of the reaction kinetics of CO oxidation and NO_x reduction[95,102]. The addition of ceria to an alumina supported catalyst was shown to increase NO reduction activity at low temperatures by lowering the apparent activation energy for the reaction with CO and shifting the dependence on the rate on the NO partial pressure to positive order[103]. Improvement of the catalyst performance at low temperatures is needed to decrease the emissions immediately following the start up of the vehicle. The location of the vehicle determines the operating temperature of the catalyst, with temperatures in the order of 350°C-650°C within the desired range for catalysis, without significant degradation of the catalyst or support[95]. For a Pt/ceria/alumina catalyst, it has been shown that a reduction in particle size of the ceria from 270Å to 120Å, lowers the temperature for 25% NO reduction by 80°C in a laboratory simulated exhaust gas[104]. This particle size effect has been attributed to increased interactions between the platinum and the ceria.

Other additives to the catalyst include lanthanum, which is added to the alumina washcoat to provide thermal stabilisation[105,106], and nickel, which is added to suppress the formation of hydrogen sulphide.

There has been much recent interest in replacing rhodium and/or platinum with palladium because of its much lower cost[95,107,108]. Comparison of the reactivity of these three metals for the reduction of NO_x reduction has shown rhodium to be favoured for its high activity, low NH_3 formation and a NO_x conversion window, which extends to leaner (more oxidising) conditions. Palladium is known to be less active than rhodium and has a narrower air/fuel ratio for NO_x conversion[109]. Palladium is more susceptible to lead poisoning than platinum, but is more durable under high temperature oxidising conditions in the absence of poisons. Studies on the conversion performance of vehicle aged catalysts have shown the main disadvantage of the palladium catalyst relative to rhodium and platinum is in the NO_x conversion under fuel rich (net reducing) conditions[95]. This disadvantage may be partially

overcome by tight control over the air/fuel ratio[110]. Muraki *et al* have suggested that poor NO_x conversion under net reducing conditions is due to poisoning by hydrocarbons, and that NO_x reduction activity is improved by adding lanthanum to the catalyst[111]. Further studies have investigated the use of palladium/ tungsten and platinum/ molybdenum in light of the intended reduction in rhodium usage[112,113].

1.7.3 Catalytic Reactions

The maintenance of exhaust composition close to the stoichiometrically balanced requirements for simultaneous reduction of nitric oxide and oxidation of carbon monoxide and hydrocarbons has been a target in the development of engine control systems. The reaction that attracts most interest is that between CO and NO over rhodium[95,114,115,116,117]. Other studies have also investigated the reduction of NO by H_2[98,118]. The mechanism of the reaction between NO and CO over rhodium is considered to proceed as follows[115].

$NO + S \leftrightarrow NO_a$ (1) (S is the surface under consideration)

$CO + S \leftrightarrow CO_a$ (2)

$NO_a + S \rightarrow N_a + O_a$ (3)

$NO_a + N_a \rightarrow N_2O + 2S$ (4)

$NO_a + N_a \rightarrow N_2 + O_a + S$ (5)

$CO_a + O_a \rightarrow CO_2 + 2S$ (6)

Also[95]:

$2N_a \rightarrow N_2$

$N_2O \rightarrow O_a + N_2$

This mechanism has been proposed by Hecker and Bell, who have also reported the formation of Rh-NCO groups during the reduction of NO by CO[115]. This species is characterised by an infrared stretch at 2170-2190cm^{-1}, with the surface coverage being strongly dependant on reactions conditions, and greatest at low NO and high CO partial pressures. The formation of the Rh-NCO species is greatest if the reaction is performed at 230°C, though there is no conclusive evidence that its formation affects the rate of the catalytic reaction[114]. The coverage on the surface of these species is low compared to that by NO and N atoms. The formation of the Rh-NCO species is believed to occur as follows[114,115]:

$N_a + CO \leftrightarrow$ Rh-NCO

$N_a + CO_a \rightarrow$ Rh-NCO + S

A steady state population of the Rh-NCO species is reached under reaction conditions, but this is readily destroyed upon the cessation of NO reduction by decomposition to form N_2 and CO:

$2Rh\text{-}NCO \rightarrow N_2 + 2CO + 2Rh$

1.7.4 Bimetallic Catalysts

The properties of bimetallic supported catalysts are often improved activity, selectivity, thermal stability and poison resistance relative to the constituent metals[95]. Rhodium and platinum have been shown to form alloy particles in the working three-way catalyst[119,120]. Few publications on bimetallic catalytic systems exist, despite the widespread use of rhodium/ platinum catalysts in the automotive industry.

Nieuwenhuys *et al* found that the gas phase composition, the bulk composition of the alloy particles and the reaction temperature influenced the properties of a platinum/ rhodium catalyst[98]. Segregation of rhodium to the surface has been reported above 600K, under

oxidising conditions, though platinum/ rhodium alloy formation was observed under reducing conditions in the same study[98]. No synergistic effects due to the alloying of platinum and rhodium were observed for the NO-H_2 reaction were reported, while the differences in activity between the various catalysts tested could be explained in terms of the specific properties of the individual metals towards the adsorbates[98,118]. The relative concentrations of the adsorbed gases on the surfaces were used to determine the selectivity of the systems under investigation.

Neiuwenhuys *et al* also investigated the reduction of NO by CO over a platinum/ rhodium alloy supported on silica. Once again, there was no synergic enhancement of the reaction rate by this alloy catalyst[121]. Rhodium was shown to be a much better catalyst for the reduction of NO and CO than platinum. This was due to the fact that the dissociation of NO is considered to be one of the slowest stages of the reaction, and this step is more difficult on platinum than rhodium[122]. Once again, a rhodium surface segregation was observed, induced by oxygen and NO in the gas phase, because of the high Rh-O bond strength relative to the Pt-O bond strength[121].

The alloying of particles in platinum/ rhodium systems resulting in possible synergistic performance effects, has been debated for many years[123]. For a bimetallic system containing an active metal A, and a less active metal B, the reactivity of the bimetallic system might be expected to be an average of these two activities[123]. The A-B alloy may show improved performance over the system just containing A, however. This effect, in which the addition of the addition of metal B, which has a low activity, has improved the performance of A, is referred to as synergistic. Alternatively, metal B could interfere with the reaction over metal A and give a combined activity below the calculated average. Synergistic alloying effects are not limited to catalytic activity, but may also include improvements in the selectivity and durability of the catalyst.

The kinetic performances of various compositions of platinum/ rhodium bimetallic catalysts for NO reduction by CO and H_2, have been investigated by Stenger *et al*[123]. A catalyst with the platinum: rhodium ratio at 95:5 (mole ratios, 1.42% Pt, 0.078% Rh), prepared by consecutive impregnation (Pt first) onto alumina, displayed enhanced reactivity

for the NO-H_2 reaction compared with that of the more active single metal, platinum. Enhanced activity for the reduction of NO by CO was observed by this system. There was no information about the surface composition of the individual alloy particles, thus there is the possibility of surface segregation of one component. A rhodium rich system with the platinum; rhodium ratio of 17:83 (0.21% Pt, 1.02% Rh), performed only slightly better for the NO-H_2 reaction than a monometallic rhodium catalyst would have done. This rhodium rich catalyst performed worse than the sum of its constituent metals, for the catalytic reduction of NO by CO.

1.8 Aims of this Thesis

Transition metal catalysts supported on high area oxides are of great industrial importance. The aim of this thesis is to investigate the formation and reactivity of surface supported organometallic species, with likely catalytic applications. These systems have been prepared by MOCVD of volatile Rh and Pd precursors onto partially dehydroxylated, high surface area titania and alumina. MOCVD has been used as the preparatory technique to allow direct comparison with results obtained using single crystals in UHV systems. The reactivity of these systems towards small molecules of catalytic importance, such as CO, NO, and H_2, have been investigated.

The techniques used in this study have been EXAFS, energy dispersive EXAFS (EDE), DRIFTS spectroscopy and temperature programmed desorption (TPD). Each of these techniques allows *in situ* monitoring of the systems under observation during thermolysis or reaction with small gas molecules. In previous studies of supported organometallic systems, EXAFS has been the main structural technique employed for the characterisation of metal bound ligands. In this thesis, energy dispersive EXAFS has also been used to investigate the local structure of supported organometallics during the course of a reaction, presenting the opportunity for *in situ* characterisation of intermediate species. The use of a controlled environment DRIFTS cell also allows reactions of surface supported organometallics to be studied *in situ*, offering a considerable advantage over conventional wafer-thin, pressed discs

used in transmission infrared studies. TPD studies enable the species evolved upon thermolysis of supported organometallic systems to be identified using mass spectroscopy.

A variety of rhodium and palladium organometallics have been used to allow for comparison of adsorption behaviour, and to see how different ligands affect the stability of the supported metal centres, and the size of the metal particles formed on thermolysis or reduction.

1.9 References

1. W. Keim, *Angew. Chem., Intl. Ed. Engl.*, 1990, **29**, 235.
2. N. A. Williams, PhD Thesis, University of Southampton, 1992.
3. B. C. Gates, *Catalytic Chemistry*, J. Wiley, 1992.
4. F. R. Hartley, S. G. Murray and P. N. Nicholson, *J. Mol. Catal.*, 1982, **16**, 363.
5. Y. Iwasawa, *Adv. Catal.*, 1987, **35**, 187.
6. F. J. Carol, C. Wu, W. T. Reichle and N. J. Maraschin, *J. Catal.*, 1979, **60**, 68.
7. R. Buffon, M. Leconte, A. Choplin and J. M. Basset, *J. Chem. Soc. Dalton Trans.*, 1994, 1723.
8. P. Dufour, S. L. Scott, C. C. Santini, F. Lefebvre and J. M. Basset, *Inorg. Chem.*, 1994, **33,** 2509.
9. S. L. Scott and J. M. Basset, *J. Mol. Catal.*, 1994, **86**, 5.
10. S. L. Scott, P. Dufour, C. C. Santini, J. M. Basset, *J. Chem. Soc. Chem. Comm.*, 1994, 2011
11. S. L. Scott, J. M. Basset, A. Choplin, M. Leconte, F. Quignard, C. Santini and A. Theolier, *Elementary Steps in Heterogeneous Catalysis,* Ed. R. W. Joyner and R. A. van Santen, Kluwer Academic, 1993, p39-49.
12. P. Doufour, C. Houtman, C. C. Santini. C. Nedez, J. M. Basset. L. Y. Hsu and S. G. Shore, *J. Am. Chem. Soc.*, 1992, **114**, 4248.
13. H. C. Foley, S. J. DeCanio, K. D. Tau, K. J. Chau, J. H. Uneferko, C. Dybowski and B. C. Gates, *J. Am. Chem. Soc.*, 1983, **105**, 3074.
14. M. D. Ward and J. Schwartz, *J. Mol. Catal.*, 1981, **11**, 397.
15. G. M. Guglielminotti, C. Dossi, R. Ugo, R. Psaro, A. Theolier, A. Choplin, L. D'Ornelas and J. M. Basset, *J. Organomet. Chem.*, 1985, **296**, 127.
16. A. Theolier, A. Choplin, L. D'Ornelas, J. M. Basset and C. Sourisseau, *Polyhedron*, 1983, **2**, 491.
17. S. L. Cook, J. Evans and G. N. Greaves, *J. Chem. Soc. Chem. Commun.*, 1983, 1287.
18. V. D. Alexiev, N. Binsted, J. Evans, G. N. Greaves and R. J. Price, *J. Chem. Soc. Chem. Commun.*, 1987, 395.
19. J. Robertson and G. Webb, *Proc. R. Soc. Lond. A.*, 1974, **341**, 383.
20. V. L. Kuznetsov and A. T. Bell, *J. Catal.*, 1980, **65**, 374.

21. D. J. Hunt, P. B. Moyes, P. B. Wells, S. D. Jackson and R. Whyman, *J. Chem. Soc. Faraday Trans. I*, 1986, **82**, 189.

22. F. Hugues, J. M. Basset, Y. Ben Taarit, A. Choplin, M. Primet, D. Rojas and A. K. Smith, *J. Am. Chem. Soc.*, 1982, **104,** 7020.

23. A. Zecchina, E. Guglielminotti, A. Bossi and M. Camia, *J. Catal.*, 1982, **74**, 225.

24. S. L. Scott and J. M. Basset, *J. Mol. Catal.*, 1994, **86**, 5.

25. F. Quignard, C. Lecuyer, C. Bougault, F. Lefebvre, A. Choplin, D. Olivier and J. M. Basset. *Inorg. Chem.*, 1992, **31**, 928.

26. F. Quignard, C. Lecuyer, A. Choplin, D. Olivier and J. M. Basset, *J. Mol. Catal.*, 1992, **74**, 353.

27. J. Corker, F. Lefebvre, C. Lecuyer. V. Dufuad, F. Quignard, A. Choplin, J. Evans and J. M. Basset, *Science*, 1996, **271**, 966.

28. C. Lecuyer, A. Choplin, D. Olivier and J. M. Basset, *Agnew. Chem. Int. Ed. Engl.*, 1991, **30**, 1660.

29. F. Quignard, A. Choplin and J. M. Basset, *J. Chem. Soc. Chem. Commun.*, 1991, 1589.

30. J. Schwartz and M. D. Ward, *J. Mol. Catal.*, 1980, **8**, 465.

31. A. K. Smith, F. Hugues, A. Theolier, J. M. Basset, R. Ugo, G. M. Zanderighi, J. L. Bilhou, V. Bilhou-Bougnol and W. F. Graydon, *Inorg. Chem.*, 1979, **18**, 3104.

32. J. M. Basset, B. Besson, A. Choplin, F. Hugues, M. Leconte, D. Rojas, A. K. Smith, A. Theolier, Y. Chauvin, D. Commereuc, R. Psaro and R. Ugo, in *Fundamental Research in Homogeneous Catalysis*, Ed. M. Graziani and M. Giongo, Vol. 4, New York, 1984, 19.

33. J. M. Basset, A. Theolier, D. Commereuc and Y. Chauvin, *J. Organomet. Chem.*, 1985, **279**, 147.

34 N. Binsted, J. Evans, G. N. Greaves and R. J. Price, *Organometallics*, 1989, **8**, 613.

35. J. A. Chudek, M. W. Quire, G. W. McQuire and C. H. Rochester, *J. Chem. Soc. Faraday Trans.*, 1994, **90,** 3699.

36. G. L. Haller and D. E. Resasco, *Adv. Catal.*, 1989, **36**, 173.

37. M. Primet, P. Pichat and M. V. Mathieu, *J. Phys. Chem.*, 1971, **75**, 1216.

38. H. P. Boehm, H. Knözinger, *Catal. Sci. Technol.*, 1983, **4**, 39.

39. C. Morterra, G. Ghiotti, E. Garrone, E. Fiscaro, *J. Chem. Soc. Faraday Trans. I,* 1980, **76**, 2101.

40. S. J. Tauster, S. C. Fung and R. L. Garten, *J. Am. Chem. Soc.*, 1980, **100**, 170.

41. G. C. Bond and R. Burch, *Catalysis*, 1983, **6**, 27.

42. J. A. Horsley, *J. Am. Chem. Soc.*, 1979, **101**, 2870.

43. P. Meriaudeau, J. F. Ducel, M. Dufuax and C. Naccache, *Stud. Surf. Sci. Catal.*, 1982, **11**, 95.

44. H. R. Sadeghi and V. E. Henrich, *J. Catal.*, 1984, **87**, 279.

45. J. Santos, J. Philips and J. A. Dumesic, *J. Catal.*, 1983, **81**, 147.

46. J. G. Chen, M. L. Colianni, P. J. Chen, J. T. Yates and G. B. Fisher, *J. Phys. Chem.*, 1990, **94**, 5059.

47. C. Wong and R. W. McCabe, *J. Catal.*, 1989, **119**, 47.

48. T. Ioannides and X. E. Verykios, *J. Catal.*, 1994, **145**, 479.

49. T. Ioannides and X. E. Verykios, *J. Catal.*, 1994, **145**, 491.

50. Z. Zhang, A. Kladi and X. E. Verykios, *J. Catal.*, 1994, **148**, 737.

51. F. A. Cotton and G. Wilkinson, in *Advanced Inorganic Chemistry (4^{th} ed)*, John Wiley and Sons, 1980, p329.

52. D. F. Shiver, P. W. Atkins and C. H. Langford, *Inorganic Chemistry*, Oxford University Press, 1994, pp 355-356.

53. S. D. Worley, G. A. Mattson and R. Caudill, *J. Phys. Chem.*, 1983, **87**, 1671.

54. P. Basu, D. Panayotov and J. T. Yates Jr., *J. Phys. Chem.*, 1987, **91**, 3133.

55. J. Evans, B. Hayden, F. Mosselmans and A. Murray, *J. Am. Chem. Soc.*, 1992, **114**, 6912.

56. Z. L. Zhang, A. Kladi and X. E. Verykios, *J. Mol. Catal.*, 1994, **89**, 229.

57. V. M. Browne, S. G. Fox and P. Hollins, *Catal. Today*, 1991, **9**, 1.

58. R. R. Cavanagh and J. T. Yates, *J. Chem. Phys.*, 1981, **74**, 4150.

59. B. E. Hayden, Reflection Absorption Infrared Spectroscopy, in-*Vibrational Spectroscopy of Molecules at Surfaces*, Eds. J. T. Yates and T. E. Madley, Plenum, New York, 1987, p 267-344.

60. L. H. Dubois and G. A. Somorjai, *Surf. Sci.*, 1980, **91**, 514.

61. V. E. Heinrich, G. Dresselhaus and H. J. Zeiger, *Phys. Rev. Lett.*, 1972, **36**, 1335.

62. G. A. Hyde, R. Rudham and C. H. Rochester, *J. Chem. Soc. Faraday Trans.*, 1983, **79**, 2405.

63. S. D. Worley, C. A. Rice, G. A. Mattson, C. W. Curtis, J. A. Guin and A. R. Tarrer, *J. Phys. Chem.*, 1982, **76**, 20.

64. G. M. Nunez, A. R. Patrignani and A. J. Rouco, *J. Catal.*, 1986, **98**, 554.

65. S. D. Worley, C. A. Rice, G. A. Mattson, C. W. Curtis, J. A. Guin and A. R. Tarrer, *J. Phys. Chem.*, 1982, **76**, 2714.

66. T. Ioannides and X. Verykios, *J. Catal.*, 1993, **140**, 353.

67. V. E. Heinrich. G. Dresselhaus and H. J. Zeigler, *Phys. Rev. Lett.*, 1972, **36**, 1335.

68. J. T. Yates Jr, T. M. Duncan. S. D. Worley and R. W. Vaughan, *J. Chem. Phys.*, 1979, **70**, 1219.

69. J. T. Yates Jr, T. M. Duncan and R. W. Vaughan, *J. Chem. Phys.*, 1979, **71**, 3908.

70. J. T. Yates Jr and K. Kolasinski, *J. Chem. Phys.*, 1983, **79**, 1026.

71. S. Trautmann and M. Baerns, *J. Catal.*, 1994, **150**, 335.

72. J. Evans, B. E. Hayden, J. F. W. Mosselmans and A. Murray, *Surf. Sci.*, 1994, **301**, 61.

73. H. P. Wang and J. T. Yates, *J. Chem. Phys.*, 1984, **89**, 79.

74. M. Primet, *J. Chem. Soc., Faraday Trans. I*, 1978, **74**, 2570.

75. J. T. Yates Jr., E. D. Williams and W. H. Weinberg, *Surf. Sci.*, 1980, **91**, 526.

76. H. F. J. van't Bilk, J. B. A. D. van Zon, T. Huizinga, J. C. Vis, D. C. Koningsberger and R. Prins, *J. Phys. Chem.*, 1985, **107**, 3189.

77. E. A. Hyde, R. Rudham and C. H. Rochester, *J. Chem. Soc., Faraday Trans. I*, 1980, **79**, 562.

78. A. Brenner and D. A. Hucul, *J. Catal.*, 1980, **61**, 216.

79. D. A. Hucul and A. Brenner, *J. Phys. Chem.*, 1981, **85**, 496.

80. F. Solymosi and M. Pasztor, *J. Phys. Chem.*, 1986, **90**, 5312.

81. J. E. Gozum, D. M. Pollina, J. A. Jensen and G. S. Girolami, *J. Am. Chem. Soc.*, 1988, **110**, 2688.

82. L. H. Dubois and G. A. Somorjai, *Surf. Sci.*, 1980, **91**, 514.

83. A. Erdohelyi and F. Solymosi, *J. Catal.*, 1983, **84**, 446.

84. D. C. Koningsberger, J. B. A. D. van Zon, H. F. J. van't Blik and D. E. Sayers, *J. Chem. Phys.*, 1985, **82**, 5742.

85. P. Johnson, R. W. Joyner and P. A. Pudney, *J. Phys. Condens. Matter*, 1989, **1**, SB171.

86. P. Johnson, R. W. Joyner, P. A. Pudney, E. S. Shpiro and B. P. Williams, *Faraday Discuss. Chem. Soc.*, 1990, **89**, 91.

87. R. Dictor and S. Roberts, *J. Phys. Chem.*, 1989, **93**, 2526.

88. J. W. Gleeson and R. W. Vaughan, *J. Chem. Phys.*, 1983, **78**, 5384.

89. T. M. Duncan, J. T. Yates and R. W. Vaughan, *J. Chem. Phys.*, 1980, **73**, 975.

90. T. M. Duncan and T. W. Root, *J. Phys. Chem.*, 1988, **92**, 4426.

91. I. D. Gay, *J. Magn. Reson.*, 1984, **58**, 413.

92. N. Takahashi, K. Miura and H. Fukui, *J. Phys. Chem.*, 1986, **90**, 2797.

93. R. K. Shoemaker and T. M. Apple, *J. Phys. Chem.*, 1985, **89**, 3185.

94. A. M. Thayer and T. M. Duncan, *J. Phys. Chem.*, 1989, **93**, 6763.

95. K. C. Taylor, *Catal. Rev. Sci. Eng.*, 1993, **35**, 457.

96. S. H. Oh and J. E. Carpenter, *J. Catal.*, 1986, **98**, 178.

97. Platinum 1993, Johnson Matthey, London.

98. B. E. Nieuwenhuys, J. Siera, K. Tanaka and H. Hirano, *ACS Symp. Ser.*, 1994, **V552**, pp114-39.

99. K. C. Taylor, *Automotive Catalytic Converters*, Springer Verlag, Berlin, 1984.

100. B. Harrison, A. F. Didwell and C. Hallett, *Platinum Metals Rev.*, 1988, **32**, 73.

101. H. S. Ghandi, A. G. Piken, M. Shelef and R. G. Delosh, *Soc. Automotive Engineers*, Publ. No. 760201.

102. P. Loof, B. Kasemo, S. Anderson and A. Frestad, *J. Catal.*, 1991, **130**, 181.

103. S. H. Oh, *J. Catal.*, 1980, **124**, 477.

104. J. G. Nunan, H. J. Robota, M. J. Cohn and S. H. Bradley, *J. Catal.*, 1992, **133**, 309.

105. H. Schaper, E. B. M. Doesburg and L. L. van Reijen, *Appl. Catal.*, 1983, **7**, 211.

106. F. Oudet, P. Courtine and A. Vejux, *J. Catal.*, 1988, **114**, 112.

107. H. Muraki, K. Yokota and Y. Fujitani, *Appl. Catal.*, 1989, **48**, 93.

108. G. S. Sims, *Soc. Automotive Engineers*, Publ. No. 912369.

109. K. C. Taylor and J. C. Schlatter, *J. Catal.*, 1980, **63**, 53.

110. J. C. Summers, J. J. White and W. B. Williamson, *Soc. Automotive Engineers*, Publ. No. 890794.

111. H. Muraki, *Soc. Automotive Engineers*, Publ. No. 910842.

112. K. M. Adams and H. S. Ghandi, *Ind. Eng. Chem. Prod. Res. Dev.*, 1983, **22**, 207.

113. H. S. Ghandi, H. C. Yao and H. K. Stepien, *ACS Symp. Ser.*, 1982, **178**, 143.

114. O. V. Krylov and V. A. Matyshak, *Russ. Chem. Rev.*, 1995, **64**, 61.

115. W. C. Hecker and A. T. Bell, *J. Catal.*, 1984, **85**, 389.

116. W. C. Hecker and A. T. Bell, *J. Catal.*, 1983, **84**, 200.

117. J. Kaspar, C. de Leitenburg, P. Fornasiero, A. Trovarelli and M. Graziani, *J. Catal.*, 1994, **146**, 136.

118. L. Heezen, V. N. Kilian, R. F. van Slooten, R. M. Wolf and B. E. Nieuwenhuys, in *Catalysis and Automotive Pollution Control II*, Ed. A. Crucq, Elsevier, Amsterdam, 1991, p. 381-393.

119. B. R. Powell and C. Len-Lung, *Appl. Catal.*, 1989, **53**, 233.

120. S. Kim, M. J. d'Aniello, *Appl. Catal.*, 1989, **56**, 23.

121. A. G. v.d.Bosch-Driebergen, M. N. H. Kieboom, A. v.Dreumel, R. M. Wolf, F. C. M. K. M. v.Delft and B. E. Neiuwenhuys, *Catal. Lett.*, 1989, **2**, 235.

122. B. E. Neiuwenhuys, *Surf. Sci.*, 1985, **126**, 307.

123. R. E. Lakis, Y. Cai, H. G. Stenger Jr and C. E. Lyman, *J. Catal.*, 1995, **154**, 276.

Chapter 2

Experimental Techniques

2.1 Introduction

The surface organometallic systems under investigation in this thesis have been studied using a variety of analytical techniques. These include EXAFS (Extended X-Ray Absorption Fine Structure), EDE (Energy Dispersive EXAFS), DRIFTS (Diffuse Reflectance Infrared Fourier Transform Spectroscopy) and TPD (Temperature Programmed Desorption). These techniques are complementary, and have assisted in understanding the structure and chemistry of surface supported organometallic systems. EXAFS and EDE provide information regarding the local structure around the absorbing metal centre, including types of coordinating atoms, coodination numbers and bond distances. DRIFTS provides information regarding the type and bonding of ligands attached to the metal centre, and the extent of dehydroxylation of the oxide support. Both these techniques can be applied *in situ*, allowing changes to the metal coordination and ligands to be monitored during the course of a reaction. TPD provides information regarding gaseous products made from surface reaction or decomposition of catalytically relevent surface species.

2.2 X-Ray Absorption Spectroscopy

2.2.1 Introduction

Extended X-Ray Absorption Fine Structure spectroscopy (EXAFS) is an analytical technique, which has been employed to provide local structural characterisation of surface-supported organometallic species during the course of this study. Highly intense, tuneable X-rays, in addition to other forms of electromagnetic radiation, are obtained in a synchrotron source, by accelerating electrons in a curved orbit, at close to the speed of light at a synchrotron source. The development of such synchrotron sources over the last twenty years, and their increasing availability has enhanced the development of X-ray absorption spectroscopy.

EXAFS is an element specific technique for determination of local structure, as X-rays can be tuned to an absorption edge of a particular element under investigation. EXAFS can yield structural information on non-crystalline solids, providing the average number and type of neighbouring atoms, and their distance from the absorbing atom. This technique can be applied to all elements with the exception of monatomic gases, as there are no neighbouring atoms fixed near to the absorbing atom[1,2].

In a typical experiment, the X-ray photon energy is tuned to the binding energy of a core electron. Photoejection of the electron occurs, accompanied by a sharp jump in the absorption coefficient, known as an absorption edge[3]. The element and the shell from which the electron is ejected define such edges. Ejection of the 1s electron is referred to as a K-edge, a 2s electron as an L_I-edge, that of a $2p_{1/2}$ electron as an L_{II}-edge and an L_{III}-edge corresponding to photoejection of a $2p_{3/2}$ electron. Neighbouring atoms in a molecule or in a condensed phase impose a modulation upon the absorption coefficient profile. This fine structure is called EXAFS and may extend up to 1000eV past the absorption edge. Its amplitude is usually 1-20% of the edge jump.

A typical X-ray absorption spectrum is shown in figure 2.1. From just prior to the edge to approximately 30eV after it, sharp spikes and oscillations are observed. These are caused by electronic transitions between bound states and are known as the **X**-ray **A**bsorption **N**ear **E**dge **S**tructure (XANES). The structure of this region is dominated by complex backscattering and multiple scattering effects, which are largely dictated by the geometry and symmetry of the first coordination shell[4]. Full analysis of the XANES region is extremely complex, but it is often used as a comparative tool, with reference to a known standard, particularly with oxide supported metal systems[5]. As stated previously, the EXAFS part of the spectrum consists of sinusoidal oscillations in the absorption occurring between approximately 30 and 1000eV after the edge. Analysis of the EXAFS spectrum by computer programs can provide accurate interatomic distances, as well as the type and number of neighbouring atoms in a coordination shell. The global errors for EXAFS analysis have been determined as 1.5% for bond lengths[6] and 10-30% for coordination numbers[7,8].

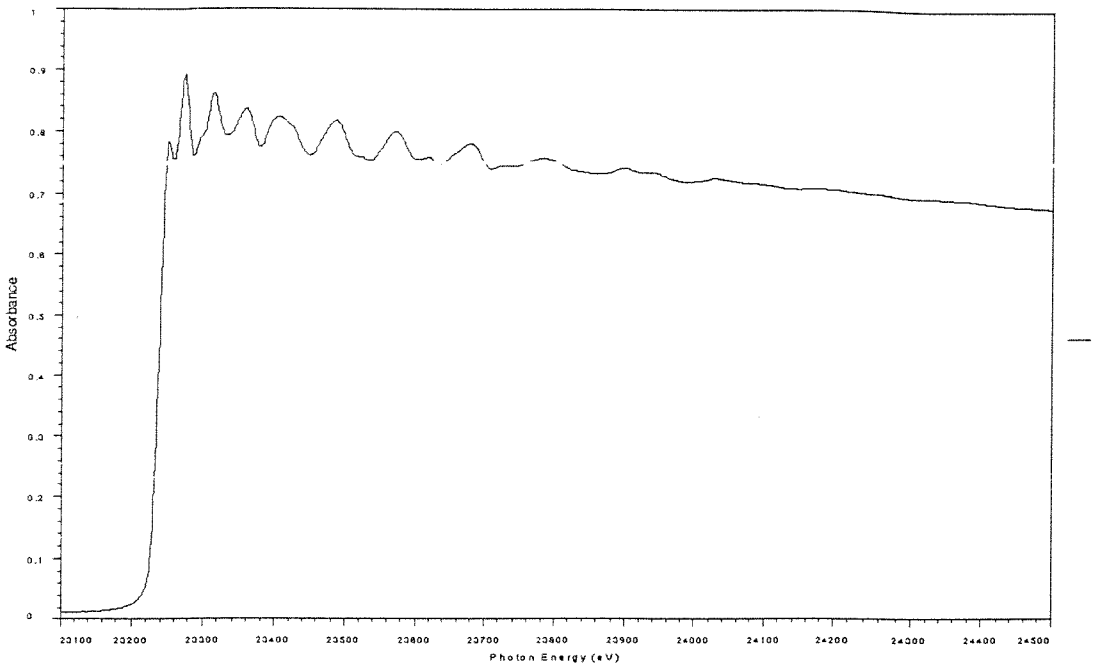

Figure 2.1 Rh K-Edge XAS Spectrum for Rhodium Foil- Acquired at Station ID24 at the ESRF in Grenoble (acquisition time = 3.2 seconds)

2.2.2 EXAFS Studies in Catalysis

EXAFS can yield structural information on noncrystalline solids, and is of particular use for the characterisation of heterogeneous transition metal catalysts. A metal supported on an amorphous oxide surface cannot easily be characterised by diffraction techniques, which requires a degree of atomic ordering. The data obtained by EXAFS about the local structure around a metal atom may then give information about the metal particle size[9,10], morphology, atomic distribution and both metal-support and metal-adsorbate interactions[3]. The supported metal particles will strongly absorb X-rays, while the quality of the spectra will also be aided by the high degree of ordering within the metal particles, and high coordination numbers[11]. The standard of the sample preparation is also fundamental to the quality of the spectra acquired.

Gurman et al have shown that an estimate of metal particle size can be obtained (assuming a particle structure exists) using the first shell coordination

number obtained from EXAFS analysis[4,10]. Two particular effects are apparent for small metal particles supported on a surface. The first of these is a reduction in the coordination number relative to the bulk metal, due to the large proportion of surface atoms present. A higher proportion of surface atoms is also responsible for an apparent reduction in metal-metal bond length for small particles, an effect which becomes more marked with decreasing particle size. The observed contraction in metal-metal interatomic distance may be as much as 0.1Å for small metal particles[12]. The relationship between particle size and coordination number derived from assuming a regular fcc structure[13], can be used to estimate the particle size of surface supported rhodium or palladium particles[4].

Particle shape can also be investigated by EXAFS spectroscopy. Greegor *et al*, and Joyner *et al* have shown that ratio of non-nearest neighbour coordination number to nearest coodination number varies with particle shape quantitatively[9,14]. The relationship between the nearest neighbour coordination number and cluster size and geometry has been determined for icosahedral and cuboctahedral clusters[15]. An indication of the extent of metallic nature of a cluster can be obtained from the nearest neighbour coordination number.

2.2.3 EXAFS Theory

2.2.3.1 The Origin of EXAFS

A basic theory of EXAFS was formulated by Stern, Lytle and Sayers, which led to a short-range single electron, single scattering theory[16]. This work fully recognised the structural content of EXAFS for the first time. Lee and Pendry published a more formal derivation of the EXAFS formula[17], which is subsequently discussed.

The probability of absorption of an X-ray photon by a core electron is dependent on the initial and final states of the excited electron. The initial state is that of the core electron, whilst the final state is less easily defined. Absorption of the X-

rays causes ionisation, and generation of a photoelectron, which can be defined as a spherical wave originating from the absorbing atom. This wave can then be backscattered by any neighbouring atoms, causing a sinusoidal variation in X-ray absorption with energy, which characterises an EXAFS spectrum. This is illustrated in figure 2.2 (R_{as} is the distance between the absorbing and backscattering atoms). The final state will be the superposition of the original and backscattered waves. The resulting interference can be constructive or destructive, causing the oscillations in the absorption coefficient[18].

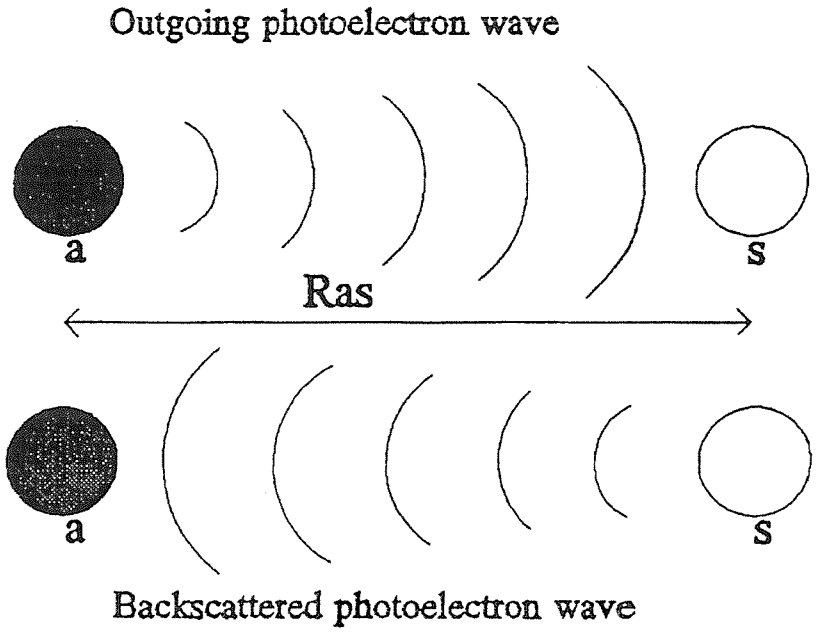

Figure 2.2 Schematic Diagram of the Backscattering Process

2.2.3.2 Plane wave theory

The spherical photoelectron wave can be approximated as a plane wave, within the vicinity of the backscattering atoms (the small atom approximation). This is justified because the radius of the backscattering atom is far smaller than the

interatomic distance between the absorber and the said backscattering atom. The expression resulting from the interaction between the invariant initial state and the interference state wavefunction describes the EXAFS intensity, χ, as a function of the photoelectron wavevector, k, and is known as the plane wave equation[16,17,19].

$$\chi(k)=1/k\ \Sigma_s\ S_i N_{si}\ |f_s(\pi,k)|\ /\ R^2_{as}\ \exp(-2\sigma^2_{as}\ k^2\ )\exp(-2R_{as}/\lambda)\sin(2kR_{as}+2\delta_1+\alpha_s)$$

S_i amplitude reduction factor

N_{si} number of equivalent backscatterers in each shell s

R_{as} interatomic distance between absorber and backscatterer

$f_s(\pi,k)$ backscattering amplitude of the backscattering atom

σ^2_{as} mean square variation of R_{as}

λ elastic mean free path

δ_1 phaseshift due to the absorber

α_s phaseshift due to the backscatterer

An individual interference pattern is produced by each shell of backscattering atoms . If these pathways are independent and do not interact with each other, then the interference patterns for the various backscattering shells may be summed, giving the relatively simple plane wave equation. The term $\sin(2kR_{as}+2\delta_1+\alpha_s)$ describes the phaseshifts caused by the atoms present, while the expression $\exp(-2\sigma^2_{as}\ k^2\ )$ gives a theoretical description of the Debye-Waller factors, and the variation in bond length between the absorbing and backscattering atoms. Contributions to the Debye-Waller factor also come from static and thermal disorder within the system.

2.2.3.3 Curved Wave Theory

The small atom approximation used in plane wave theory, breaks down for low energy data ($k < 4$ Å^{-1})[11,12]. This is particularly important if multiple scattering is prominent or light atoms are present. Therefore, the plane wave theory is only really useful as a tool to explain the theoretical methods involved. For practical EXAFS

analysis the curved wave theory is applied.[13] This considers all the effects of the scattering atom, describing the initial and final states in terms of angular momentum. This gives a complex expression, with the effects of the scattering atoms included in matrix form. Gurman et al have modified curved wave theory in such a way that computing time is reduced whilst the exactness of the original method is maintained[20].

2.2.3.4 Multiple Scattering

The phenomenon of multiple scattering occurs if the emitted photoelectron encounters more than one backscattering atom before returning to the absorber. If one atom is behind another, relative to the absorbing atom, this will give a significant contribution to the EXAFS. The first neighbour in the system will have a focusing effect on the photoelectron, forward scattering it with increased intensity and a change of phase. This will result in the second backscattering shell giving a greatly enhanced signal. Multiple scattering pathways have been included in an extended description of the curved wave theory[21], while a further simplification of the theory obtained by an approximation to the wavefunction has enabled multiple scattering calculations to be included in the iterative procedure of EXAFS analysis[22,23]. Multiple scattering calculations are likely to be required if two different backscattering shells are bonded to each other with a bond angle of >120°. As the bond angle increases, the effects of multiple scattering become more pronounced, such that its inclusion in the fitting calculations will be vital for compounds containing CO as a ligand with a bond angle of 180°.

2.2.4 Data Acquisition

2.1.4.1 Synchrotron Radiation

Standard EXAFS spectra were collected at the CLRC Synchrotron Radiation Source (SRS) at Daresbury Laboratory, using station 9.2. Energy Dispersive EXAFS

(EDE) data (section 2.3) were collected at the European Synchrotron Radiation Facility (ESRF) in Grenoble, France using station ID24.

Electrons are initially injected into a storage ring, at the SRS, where their trajectory is maintained by bending magnets with a field strength of 1.2T. The acceleration of the electrons, travelling close to the speed of light in ultra high vacuum, due to the magnetic field causes them to emit intense white radiation tangentially to their path. The radiation emitted covers a wide range of energies, from infrared to hard X-rays. Ports are situated at tangents around the ring to enable the radiation to exit and travel along a beam line to experimental stations. The maximum photon energy available is determined by the energy of the stored electrons and the radius of curvature in which they travel. The beam lines have beryllium windows to absorb photons with wavelengths of 3.2Å or greater (< 3.9keV). Most stations at Daresbury have insufficient photons with wavelengths below 0.9 Angstroms to obtain EXAFS spectra.

The presence of a 5T wiggler magnet in the straight section before Station 9.2 enables high energy photons with wavelengths as low as 0.3Å (41.3keV) available. The wiggler consists of three magnets of alternating polarity; this reduces the radius of curvature through which the electrons travel, increasing the energy of the radiation. This enables the study of the K-edges of second row transition elements such as rhodium and palladium.

2.2.4.2 EXAFS Stations

Station 9.2 has a double Si(220) crystal monochromator, which allows the energy of the X-ray photons to be altered, permitting the desired energy range to be scanned. The monochromator allows the energy of the X-ray photons passing through to be altered. such that a set energy range may be scanned for any given sample. The wavelength of X-rays required is selected according to Bragg's equation:

$$n\lambda = 2d\sin\theta$$

where n is an integer (1 for the fundamental), d is the crystal spacing and θ the angle between the monochromator crystals and the beam. Light reflected off the first crystal contains higher order harmonics in addition to the fundamental. These harmonics can complicate the fine structure, and are removed by slightly misaligning the second crystal. This misalignment works due to the fact that the rocking curve for higher order harmonics is narrower than that for the fundamental, resulting in a greater loss of intensity for the higher harmonics than for the fundamental reflection.

If maximum I_0 is measured at the beginning and end points of the scan, interpolation between the two allows the coarse motor to maintain the harmonic rejection at 50% (on the negative side of the rocking curve), despite uneven heating of the crystals by the incident beam (the first crystal of the monochromator is water cooled to reduce these heating effects). The entrance and exit slits of the monochromator control the size of the beam incident upon the sample, whilst the vertical height of the beam controls the resolution.

Spectra may be recorded in transmission mode at station 9.2, if the absorbing atom is in sufficiently high enough concentration. In this instance, ion chambers are positioned before and after the sample. The ion chambers contain plates, with a potential difference of 400V across them, in an atmosphere of noble gas. The gases used, and the pressure required, are selected such that I_0 absorbs approximately 20% of the beam and I_t absorbs approximately 80%. The relative absorbance is then calculated from the log of the ratio between the two readings. A schematic of the experimental setup for recording spectra in transmission mode is shown in figure 2.3.

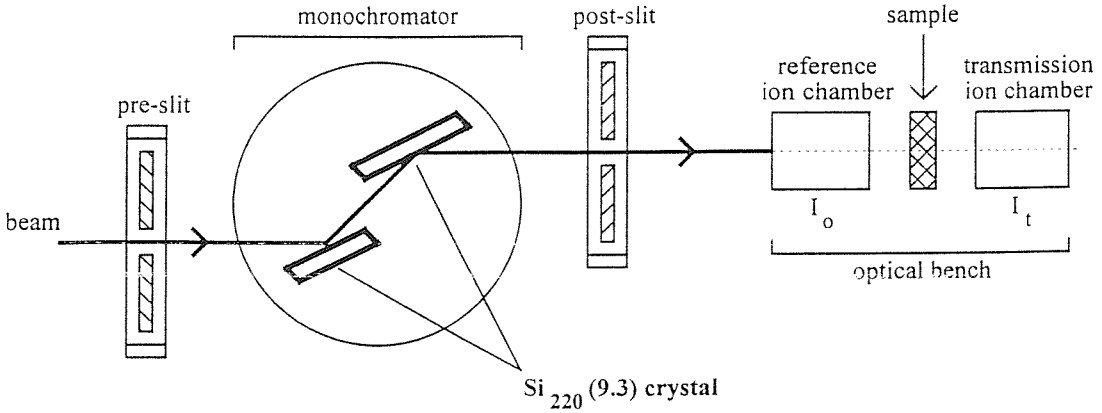

Figure 2.3 Experimental Arrangement for Recording Transmission XAS Spectra

For a sample in which the absorbing atom is present in low concentrations, such as with the oxide-supported organometallics used in this study, the spectrum is recorded in fluorescence mode. Station 9.2 uses a Canberra 13 element solid state germanium detector, on which the window used for detection can be defined very specifically in order to cut out interference which arises from Rayleigh and Compton scattering. The sample is oriented at 45° to both the beam and the detector for collection of fluorescence data. A schematic of the experimental setup for recording spectra in fluorescence mode is shown in figure 2.4.

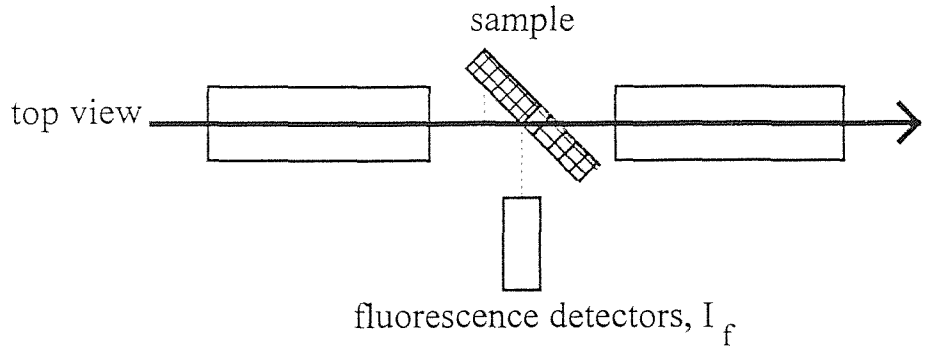

Figure 2.4 Experimental Arrangement for Recording Fluorescence XAS spectra

2.2.4.3 The *In Situ* EXAFS Cell

Standard EXAFS experiments conducted at station 9.2, at the SRS, were performed using a controlled environment *in situ* EXAFS cell. The design of the cell is shown in figures 2.5-2.6. The cell was originally designed by T. Gauntlett, and modified by C. Rudkin and D. Burnaby. The cell consists of a steel block with a circular recess cut into the front to accommodate the sample. A vacuum tight window of polyimide film can then be positioned over the sample, sealing vacuum tight against an O-ring when bolted in place. Lines to the vacuum and gas system run from the sample through the block of the cell, with the sample being maintained in position by means of glass sinters placed in the gas lines. The cell can be rapidly heated to temperatures of up to 330°C by means of two 100W cartridge heaters, which are inserted into the block of the cell. The heating is controlled by a Cole Palmer 2186-15A temperature controller which includes a k-type thermocouple which is inserted into the cell between the cartridge heaters and the sample.

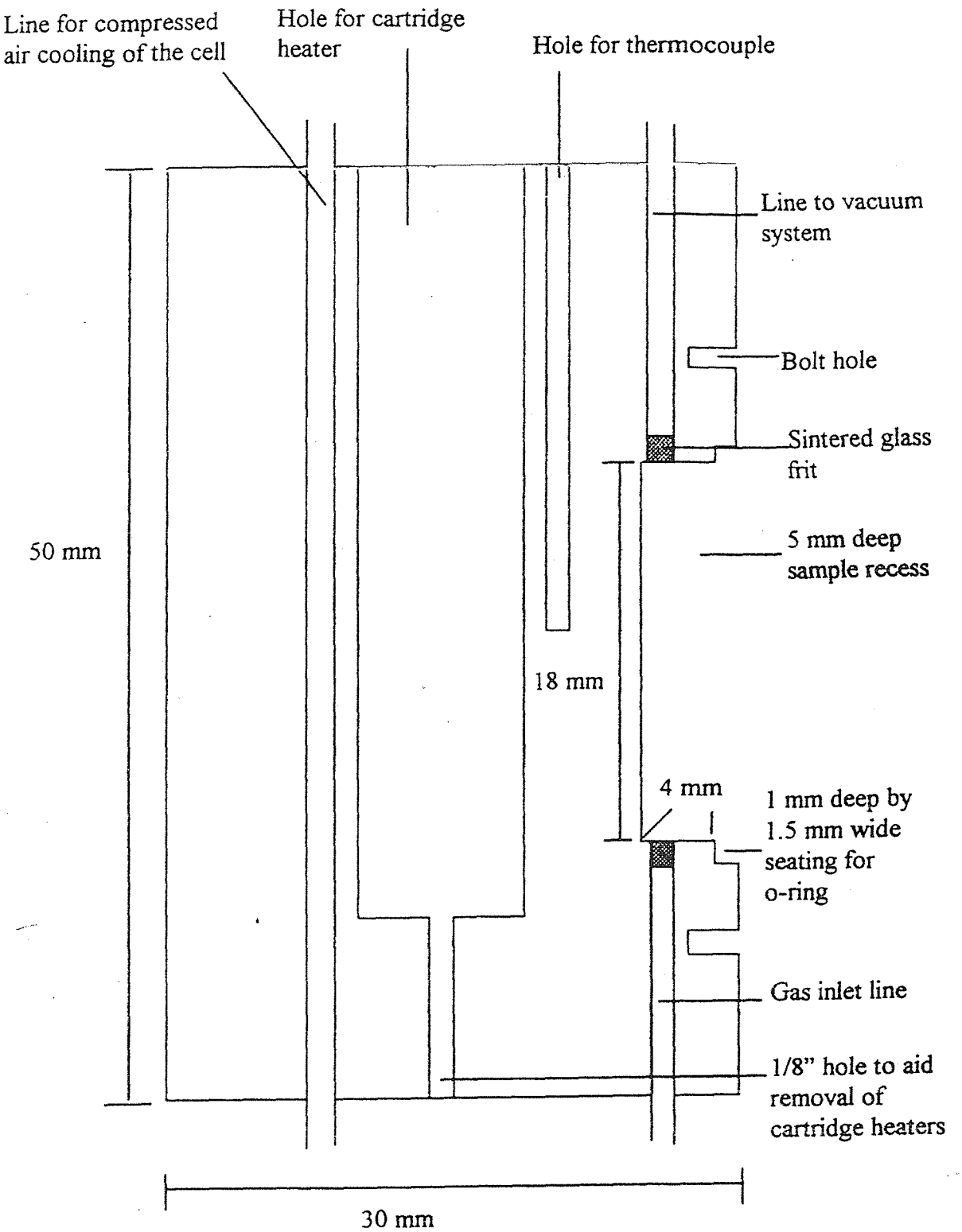

Figure 2.5 Cross Section (side view) of the *in situ* EXAFS cell

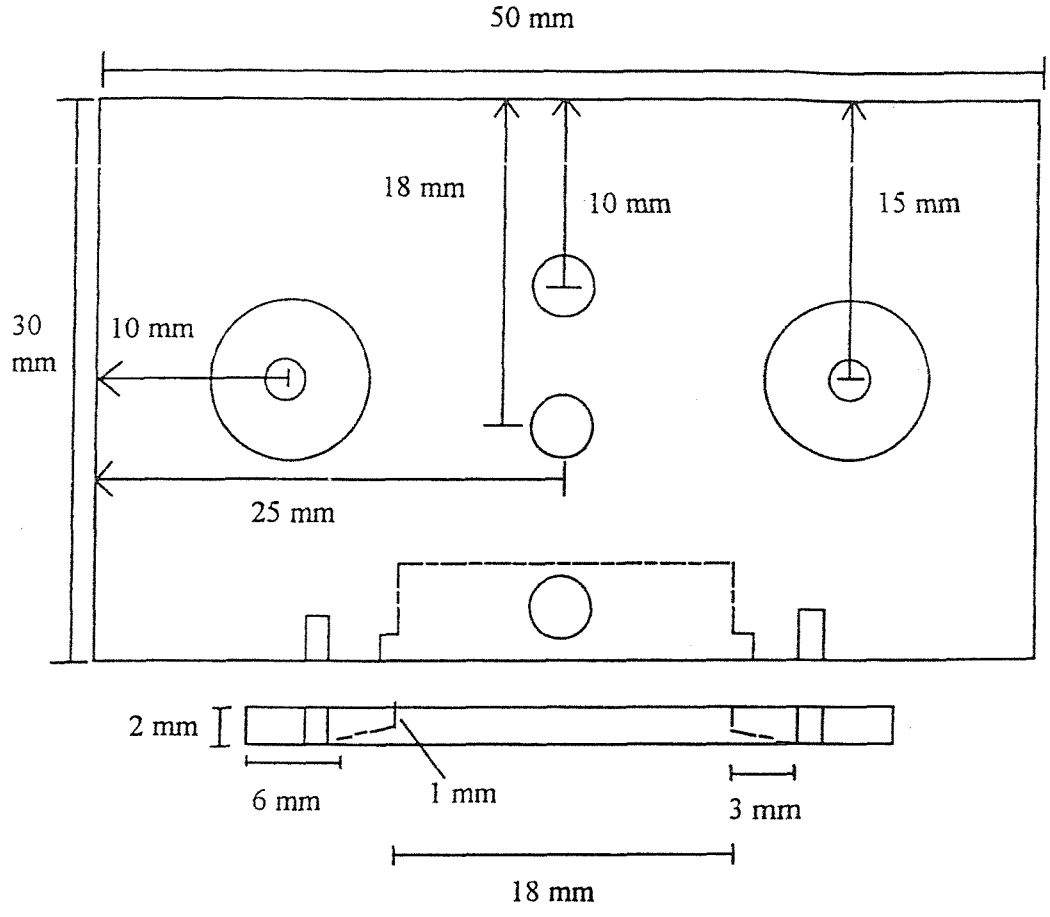

Figure 2.6 Plan View of the *in situ* EXAFS cell, showing cross sections through the sample area and clamping ring

The cell is cooled by means of connection to a compressed air line, which runs through the block close to the sample. The cell can be evacuated down to 1×10^{-5} mbar and gases can be dosed up to atmospheric pressure. This enables a cell temperature of 300°C to be reached in 8 minutes, while cooling from this temperature would take approximately 30-35 minutes. The design of the cell is such that data can only be collected in fluorescence mode, which is ideal for the oxide supported organometallic systems under investigation in this study. Spectra of pure organometallic samples were collected using standard sample holders, in transmission mode.

2.2.4.4 Data Analysis

There are two distinct stages involved in the analysis of EXAFS data. Firstly, the EXAFS spectrum must be isolated from the background absorption. This background subtraction is performed by the computer program PAXAS, developed by Binsted[24].

The resulting spectrum of $\chi(k)$ (intensity) versus k (reciprocal space), is then curve fitted by applying theoretical models of the system under investigation, using the EXCURV98 program[23] on the xrsserv1 computer at Daresbury.

2.2.4.5 PAXAS

The EXAFS data is recorded experimentally as a set of points of absorption versus monochromator angle. Upon reading the data into PAXAS it is converted into a plot of absorption versus energy (eV) using the appropriate monochromator d-spacing. Multiple data sets which have been acquired are first aligned in the x-direction, if required, before averaging the spectra to improve the signal to noise ratio. Obvious glitches can be editing out of the spectrum at this stage, as they would later be amplified by k^3 weighting. The subsequent procedure for preparation of EXAFS data prior to analysis in EXCURVE is schematically illustrated in Fig 2.7 and described below.

Pre-edge background subtraction involves the subtraction of a second or third order polynomial from the absorption spectrum to remove the effect of background absorption. The polynomial is defined by three points: L1 and U1 are pre-defined at the beginning and end of the pre-edge region. P1 is given a weighting such that the polynomial will pass through it and its Y coordinate is changed until the background subtracted absorption (BSA) obtained on subtracting the polynomial is approximately horizontal above the edge.

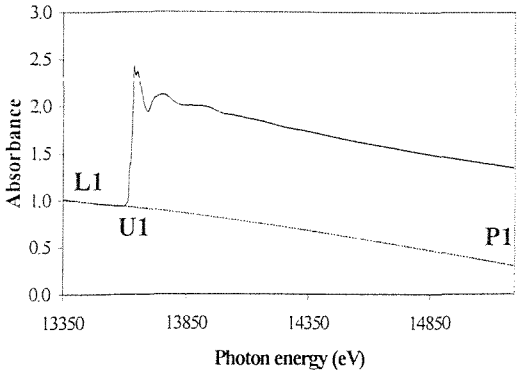

(a) pre-edge

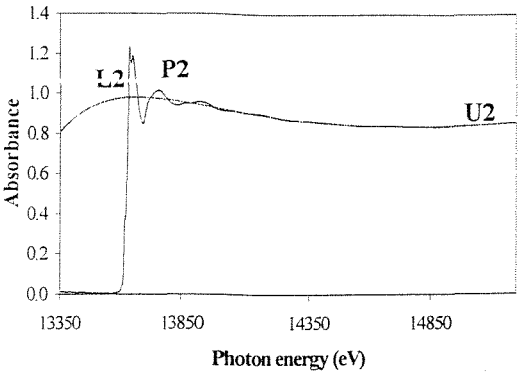

(b) post-edge

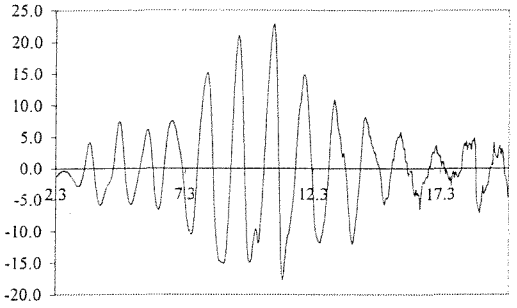

(c) k^3-weighted EXAFS

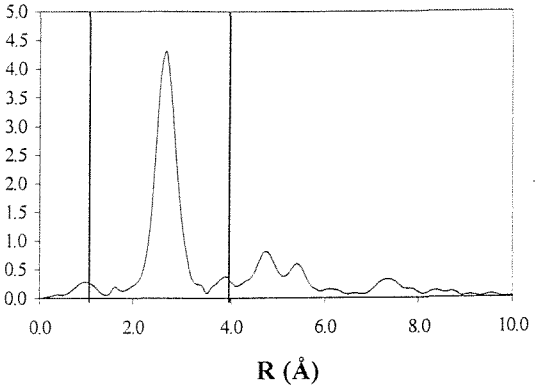

(d) Fourier transform

Figure 2.7. Background removal in PAXAS for bromine K-edge (background subtraction method identical to that used for rhodium and palladium)

a. X-ray absorption curve in pre-edge background subtraction.
b. Background subtracted absorption in post-edge background subtraction.
c. k^3-weighted experimental EXAFS.
d. radial distribution curve showing window for back transform.

The post edge background due to 'atomic' absorption is subtracted by fitting a high order, inverse or two linked polynomials, or a cubic spline such that this fits through the centre of the oscillations at the top of the edge. The weighting of the polynomials usually governs the quality of the subtraction, but a weighted point can be added at the top of the edge to give further refinements. The EXAFS intensity is normalised versus the edge jump and plotted against the photoelectron wavevector, k. The presence of noise in the spectrum, or a poor background subtraction are manifested as peaks at very low radius (<1 Å) in the Fourier transform. A window can be set up around the real peaks in the Fourier transform and the EXAFS due to these shells is then calculated by back transformation. Refinement of the variables in the polynomial expression can then be performed to minimise the difference between the experimental and calculated EXAFS

2.2.4.6 EXCURVE98

The EXAFS data produced from PAXAS were curve fitted using the program EXCURV98 at Daresbury Laboratory, which can be accessed from Southampton. EXCURV98 employs the rapid curved wave theory of Gurman[22], to fit the background subtracted experimental data to the calculated theoretical spectrum.

Correct phaseshifts are required for the accurate determination of interatomic distances from peaks in the Fourier transform. The phaseshifts used are determined by *ab initio* calculations, with the atomic wavefunctions determined using muffin-tin radii and complex Hedin-Lundqvist potentials[25]. EXCURV98 treats each element as part of a 3D lattice, for which the other atom type has to be defined as the nearest neighbour. With the excited atom, the core hole is assumed to have decayed and the outer electrons are treated as fully relaxed.

The theoretical spectrum, which is compared with the experimental data is calculated from various parameters. These can be adjusted manually and refined by least squares iteration in order to give the best fit. The relevant parameters are:

E_o The magnitude of the photoelectron energy at zero wavevector. This affects k across the whole spectrum.

VPI The constant imaginary potential which accounts for the effects of inelastic scattering on the lifetime of the core hole. It is chemically dependent and lies between -1 and -5 eV.

Ef In EXCURVE98, E_o and VPI are combined and iterated as one parameter, Ef. This is the difference between the calculated Fermi level energy, and the known value for the element (in a vacuum).

AFAC This amplitude factor accounts for reductions in the EXAFS amplitude caused by dampening resulting from multiple excitations at the central atom. It is virtually chemically independent and is kept fixed (default value 0.8) for a particular element.

EMIN The minimum energy used to calculate the spectrum and fit the EXAFS. It is measured as the energy above the edge.

EMAX The maximum energy used to calculate the spectrum and fit the EXAFS. If a spectrum becomes noisy at high k values, EMAX is reduced to improve the fit.

Ns The number of shells, each of which contains a group of identical atoms the same distance from the absorber.

Tn The types of atoms in the nth shell.

Nn The number of atoms of type Tn in the nth shell. Can be determined with an accuracy of ± 20%.

Rn The distance of the nth shell from the central atom. This can be determined with an accuracy of ± 0.02 Angstroms (in an ideal situation, not accounting for limitations inherent in the data.

An The Debye-Waller factor for shell n, defined as $2\sigma^2$, where σ is the root mean square variation in the interatomic distance Rn. These should normally be of the order 0.003 to 0.03Å^2.

The shell distances, Debye-Waller factors and Ef are refined during the iteration process, as the program attempts to fit the data to a proposed model. As the coordination numbers are highly correlated to the Debye-Waller factors, they are not normally refined together. The coordination numbers are instead set to a sensible value at the start of the procedure, and may be altered manually, or refined separately. the quality of the fit between the experimental and theoretical spectra is measured in two ways. the R-factor (R) calculates the total sum of the errors between all the data points, and quotes the result as a percentage against the experimental spectrum. the second measure is the fit index (FI), which calculates the sum of the square of the differences between the experimental and theoretical data points. The R-factor would not be expected to exceed ≈30% for standard compounds. However, with supported systems containing a low percentage of the absorbing atom, and exhibiting a lower signal to noise ratio, the R-factor is expected to exceed this value significantly, with values up to 45% observed in this study. The fit index will have a value of less than 8×10^{-4}. Multiple scattering units can be defined and included in the least squares iterations, although this process requires significantly more computing time. The interatomic distances obtained from EXAFS analysis can be considered accurate to the order of ≈ 0.02Å[6], with coordination numbers having an error of at best 10%[7,8]. The figures quoted in parentheses with the derived structural parameters from an EXAFS spectrum, represent the statistical errors in the last quoted figure, as calculated by EXCURV98. These statistical errors include fluctuations in the beam position, sample inhomogeneities and electronic noise. However, this takes no account of the non-statistical errors, which arise during data acquisition and analysis, or of errors caused by correlation between parameters. The total actual errors will therefore be higher than those quoted. As the Debye-Waller factors include contributions from both lattice and thermal effects, these errors will be higher for experiments performed at elevated temperatures by 10-20%.

2.3 Energy Dispersive EXAFS

2.3.1 Introduction

The identification of intermediate species during a chemical reaction, can serve to provide valuable information regarding the reaction mechanism. Identification of reaction intermediates is particularly important during catalytic cycles, as this can shed light on the often-complex mechanisms involved. In addition to kinetic studies, EXAFS studies can provide the structures of intermediate species in catalytic systems[26]. However, the time scale required for acquisition of traditional scanning EXAFS spectra has meant that the technique has often been unsuitable for the investigation of fast processes, such as many *in situ* catalytic reactions[27]. The common approach to this problem has been to trap labile intermediates at low temperatures to allow sufficient time for collection of the spectra[28]. However, the timescale required for the acquisition of EXAFS spectra has been reduced by the increased use of insertion devices on synchrotron sources, in conjunction with the construction of third generation light sources and improvements to the associated station instrumentation[29].

The technique of Quick EXAFS (QuEXAFS) enables EXAFS spectra to be acquired over a range of approximately 500eV in less than two minutes[29]. This is achieved with a continuously driven, water cooled monochromator in conjunction with a fast solid state detector[28,30]. While the smaller k range employed and lower signal to noise ratio of the QuEXAFS data meant that data analysis could only support a restricted number of shells, results have shown that analysable EXAFS data can be obtained for solutions of organometallic species from this rapid scanning method[30]. QUEXAFS has been applied to heterogeneous systems by Clausen *et al*[31] , and Neilsen *et al*[32]. Both of the above have used a microreactor system, avoiding pressing disks of samples, investigating Cu K-edge EXAFS in working methanol synthesis catalysts. In the latter case QUEXAFS spectra were acquired in 3-4 seconds. However, the data range obtained only covers the XANES region and therefore *a priori* structure determination is not possible and references to known standards have to be employed.

Energy Dispersive EXAFS (EDE) employs an elliptically bent crystal monochromator (in either transmission or reflection geometry) to simultaneously provide the required spectral range[27,28,33,34]. The sample under investigation is positioned at the focal length of the monochromator, with the intensity of the different wavelengths being measured on a position-sensitive detector (typically a photodiode array or CCD camera)[27,35]. Due to the fixed energy-position correlation on the detector, a full absorption spectrum can be obtained by measuring the intensity distribution on the detector with and without a sample. The layout of the experimental station for EDE on beamline 8 (ID24) at the ESRF is shown in figure 2.8[36]. Since no movement of the monochromator is required, the acquisition time is determined by the X-ray intensity, and the response time of the detector, leading to a millisecond timescale[27,28].

EDE is a relatively new experimental technique and thus there are few publications regarding EDE studies on catalytic systems. An early study employed EDE to follow structural changes at the nickel edge during reduction of nickel oxide on α-alumina, and activation of Ni exchanged zeolite Y[37]. This experiment employed a collection time of 100s for each spectrum and was able to produce plots showing how the reactions proceeded as a function of time. Later work by this group investigated the reaction between N_2O and Cu supported on silica[38]. For this study, each spectrum was recorded in 100ms, though an average of 500 scans were taken in order to improve the signal to noise ratio.

Hagelstein *et al*[27], have investigated heterogeneous systems using pressed disks. Here, kinetic oscillations are associated with the reaction rate of CO with O on Pt. However the data is not analysed explicitly, but instead rely upon white line changes and other XANES structure variations.

The studies references to above refer to above have all used pressed disks as samples. One of the problems encountered in the preparation of such systems is that sample pressing can lead to reduction of the surface organometallic species to metallic particles[39,40]. Evans *et al*[41,42], have successfully performed EDE on powder samples

that have not been pressed. They are also the fastest examples of EDE where *a priori* EXAFS analysis has been shown to be possible.

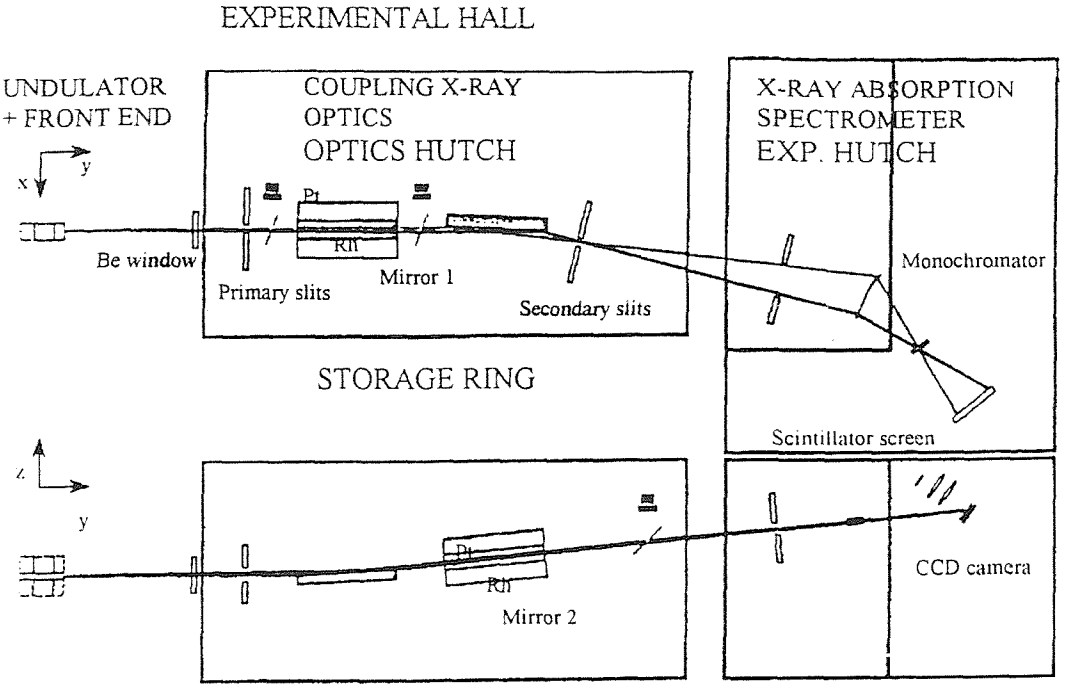

Figure 2.8 Layout of the Experimental Station on ID24 at the ESRF

Stacked plots of the X-ray absorption spectra versus time showed the conversion of the reduced Cu/SiO_2 catalyst to a surface oxide species. Though EDE data showed the extent of the reaction with time and temperature, structural parameters for the system were obtained from conventional EXAFS studies of the reaction.

EDE has been employed to study alkene oligomerisation, performed by a homogeneous nickel catalytic system[37]. The nickel K-edge spectrum of $[Ni(acac)_2]_3$ (100mM in toluene) was acquired in 14.5s by averaging 1000 × 14.5ms scans and was found to agree closely with that from scanning EXAFS experiments. Spectra of a solution of $[Ni(acac)_2]_3$ (140 mM) and hex-1-ene added to $AlEt_2(OEt)$ (280mM) in toluene were recorded in two seconds (average of 100 × 20ms scans) with a cycle

time of 10-15s, to give data from which structural parameters could be obtained, showing partial substitution of the acac ligands by alkene and alkyl groups.

Structural analysis of EDE on a heterogeneous catalyst were first reported for a 5% Pd on γ Al_2O_3 system[31]. These studies were performed on the Pd K-edge, and employed a monochromator crystal with Laue geometry (100μm Si(111) asymmetric cut at 6° and 4°), which was shown to produce none of the distortions (due to penetration of the high energy X-rays into the crystal, resulting in diffraction from a significantly different position within the crystal and a spread over several pixels) which had been observed at high photon energies with Bragg crystals. The authors noted additional experimental precautions for studies on powder samples. These included perfect focusing of the curved monochromator and exact positioning of the homogeneously thick sample in the polychromatic focus of the X-rays. Spectra were acquired every 30s by averaging 240 × 109ms scans. The initial sample was observed to consist of a mixture of Pd metal and PdO, while the Pd was completely reduced to the metallic state upon exposure to CO for 1 hour at 373K.

Further studies on Pd catalysts (10% weight Pd/C) investigates chemical oscillations during the oxidation of CO by O_2, using an integration time of 15s for each spectrum[27]. Observed alterations in the EXAFS parameters were found to agree with theoretical calculations of the Pd K-edge $\chi(k)$, showing that the catalyst alternates between an O_2 covered and CO covered surface during the observed chemical oscillations.

2.3.2 Experimental

EDE spectra were recorded at ID24 of the ESRF at Grenoble, one of the most brilliant X-ray sources in the world. The ESRF is a third generation synchrotron light source, in that it was built to incorporate magnetic insertion devices such as wigglers and undulators into its structure[28]. Wiggler magnets cause a substantial deviation in the electron path and serve to enhance the intensity of the broad band light source. However, the difference between the two beamlines employed during this study (the

SRS at Daresbury, and the ESRF at Grenoble), is the added presence of an undulator at the ESRF, which causes a much smaller deviation in the electron path, producing intense peaks of highly collimated radiation.

The X-ray beam at the ESRF is generated by a tapered undulator (1.6 m long and 40 mm period) in a high-β section of the storage ring as shown schematically in Figure 2.8. The undulator and the front end are positioned in the ring tunnel. The coupling optics are Kirkpatrick Baez type contains two X-ray focusing mirrors in a Laue (*ie* transmission) geometry. The first mirror has three different strips (Rh and Pt coated and a bare strip), which allows different cutoffs without changing the overall geometry of the beamline, and is placed 29.2m from the source. The vertical focussing thus provided, leads to imaging of the source on to the sample position. The second mirror strongly magnifies the horizontal divergence of the undulator beam, to give a bright focus on the sample of 0.1 mm or less. The dispersive spectrometer consists of θ-2θ goniometer with the dynamically bent Si(220) crystal monochromator on the axis and an optical bench supporting the sample are mounted on individual circles. The monochromator was immersed partly in a liquid GaIn eutectic. The Laue geometry monochromator establishes an energy-angular correlation and focuses the beam onto the sample. A position-sensitive Princeton TE-CCD-1242-E-1-UV detector, converts this correlation into an energy-position correlation. Spectra are then recorded simultaneously for all energies in a XAS spectrum in a single X-ray shot. Spectra consist of 1242 × 1152 pixels. 64 pixels are unmasked and used to take the data.

Figure 2.9 shows a representation of the experimental set up employed for EDE investigations of heterogeneous catalysts on beamline ID24 at the ESRF. Samples of oxide supported organometallics were sieved to a particle size of 150-100μm and packed into a flow microreactor (figure 2.10) based upon thin walled quartz tubes (2mm outer diameter and 0.1mm wall thickness). A second tube, the I_o reference, was packed in the same way with unsupported oxide (alumina or titania). The reactor can be heated to a temperature of 400°C, using cartridge heaters, inserted in close proximity to the sample, and controlled by a 900 EPC Eurotherm. A 0.25mm, mineral insulated, K-type thermocouple inserted into the quartz tube is in direct

Page 59 is missing from the volume

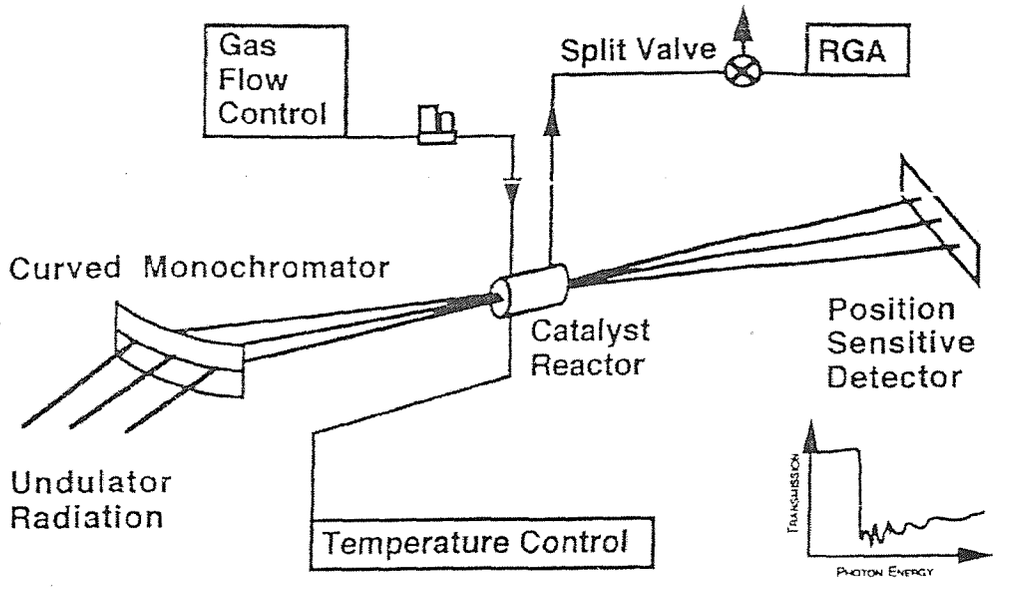

Figure 2.9 Experimental Layout for EDE Investigations of Heterogeneous Catalysts at Station ID24 at the ESRF

2.4 DRIFTS (Diffuse Reflectance Infrared Fourier Transform Spectroscopy)

2.4.1 Introduction

Infrared spectroscopy has been extensively applied to investigate the nature and reactions of surface supported organometallic systems. Transmission has been the most commonly employed method, due to its sensitivity and ease of use. The main disadvantages are that it requires the sample to be pressed into a wafer thin disk. This procedure can lead to the creation of voids[39], or a change in the oxide structure[40], as well as being experimentally tedious. Compressed disks also have poor porosities, which can lead to problems when treating samples with gases during *in situ* studies.

DRIFTS studies enable an infrared spectrum to be collected with the sample as a free powder, alleviating the above problems. The low levels of diffusely scattered light, and energy losses due to specular reflectance, means that DRIFTS provides less sensitivity than transmission experiments. There are several methods of offsetting the problems caused by the low optical efficiency of diffuse reflectance. These include averaging multiple spectra to increase the signal to noise ratio, and using a more sensitive Mercury Cadmium Telluride (MCT) detector, again to improve the quality of the spectra collected.

Other advantages of DRIFTS are that the cell can be attached to a vacuum line and heating unit, enabling thermolysis studies and treatment with gases to be carried out *in situ*. The cell can also be operated as a flow reactor in conjunction with a mass spectrometer, to monitor the gas phase, or to perform TPD experiments. Samples can be analysed whilst under vacuum (1×10^{-4} atm), or under an inert atmosphere of helium or argon.

2.4.2 Experimental

A Spectratech controlled environment DRIFTS cell is inserted into a diffuse reflectance attachment, which is mounted in a Perkin Elmer FT-IR 1710 spectrometer. The cell is also connected to a vacuum line connected to an Edwards rotary pump and lecture bottles of He, H_2, CO and NO supplied by Aldrich. The temperature is controlled by a variable resistor in series with the heating element, which is housed inside the sample post. The temperature is measured by a K-type thermocouple, which is in direct contact with the sample. This experimental set up is illustrated in figure 2.11. The main body of the DRIFTS cell is water cooled, preventing the O-ring seal between the shroud and the cell from perishing and protects the KBr windows. A cross section through the DRIFTS cell is illustrated in figure 2.12. Background spectra were collected with untreated titania or alumina in place of the supported organometallic. The mirror positions of the DRIFTS attachment and the sample height are continually adjusted to maintain a maximum energy throughput to the detector. Typical energy throughput with an oxide-supported organometallic in the sample

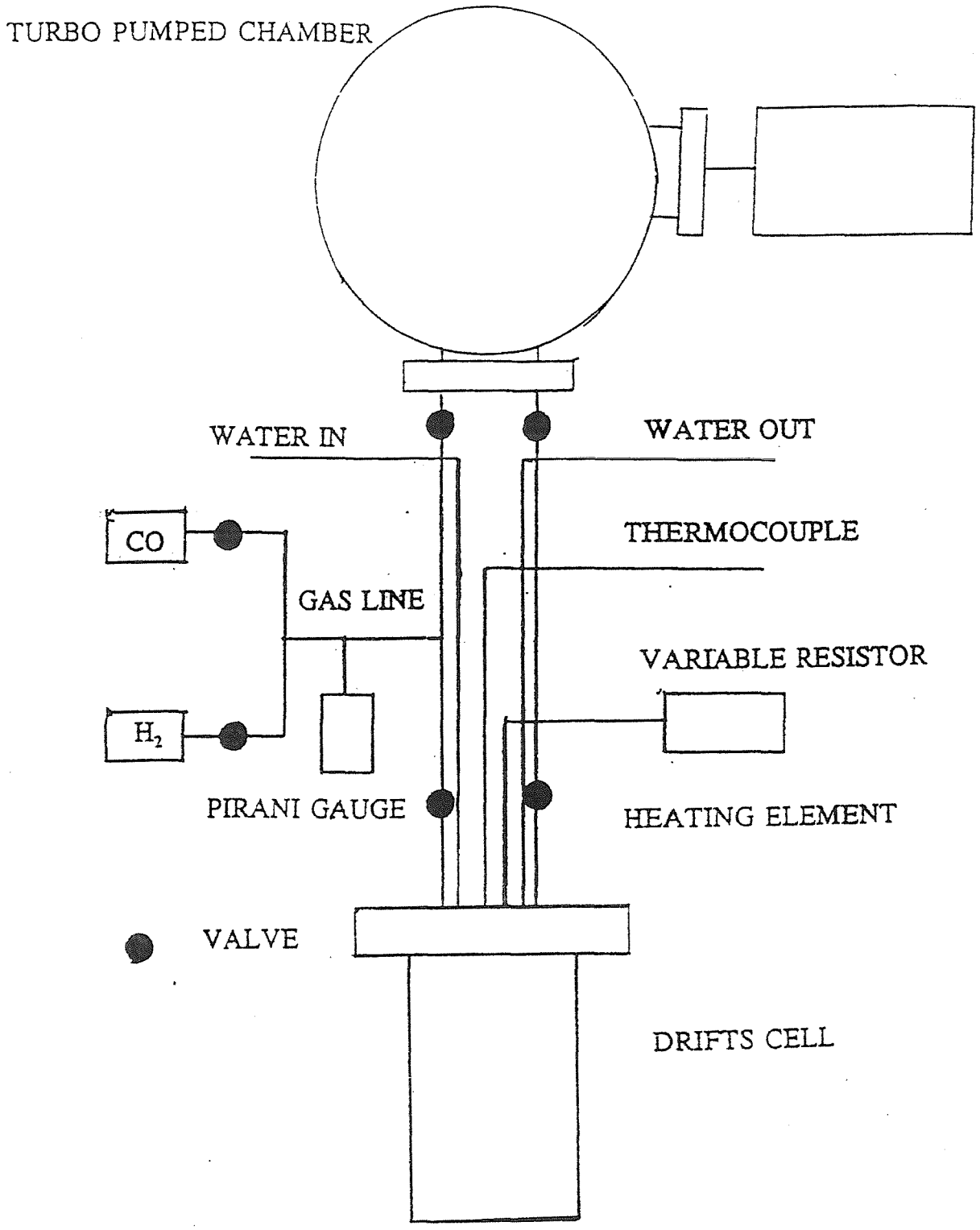

Figure 2.10 Experimental Arrangement for DRIFTS Experiments[44]

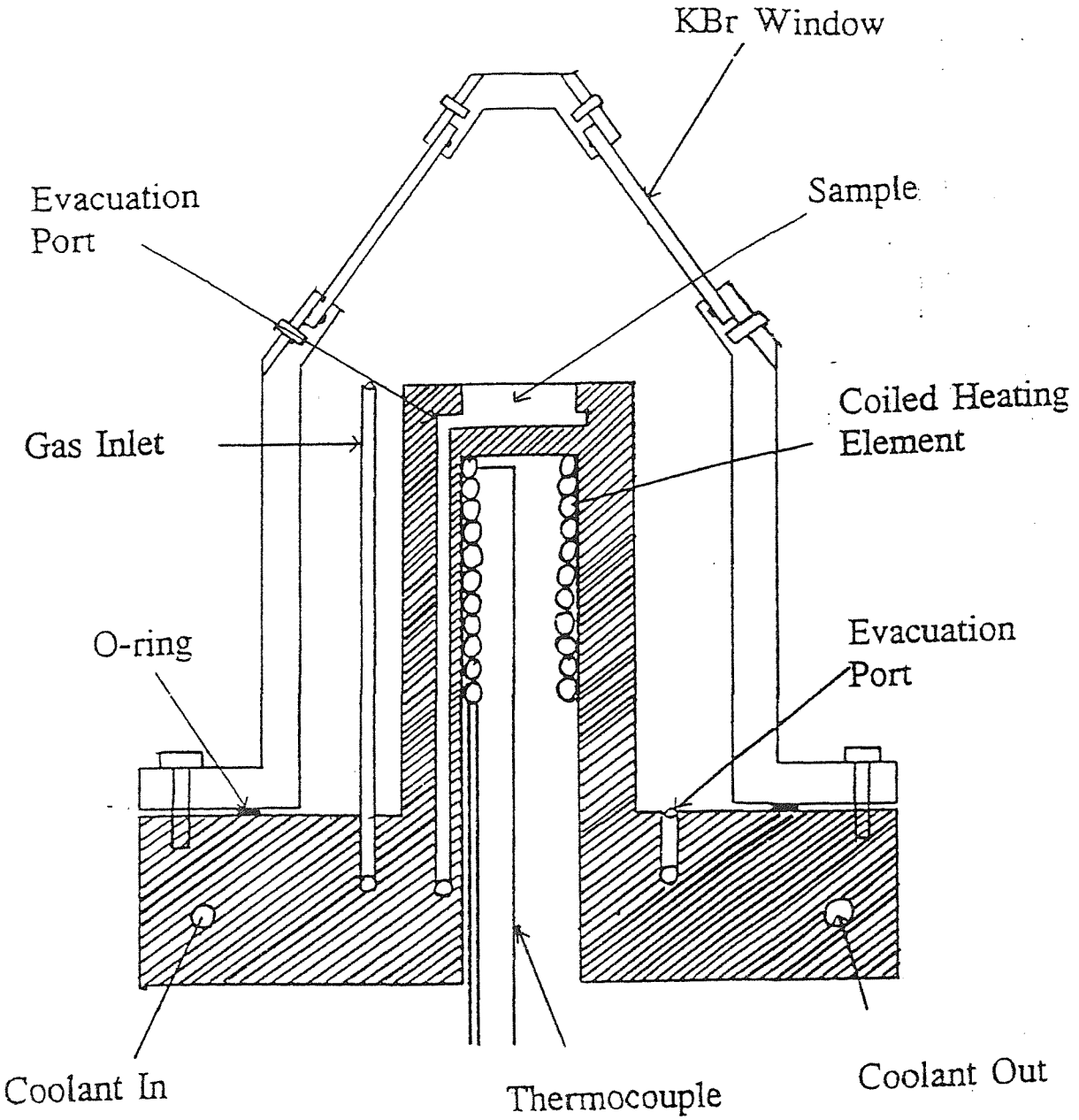

Figure 2.11 Cross section through Controlled Environment DRIFTS Cell[44]

receptacle was 1% of the maximum. The spectra were generally obtained by signal averaging 100 scans at $4cm^{-1}$ resolution, with an acquisition time of 7 minutes 30 seconds.

2.4.3 Sample Preparation

Samples for DRIFTS experiments are prepared by the usual MOCVD method (section 2.5). The oxide supported organometallic samples are transferred to the DRIFTS cell rapidly from Schlenk tubes, under a helium atmosphere, and flattened in the sample holder using a spatula. The DRIFTS cell is rapidly evacuated, and flushed with helium to minimise exposure of the sample to air. Thereafter, the sample is maintained under an inert atmosphere.

2.5 TPD (Temperature Programmed Desorption)

Temperature Programmed Desorption is a useful technique for the characterisation of surface species. It provides information regarding the chemical composition and stability of such species. In a typical experiment, the chamber containing the sample is evacuated, and the sample is gradually heated, and the evolved gases are monitored as a function of increasing temperature.

The apparatus used to perform TPD experiments is identical to that used to for EDE experiments (section 2.2.2). The oxide supported organometallic samples are loaded into a quartz tube (2mm outer diameter and 0.1mm wall thickness), though they are not sieved prior to this. The temperature control, gas flow control and thermocouple used, are identical to that described in section 2.2.2. A mass spectrometer is attached directly to the end of the quartz tube containing the sample. This is evacuated to a pressure of 10^{-7}mbar by a Balzers TSU 240 turbomolecular pump, which is backed by an Edwards E2M2 rotary pump. Gaseous products from reactions are drawn into the mass spectrometer for analysis.

2.6 Preparation of Surface Supported Organometallic Compounds by MOCVD

The oxide supports used in this study are P25 Degussa titania and Degussa γ alumina. These were partially dehydroxylated by heating at 220°C under vacuum at 10^{-6}mbar for 6 hours, prior to reaction with organometallics. The organometallic precursor and oxide were loaded into two different porcelain boats in a glove box. The two samples were then placed in a quartz tube, with the organometallic at the far end from the B19 ground joint. The tube was sealed with a Young's tap adapter. While being maintained in a horizontal position, the tube was evacuated, with the heating of the organometallic precursor to 40-60°C if necessary, in order to caused sublimation. As the organometallic vapour is drawn over the oxide support, it will react with the surface. This was continued until all the precursor had sublimed, or no more of the organometallic would appear to react with the oxide surface, instead subliming onto the sides of the vessel. The resultant supported organometallic sample was transferred to storage in a solvent Schlenk tube within a glove box. The samples were then stored in a refrigerator at -10°C to prevent thermal decomposition. This procedure was employed for preparation of all samples in this study. Transfer of samples to the *in situ* EXAFS cell were performed in a glove box, whilst transfer to the DRIFTS cell was conducted under a gentle flow of argon.

2.7 References

1. P. Andrews, PhD Thesis, University of Southampton, 1993.
2. P. A. O'Day, J. J. Rehr, S. I. Zabinsky and G. E. Brown, *J. Am. Chem. Soc*, 1994, **116**, 2938
3. J. Evans, *Catalysis,* 1989, **8**, 1.
4. K. M. Tearle, PhD Thesis, University of Southampton, 1995.
5. D. E. Resasco, R. S. Weber, S. Saskellom, M. McMillan and G. L. Haller, *J. Phys. Chem.*, 1988, **92**, 189.
6. J. M. Corker, J. Evans, H. Leach and W. Levason, *J. Chem. Soc., Chem. Commun.*, 1989, 181.
7. B. K. Teo, *EXAFS: Basic Principles and Data Analysis,* Springer Verlag, Berlin, 1986.
8. S. J. Gurman, in *Applications of Synchrotron Radiation,* Blackies, Glasgow, 1989.
9. R. B. Greegor, F. W. Lyttle, *J. Catal.*, 1980, **63**, 476.
10. J. M. Corker and J. Evans, *J. Chem. Soc., Chem. Commun.,* 1994, 1027.
11. R. W. Joyner, in *Elementary Steps in Heterogeneous Catalysis,* Ed. R. W. Joyner and R.A.van Santen, Kluwer Academic Publishers, 1993, p249-265.
12. E. S. Shpiro, R. W. Joyner, K. M. Minachev and P. D. A Pudney, *J. Catal.*, 1991, **127**, 366
13. O. M. Poltorak and V. S. Boronin, *Russian J. Phys. Chem.*, 1996, **40**, 1436.
14. R. W. Joyner, in *Characterisation of Catalysts*, Ed. J. M. Thomas and R. M. Lambert, J. Wiley, Chichester, 1980, pp.237.
15. R. E. Benfield, *J. Chem. Soc. Faraday Trans.*, 1992, **88**, 1107.
16. D. E. Sayers, E. A. Stern and F. W. Lytle, *Phys. Rev. Lett.* 1971, **27**, 1204.
17. P. A. Lee and J. B. Pendry, *Phys. Rev. B,* 1975, **11**, 2795.
18. H. Bertagnolli and T. S. Ertel, *Angew. Chem. Int. Ed.*, 1994, **33**, 45.
19. C. A. Ashley and S. Doniach, *Phys. Rev. B*, 1975, **11**, 1279.
20. S. A. Gurman, N. Binsted, I. Ross, *J. Phys. C,* 1984, **17**, 143.
21. S. A. Gurman, N. Binsted, I. Ross, *J. Phys. C,* 1986, **19**, 1845.
22. S. J. Gurman, *J. Phys. C*, 1988, **21**, 3699.
23. S. A. Gurman, N. Binsted, J. W. Campbell and P. C. Stephenson, *EXCURVE92, EPSRC Daresbury Laboratory Computer Program,* **1992**.

24. N. Binsted, PAXAS (Program for the Analysis of X-ray Absorption Spectra), University of Southampton, 1988.

25. S. J. Gurman, *J. Phys. C*, 1983, **16**, 2987.

26. B. Chance, in *EXAFS and Near Edge Structure III*, Ed. K. O. Hodgson, B. E. Hedman and J. E. Penner-Hahn, Springer Verlag, 1984.

27. T. Ressler, M. Hagelstein, U. Hatje and W. Metz, *J. Phys. Chem.*, 1997, **101**, 6680.

28. J. Evans, *Chem. Industry*, 1995, 135.

29. N. A. Cruise and J. Evans, *J. Chem. Soc. Dalton Trans.*, 1995, 3089.

30. G. Sankar, P. A. Wright, S. Natarajan, J. M. Thomas, G. N. Greaves, A. J. Dent, B. R. Dobson, C. A. Ramsdale and R. H. Jones, *J. Phys. Chem.*, 1993, **97**, 9550.

31. B. S. Clausen, L. Grabaek, G. Stefferson, P. L. Hanson and H. Topsoe, *Catal. Lett.* 1993, **20**, 23.

32. J. Als. Neilson, G. Grubel and B. S. Clausen, *Nucl. Instr. & Methods*, 1995, **97**, 522.

33. M. Hagelstein, C. Ferrero, U. Hatje, T. Ressler and W. Metz, *J. Synchrotron Rad.*, 1995, **2**, 174.

34. M. Hagelstein, C. Ferrero, M. Sanchez del Rio, U. Hatje, T. Ressler and W. Metz, *Physica B*, 1995, **208-209**, 223.

35. G. E. Derbyshire, W. I. Helsby, A. J. Dent, S. A.Wright, R. C. Farrow, G. N. Greaves, C. Morrell and G. I. Baker, *Daresbury Synchrotron Technical Memorandum*, DL/SCI/P723E

36. ESRF, M. Hagelstein, Personal Communication.

37. G. Baker, A. J. Dent, G. Derbyshire, G. N. Greaves, C. R. A. Catlow, J. M. Couves and J. M. Thomas, in *X-Ray Absorption Fine Structure*, Ed. S. Samar Hasnain, Ellis Horwood, Chichester, 1991.

38. G. Sankar, J. M. Thomas, D. Waller, J.W. Couves, C. R. A. Catlow and G. N. Greaves, , *J. Phys. Chem*, 1992, **96**, 7485.

39. D. Bogg, M. Conyngham. J. M. Corker, A. J. Dent, J. Evans, R. C. Farrow, V. L. Kambhampati, A. F. Masters, D. N. McCleod, C. A. Ramsdale and G. Salvini, *Chem. Commun.*, 1996, 647.

40. J. L. Van der Venne, J. P. M. Rindt and G. J. M. M. Coenen, *J. Colloid. Interface. Sci.*, 1980, **74**, 287.

41. W. C. Conner, E. L. Weist, T. Ito and J. Fraissard, *J. Phys. Chem.*, 1989, **93**, 4138.

42. S. G. Fiddy, M. A. Newton, A. J. Dent, G. Salvani, J. M. Corker, S. Turin, T. Campbell and J. Evans, *J. Chem. Soc., Chem. Commun.*, 1999, **851**

43. A. J. Dent, J. Evans, M. A. Newton, J. M. Corker, A. Russell, M. B. A. Rahman, S. Fiddy, R. Matthew, R. Farrow and G. Salvani, , *J. Synchrotron Rad.*, 1999, **6**, 381.

44. N. A. Williams, PhD Thesis, University of Southampton, 1992.

Chapter 3

The Surface Organometallic Chemistry of $[Rh(CO)_2Cl]_2$ Supported on Titania

3.1 Introduction

3.1.1 The Chemistry of $[Rh(CO)_2Cl]_2$ Supported on Inorganic Oxide Surfaces

The rhodium carbonyl chloride dimer $[Rh(CO)_2Cl]_2$ is an ideal precursor for MOCVD as it is relatively air stable and volatile. The molecular structure of $[Rh(CO)_2Cl]_2$ has been established by single crystal X-ray diffraction[1], and has been found to have C_{2v} symmetry. Three IR active bands are predicted and the vibrational modes are illustrated in figure 3.1. The three IR bands serve as a useful fingerprint to indicate the presence of two rhodium dicarbonyl units coupled together.

The surface organometallic chemistry of $[Rh(CO)_2Cl]_2$ supported on high area silica and alumina has been studied by various groups. $[Rh(CO)_2Cl]_2$ supported on alumina has been shown to be active towards the hydrogenation of pentynes[2] and the water gas shift reaction[3,4].

Despite the extent of study that has taken place on surface supported $[Rh(CO)_2Cl]_2$, the exact nature of the interaction of the parent molecule with the oxide surface is unclear. Evans et al. have shown that MOCVD of $[Rh(CO)_2Cl]_2$ onto a single crystal [rutile(110)] surface under UHV conditions results in the formation of the $Rh^I(CO)_2$ *gem* dicarbonyl species[5,6,7], characterised by infrared bands at $2112cm^{-1}$ and $2028cm^{-1}$. The formation of the *gem* dicarbonyl species has also been observed by infrared studies of MOCVD onto high surface area titania by Rudkin and Williams, with the characteristic bands found at $2103cm^{-1}$ and $2026cm^{-1}$. These studies have shown that reaction with the titania surface is not merely a weak physisorption of the parent molecule.

Although the consumption of hydroxyl groups was not observed, Robbins suggested that isolated square planar $[Al\text{-}O]_2Rh(CO)_2$ units were formed on adsorption, with Rh-Cl bonds being replaced by Rh-O support bonds and HCl evolved[10]. This assignment was based on infrared studies with ^{13}CO exchange, solid

state NMR with magic angle spinning, and low temperature ESR, which all indicated the presence of a single type of isolated rhodium dicarbonyl species. At 20K ESR showed no evidence of paramagnetic rhodium species, which is consistent with the presence of diamagnetic $4d^8$ $Rh^{I}(CO)_2$ species. Monomeric Rh^0 and Rh^{II} have d^9 and d^7 ground state electron configurations, which in strong crystal fields of trigonal, tetrahedral, square planar or pyramidal symmetry, would have one unpaired electron, which would give rise to an ESR signature.

Although these studies have conclusively shown that a $Rh^{I}(CO)_2$ surface species is formed, the fate of the chlorine from the precursor upon reaction with the surface is less well understood. XPS measurements on a rutile (110) surface have shown that the chlorine remains upon the surface with a binding energy [$Cl(2p_{3/2})$ = 198.5eV] shifted from that of the physisorbed parent molecule [$Cl(2p_{3/2})$ = 199.1eV], which has led the authors to propose that the dimer dissociates, with the chlorine being adsorbed on the titania surface[7]. EXAFS studies of the species supported on high surface area titania have again shown isolated rhodium dicarbonyl units, though with the chlorine bound to the rhodium[9]. Such a system could be caused by the averaging of the signals from $[Rh(CO)_2Cl]_2$ and the $[Ti\text{-}O]Rh(CO)_2$ groups, though no rhodium neighbour signal which would be expected for the parent molecule has been observed. The existence of discrete, surface bound $Rh(CO)_2Cl$ species has therefore been concluded from EXAFS and infrared studies on this system.

Johnson et al. prepared $1\%Rh/Al_2O_3$, by wet impregenation of $RhCl_3$ followed by reduction in hydrogen at 473K. Following exposure to one atmosphere of CO at room temperature, they observed a *gem* dicarbonyl species and coordintion to two chlorine atoms at 2.33Å, using EXAFS spectroscopy[11]. The retention of Rh-Cl bonds has been observed in EXAFS studies of $[Rh(CO)_2Cl]_2$ chemisorbed onto Al_2O_3 from a dichloromethane solution to give a Rh loading of approximately 2%. These results have shown a Rh-Cl bond length of 2.39Å and considered chlorine as a directly bound ligand on the $Rh(CO)_2$ centre. Furthermore, these and later studies by Barnes at al. have failed to show any Rh-Rh EXAFS signal for the adsorbed species, even at low temperature, suggesting that reaction with the oxide surface breaks up the dimeric structure of the parent molecule[11].

The behaviour of the supported Rh can be severely modified through variation of the support material used, and the Rh containing precursor used in the catalyst preparation[12-15]. For example, catalysts prepared from $RhCl_3$ and supported on SiO_2[12] act (almost exclusively) as methanation catalysts. The same precursor supported on TiO_2 produces a catalyst that, in terms of turnover number, is a more efficient methanation catalyst, but shows a considerably poorer selectivity, as it produces a significant number of C_2-C_5 hydrocarbons[12,13]. Further, changing the Rh precursor produces yet more variation in the final catalyst[13,16]. Specifically, SiO_2 supported catalysts derived from $Rh(CO)_2(acac)$ showed a significant selectivity for CH_3CHO synthesis, whereas those derived from $[Rh(CO)_2Cl]_2$ showed a significant selectivity toward C_2-C_3 hydrocarbons[13].

Purely electronic interactions due to charge transfer from TiO_2 to Rh have been invoked to explain the enhanced selectivity of Rh/TiO_2 in CO hydrogenation compared to other, less reducible supports[12]. However, it is also known that reaction above 623K for these $RhCl_3$ derived systems, results in both a lowering in the level of surface carbon maintained upon the catalyst. The level of carbonaceous material retained by the working catalyst has been linked to the selectivity the Rh catalyst displays in CO hydrogenation reactions[13].

3.1.2 Reaction of the Surface Species with Hydrogen

Since the MOCVD of $[Rh(CO)_2Cl]_2$ onto titania has been shown to generate $Rh^I(CO)_2$ units, the reactivity of this system can serve to model that of catalytic systems which contain rhodium carbonyl surface species. The reaction of the surface rhodium *gem* dicarbonyl species with hydrogen has been subject to much investigation due to its importance in industrial catalytic systems[17-20].

The reactivity of titania supported rhodium carbonyl species with hydrogen has been investigated by Zhang et al[21]. Results, using DRIFTS spectroscopy, showed a decrease in intensity of the *gem* dicarbonyl infrared bands upon exposure to 1 bar at room temperature, though their frequencies remained constant. This decarbonylation of the *gem* dicarbonyl species was observed to occur at lower temperatures in the

presence of a higher pressure of hydrogen, indicating that hydrogen has a promoting effect on the reductive agglomeration of Rh^I. The absence of signals from any intermediate species led the authors to propose the following mechanism for the hydrogen promoted decarbonylation of the *gem* dicarbonyl:

$$Rh^I(CO)_2 + \tfrac{1}{2} H_2 + O^{2-} \rightarrow Rh^O + 2CO + OH^-$$

Though the $Rh^I(CO)_2$ was not considered to react directly with hydrogen, the hydrogen promoted enhanced decarbonylation of the species will alter the dispersive state of the rhodium, affecting the reaction between the H_2 and other adsorbed carbonyl species (e.g. bridging or linear).

Studies by Evans et al. on the rutile (110) surface under UHV conditions found that exposure of the *gem* dicarbonyl species to hydrogen at 300K caused a loss in intensity and eventual removal of the characteristic infrared bands, accompanied by the reduction of the rhodium[7]. XPS studies of the C(1s) core level during this reaction have shown that although the CO ligands are removed, 40-50% of the original CO has been reduced to a graphitic or carbidic form of carbon, resulting from the disproportionation of the CO groups on the surface. More recent studies have observed the growth of an infrared band at $2065cm^{-1}$ upon exposure to hydrogen, which has been assigned to a RhH(CO) or $RhH_2(CO)$ species[22]. Rh 3d XPS measurements indicated that a small amount of clustering may have occurred.

Studies by Rudkin of the reaction between $[Ti\text{-}O]Rh(CO)_2Cl$ and hydrogen, using EXAFS and infrared spectroscopy have shown that a pressure of 1bar is required for the reaction to proceed at room temperature[9]. EXAFS results have shown the complete loss of all carbonyl coordination and the formation of very small metal particles to occur. The reaction involves the loss of the *gem* dicarbonyl infrared signal without the formation of any infrared bands, which could be assigned to any other species. Elevation of the reaction temperature to 339K enabled it to proceed rapidly at a lower pressure to an extent from which much of the *gem* dicarbonyl could be regenerated upon re-exposure to CO. At a temperature of 350K, the presence of hydrogen can be considered to promote the reductive agglomeration of $Rh^I(CO)_2$ to

metal particles. Conducting the reaction at 400K causes a more rapid initial loss in intensity from the *gem* dicarbonyl bands, though the final extent of the reaction is little more than which could be achieved from prolonged heating at such a temperature.

3.1.3 Reaction of the Surface Species with NO

The reaction between CO and NO over rhodium is of great importance within three-way automotive catalysts[23,24]. Studying the reaction of NO with surface supported rhodium carbonyl species can provide valuable information on this catalytic system.

Arai and Tominaga have studied the reaction of NO with rhodium supported on alumina by infrared spectroscopy[25]. When NO is adsorbed on rhodium, two surface species are identified. A cationic ($Rh\text{-}NO^{+}$) is produced by donation of an electron from the NO antibonding (π_{2pz*}) orbital to the d orbitals of the rhodium to strengthen the NO bond. An anionic ($Rh\text{-}NO^{-}$) species is also observed, produced by transfer of a d electron of the metal to the (π_{2pz*}) orbital of NO to weaken the NO bond. They also observed *cis*-coordination of NO and CO to one rhodium atom. It was also discovered that when NO is first adsorbed onto rhodium followed by the introduction of CO, an M-NCO (isocyanate) is formed, which is stable up to 400°C under vacuum.

Srinivas et al. investigated the reactivity of NO and CO on rhodium supported on high area silica by infrared and mass spectroscopy[26]. Exposure of preadsorbed CO to a gaseous NO pulse on Rh/SiO_2 resulted in desorption of linear CO and formation of a low wavenumber NO^{-} ($1650\text{-}1700cm^{-1}$) species on the reduced Rh site (Rh-NO- typically appears at $1740\text{-}1750cm^{-1}$). The frequency of the asymmetric band of an $Rh(NO)_2$ species will overlap with the species at $1740\text{-}1750cm^{-1}$. Its existence is verified by the appearance of the symmetric band at $2140cm^{-1}$. Exposure of preadsorbed CO on oxidised Rh/SiO_2 to a gaseous NO pulse resulted in displacement of the *gem* dicarbonyl without formation of CO_2 at 298-423K. Increasing NO

exposure time led to the desorption of all adsorbed CO and formation of NO^+ species, a high wavenumber NO^- ($1740\text{-}1770cm^{-1}$) species, and a bidentate nitrato species. Prolonged exposure of preadsorbed NO to CO resulted in displacement of the adsorbed NO^+ and chemisorption of CO as gem dicarbonyl and linear CO on Rh^+. Exposure of the catalyst to a mixture of NO-CO-He (1:1:3) at 373K at 0.1MPa resulted in the formation of CO_2. The formation of CO_2 from the reaction of adsorbed CO with oxygen produced from dissociated NO was more rapid than the desorption of adsorbed CO.

A UHV study by Hayden et al[22]. of the reaction of NO with the rhodium *gem* dicarbonyl species on TiO_2 (110), prepared by MOCVD of $[Rh(CO)_2Cl]_2$, observed formation of a band at $1920cm^{-1}$, which was assigned to the Rh-NO^+ species. There is also evidence that a proportion of the starting surface species reacts to form Rh(CO)(NO), which at room temperature reacts no further. Both infrared and XPS measurements on this system suggested that the rhodium remained in a highly dispersed state, though a small degree of clustering may have occurred.

3.2 Adsorption of $[Rh(CO)_2Cl]_2$ onto TiO_2 and γ Al_2O_3

3.2.1 Vibrational Study of the Adsorption of $[Rh(CO)_2Cl]_2$ onto TiO_2 and γ Al_2O_3

The parent molecule, $[Rh(CO)_2Cl]_2$, shows three distinct infrared bands at $2105cm^{-1}$(m), $2090cm^{-1}$(s) and $2035cm^{-1}$(s), accompanied by weak ^{13}C satellites at $2079cm^{-1}$ and $2002cm^{-1}$, shown in figure 3.1. The spectrum was acquired in a hexane solvent, and the infrared frequencies are in agreement with the literature values[30].

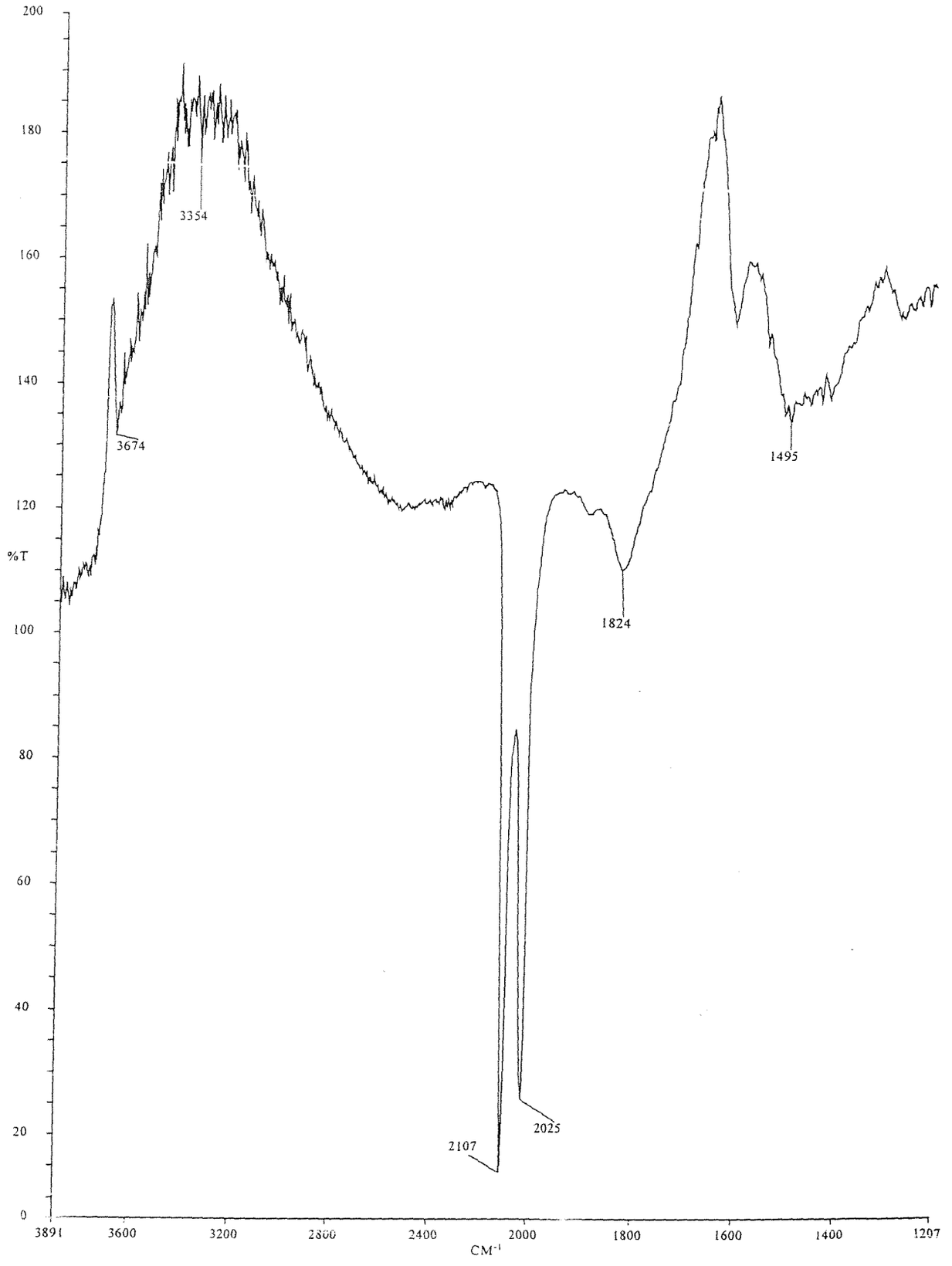

Figure 3.2 DRIFTS difference spectrum of $[Rh(CO)_2Cl]_2$ supported on partially dehydroxylated titania

titania has been partially dehydroxylated prior to absorption of the organometallic, and that the reaction with the organometallic results in the consumption of surface hydroxyl groups. This supports the idea that reaction of $[Rh(CO)_2Cl]_2$ with the surface is not merely a weak physisorption of the parent molecule, but a chemisorbed [Ti-O]-$Rh(CO)_2$ bond. This experiment gives no information on the whereabouts of the chlorine from the precursor. Table 3.1 compares the frequencies of titania-supported $[Rh(CO)_2Cl]_2$ with some analogous systems.

This experiment was repeated using alumina as the support. The procedure followed was exactly the same, with the alumina partially dehydroxylated by vacuum heating to 220°C before reacting with the organometallic by MOCVD. The DRIFTS spectrum is shown in figure 3.3. The spectrum was acquired by taking 100 scans at $4cm^{-1}$ resolution. The spectrum displays the same characteristics as that of the titania supported sample. The broad positive band in the hydroxyl region of the spectrum indicates that the alumina has less surface water and hydroxyl groups than the hydroxylated background sample, due to their removal in the pretreatment of the oxide, and consumption on reaction with the organometallic. The frequencies of the *gem* dicarbonyl stretches are at $2107cm^{-1}$ and $2028cm^{-1}$, slightly higher than the literature values, which may be due to the high metal loading of the samples.

Sample	**ν(sym) cm^{-1}**	**ν(sym) cm^{-1}**	**ν(assym) cm^{-1}**
$[Rh(CO)_2Cl]_2$/ Hexane	2105	2090	2035
$[Rh(CO)_2Cl]_2$/ TiO_2		2103	2026
$[Rh(CO)_2Cl]_2$/ SiO_2[2]	2112	2097	2035
$[Rh(CO)_2Cl]_2$/ Al_2O_3[3]		2104	2025
$(Al\text{-}O)_xRh(CO)_2$ 2% wt Rh[14]		2101	2031
$(Ti\text{-}O)_xRh(CO)_2$ 0.5% wt Rh[14]		2096	2026
$(Ti\text{-}O)_xRh(CO)_2$ 10% wt Rh[14]		2102	2035

Table 3.1 A comparison of the values of the frequency of the carbonyl stretch for a variety of oxide-supported $[Rh(CO)_2Cl]_2$ and $Rh(CO)_2$ species.

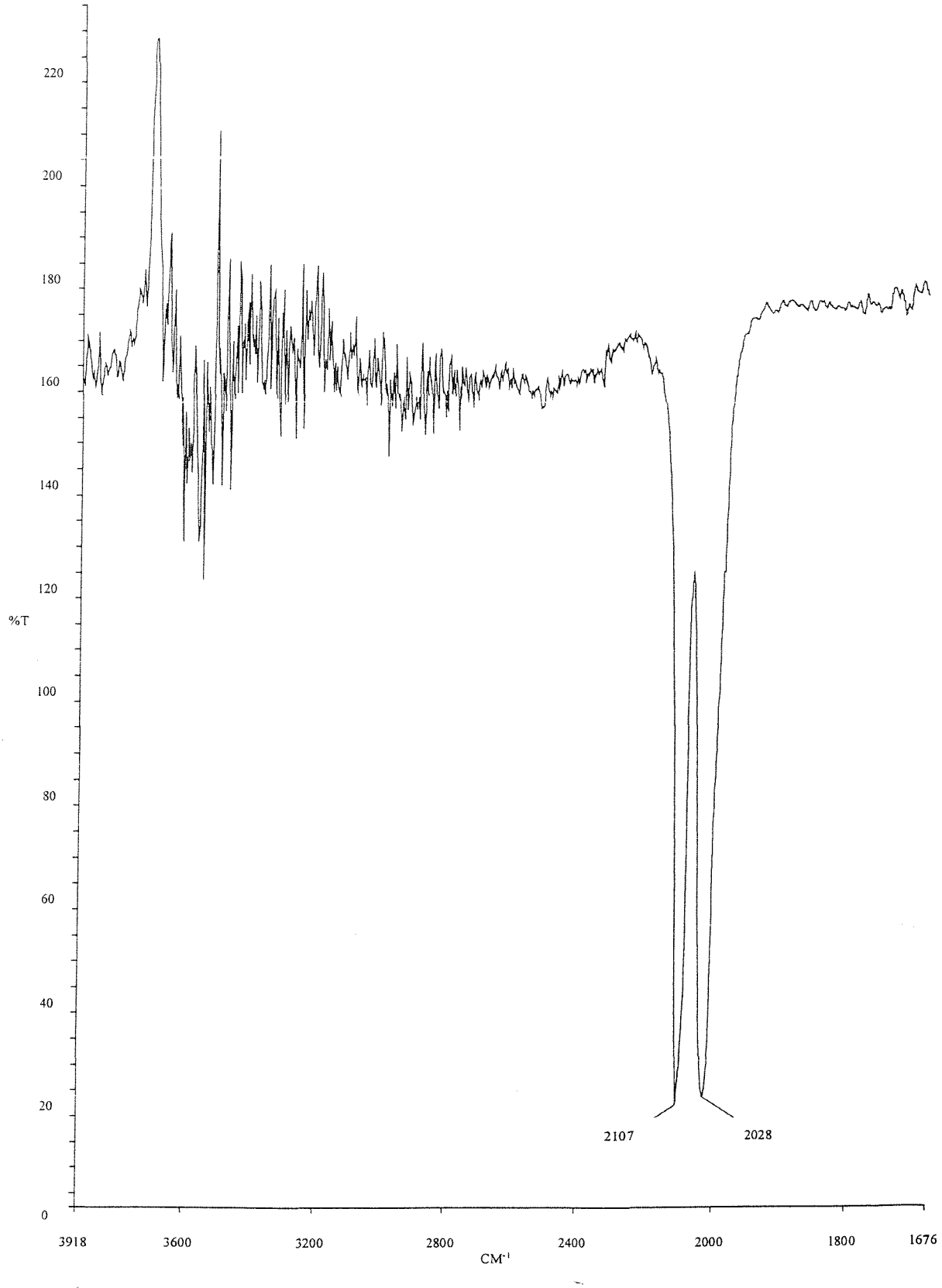

Figure 3.3 DRIFTS difference spectrum of $[Rh(CO)_2Cl]_2$ supported on partially dehydroxylated alumina

3.2.2 Energy Dispersive EXAFS Study of the Adsorption of $[Rh(CO)_2Cl]_2$ onto γ Al_2O_3

The Rh K-edge Energy Dispersive EXAFS (EDE) spectrum and its Fourier transform for a rhodium foil is shown in figure 3.4 The spectrum is an average of 100 scans, each lasting 36 ms (18 frames at 2ms), resulting in a total acquisition time of 3.6s. The bond lengths obtained for rhodium metal by X-ray crystallography are also shown. The spectrum shows coordination numbers expected for a face centred cubic structure up to the fifth coordination shell. It is only with the fourth coordination shell that the bond length shows any appreciable disagreement with the X-ray value. Crystallographic values were obtained from the CDS database using CCDL. The spectrum compares very closely with a standard EXAFS scan acquired at the SRS at Daresbury, shown in section 7.2, which was (incidentally) recorded in 80 minutes.

The Rh K-edge Energy Dispersive EXAFS (EDE) spectrum and its Fourier transform for $[Rh(CO)_2Cl]_2$ supported on partially dehydroxylated alumina, is shown in figure 3.5. The spectrum is an average of 100 scans, each lasting 18 ms (18 frames at 1ms), resulting in a total acquisition time of 1.8s.

The Fourier transform shows the presence of four coordination shells, the first and third of which are fitted to two carbonyl groups with a Rh-C distance of 1.88Å and the oxygen shell 2.97Å from the rhodium. The successful fitting of these groups requires the use of multiple scattering calculations[27], which have employed a Rh-C-O bond angle of 180°. This bond angle showed no noticeable variation upon iteration. The observed C-O bond length of 1.09 Å agrees well with that of 1.11Å found by Rudkin[9].

The second coordination sphere is fitted by including contributions from two different shells. An Rh-$O_{surface}$ distance of 2.18Å is observed, along with a Cl atom at 2.36Å. These assignments are in agreement with previous studies by Rudkin and Williams. The Rh-Cl distance of 2.36Å is close to the average value of 2.355Å observed in the precursor[1] and shows the chlorine, under these conditions, to be bound to the rhodium rather than merely to the alumina surface.

Figure 3.4 Rh K-Edge EXAFS and Fourier transform for Rhodium foil. Solid lines show actual spectra, dotted lines show theoretical spectra (for this and all subsequent spectra).

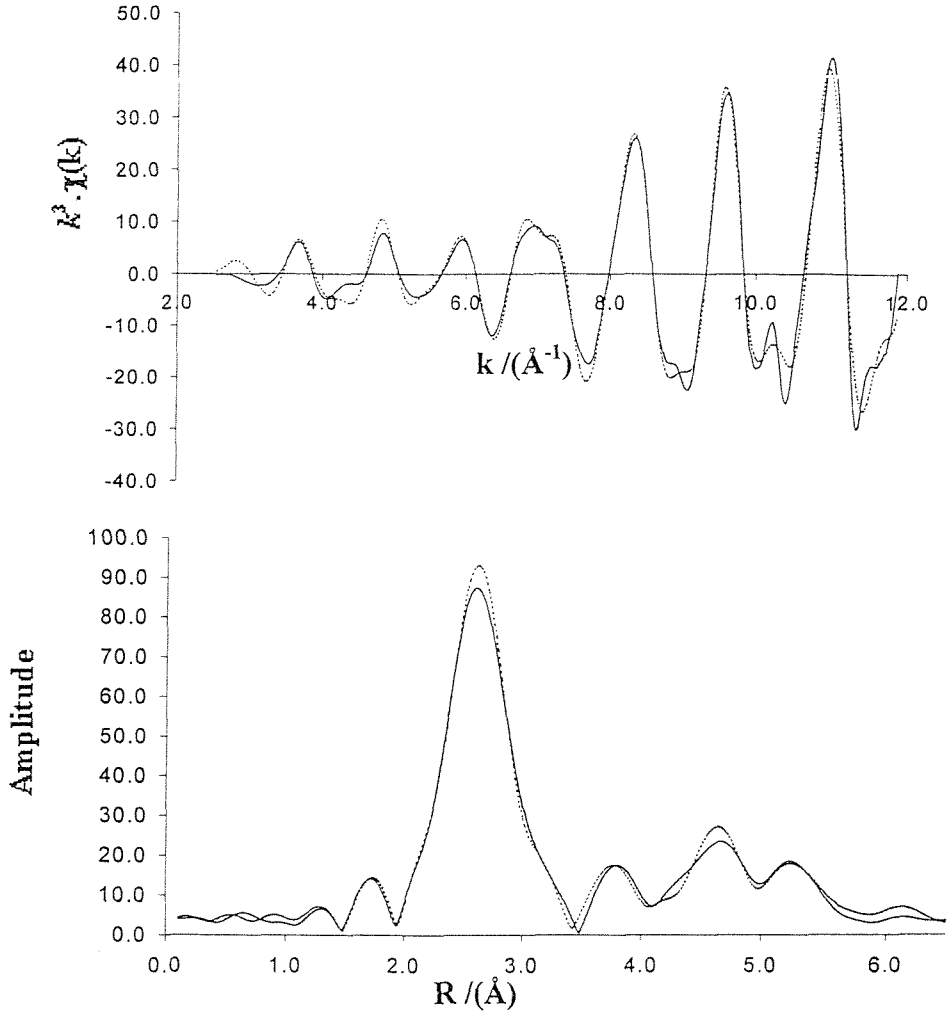

Atom	C.N.	r/Å	X-Ray Bond Length / Å	$2\sigma^2$ / Å^2 (D.W)
Rh	12	2.701(1)	2.69	0.009(1)
Rh	6	3.805(3)	3.80	0.013(1)
Rh	24	4.684(2)	4.66	0.014(1)
Rh	12	5.270(3)	5.38	0.015(1)
Rh	24	6.017(5)	6.01	0.018(2)

R= 17.82 %

Ef= -0.44 eV

Figure 3.5 Rh K-Edge EXAFS and Fourier transform of $[Rh(CO)_2Cl]_2$ supported on Al_2O_3

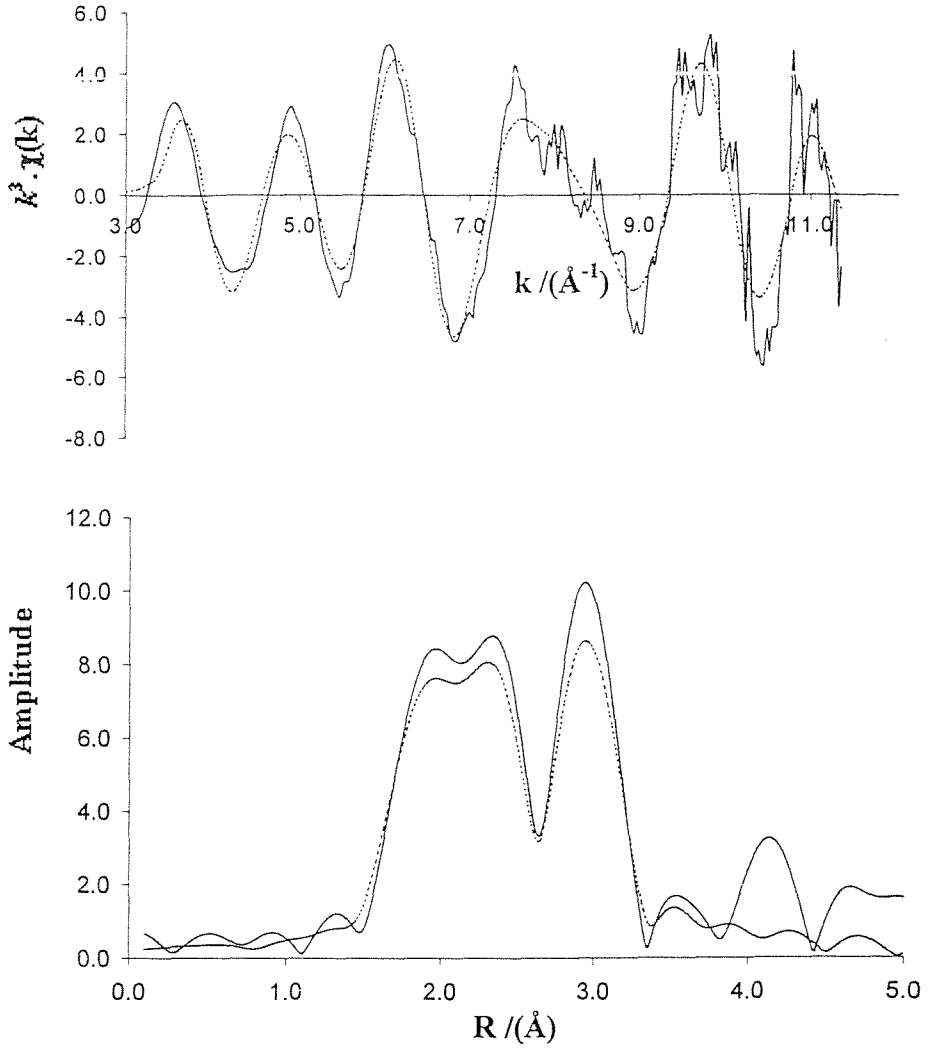

Atom	C.N.	r/Å	$2\sigma^2$ / Å^2
C	2(0.1)	1.871(2)	0.007(1)
O	1(0.1)	2.150(4)	0.002(1)
Cl	1(0.2)	2.360(3)	0.008(3)
O	2(0.2)	3.006(4)	0.016(1)
Al	1(0.3)	3.609(8)	0.019(3)

R = 37.85%
Ef =2.31eV

A third coordination sphere is also observed which arises from an $Al_{surface}$ atom at a distance of 3.60Å. This is bound to the oxygen atom, which is in turn bound to the rhodium atom.

As with the work of Rudkin[9], the EXAFS results show an average coordination sphere of [Al-O]$Rh(CO)_2Cl$, which could either arise from the averaging of signals from $[Rh(CO)_2Cl]_2$ molecules physisorbed on the surface and $Rh(CO)_2$ units, or from the presence of a discrete surface supported $Rh(CO)_2Cl$ species. Previous studies on this system have repeatedly shown that this coordination sphere, which is stable under vacuum, does not show any signal for a rhodium neighbour, which would be expected for the physisorbed dimeric precursor. EXAFS spectra for the precursor clearly indicate a rhodium neighbour feature at 3.18Å, as shown by Rudkin[9].

3.3 Helium Thermolysis of $[Rh(CO)_2Cl]_2$ Supported on Titania and Alumina

The reactivity of surface supported dicarbonyl species with helium has been investigated by DRIFTS and Energy Dispersive EXAFS spectroscopies, as well as temperature programmed desorption.

3.3.1 DRIFTS studies of the Helium Thermolysis of $[Rh(CO)_2Cl]_2$ Supported on Titania and Alumina

The thermolysis of 5% wt $[Rh(CO)_2Cl]_2$ supported on partially dehydroxylated alumina and titania was studied by DRIFTS spectroscopy. The samples were heated *ex-situ* under an argon atmosphere and transferred to the DRIFTS cell where they were maintained under an argon atmosphere while spectra were collected. In each experiment 100 scans were accumulated, with a spectral resolution of $4cm^{-1}$. The

changes in the DRIFTS spectra during the thermolysis experiment are illustrated in figure 3.6.

At a temperature of 110°C, the intensity of the *gem* dicarbonyl band had decreased by 20%, though the frequencies remained unchanged. The symmetric band began to develop a negative shoulder (at lower frequencies), which indicates the development of a linear carbonyl band at ≈ 2090cm^{-1}. By 140°C the *gem* dicarbonyl band had disappeared, and had been replaced by a linear carbonyl band at 2089cm^{-1}. These linear carbonyl species are believed to be adsorbed on small rhodium particles[9,11], and are an indication of the commencement of the reduction of the rhodium to metallic clusters. The intensity of this linear band decreased as the temperature was raised further, and the frequency decreased steadily to a value of 2065cm^{-1} by 190°C. This corresponds to a decrease in the population of the carbonyl species which results in a reduction in infrared frequency due to increasing backbonding into the unoccupied states of the CO due to increasing metal particle size. By 220°C, there are no surface carbonyl species evident on the rhodium, and it can be concluded that metallic rhodium clusters have been formed. The reduction process has also resulted in the removal of the bridging carbonyl species. The mechanism of this process is as yet unknown. The species apparent at ≈ 3000cm^{-1} in spectra (g) and (h) are likely to be hydrocarbon impurities, which have sublimed from the TiO_2 surface onto the KBr windows of the DRIFTS cell. They are probably drawn out of the cell by the He flow and are thus not apparent in spectra acquired at higher temperatures.

This experiment was repeated for an alumina supported sample of $[Rh(CO)_2Cl]_2$ to aid comparison with results from EXAFS experiments. The results of this experiment were identical to that of the titania supported sample to within 5°C. This involved the rhodium *gem* dicarbonyl species progressing through a linear carbonyl species and the subsequent formation of rhodium clusters on the alumina surface. The quality of the DRIFTS spectra for the alumina supported $[Rh(CO)_2Cl]_2$ was inferior to that of the titania supported sample due to the poorer reflectivity of alumina to that of titania. Therefore the spectra from the titania supported sample are presented.

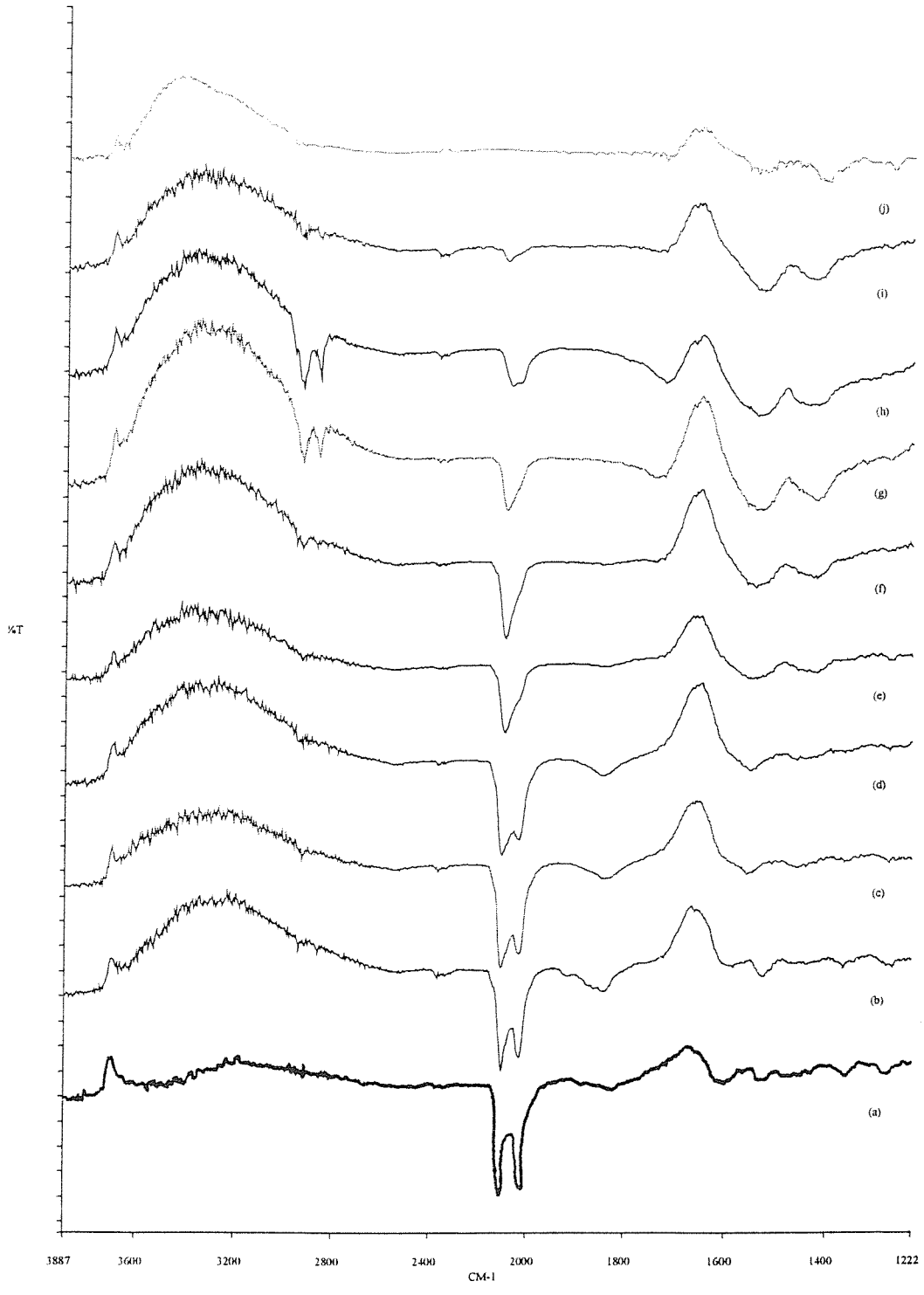

Figure 3.6 DRIFTS difference spectra of helium thermolysis of $[Rh(CO)_2Cl]_2$ supported on partially dehydroxylated titania: (a) Room temp, (b) 100°C, (c) 130°C, (d) 150°C, (e) 160°C, (f) 170°C, (g) 180°C, (h) 190°C, (i) 200°C, (j) 220°C.

3.3.2 Energy Dispersive EXAFS studies of the Thermolysis of $[Rh(CO)_2Cl]_2$ Supported on Alumina

The Rh K-edge energy dispersive EXAFS experiment for the thermolysis of $[Rh(CO)_2Cl]_2$ supported on partially dehydroxylated alumina was performed at the ESRF in Grenoble at station ID24. The samples were heated at a rate of 5°C per minute, under a flow of 5ml/min of helium. Spectra were collected every 5 minutes until the temperature reached 400°C. The EXAFS spectrum and its Fourier transform for the thermolysis of $[Rh(CO)_2Cl]_2$ supported on partially dehydroxylated alumina are shown in figures 3.7 to 3.11. A stack plot for the thermolysis experiment is shown in figure 3.12.

The starting spectrum shows the [Al-O]$Rh(CO)_2Cl$ species, and is shown in figure 3.4, as it was this sample which was used for the thermolysis experiment.

Figure 3.7 shows a spectrum of the sample after heating to 120°C. This spectrum was acquired in 1.3 seconds. The EXAFS and Fourier transform indicate that the [Al-O]$Rh(CO)_2Cl$ species is still present on the surface at this temperature. There is no noticeable change in the coordination numbers, bond distances or Debye-Waller factors, to suggest any change has taken place. This is in agreement with DRIFTS results, which also indicate no change at this temperature.

Figure 3.8 shows the EXAFS and Fourier transform of the sample after heating to 140°C. This spectrum was acquired in 1.3 seconds. Though the EXAFS shows slightly greater intensity at greater 'k' values and the Fourier transform has assumed a marginally different shape, the sample still appears to remain unchanged. A variety of other models were attempted to fit the data, including a linear carbonyl species and a mixture of *gem* dicarbonyl surface species, and rhodium clusters However, the [Al-O]$Rh(CO)_2Cl$] model fitted the data considerably better than these. This result suggests that although the system may be in transition from a [Al-O]$Rh(CO)_2Cl$] species to a linear carbonyl species, the former is by far the most prevalent of these at 140°C. The spectra also suggest that some clustering of the

Figure 3.7 Rh K-Edge EXAFS and Fourier transform of $[Rh(CO)_2Cl]_2$ supported on Al_2O_3 after heating to 120°C in helium

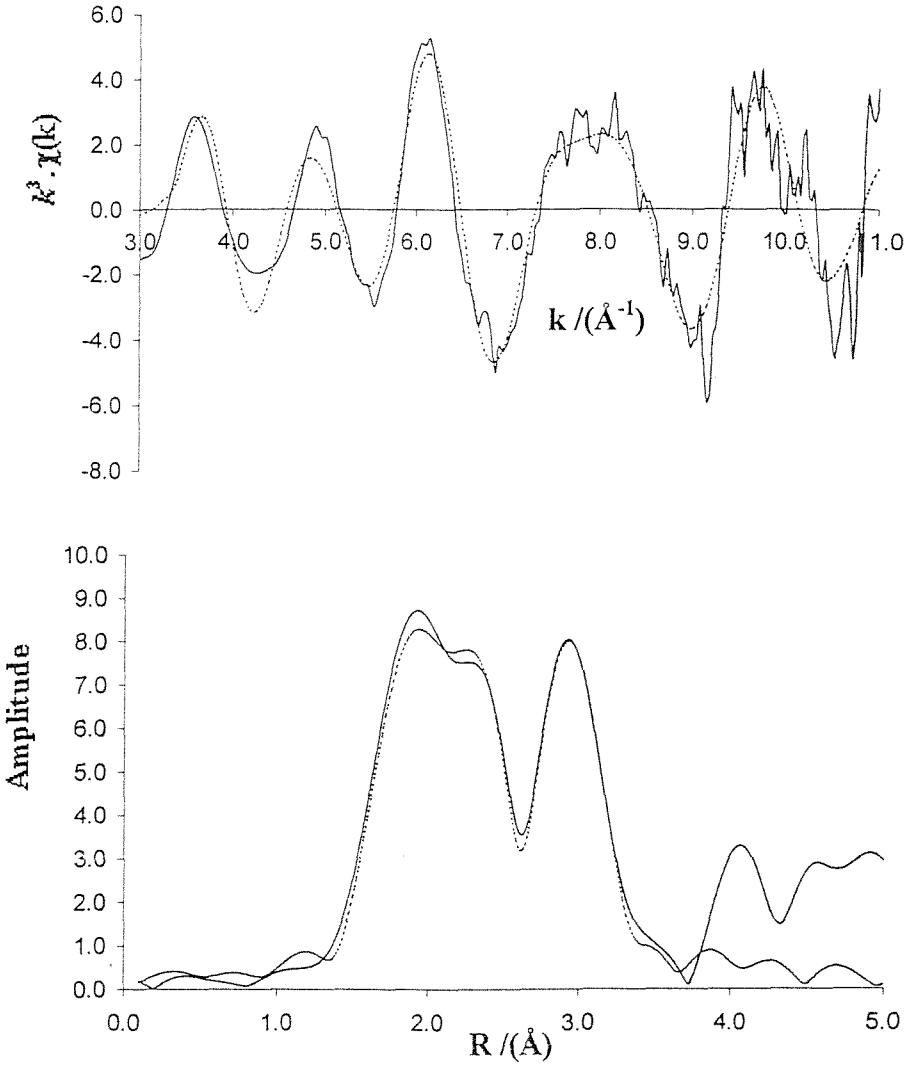

Atom	C.N.	r/Å	$2\sigma^2$ / Å^2
C	2(0.1)	1.882(1)	0.001(1)
O	1(0.1)	2.147(2)	0.002(1)
Cl	1(0.1)	2.375(3)	0.013(3)
O	2(0.2)	2.992(3)	0.020(5)
Al	1(0.3)	3.590(6)	0.023(3)

R = 39.99%
Ef =2.23eV

Figure 3.8 Rh K-Edge EXAFS and Fourier transform of $[Rh(CO)_2Cl]_2$ supported on Al_2O_3 after heating to 140°C in helium

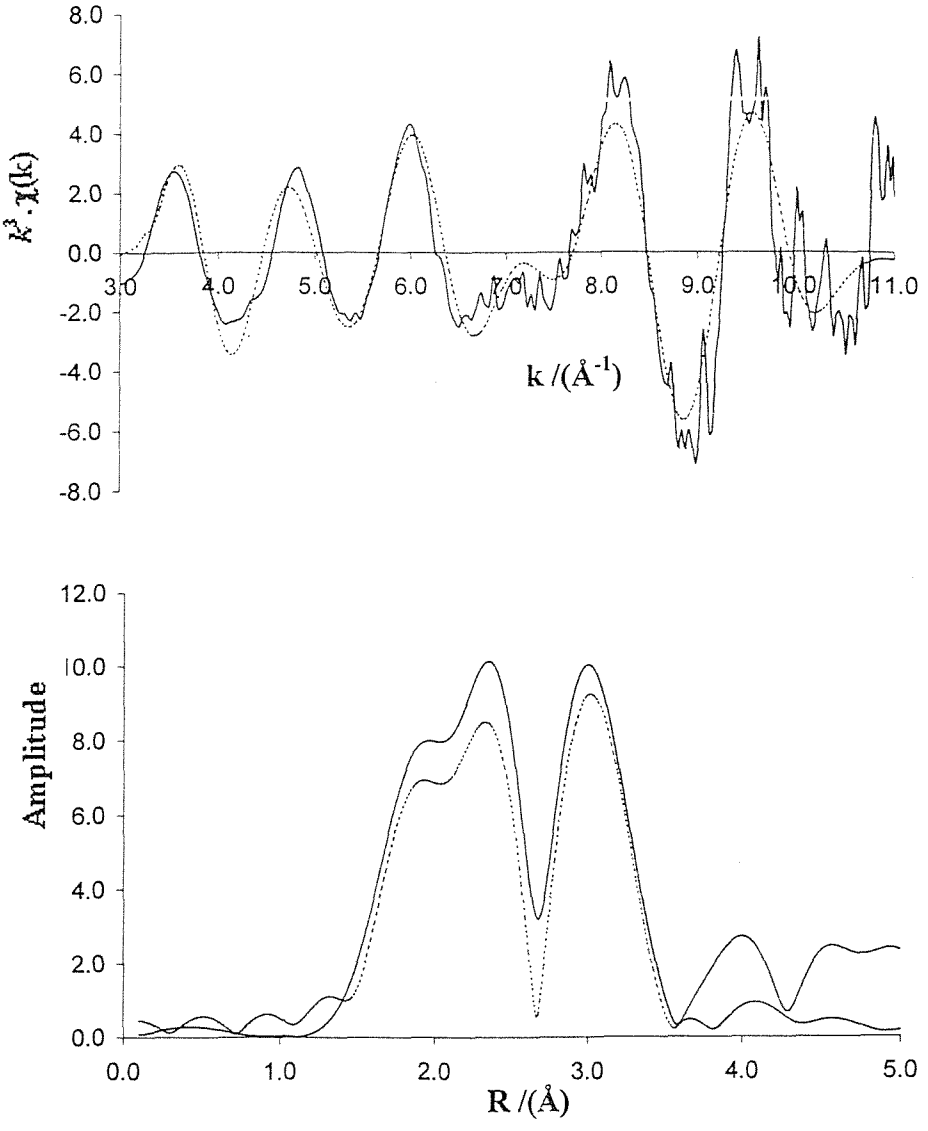

Atom	C.N.	r/Å	$2\sigma^2$ / Å^2
C	2(0.1)	1.877(2)	0.001(2)
O	1(0.2)	2.168(2)	0.002(1)
Cl	1(0.1)	2.348(4)	0.012(1)
O	2(0.2)	3.014(3)	0.019(5)
Al	1(0.3)	3.579(7)	0.026(2)

R = 42.45%
Ef = 2.11 eV

rhodium may have occurred, indicated by the presence of greater intensity at higher 'k' numbers. However, as stated above, a rhodium-rhodium shell could not be fitted.

Figure 3.9 shows the EXAFS and Fourier transform of the sample after heating to 170°C. This spectrum was acquired in 1.3 seconds. It can be seen that the EXAFS has changed considerably from before in that the greatest intensity is at larger k values, suggesting the presence of heavier backscattering atoms such as rhodium. The Fourier transform also has a very different shape to that of the [Al-O]Rh(CO)$_2$Cl] species. There are four peaks in the Fourier transform, the first of much greater intensity than the other three, which are of similar intensity. Such a shape in the Fourier transform is diagnostic of a rhodium cluster. Several models were again attempted to fit the data, the best being a rhodium cluster with four shells. The coordination number was refined and the result was a series of four nearly complete shells. The bond distances are in close agreement with the values found for a rhodium cluster to within 0.05Å.

Figure 3.10 shows the EXAFS and Fourier transform of the sample after heating to 200°C. This spectrum was acquired in 1.3 seconds. The EXAFS and Fourier transform are very similar in shape to that of the sample after heating to 170°C. A rhodium cluster model was employed and the coordination number was refined. The results of this show the rhodium clusters to have grown in size by a small amount relative to the previous experiment. The first two shells have twelve and six rhodium atoms respectively, which is the same number as that for bulk rhodium metal. The third shell has a coordination number of twenty, which is four short of that for bulk metal, and the fourth has a coordination number of eight, relative to twelve for bulk metal. It can be seen that the coordination number has only increased for the first two shells relative to the sample heated to 170°C.

Spectra for samples heated beyond 200°C were of poorer quality, which rendered background subtraction impossible. However, a final spectrum was acquired after heating to 400°C, and allowing the sample to cool to room temperature. The EXAFS and Fourier transform for this sample is shown in figure 3.11. There are five peaks in the Fourier transform, the first of which is much more intense than the other

Figure 3.9 Rh K-Edge EXAFS and Fourier transform of $[Rh(CO)_2Cl]_2$ supported on Al_2O_3 after heating to 170°C in helium

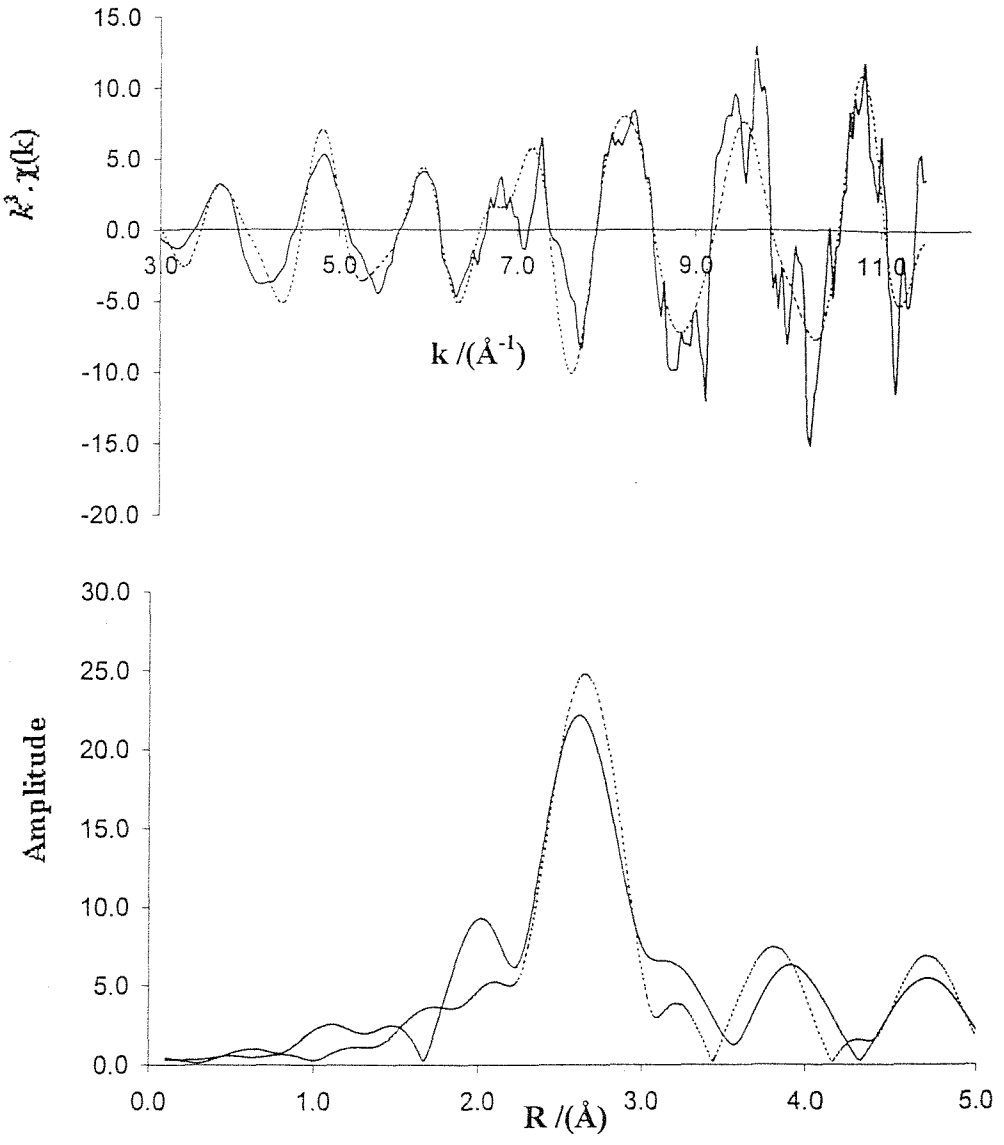

Atom	C.N.	r/Å	$2\sigma^2$ / Å^2
Rh	9(1.0)	2.272(3)	0.018(3)
Rh	5(1.2)	3.840(2)	0.016(2)
Rh	20(2.5)	4.793(3)	0.023(4)
Rh	9(2.8)	5.328(6)	0.027(5)

R = 47.24 %
Ef = 0.25 eV

Figure 3.10 Rh K-Edge EXAFS and Fourier transform of $[Rh(CO)_2Cl]_2$ supported on Al_2O_3 after heating to 200°C in helium

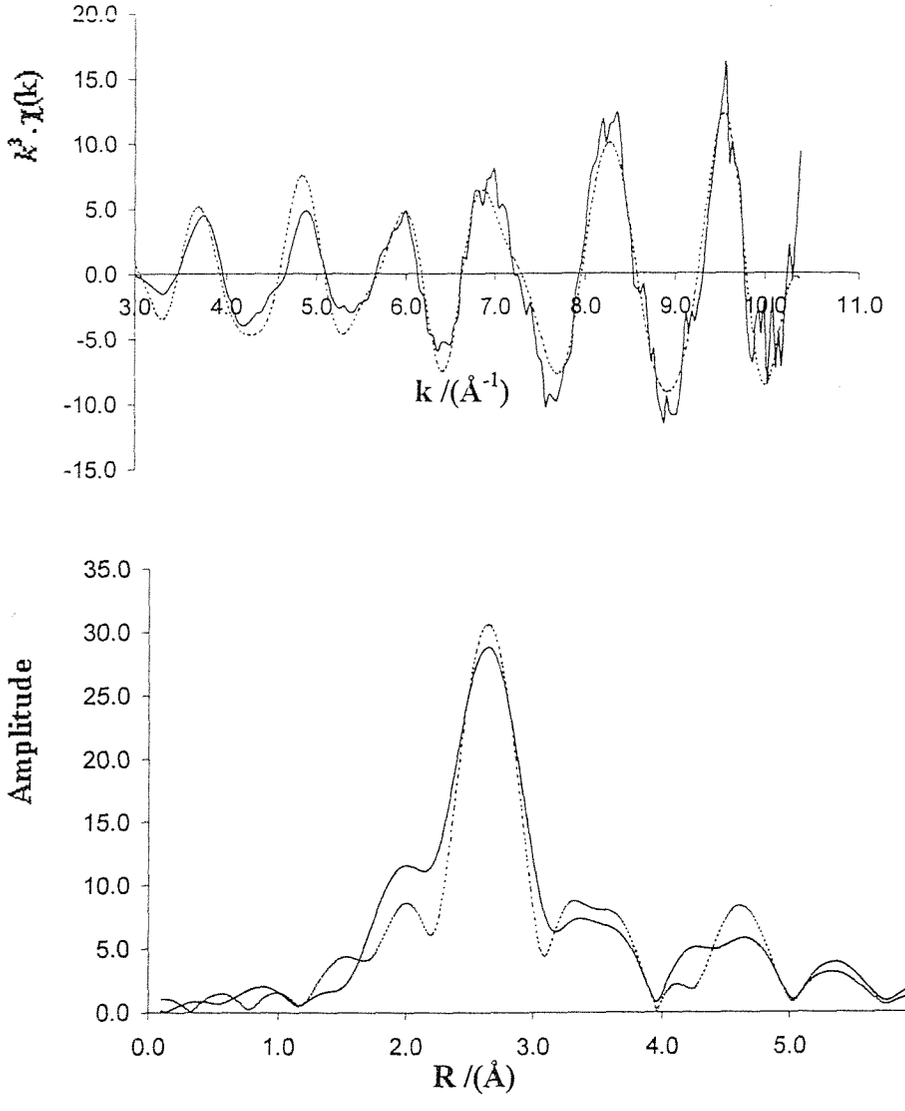

Atom	C.N.	r/Å	$2\sigma^2$ / Å^2
Rh	12(1.4)	2.218(2)	0.021(2)
Rh	6(1.5)	3.778(1)	0.016(2)
Rh	20(3.0)	4.697(3)	0.022(2)
Rh	10(2.4)	5.298(4)	0.024(3)

R = 36.04 %
Ef = 2.41 eV

Figure 3.11 Rh K-Edge EXAFS and Fourier transform for $[Rh(CO)_2Cl]_2$ supported on Al_2O_3 after heating to 400°C in helium

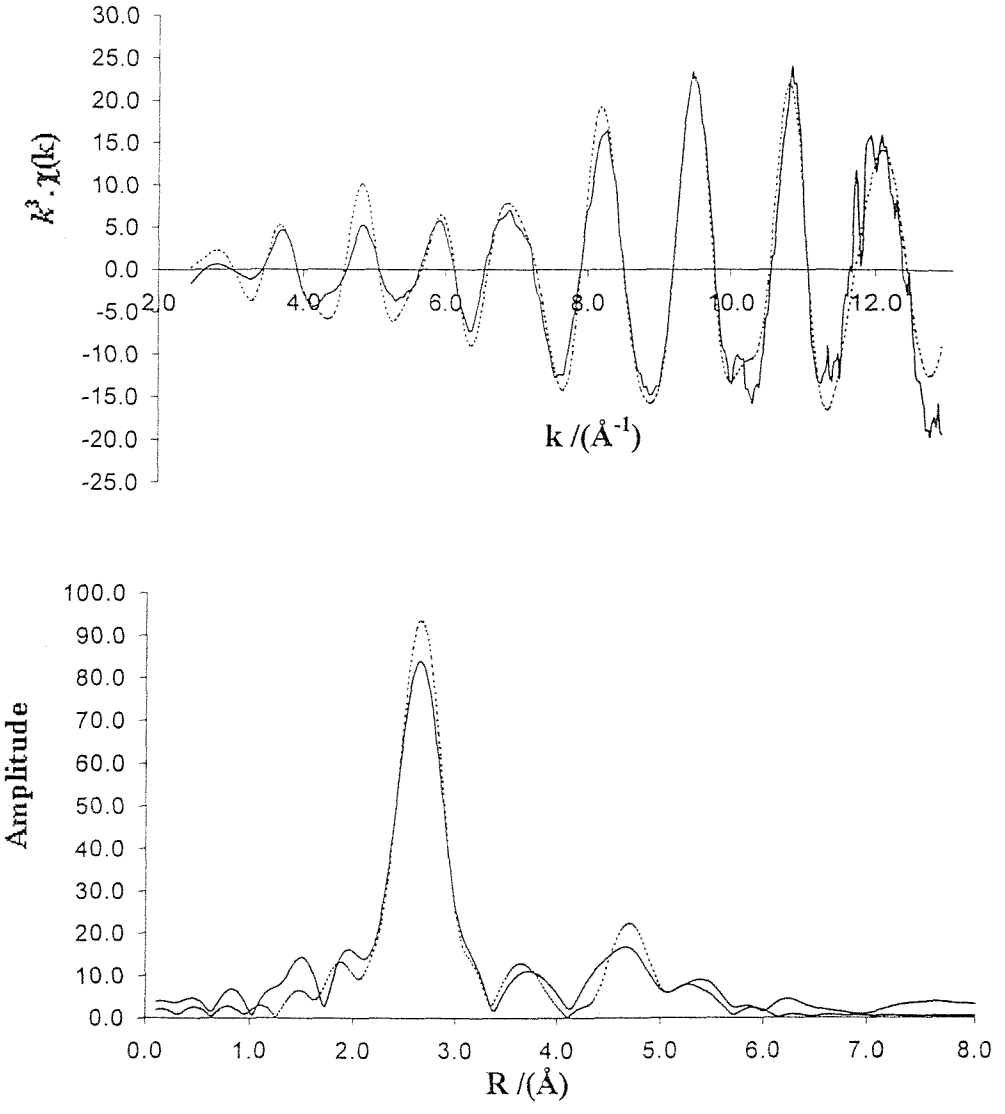

Atom	C.N.	r/Å	$2\sigma^2$ / Å^2
Rh	12(0.6)	2.727(3)	0.012(1)
Rh	6(1.1)	3.837(2)	0.017(1)
Rh	24(3.2)	4.734(3)	0.019(3)
Rh	12(1.5)	5.354(6)	0.022(2)
Rh	6(3.3)	5.998(8)	0.028(7)

R = 26.64%
Ef =1.85eV

four. A rhodium cluster model was applied to these data, and the coordination number was refined. The results indicate that the thermolysis experiment has generated large clusters of rhodium, as the coordination numbers for the five shells resemble those of bulk metal. Only the fifth shell has a coordination number slightly lower than that for bulk metal. The bond distances also match those found in bulk rhodium, with deviations no greater than 0.05Å.

The results of these experiments agree well with those for the DRIFTS study of the same reaction in terms of the removal of the *gem* dicarbonyl species and the formation of rhodium clusters on the alumina surface. The temperature at which the transition takes place is consistent in both experiments. The differences in results between the DRIFTS and EDE studies can be explained in terms of the varying sensitivities of the two techniques. Infrared spectroscopy is particularly sensitive to the intense bands caused by the C-O stretch, while it will not observe any signal for metal particles. Conversely, EXAFS spectroscopy is sensitive to large backscattering atoms such as rhodium. Since EXAFS observes an average signal from all absorbing atoms, the presence of small metal particles will swamp the signal for any residual carbonyl groups, which would still be detectable by infrared spectroscopy. This probably explains why it was impossible to fit a linear carbonyl species to any of the spectra obtained in this study, as the onset of this species was coincident with the formation of rhodium clusters.

Figure 3.12 shows a stack plot for the helium thermolysis. The spectra clearly illustrate the onset of oscillations at higher energies between 170 and 205°C. These oscillations are indicative of the presence of heavier backscattering atoms, which indicate the onset of formation of rhodium clusters on the alumina surface.

The experiment was repeated for another identical sample of 5% weight $[Rh(CO)_2Cl]_2$ supported on partially dehydroxylated alumina, to test the repeatability of the experiment. The data obtained was found to closely match that of the previous run, despite being of somewhat poorer quality (weaker edge jump and poorer background subtraction). The onset of metal particle formation was found to occur

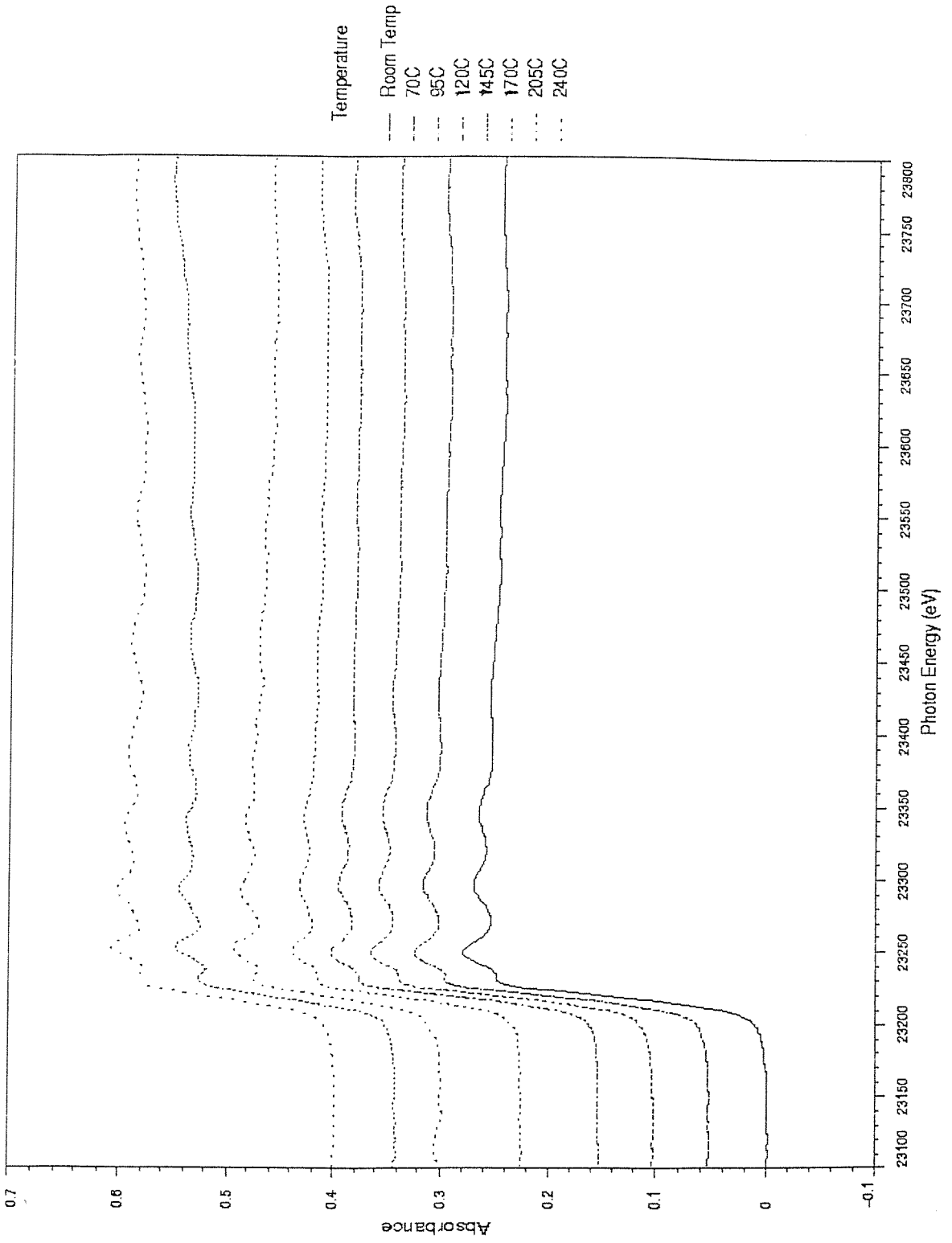

Figure 3.12 Stacked plot for helium thermolysis of 5% $[Rh(CO)_2Cl]_2$ supported on Al_2O_3

within the same temperature range, and the rhodium clusters formed were of comparable size to that found in the previous experiment.

A helium thermolysis experiment was also attempted for a sample of 2% weight $[Rh(CO)_2Cl]_2$ supported on partially dehydroxylated alumina. The purpose of this experiment was to ascertain any differences in the mode of decomposition of the *gem* dicarbonyl species, and formation of metal clusters. In particular, it was hoped the experiment would highlight differences in the sizes of the rhodium clusters formed relative to the 5% weight sample. Unfortunately, the data quality from this experiment was very poor, with a poor edge jump and low signal to noise ratio. Consequently, no meaningful conclusions could be drawn from these data. However, a stack plot for this experiment is shown in figure 3.13. The onset of metal particle formation is apparent at 180-200°C, where the number of oscillations in the spectra increases.

3.3.3 TPD Study of the Thermolysis of $[Rh(CO)_2Cl]_2$ Supported on Alumina

The temperature programmed desorption study of the thermolysis of 5% $[Rh(CO)_2Cl]_2$ supported on partially dehydroxylated alumina, was conducted using the microreactor in Southampton. The sample was heated under a flow of helium at 5K per minute, whilst the gaseous products were monitored by mass spectroscopy. The TPD profile in figure 3.14, indicates a CO evolution peak (mass 28) at 160°C, with a shoulder at 155°C. The shoulder is believed to correspond to the initial desorption of CO from the $[Al\text{-}O]Rh(CO)_2Cl$ surface species, resulting in the formation of linear carbonyl and bridging carbonyl species. The clustering of these electron deficient species, with the evolution of CO is believed to correspond to the main peak in the TPD profile.

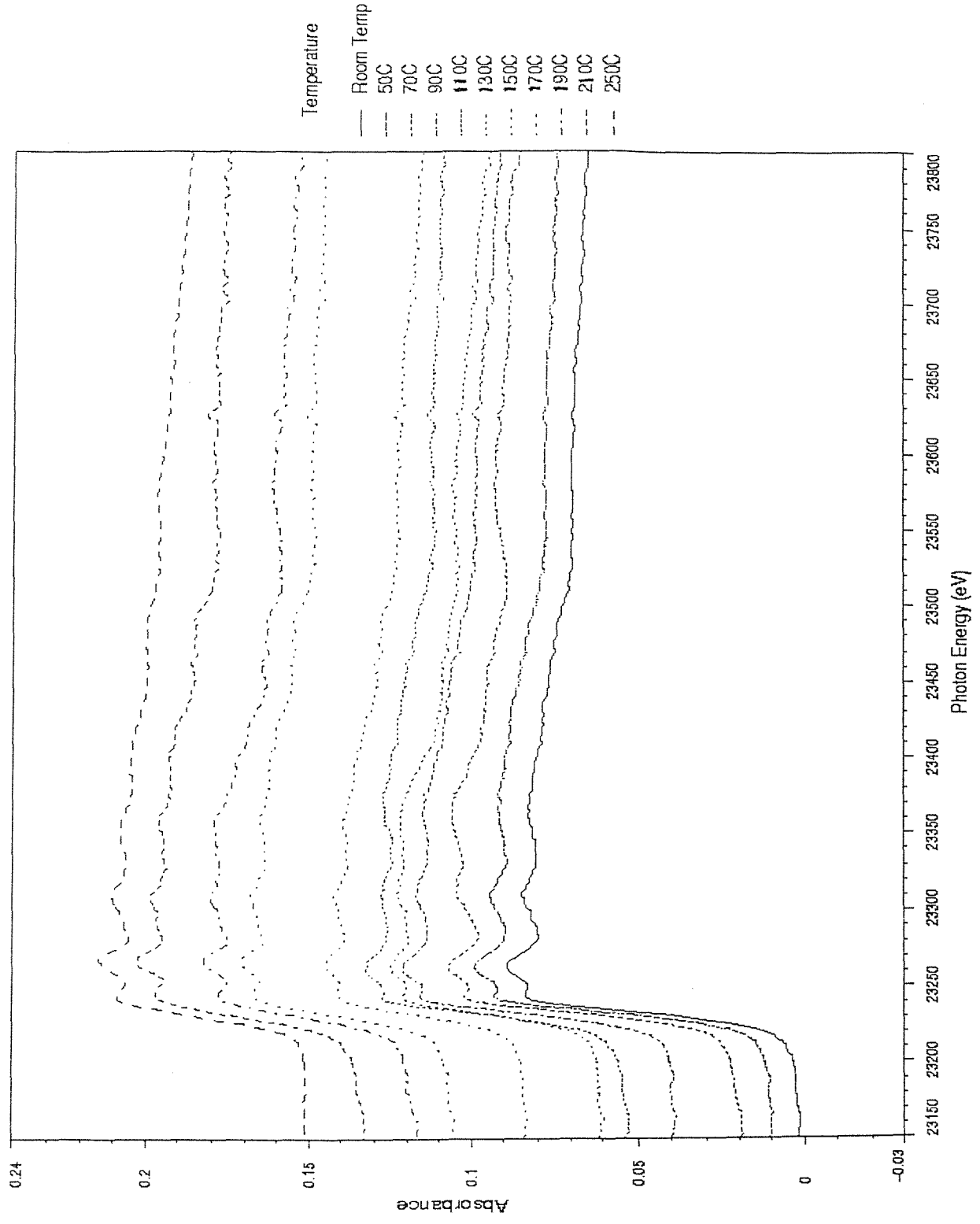

Figure 3.13 Stacked plot for helium thermolysis of 2% $[Rh(CO)_2Cl]_2$ supported on Al_2O_3

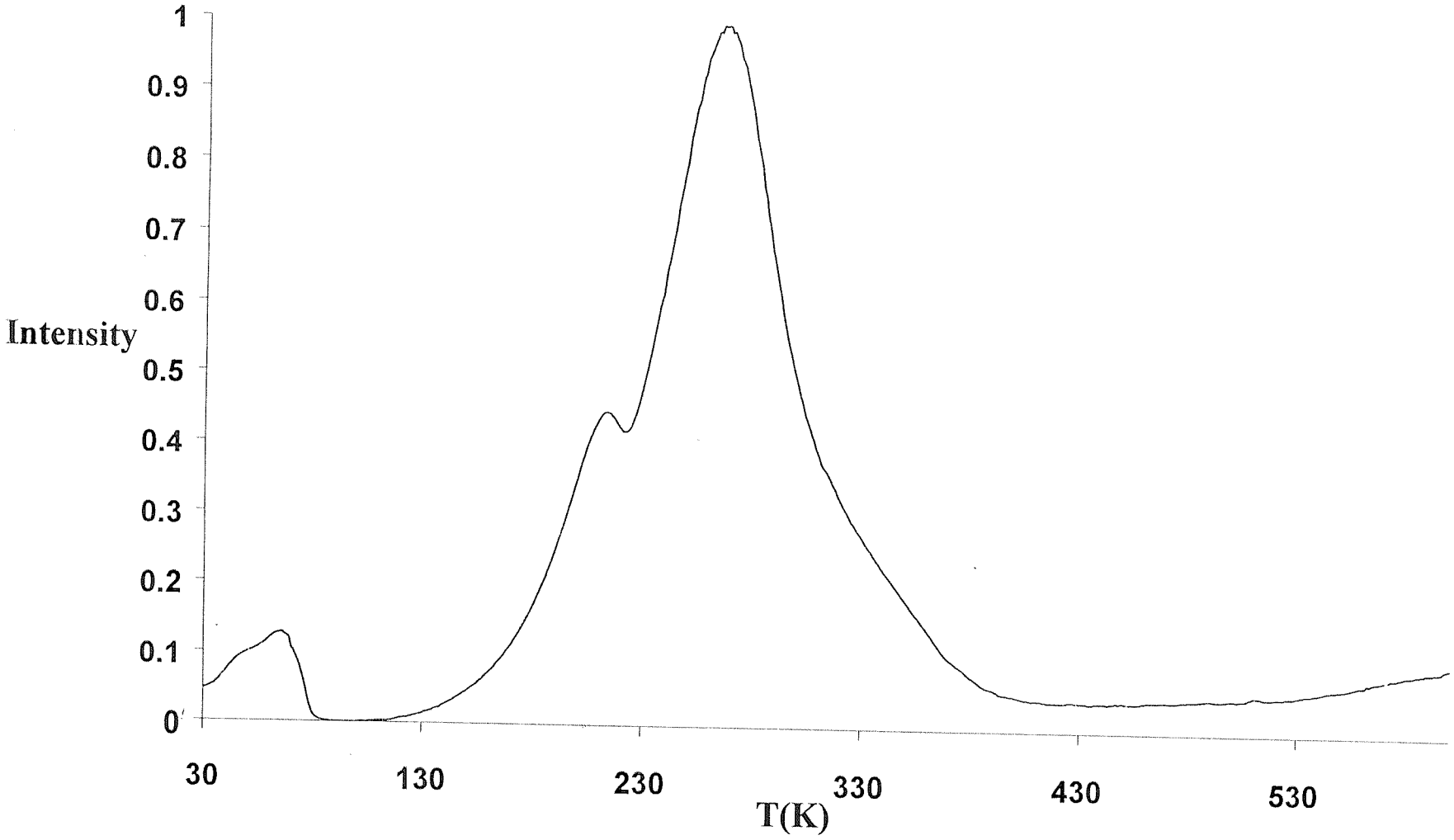

Figure 3.14 TPD profile for CO evolution (mass 28) during helium thermolysis of 5% $[Rh(CO)_2Cl]_2$ supported on Al_2O_3

3.4 Re-adsorption of CO onto Thermolysed Species

3.4.1 DRIFTS Study of Re-adsorption of CO onto Thermolysed Species

Following the thermolysis to 220°C of the $[Rh(CO)_2Cl]_2$ supported on partially dehydroxylated titania, the sample was exposed to 1bar of CO for 2 hours at room temperature, in an attempt to regenerate the *gem* dicarbonyl species. This experiment serves as a probe for investigation of the size of the rhodium clusters formed from the thermolysis experiment. Koningsberger *et al*[25] have observed that larger metallic particles (Pt) supported on SiO_2 (first shell coordination number >5) were stable under a CO atmosphere. By contrast, the smaller particles (first shell coordination number <5) reconstructed with the formation of linear Pt-CO aggregates at room temperature. A similar study by Koningsberger *et al*[26] on Al_2O_3 supported Rh catalysts attempted to assess to role of particle size in the CO re-dispersion reaction, using EXAFS. They again observed that linear and bridging rhodium carbonyl species were formed from smaller Rh clusters, whereas larger clusters (first shell coordination number >5) were unaffected by CO at room temperature. If large particles of rhodium have been generated by the thermolysis experiment, only a small fraction of the rhodium will be at the surface, leading to only a small concentration of rhodium carbonyl species regenerated. The *gem* dicarbonyl species only exists on monodispersed rhodium, whereas the linear and bridging carbonyl species also exist on larger clusters. CO may only re-disperse relatively small clusters[25,26], so the presence of a high concentration of the *gem* dicarbonyl species upon regeneration indicates that small rhodium clusters have been formed.

Figure 3.15 shows that 70% regeneration of the *gem* dicarbonyl species occurs. The frequencies of the symmetric and asymmetric bands have however, changed to $2090cm^{-1}$ and $2018cm^{-1}$ respectively, which is a reduction of $10cm^{-1}$ relative to the sample before thermolysis (to 220°C). Reasons for this could be that the chlorine is no longer bonded to the rhodium, thus allowing a greater degree of backbonding into the CO antibonding orbitals, or a lower density of rhodium *gem*

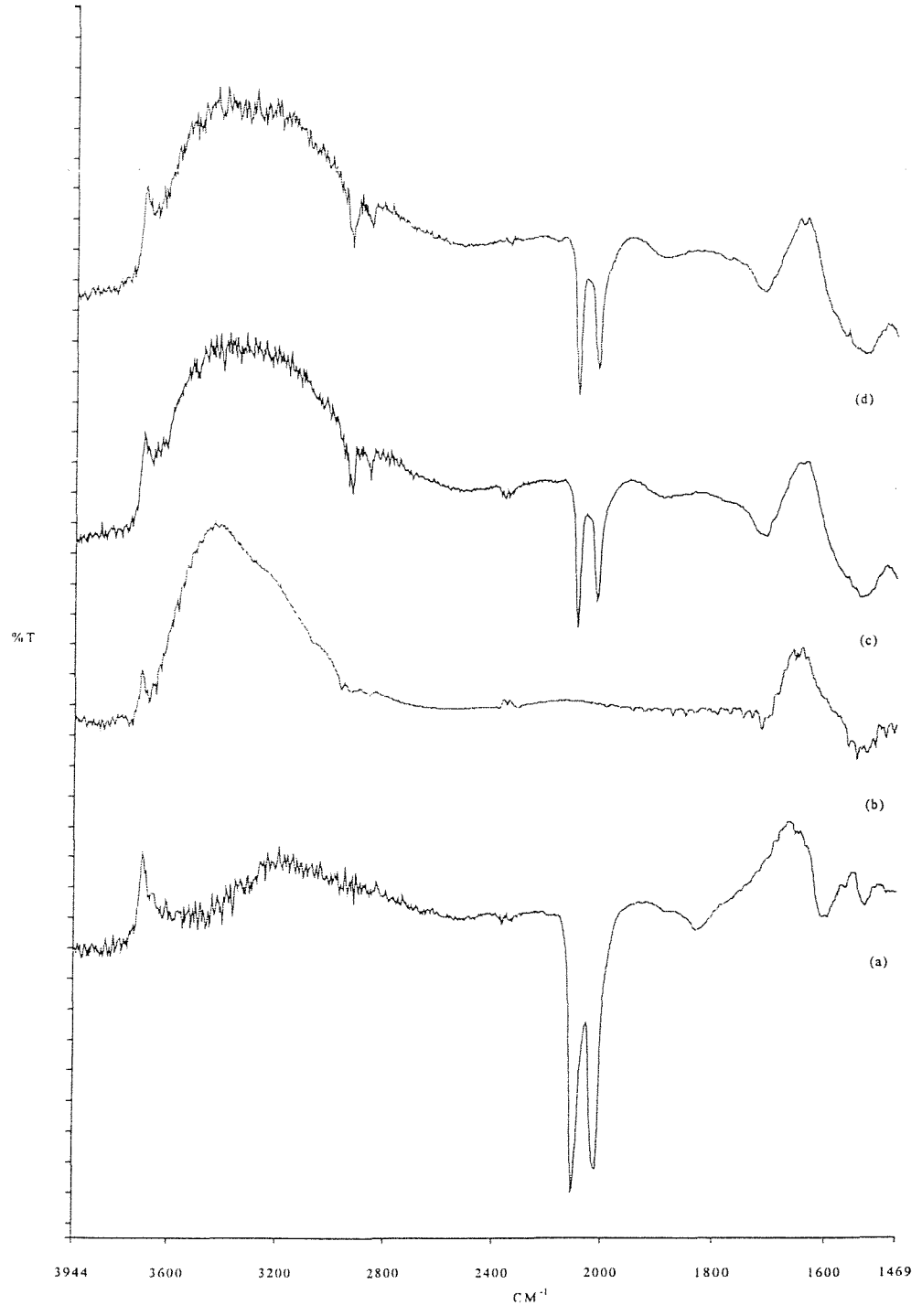

Figure 3.15 DRIFTS spectra of CO regeneration of $[Rh(CO)_2Cl]_2$ supported on partially dehydroxylated titania after helium thermolysis. (a) Room temp before thermolysis to 220°C, (b) Post thermolysis to (220°C), (c) CO exposure for 1hr, (d) CO exposure for 2 hrs

carbonyl species. This dicarbonyl frequency is similar to that of $Rh(CO)_2(acac)$, an organometallic which does not have a strongly withdrawing counter-ligand such as Cl in $[Rh(CO)_2Cl]_2$. There is also a weak, broad band at $\approx 1850 cm^{-1}$, which is attributed to a bridging carbonyl species, possibly $Rh_2(CO)_3$. The substantial regeneration of the *gem* dicarbonyl species indicates that the majority of the clusters formed were small, as this species only exists on monodispersed rhodium. CO is believed to be able to catalyse the dispersion of small rhodium clusters, whilst forming *gem* dicarbonyl bonds[28,29]. If large clusters have formed, the CO would not have been able to catalyse their dispersion. Linear and bridging carbonyl species can exist on monodispersed or larger rhodium clusters, and the presence of bridging carbonyl species after regeneration may indicate the presence of larger rhodium clusters on the titania surface. Exposure of the sample to CO for a further hour resulted in very little further regeneration of either the *gem* dicarbonyl or the bridging carbonyl species.

This experiment was repeated for an alumina supported sample of $[Rh(CO)_2Cl]_2$ to aid comparison with EDE results. The results were almost identical to that of the titania supported sample, though once again, the spectra were of inferior quality.

3.4.2 Energy Dispersive EXAFS studies of Re-adsorption of CO onto Thermolysed Species

Following the helium thermolysis to 220°C of $[Rh(CO)_2Cl]_2$ supported on partially dehydroxylated alumina, the sample was exposed to 4bar of CO for 1 hour at room temperature, at a flow rate of 5ml/min. The EXAFS and Fourier transform spectrum after CO exposure was acquired in 1 second, and is shown in figure 3.16. The shape of the EXAFS and the Fourier transform strongly resembles that of bulk rhodium metal. Thus although some of the smaller clusters may have re-dispersed to form rhodium carbonyl species (as indicated by DRIFTS results), the carbonyl signal is swamped by the majority of rhodium clusters on the surface.

Figure 3.16 Rh K-Edge EXAFS and Fourier transform of $[Rh(CO)_2Cl]_2$ supported on Al_2O_3 after He reaction at 220°C and exposure to CO for 30 mins

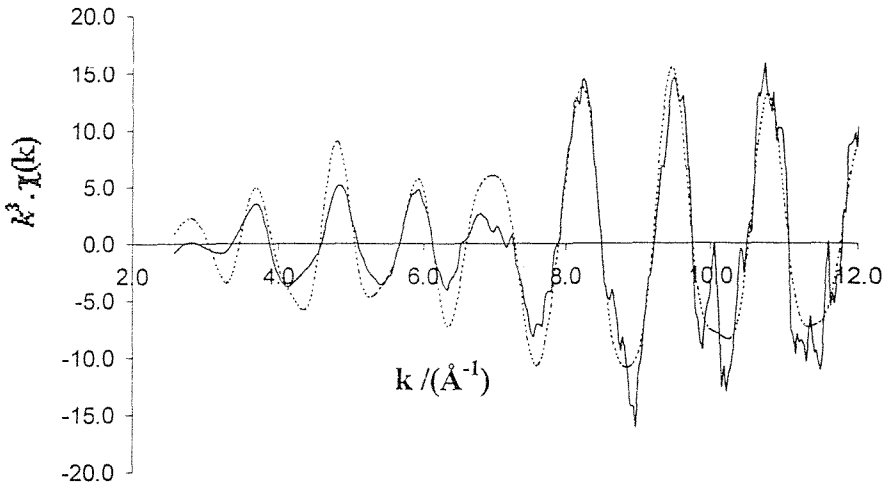

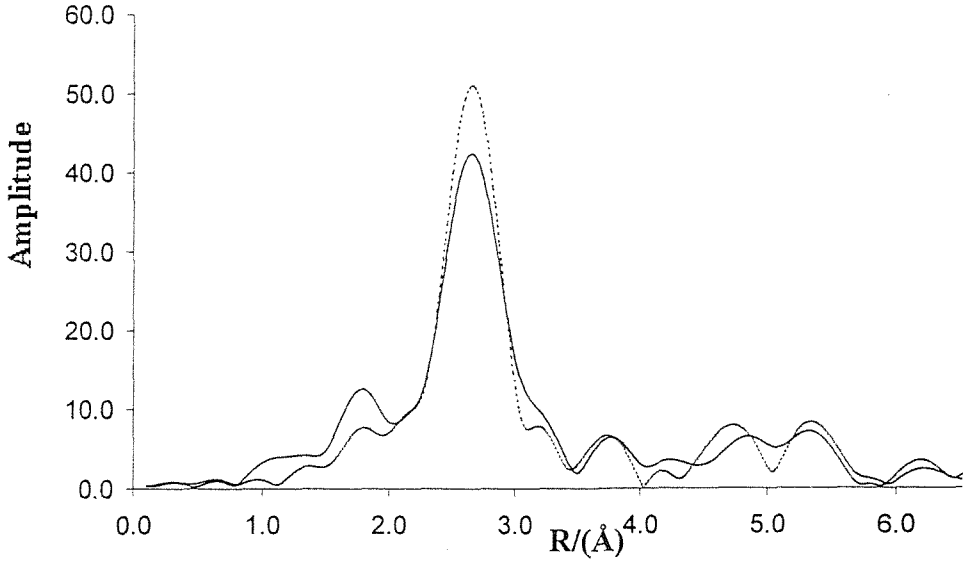

Atom	C.N.	r/Å	$2\sigma^2$ / Å^2
Rh	9(1.0)	2.272(3)	0.018(3)
Rh	5(1.2)	3.840(2)	0.016(2)
Rh	20(2.5)	4.793(3)	0.023(4)
Rh	9(2.8)	5.328(6)	0.025(5)

R = 47.24 %
Ef = 0.25 eV

3.5 Reaction of $[Rh(CO)_2Cl]_2$ Supported on Titania and Alumina with Hydrogen

The reactivity of surface supported dicarbonyl species with hydrogen has been investigated by DRIFTS and Energy Dispersive EXAFS spectroscopies, as well as Temperature Programmed Desorption.

3.5.1 DRIFTS studies of Reaction of $[Rh(CO)_2Cl]_2$ Supported on Titania with Hydrogen

The hydrogen themolysis of 5%wt $[Rh(CO)_2Cl]_2$ supported on partially dehydroxylated alumina and titania has been investigated by DRIFTS spectroscopy. The samples were heated *in-situ* under a hydrogen atmosphere while spectra were collected. In each experiment 100 scans were accumulated, with a spectral resolution of $4cm^{-1}$. The changes in the DRIFTS spectra during the thermolysis experiment are illustrated in figure 3.17.

The room temperature spectrum shows the characteristic *gem*-dicarbonyl bands at $2030cm^{-1}$ and $2107cm^{-1}$. There is also a broad band at $1830cm^{-1}$, which is attributed to a bridging rhodium carbonyl species, $Rh_2(CO)_3$[11].

At room temperature, after 1 hour, it can be seen that 50% of the *gem* dicarbonyl intensity has disappeared, with the development of a band at $2070cm^{-1}$, which is attributed to a linear carbonyl species. It is to be noted that no change in the frequency of the *gem* dicarbonyl band is observed during this stage of the experiment. At a temperature of 55°C, the *gem* dicarbonyl band has almost disappeared and been replaced by the linear carbonyl species at $2070cm^{-1}$. The intensity of the bridging carbonyl band remains constant, but has shifted to $1870cm^{-1}$. This may be due to an increase in the population of the bridging species, which is seen to occur upon the onset of clustering of the rhodium (3.3.1). This increased concentration of bridging species will result in increased competition for Rh electrons, and dipole coupling

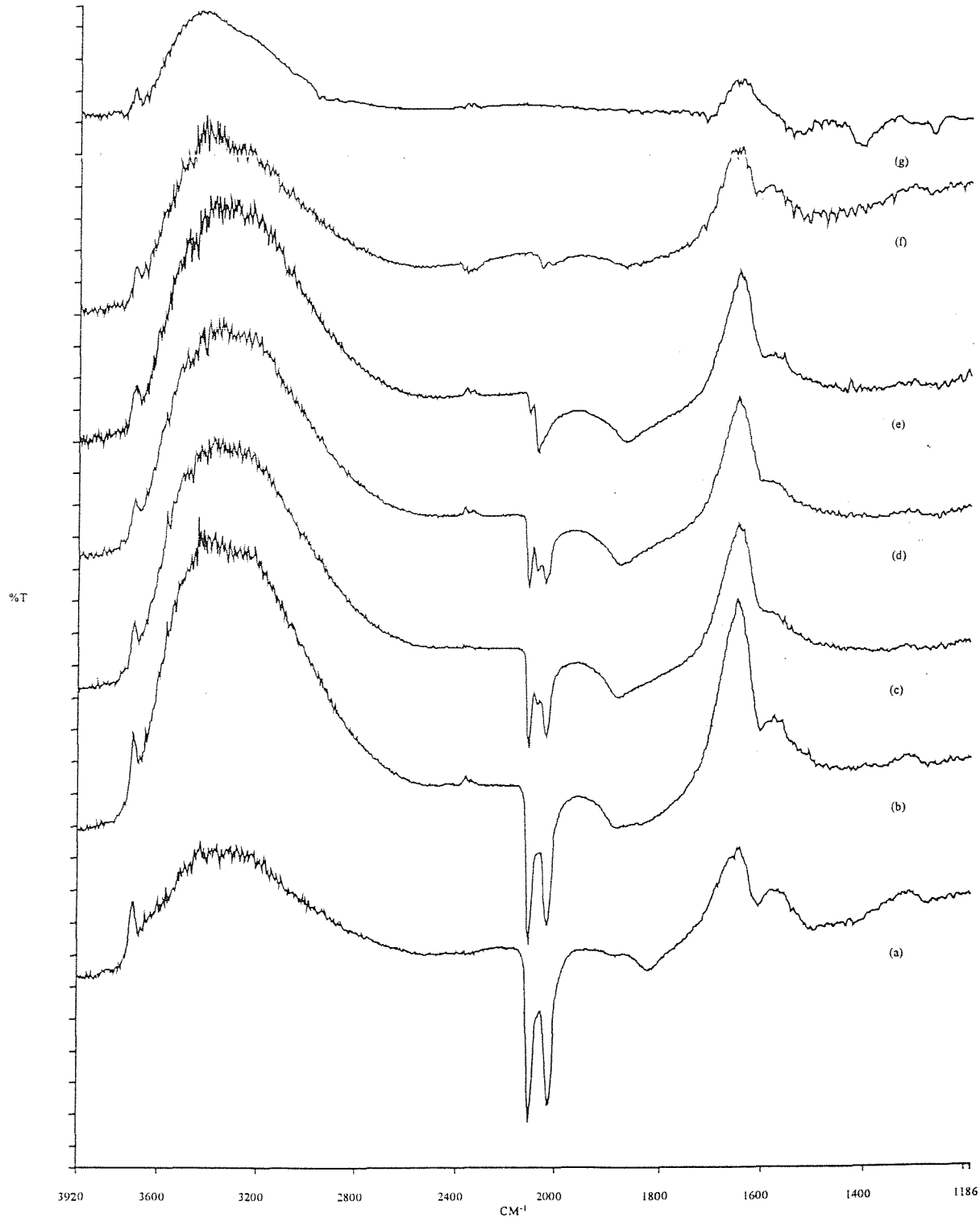

Figure 3.17 DRIFTS difference spectra of hydrogen thermolysis of $[Rh(CO)_2Cl]_2$ supported on partially dehydroxylated titania. (a) Room temp before exposure (b) Room temp 10 mins, (c) Room temp 30 mins, (d) Room temp 1 hour, (e) 55°C. (f) 85°C, (g) 100°C.

effects, both of which lead to less backbonding into the CO antibonding orbitals and a higher CO frequency. By 85°C the intensity of the linear carbonyl band has almost disappeared, along with the intensity from the bridging band. At 100°C, there are no remaining carbonyl species on the surface, and it can be inferred that the system consists of metallic Rh^0 clusters on the alumina surface. In conclusion, this experiment has shown that the reduction of the [Al-O]$Rh(CO)_2Cl$ species to Rh^0 is complete at 100°C, some 120°C lower than under a helium atmosphere. As in the helium thermolysis experiment, the *gem* dicarbonyl species progresses to metal particles via a linear carbonyl species.

3.5.2 Energy Dispersive EXAFS studies of Reaction of $[Rh(CO)_2Cl]_2$ Supported on Alumina with Hydrogen

The Rh K-edge energy dispersive EXAFS experiment for the reaction of $[Rh(CO)_2Cl]_2$ supported on partially dehydroxylated alumina with hydrogen, was performed at the ESRF in Grenoble at station ID24. The samples were heated at a rate of 5°C per minute, under a flow of 5ml/min of hydrogen. Spectra were collected every 5 minutes until the temperature reached 400°C. The EXAFS spectra and their Fourier transforms for the thermolysis of $[Rh(CO)_2Cl]_2$ supported on partially dehydroxylated alumina are shown in figures 3.18 to 3.23. A stack plot for the hydogen thermolysis experiment is shown in figure 3.24.

Figure 3.18 shows the EXAFS and Fourier transform for the sample of $[Rh(CO)_2Cl]_2$ supported on alumina prior to exposure to hydrogen. This spectrum was acquired in 2.3 seconds. The EXAFS and Fourier transform strongly resemble that previously observed for the [Al-O]$Rh(CO)_2Cl$ species, and the data fits the model very well. The bond distances and coordination numbers are consistent with those of the previous sample (figure 3.4).

Figure 3.18 Rh K-Edge EXAFS and Fourier transform of $[Rh(CO)_2Cl]_2$ supported on Al_2O_3

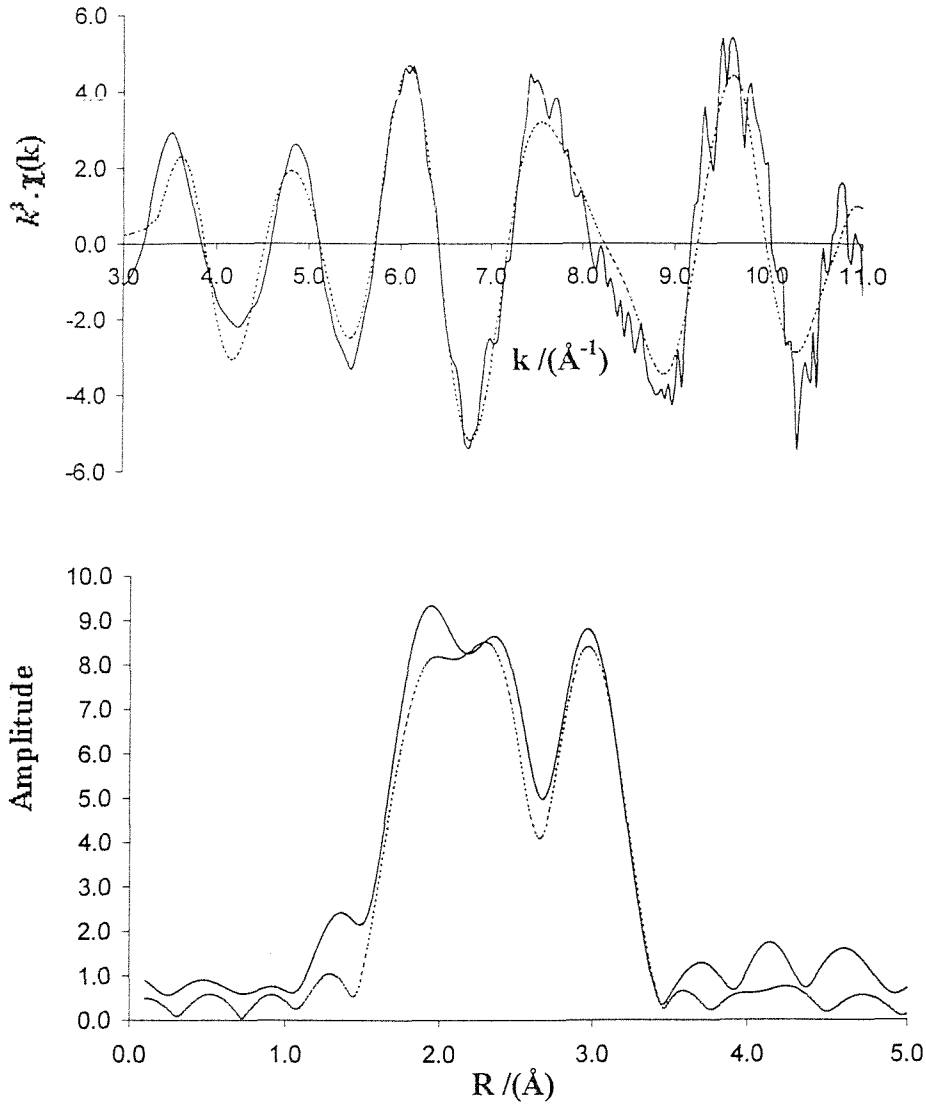

Atom	C.N.	r/Å	$2\sigma^2$ / Å^2
C	2(0.1)	1.893(3)	0.001(1)
O	1(0.2)	2.180(4)	0.005(1)
Cl	1(0.2)	2.390(2)	0.001(1)
O	2(0.1)	3.028(1)	0.011(4)
Al	1(0.2)	3.572(6)	0.031(2)

R = 33.08 %
Ef = 1.46 eV

Figure 3.19 shows the EXAFS and Fourier transform of the sample after exposure to hydrogen at room temperature for 30 minutes. The EXAFS and Fourier transform are virtually identical to that of the starting spectrum, and the data fits the [Al-O]Rh(CO)$_2$Cl model very well. There were no rhodium shells detected, nor a linear carbonyl species. These findings agree well with the results observed in the DRIFTS experiment, which were that the *gem* dicarbonyl species is still the dominant surface species after exposure to hydrogen at room temperature, despite some decomposition to a linear carbonyl species.

Figure 3.20 shows the EXAFS and Fourier transform of the sample after exposure to hydrogen at 57°C. The shape of the EXAFS is different to that of the starting species, in that there is greater intensity at higher energies, which is diagnostic of the presence of heavy backscatterering atoms such as rhodium. The Fourier transform has the basic shape of that of the [Al-O]Rh(CO)$_2$Cl species, but with greater intensity in the second and third peaks. These peaks correspond to the distances of the first and second rhodium shells in a rhodium cluster. Several models were used to try and fit to the data, including a linear carbonyl species and metal clusters. The best fit came from a model with a mixture of the *gem* dicarbonyl species and two shells of rhodium. The bond lengths of the *gem* dicarbonyl species are consistent with those found on the previous spectra in this experiment. The rhodium distances are at 2.74 and 3.80Å, which are consistent with the distances found in the bulk metal.

Figure 3.21 shows the EXAFS and Fourier transform of the sample after exposure to hydrogen at 102°C. The shape of the EXAFS is very similar to that of the previous spectrum, with more intense oscillations at higher energies. The Fourier transform again has a resemblance of the shape of the [Al-O]Rh(CO)$_2$Cl species, but also has peaks at the positions of rhodium-rhodium distances. After attempting a variety of possible models, the best fit was achieved by fitting a *gem* dicarbonyl species and a series of four rhodium shells. The coordination number was refined and it was found that these shells had increased in their respective coodination number relative to the spectrum acquired at 57°C. The bond distances for the *gem* dicarbonyl species and rhodium-rhodium distances are consistent with previous observations.

Figure 3.19 Rh K-Edge EXAFS and Fourier transform of $[Rh(CO)_2Cl]_2$ supported on Al_2O_3 after reaction with H_2 at room temperature for 30 minutes

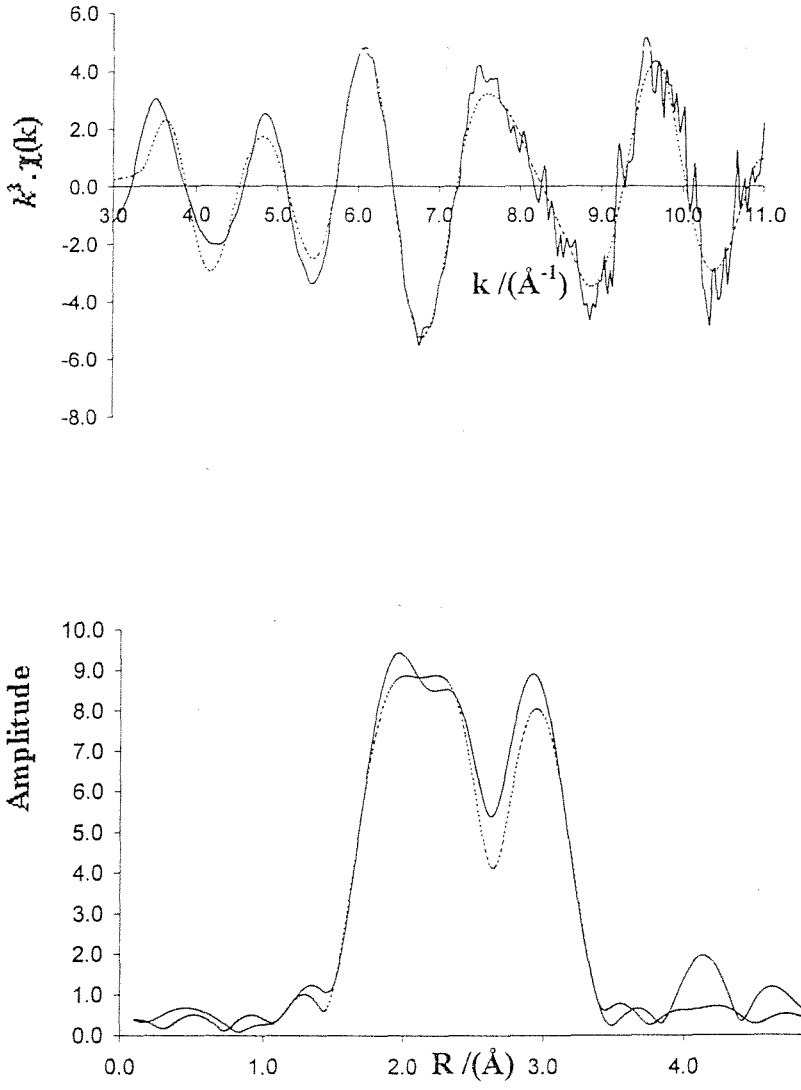

Atom	C.N.	r/Å	$2\sigma^2$ / Å^2
C	2(0.1)	1.885(2)	0.001(1)
O	1(0.2)	2.183(3)	0.001(1)
Cl	1(0.2)	2.391(2)	0.002(2)
O	2(0.1)	3.031(2)	0.016(4)
Al	1(0.2)	3.597(6)	0.014(3)

R = 28.11 %
Ef = 1.37 eV

Figure 3.20 Rh K-Edge EXAFS and Fourier transform of $[Rh(CO)_2Cl]_2$ supported on Al_2O_3 after reaction with H_2 at 57°C

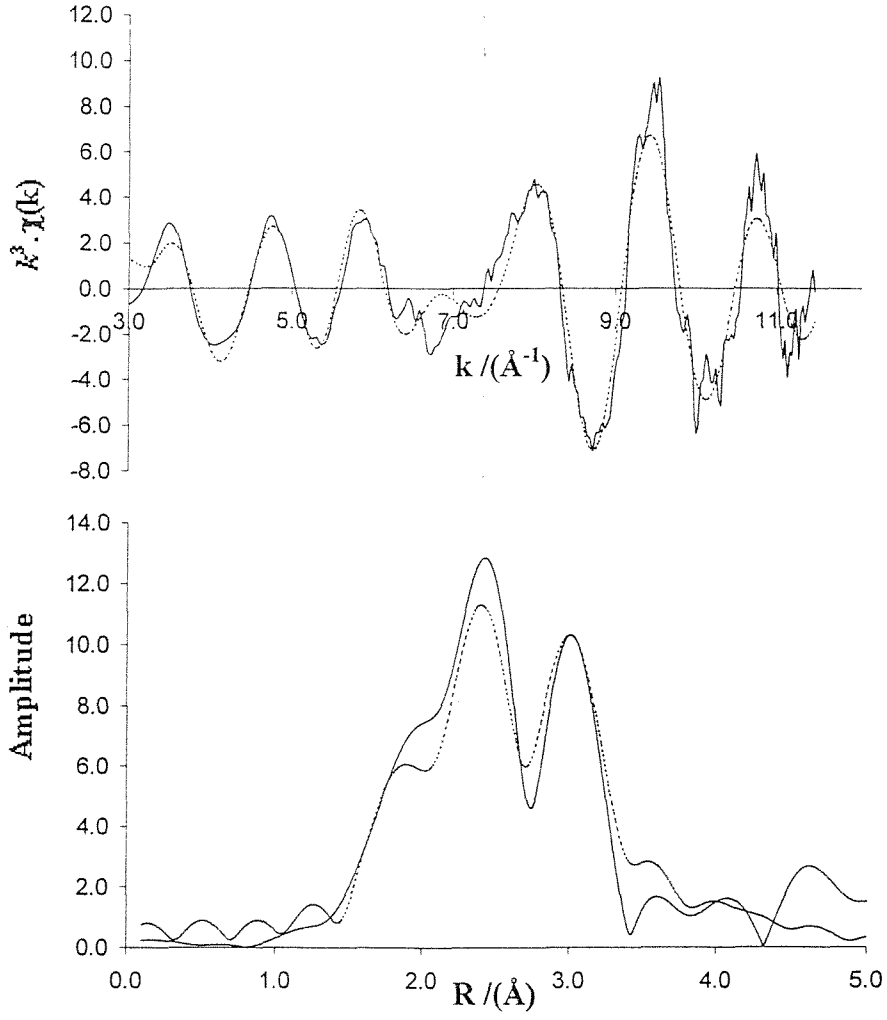

Atom	C.N.	r/Å	$2\sigma^2$ / Å^2
C	2(0.3)	1.893(3)	0.001(1)
O	1(0.2)	2.180(4)	0.002(1)
Cl	1(0.2)	2.390(2)	0.001(1)
Rh	4(1.1)	2.747(1)	0.019(4)
O	2(0.4)	3.038(4)	0.031(3)
Al	1(0.4)	3.625(5)	0.030(2)
Rh	2(1.3)	3.846(6)	0.024(2)

R = 33.50 %
Ef = 1.46 eV

Figure 3.21 Rh K-Edge EXAFS and Fourier transform of $[Rh(CO)_2Cl]_2$ supported on Al_2O_3 after reaction with H_2 at 102°C

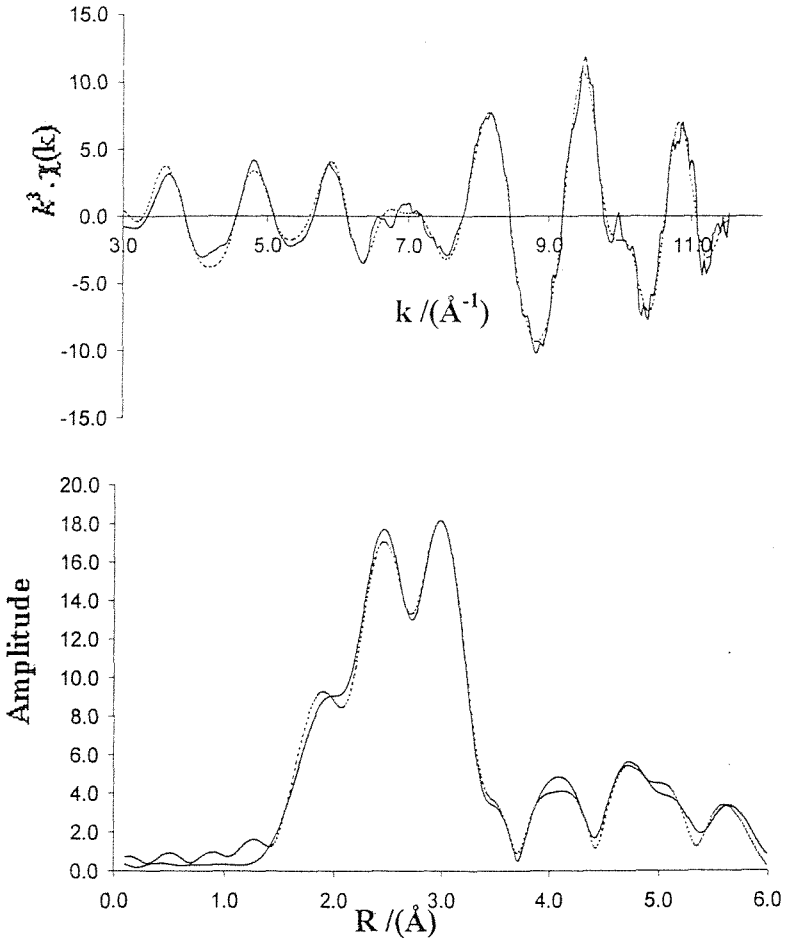

Atom	C.N.	r/Å	$2\sigma^2$ / Å^2
C	1(0.3)	1.893(3)	0.001(1)
O	1(0.2)	2.168(2)	0.002(1)
Cl	1(0.2)	2.351(4)	0.001(1)
Rh	9(1.7)	2.738(3)	0.019(4)
O	1(0.5)	3.042(4)	0.031(3)
Al	1(0.4)	3.635(4)	0.007(2)
Rh	6(1.4)	3.829(6)	0.023(2)
Rh	6(2.1)	4.768(4)	0.011(2)

R = 28.68 %
Ef = 0.55 eV

These findings are somewhat inconsistent with the observations in the corresponding DRIFTS experiment, which observes no rhodium carbonyl species at this temperature. Differences in results may be attributed to differing sample environment and temperature measurement. It is also possible that the differing timescale over which the experiments were conducted has an influence on the results obtained (EDE spectra are acquired in seconds as opposed to DRIFTS which take minutes.

Figure 3.22 shows the EXAFS and Fourier transform of the sample after exposure to hydrogen at 120°C. The shape of the EXAFS now very closely resembles that observed for bulk rhodium metal. There is now one main peak in the Fourier transform at 2.71Å, with smaller peaks at 3.78Å, 4.72Å and 5.34Å, which can all be attributed to coordination shells from the second, third and fourth coordination shells of rhodium respectively. There is no evidence in the Fourier transform of peaks in the position where carbonyl groups can be observed. Multiple scattering does not improve the fit, and it can therefore be inferred that the sample consists of rhodium clusters supported on the alumina surface. The coordination number was refined, and the results indicate that small rhodium clusters have formed. Only the first two coordination shells are fully occupied. These observations are in agreement with the DRIFTS experiment, which indicates that the reduction of the [Al-O]$Rh(CO)_2Cl$ surface species to rhodium clusters proceeds at much lower temperatures under a hydrogen atmosphere than an inert atmosphere. The reaction appears to proceed at 20°C higher in the EDE experiment, and there is no observation of the linear carbonyl species, which is observed as a reaction intermediate in the DRIFTS experiment. This could be due to differing temperature control, and rates of heat transfer in the two experiments

The spectra obtained at temperatures above 120°C were of poorer quality, but analysis showed that they consisted of rhodium particles with progressively greater cluster size and coordination number. Figure 3.23 shows the EXAFS and Fourier transform of the sample after exposure to hydrogen at 400°C, after the sample had cooled to room temperature. This spectrum shows the presence of five coordination shells.

Figure 3.22 Rh K-Edge EXAFS and Fourier transform of $[Rh(CO)_2Cl]_2$ supported on Al_2O_3 after reaction with H_2 at 120°C

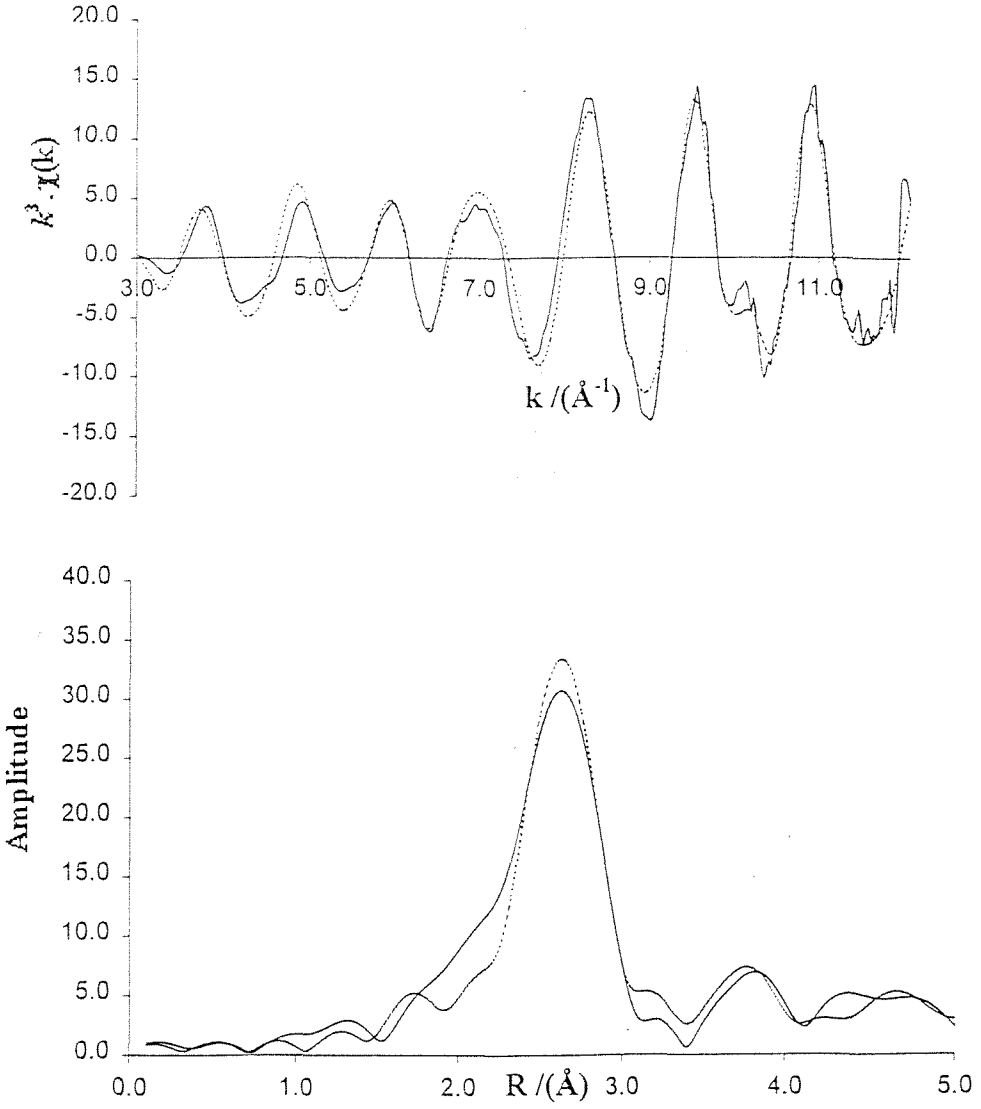

Atom	C.N.	r/Å	$2\sigma^2$ / Å^2
Rh	12(0.4)	2.705(2)	0.016(4)
Rh	6(1.1)	3.802(4)	0.016(2)
Rh	6(1.3)	4.720(3)	0.010(2)
Rh	4(1.3)	5.338(6)	0.007(4)

R = 24.51 %
Ef = 2.60 eV

Figure 3.23 Rh K-Edge EXAFS and Fourier transform for $[Rh(CO)_2Cl]_2$ supported on Al_2O_3 after reaction with H_2 at 400°C

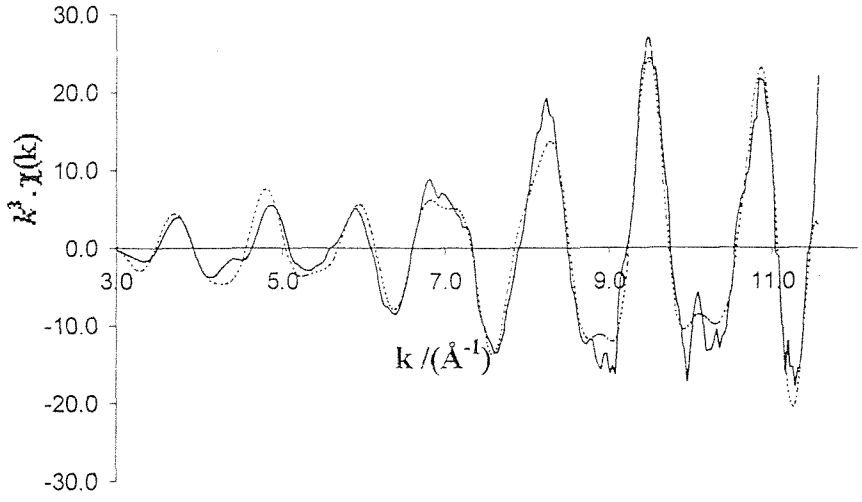

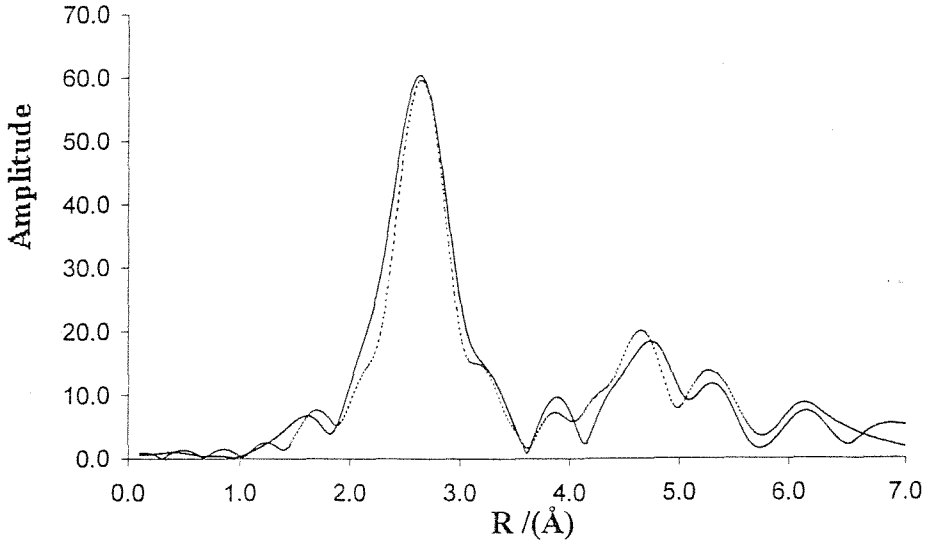

Atom	C.N.	r/Å	$2\sigma^2$ / Å^2
Rh	12(0.6)	2.725(1)	0.012(1)
Rh	6(1.1)	3.778(2)	0.022(1)
Rh	16(3.2)	4.759(2)	0.010(3)
Rh	10(1.5)	5.322(6)	0.008(2)
Rh	10(3.3)	6.012(5)	0.022(7)

R = 25.36 %
Ef =2.29 eV

Refining the coordination number reveals only the first two shells to be filled with twelve and six rhodium atoms respectively. The third shell has a coordination of twenty rhodium atoms, and the fourth and fifth both have ten rhodium atoms. This result contrasts with the analogous helium experiment, where after heating to 400°C, the first four coordination shells were completely filled, and the fifth had a coordination of twenty one rhodium atoms. This suggests that although the hydrogen causes reduction of the [Al-O]$Rh(CO)_2Cl$ species to rhodium particles at much lower temperature than helium, the clusters formed on prolonged heating are, on average, smaller in size.

Figure 3.24 shows a stack plot illustrating the progress of this reaction. It can be seen quite clearly that the number of oscillations in the spectra increases between 102 and 120°C. This is indicative of the presence of heavier backscattering atoms, and can therefore be correlated with rhodium metal particle formation on the alumina surface.

The experiment was repeated for another identical sample of 5% weight $[Rh(CO)_2Cl]_2$ supported on partially dehydroxylated alumina, to test the repeatability of the experiment. The data obtained was found to closely match that of the previous run, despite being of slightly inferior quality. The onset of metal particle formation was found to occur within the same temperature range, and the rhodium clusters formed were of comparable size to that found in the previous experiment.

A hydrogen thermolysis experiment was also attempted for a sample of 2% weight $[Rh(CO)_2Cl]_2$ supported on partially dehydroxylated alumina. The purpose of this experiment was to acertain any differences in the mode of decomposition of the *gem* dicarbonyl species, and formation of metal clusters. In particular, it was hoped the experiment would highlight differences in the sizes of the rhodium clusters formed relative to the 5% weight sample. The data quality in this experiment was much better than the helium analogue, and is thus presented.

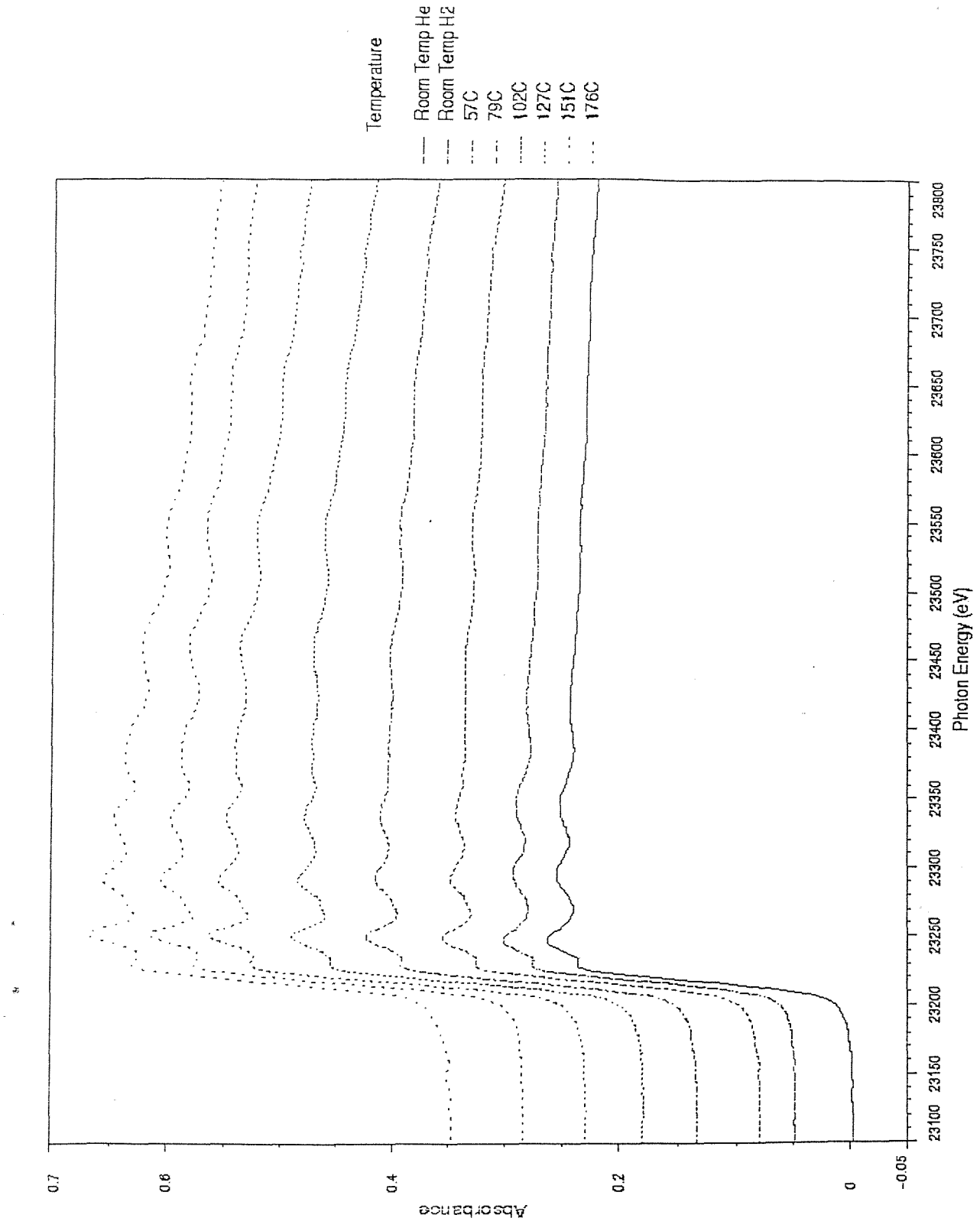

Figure 3.24 Stacked plot for hydrogen thermolysis of 5% $[Rh(CO)_2Cl]_2$ supported on Al_2O_3

Figure 3.25 shows the EXAFS and Fourier transform for the sample of $[Rh(CO)_2Cl]_2$ supported on alumina prior to exposure to hydrogen. The spectrum was acquired in 1.9 seconds. The EXAFS and Fourier transform strongly resemble that previously observed for the $[Al\text{-}O]Rh(CO)_2Cl$ species, and the data fits the model well at distances below 4Å.

Following the acquisition of the starting spectrum, the time resolved experiment was begun, in which 130 frames were taken, each with an acquisition time of 0.8 seconds. The sample was heated at a rate 5°C per minute, with a hydrogen flow of 5ml/min. Sets of 10 spectra were averaged in order to improve the signal to noise ratio of the data. The temperature variation between the first and last spectra was about 8°C.

Figure 3.26 shows the EXAFS and Fourier transform for the sample after heating to 100°C in hydrogen. The data still fits the $[Al\text{-}O]Rh(CO)_2Cl$ model well, though a variety of other models were used to try and fit the data to. This finding is in slight contrast to that at the same temperature for the 5% weight sample, in which rhodium clusters had begun to form in addition to remaining $[Al\text{-}O]Rh(CO)_2Cl$ species.

Figure 3.27 shows the EXAFS and Fourier transform for the sample after heating to 120°C in hydrogen. The shape of the EXAFS is similar to that of the previous spectrum, with more intense oscillations at higher frequencies. The Fourier transform again has a resemblance of the shape of the $[Al\text{-}O]Rh(CO)_2Cl$ species, but also has peaks at the positions of rhodium-rhodium distances. After attempting a variety of possible models, the best fit was achieved by fitting a *gem* dicarbonyl species and a series of four rhodium shells. The coordination number was refined to give the numbers shown in the table in figure 3.25. There are far fewer rhodium atoms in these shells than in the analogous experiment with the 5% weight sample, in which the first two rhodium shells are full.

Figure 3.28 shows the EXAFS and Fourier transform for the sample after heating to 140°C in hydrogen. The shape of the EXAFS now very closely resembles

Figure 3.25 Rh K-Edge EXAFS and Fourier transform of 2% $[Rh(CO)_2Cl]_2$ supported on Al_2O_3

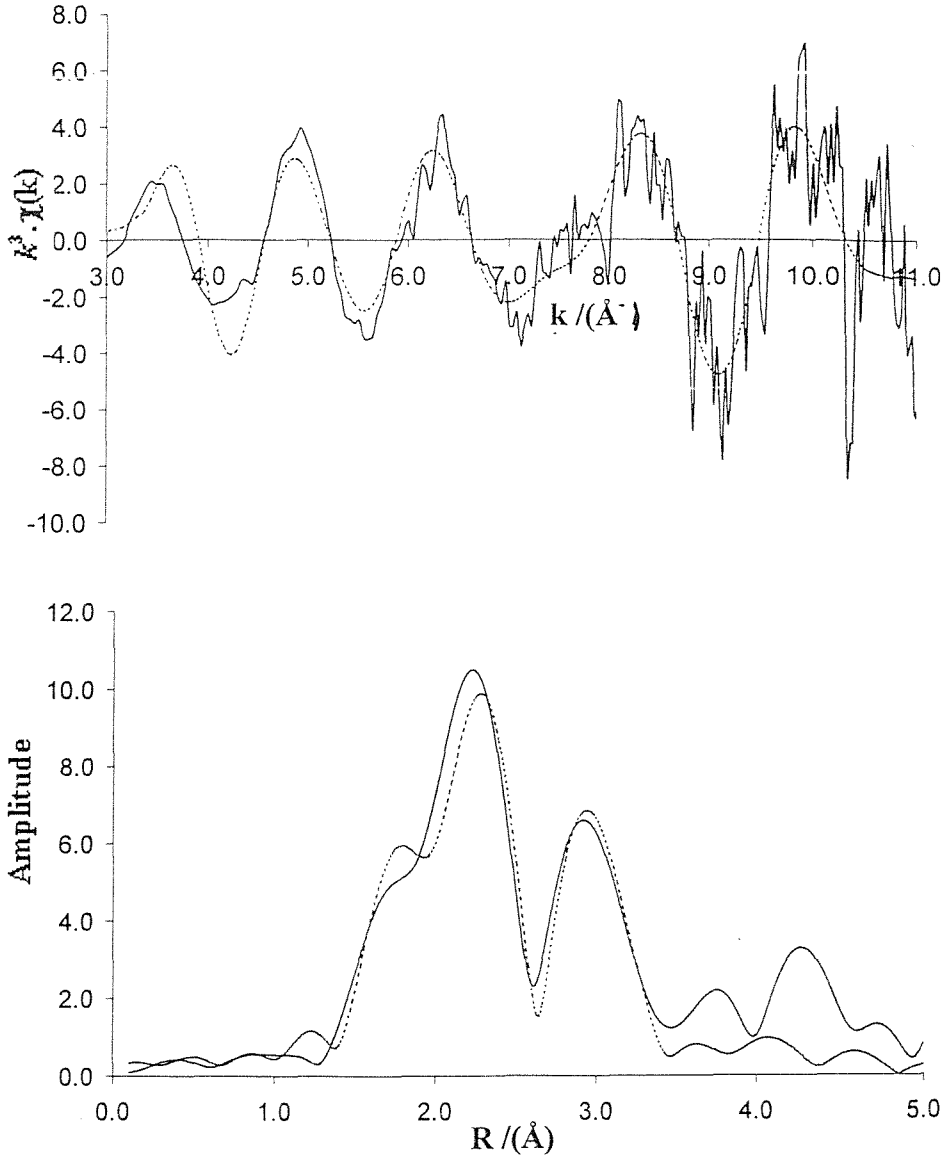

Atom	C.N.	r/Å	$2\sigma^2$ / Å^2
C	2(0.1)	1.884(2)	0.005(1)
O	1(0.1)	2.110(4)	0.009(1)
Cl	1(0.2)	2.347(3)	0.013(3)
O	2(0.2)	3.014(4)	0.020(1)
Al	1(0.3)	3.621(8)	0.029(3)

R = 55.24%
Ef = 0.79 eV

Figure 3.26 Rh K-Edge EXAFS and Fourier transform of 2% $[Rh(CO)_2Cl]_2$ supported on Al_2O_3 after reaction with H_2 at 100°C

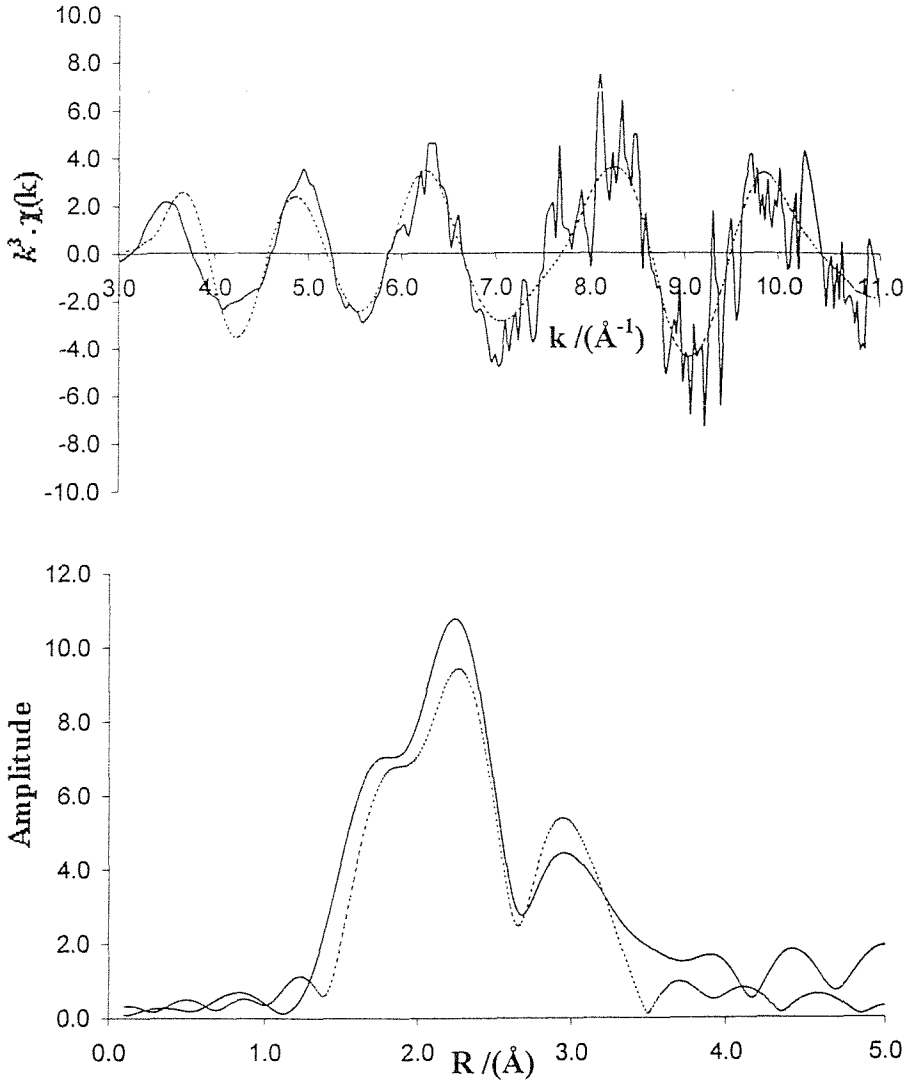

Atom	C.N.	r/Å	$2\sigma^2$ / Å^2
C	2(0.1)	1.884(2)	0.005(1)
O	1(0.1)	2.110(4)	0.002(1)
Cl	1(0.2)	2.347(3)	0.011(3)
O	2(0.2)	3.014(4)	0.023(1)
Al	1(0.3)	3.621(8)	0.028(3)

R = 48.01 %
Ef = 0.08 eV

Figure 3.27 Rh K-Edge EXAFS and Fourier transform of 2% $[Rh(CO)_2Cl]_2$ supported on Al_2O_3 after reaction with H_2 at 120°C

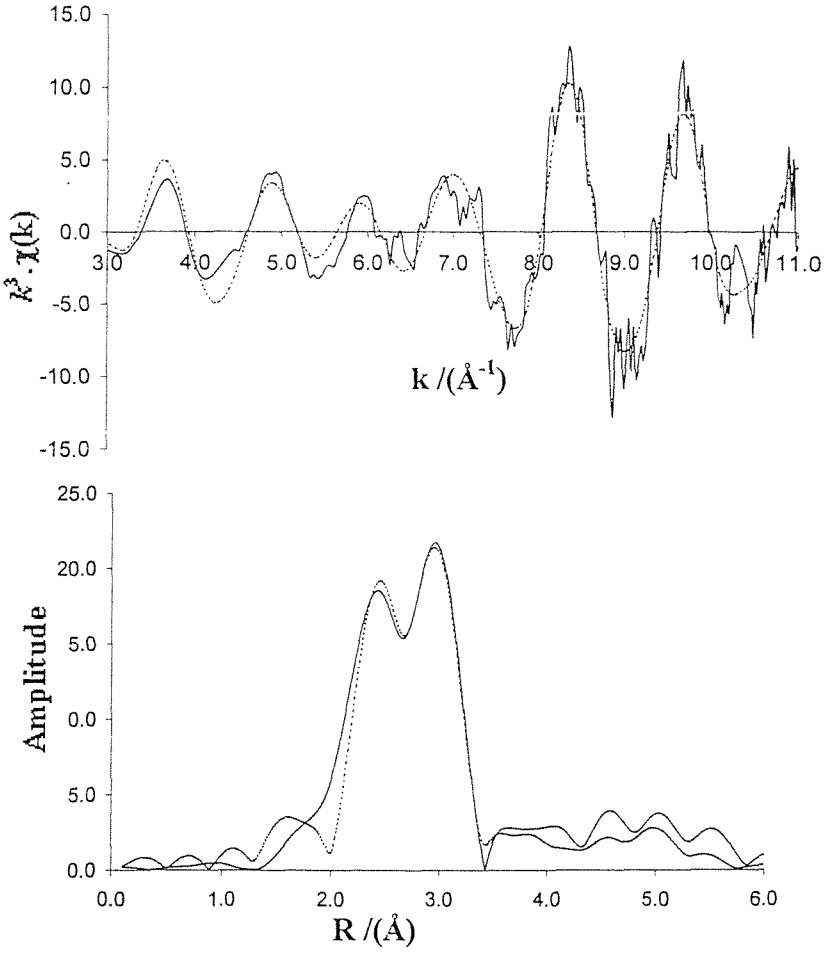

Atom	C.N.	r/Å	$2\sigma^2$ / Å^2
C	2(0.1)	1.885(2)	0.008(1)
O	1(0.1)	2.118(4)	0.001(1)
Cl	1(0.2)	2.357(3)	0.001(3)
Rh	8(1.2)	2.698(5)	0.017(2)
O	2(0.2)	3.027(4)	0.007(1)
Al	1(0.3)	3.646(8)	0.017(3)
Rh	4(0.9)	3.775(2)	0.024(2)
Rh	2(0.8)	4.628(3)	0.027(5)

R = 48.01 %
Ef = 0.06 eV

Figure 3.28 Rh K-Edge EXAFS and Fourier transform of 2% $[Rh(CO)_2Cl]_2$ supported on Al_2O_3 after reaction with H_2 at 140°C

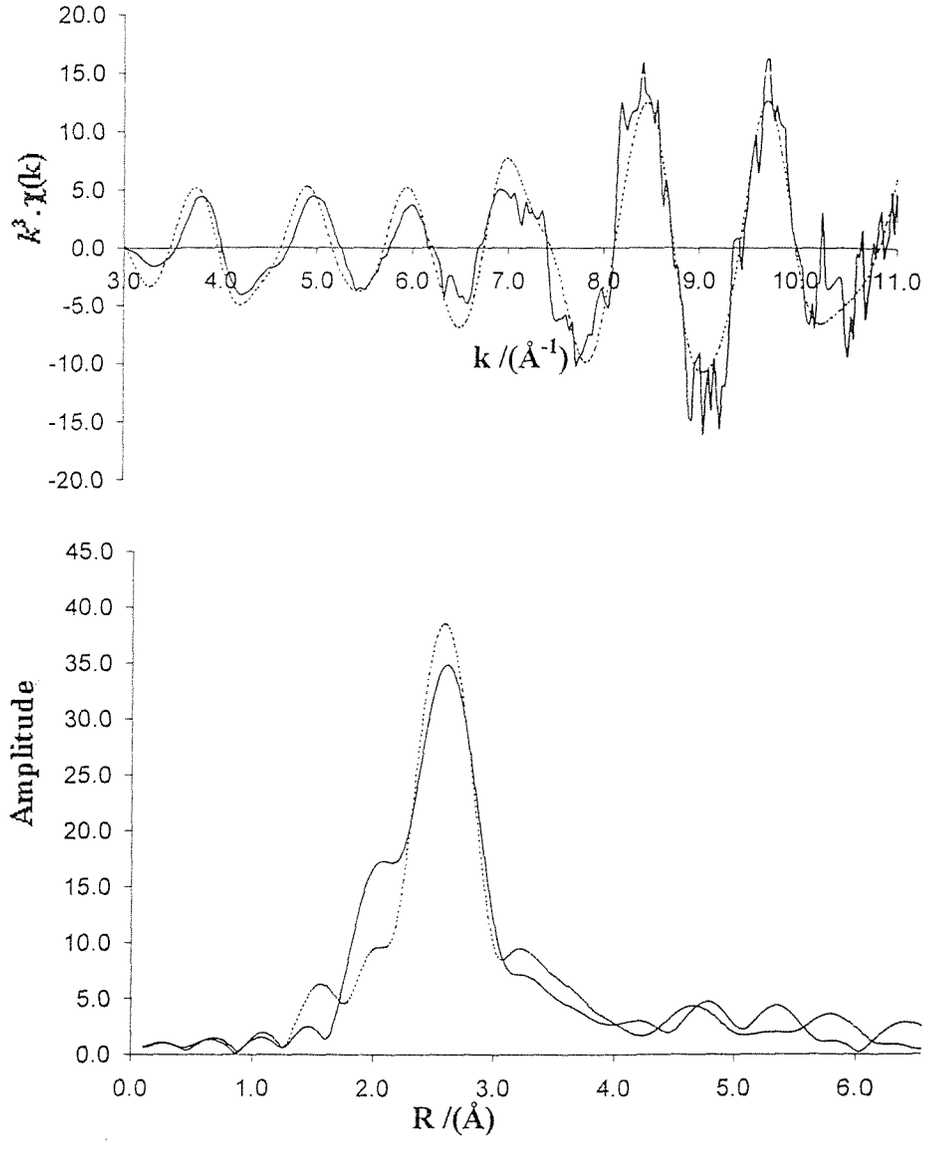

Atom	C.N.	r/Å	$2\sigma^2$ / Å^2
Rh	10(1.1)	2.679(2)	0.010(1)
Rh	6(1.3)	3.743(4)	0.009(1)
Rh	3(1.6)	4.634(3)	0.020(3)
Rh	2(1.2)	5.246(5)	0.022(2)

R = 43.03 %
Ef = 0.74 eV

that observed for bulk rhodium metal. There is now one main peak in the Fourier transform at 2.71Å, though it has a negative shoulder, and there are other smaller peaks in the positions expected for successive rhodium shells. Several fits were attempted, with a mixture of species, but the best was for a rhodium cluster with four shells. The coordination number was refined, and the first shell was still not found to be completely full. The second shell is almost full at this stage, and the third and fourth shells are beginning to fill.

Figure 3.29 shows the EXAFS and Fourier Transform for the sample after heating to 295°C in hydrogen. The data has been fitted to bulk rhodium metal, though the size of the clusters has hardly changed. Again, four rhodium shells have been fitted, and the coordination numbers in the third and fourth shells has only increased by two or three atoms. These results are consistent with the idea that samples with lower metal loading form smaller rhodium clusters upon thermolysis, due to the increased nearest rhodium neighbour distance. Unfortunately, a spectrum was not collected at 400°C in order to compare cluster sizes with the 5% weight analogue.

Figure 3.30 shows a stack plot of the thermolysis experiment, illustrating the transition to metal particles from the starting [Al-O]$Rh(CO)_2Cl$ species. It can be seen that the number of oscillations, which indicate metal particle formation, increases at 120-130°C.

3.5.3 TPD Study of the Hydrogen Thermolysis of $[Rh(CO)_2Cl]_2$ Supported on Alumina

The temperature programmed desorption study of the hydrogen thermolysis of $[Rh(CO)_2Cl]_2$ supported on partially dehydroxylated alumina was conducted using the microreactor in Southampton. The sample was heated under a flow of hydrogen at 5°C per minute, whilst the gaseous products were monitored by mass spectroscopy. The TPD profile in figure 3.31 indicates CO evolution peaks at 100°C and 130°C. The first of these peaks is much sharper than the analogous peak in the helium thermolysis TPD. The peak is again believed to correspond to the desorption of CO

Figure 3.29 Rh K-Edge EXAFS and Fourier transform of 2% $[Rh(CO)_2Cl]_2$ supported on Al_2O_3 after reaction with H_2 at 295°C

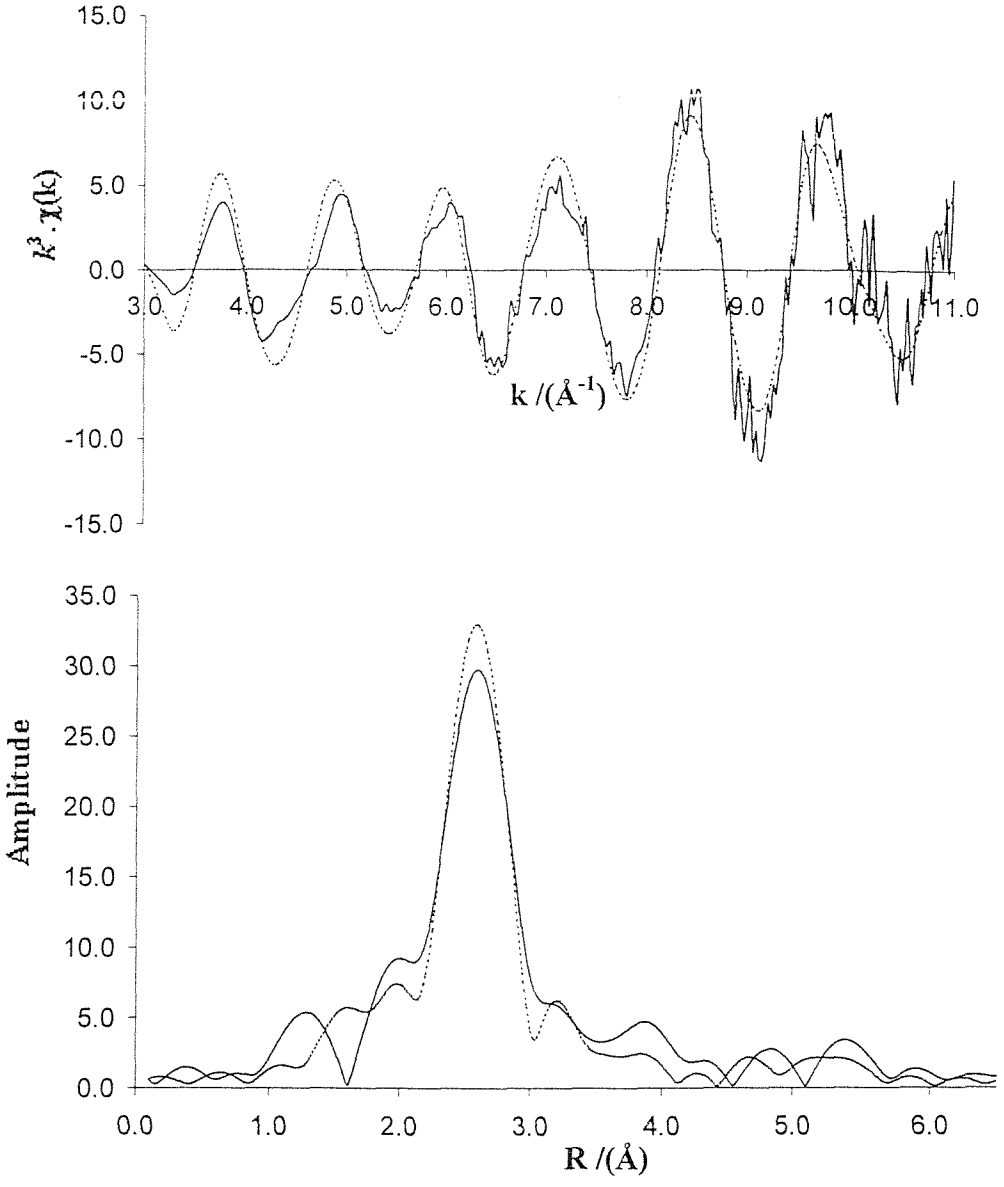

Atom	C.N.	r/Å	$2\sigma^2$ / Å^2
Rh	12(1.4)	2.665(2)	0.010(1)
Rh	6(1.5)	3.722(4)	0.010(1)
Rh	8(2.1)	4.640(3)	0.011(3)
Rh	6(2.0)	5.264(5)	0.018(2)

R = 38.89 %
Ef = -1.92 eV

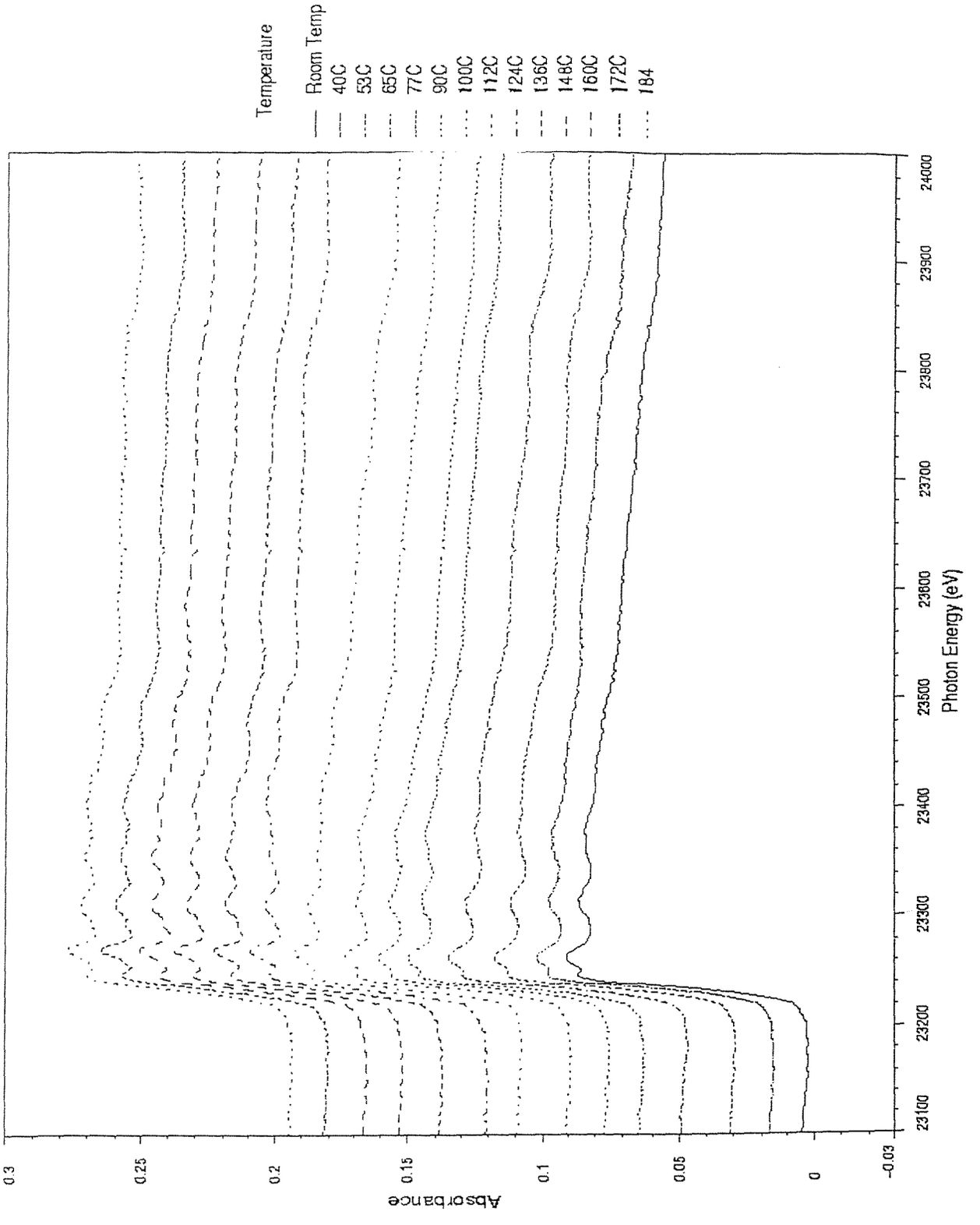

Figure 3.30 Stacked plot for hydrogen thermolysis of 2% $[Rh(CO)_2Cl]_2$ supported on Al_2O_3

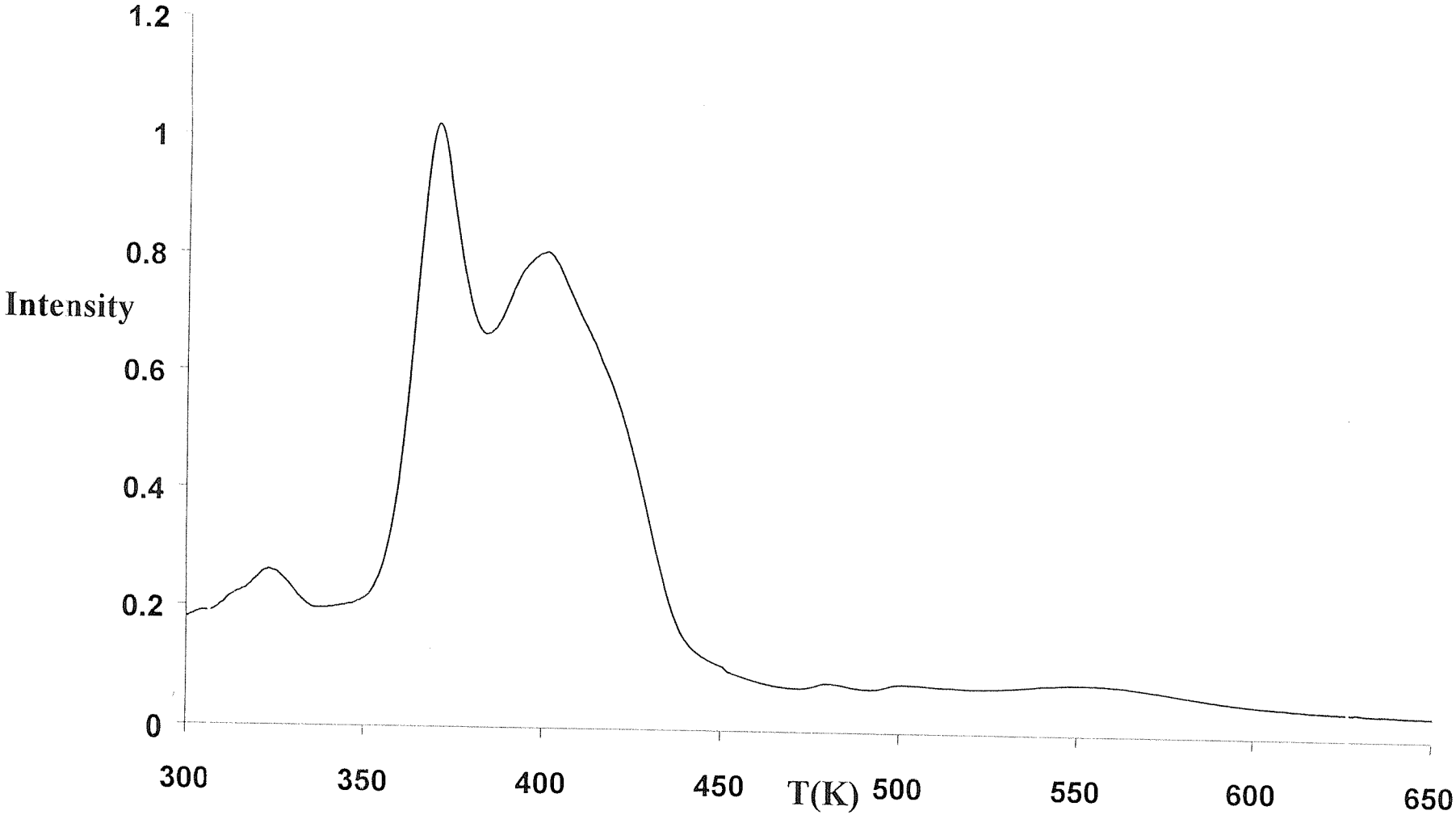

Figure 3.31 TPD profile for CO evolution (mass 28) during hydrogen thermolysis of 5% $[Rh(CO)_2Cl]_2$ supported on Al_2O_3

from the [Al-O]$Rh(CO)_2Cl$ surface species. The fact that it is sharper than in the helium thermolysis indicates that the reaction proceeds faster than in the former case, and that hydrogen is increasing the rate at which decarbonylation proceeds. Again this initial decarbonylation is believed to produce linear and bridging carbonyl species, evidenced by DRIFTS spectroscopy. The clustering of these electron deficient species, with the evolution of CO is believed to correspond to the main peak in the TPD profile, at 130°C.

3.6 Re-adsorption of CO onto Hydrogen Thermolysed Species

3.6.1 DRIFTS Study of Re-adsorption of CO onto Hydrogen Thermolysed Species

Following the hydrogen thermolysis of the $[Rh(CO)_2Cl]_2$ supported on partially dehydroxylated titania, the sample was exposed to one bar of CO for two hours at room temperature, in an attempt to regenerate the *gem* dicarbonyl species. Again, this experiment serves as a probe for investigation of the size of the rhodium clusters formed from the thermolysis experiment, as the type of rhodium carbonyl species formed is indicative of the cluster size.

After two hours of exposure to CO, there are three sets of bands visible in the DRIFTS spectrum, shown in figure 3.32. Approximately 50% of the *gem* dicarbonyl species has been regenerated, the frequencies of the symmetric and asymmetric bands being $2095cm^{-1}$ and $2027cm^{-1}$ respectively. There is an intense, sharp band at $2072cm^{-1}$, which is attributed to a linear carbonyl species. There is also a broad band at $1850cm^{-1}$ to $1890cm^{-1}$, which is attributed to a bridging carbonyl species. As discussed in section 3.4.1, the *gem* dicarbonyl species only forms on monodispersed rhodium atoms. The monodispersion process can only be fulfilled by CO for small rhodium clusters. The fact that 50% of the *gem* dicarbonyl species is regenerated suggests that the hydrogen thermolysis to 100°C generates approximately this

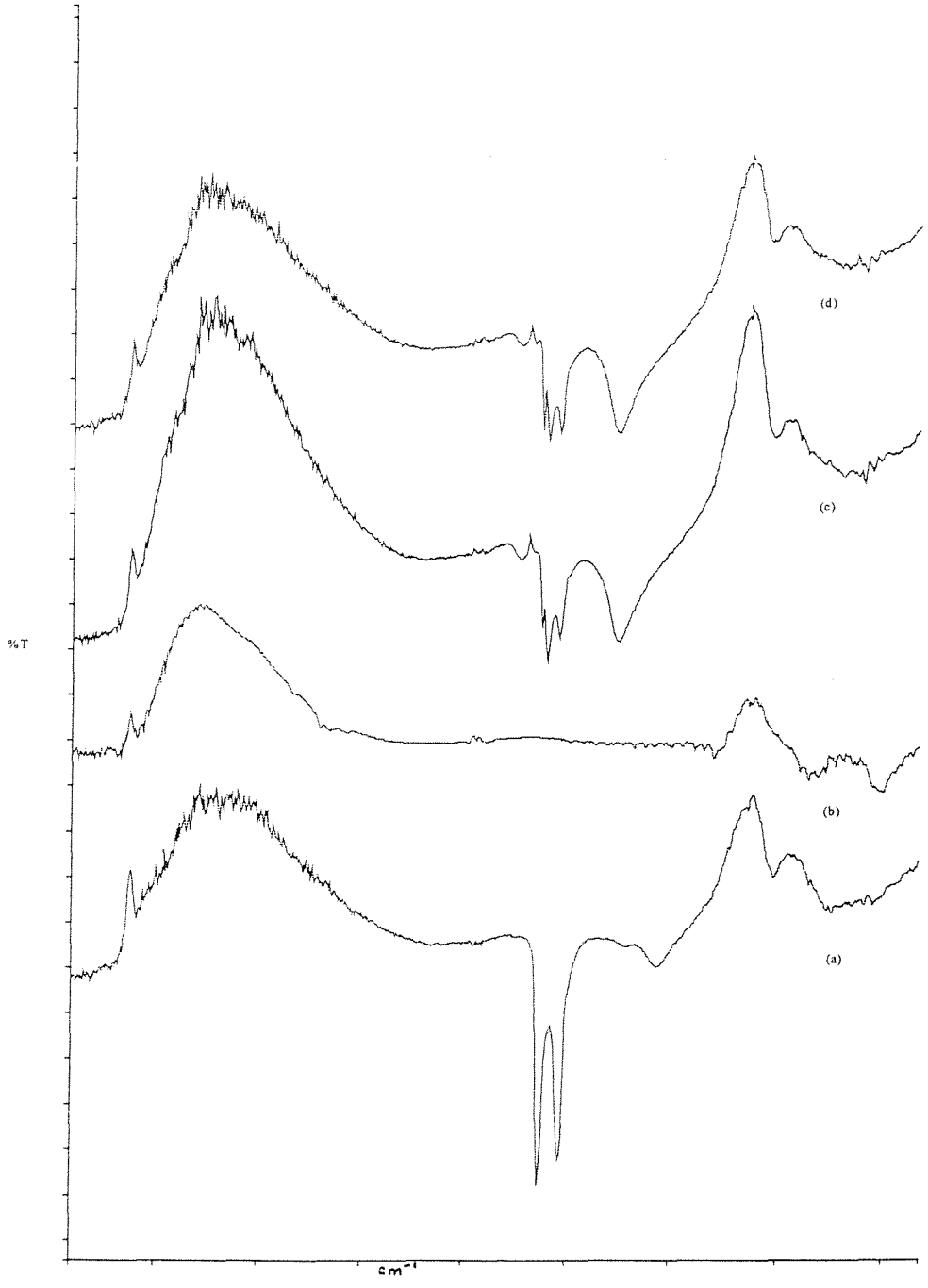

Figure 3.32 DRIFTS difference spectra of CO regeneration of $[Rh(CO)_2Cl]_2$ supported on partially dehydroxylated titania after hydrogen thermolysis. (a) Room temp before thermolysis, (b) Post thermolysis, (c) CO regeneration after 1hr, (d) CO regeneration after 2hrs.

proportion of small rhodium clusters. The linear and bridging carbonyl species are more commonly found on larger rhodium particles, and thus it can be assumed that these exist on such larger clusters in this experiment. The conclusion is that the hydrogen thermolysis to 100°C generates predominately small rhodium clusters, which are easily redispersed by CO at room temperature. There are however, a number of larger rhodium clusters formed at this temperature. The results of this experiment agree well with the EDE study of the hydrogen thermolysis, which showed the presence of rhodium clusters at 100°C, although the carbonyl ligands were not fully removed until a temperature of 120°C had been reached.

3.6.2 EDE Study of Re-adsorption of CO onto Hydrogen Thermolysed Species

Following the hydrogen thermolysis to 120°C of $[Rh(CO)_2Cl]_2$ supported on partially dehydroxylated alumina, the sample was exposed to 4bar of CO for 1 hour at room temperature, at a flow rate of 5ml/min. The EXAFS and Fourier transform spectrum after CO exposure was acquired in 1 second, and is shown in figure 3.33. The shape of the EXAFS and the Fourier transform strongly resembles that of bulk rhodium metal.

3.7 Conclusions

EXAFS and DRIFTS spectroscopies indicate that $[Rh(CO)_2Cl]_2$ is chemisorbed to the TiO_2 and Al_2O_3 surface. The chlorine is retained as the dimer is broken to produce a $[O]Rh(CO)_2(Cl)$ species. Surface hydroxyl groups are consumed during the adsorption process, evidenced by DRIFTS spectroscopy. Thermolysis of the surface species under an inert helium atmosphere, results in removal of the gem-dicarbonyl ligands by 220°C, evidenced by EDE, DRIFTS and TPD. The process of removal of the gem-dicarbonyl ligands involves passing through a linear carbonyl intermediate, evidenced by DRIFTS spectroscopy. EDE spectroscopy indicates the

Figure 3.33 Rh K-Edge EXAFS and Fourier transform of $[Rh(CO)_2Cl]_2$ supported on Al_2O_3 after H_2 reaction at 130°C and exposure to CO for 30 mins

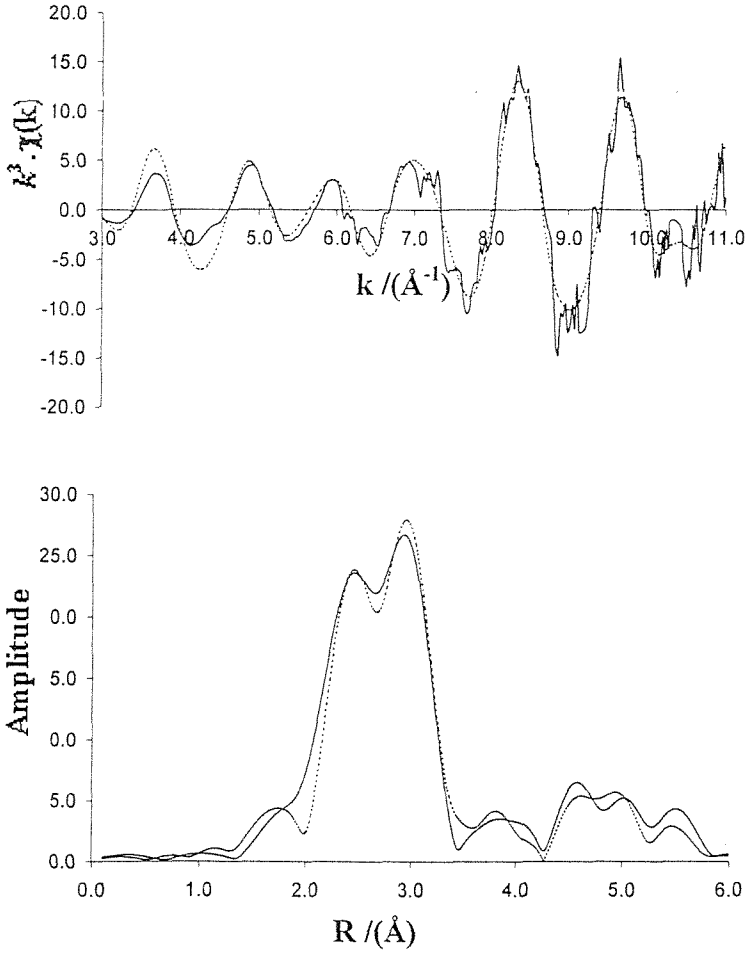

Atom	C.N.	r/Å	$2\sigma^2$ / Å^2
C	2(0.1)	1.871(2)	0.009(1)
O	1(0.1)	2.117(4)	0.001(1)
Cl	1(0.2)	2.377(3)	0.005(3)
Rh	12(1.2)	2.691(5)	0.019(2)
O	2(0.2)	3.027(4)	0.020(1)
Al	1(0.3)	3.646(8)	0.001(3)
Rh	5(0.9)	3.788(2)	0.019(2)
Rh	6(0.8)	4.661(3)	0.016(5)

R = 39.36 %
Ef = 0.50 eV

formation of small rhodium clusters during the thermolysis experiment. Re-exposure of the thermolysed sample to CO at room temperature results in 70% regeneration of the gem-dicarbonyl species, evidenced by DRIFTS spectroscopy. Thermolysis under a hydrogen atmosphere results in removal of the gem-dicarbonyl ligands by 100°C, again via a linear carbonyl intermediate. EDE spectroscopy again shows the formation of rhodium clusters during the hydrogen thermolysis. It was observed that heating to 400°C in helium led to larger clusters being formed than under hydrogen at the same temperature, despite the initial formation of clusters at lower temperatures under hydrogen. It was also observed that smaller clusters were formed during hydrogen thermolysis, for a 2% weight sample, than for a 5% weight sample. Re-exposure to CO results in the formation of a mixture of gem-dicarbonyl, linear and bridging carbonyl species, evidenced by DRIFTS spectroscopy.

3.8 Experimental

The synthesis of $[Rh(CO)_2Cl]_2$ follows the method of McCleverty and Wilkinson[30], in which a flow of CO is passed through $RhCl_3.nH_2O$ at 95°C for two hours:

$$2(RhCl_3.nH_2O) + 6CO \rightarrow [Rh(CO)_2Cl]_2 + 6H_2O + 2CO + 2Cl_2$$

The reaction was conducted in a glass tube, containing a medium porosity frit on which the starting material is placed. The sample is lowered into an oil bath and care taken such that the reaction temperature does not exceed 100°C, which would lead to the formation of unreactive $RhCl_3$. Carbon monoxide was flushed slowly through the system. For the first 5-10 minutes of the reaction, the evolved water was removed from the sides of the reaction vessel, which was required since the moisture sensitive product will sublime up the sides of the tube. After 1-4 hours, the product was collected by means of scraping it out of the reaction vessel with a spatula. The product is further purified by sublimation, resulting in the formation of red needles of the product. The purified sample was characterised by infrared spectroscopy in

pentane (see section 3.2.1): 2105cm^{-1} (m), 2090cm^{-1} (vs), 2080cm^{-1} (satellite), 2035cm^{-1} (s), 2003cm^{-1} (satellite).

Preparation of the surface supported organometallic species for DRIFTS and EXAFS studies, by MOCVD involved deposition of $[Rh(CO)_2Cl]_2$ (50-60 mg) onto partially dehydroxylated titania (Degussa P25, 0.5g) or γ alumina (Degussa, 0.5g), according to the general procedure given in section 2.7. Heating the organometallic sample to 50°C for 2 hours caused sublimation, resulting in the titania becoming a reddish brown colour, or the alumina becoming a deep yellow colour. The sample was treated as air sensitive as was thus stored in a Schlenk tube under an argon atmosphere, and refrigerated until used.

3.9 References

1. L. F. Dahl, C. Martell and D. L. Wampler, *J. Am. Chem. Soc.*, 1961, **83**, 525.
2. P. M. Lausarot, G. A. Vaglio and M. Valle, *J. Organomet. Chem.*, 1981, **204**, 249.
3. J. M. Basset, A. Theolier, D. Commeruec and Y. Chauvin, *J. Organomet. Chem.*, 1985, **279**, 147.
4. A. K. Smith, F. Hughes, A. Theolier, J. M. Basset, R. Ugo, G. M. Zanderighi, J. L. Bilhou, V. Bilhou-Bougnal and W. F. Graydon, *Inorg. Chem.*, 1979, **18**, 3104.
5. J. Evans, B. E. Hayden, F. Mosselmans and A. Murray, *Surf. Sci.*, 1992, **279**, L159.
6. J. Evans, B. E. Hayden, F. Mosselmans and A. Murray, *J. Am. Chem. Soc.*, 1992, **114**, 6912.
7. J. Evans, B. E. Hayden, F. Mosselmans and A. Murray, *Surf. Sci.*, 1994, **301**, 61.
8. N. A. Williams, PhD Thesis, University of Southampton, 1992.
9. C. J. Rudkin, PhD Thesis, University of Southampton, 1997.
10. J. L. Robbins, *J. Phys. Chem.*, 1986, **90**, 3381.
11. P. Johnson, R. W. Joyner, P. D. A. Pudney, E. S. Shpiro and B. P. Williams, *Faraday Discuss. Chem. Soc.*, 1990, **89**, 91.
12. F. Solymosi, I. Tombacz and M. Kocsis, *J. Catal.*, 1982, **75**, 78.
13. S. D. Jackson, B. J. Brandreth and D. Winstanley, *J. Chem. Soc. Faraday Trans.*, 1988, **84**, 1741.
14. S. D. Worley, C. A. Rice, G. A. Mattson, C. W. Curtis, J. A. Guin and A. R. Tarrer, , *J. Phys. Chem.*, 1982, **76**, 20.
15. E. A. Hyde, R. Rudham and C. H. Rochester, *J. Chem. Soc. Faraday Trans.*, 1983, **79**, 2405.
16. K. Gilhooley, S. D. Jackson and S. Rigby, *J. Chem. Soc. Faraday Trans.*, 1986, **82**, 431.
17. C. E. Barnes, M. Ralle, S. A. Vierkotter and J. E. Penner-Hahn, *J. Am. Chem. Soc.*, 1995, **117**, 5861.
18. S. D. Worley, G. A. Matteson and R. A. Caudhill, *J. Phys. Chem.*, 1983, **87**, 1671.
19. T. Ionnides, and X. Verykios, *J. Catal*, 1993, **140**, 353.
20. J. A. Chudek, M. W. McQuire and C. H. Rochester, *J. Catal*, 1992, **135**, 358.
21. Z. L. Zhang, A. Kladi and X. E. Verykios, *J. Mol. Catal.*, 1994, **89**, 229.

22. B. E. Hayden, M. A. Newton and A. King and N. Yoshikawa, Submitted to *J. Phys Chem.*.

23. K. C. Taylor, *Catal. Rev. Sci-Eng.*, 1993, **35**, 457.

24. W. Hecker and A. T. Bell, *J. Catal*, 1983, **84**, 200.

25. H. Arai and H. Tominga, *J. Catal*, 1975, **43**, 131.

26. G. Srinivas, S. Chuang and S. Debnath, *J. Catal*, 1994, **148**, 748.

27. N. Binsted, S. J. Gurman, J. W. Campbell and P. C. Stephenson, *EXCURV98, EPSRC Daresbury Laboratory Computer Program,* **1992**.

28. D. C. Koningsberger, J. T. Miller and B. L. Mojet; *J. Phys. Chem.*, 1999, **103**, 2724-2734.

29. D. C. Koningsberger, J. Vanzon, H. F. J. Vanblik and D. E. Sayers, *J. Phys. Chem.*, 1983, **87**, 2264-2267.

30. J. A. McCleverty and G. Wilkinson, *Inorg. Synth.*, 1965, **8**, 211.

Chapter 4

Reaction of $[Rh(CO)_2Cl]_2$ Supported on TiO_2 and Al_2O_3, with NO

4.1 Introduction

Automobiles are among the highest producers of the pollutants CO, NO, hydrocarbons, particulates and oxidants. A 'three way catalyst' simultaneously promotes the removal of each of the three major pollutants, namely CO, NO and hydrocarbons[1-7].

Platinum, which in 1992 found 34% of its total usage in such automotive catalysts[8,9], serves as an effective catalyst for the oxidation of CO and hydrocarbons[7,8]. Rhodium, which in the same year, found 87% of its usage in automotive catalysts[8,9], is superior for reduction of NO to N_2[10].

Schemes for the net reactions of the above catalysts are shown below:

$$2NO + 2CO \rightarrow N_2 + 2CO_2 \quad (1)$$

$$2NO + CO \rightarrow N_2O + CO_2 \quad (2)$$

The homogeneous analogue of reaction 2 is facilitated by $[Rh(CO)_2Cl]_2$[11], which is an active species in this reaction.

The heterogeneous systems are typically more complex than the homogeneous analogues, and NO reactions are observed to exhibit temperature and dispersion dependent behaviour. Dissociation of NO on rhodium is rate limiting due to low concentrations of clusters of sufficient size to facilitate the reaction[11].

$$NO_a \rightarrow N_a + O_a \quad (3)$$

However, larger clusters formed by raising the temperature of the system, permit the dissociation to occur with greater ease[12].

The recombination of N_a to form N_2 is also dependent on particle size:

$$2N_a \rightarrow N_{2(g)} \quad (4)$$

The reaction proceeds rapidly on large particles, and higher temperatures are required to facilitate the reaction on small particles.

There have been several investigations of the reaction of NO with high area supported Rh systems[14-22]. Several rhodium nitrosyl species have been observed in these investigations including $Rh(NO^+)$, $Rh(NO)$, $Rh(NO^-)$ and $Rh(NO)_2$. See table 4.1 for references to above species. See also 3.1.3 for a detailed discussion of some of the above studies. An isocyanate species has also been observed upon co-adsorption of CO and NO onto high area supported Rh systems[14,19,20].

The above studies have shown that the pre-treatment of the Rh affects the type of nitrosyl species formed. NO has also been shown to facilitate the disruption of Rh clusters, aiding the formation of monodipersed $Rh(CO)_2$ in the presence of CO[15,16,17].

A bridge bonded NO species has been postulated in single crystal UHV studies[23,24,25]. The validity of this claim, however, has been challenged by temperature programmed static-SIMS[26], core-level X-ray photoelectron diffraction (XPD)[27] and theoretical calculations[28], suggesting that hollow sites ($\nu \approx 1640cm^{-1}$-$1544cm^{-1}$) may also be likely.

Table 4.1 shows the infrared frequency of CO and NO species observed in previous work on Rh/NO/CO systems. This table has been provided by Dr M. A. Newton, from a pre publication version of reference 29.

Adsorbed Species	**Frequency (cm^{-1})**	**Support and References**
$Rh_2(CO)$ bridge	1900-1830	Al_2O_3[14], SiO_2[15], $TiO_2(110)$[30]
$Rh_x(CO)$ $(x \geq 2)$ linear	2020-2090	Al_2O_3[14], SiO_2[15,16], $TiO_2(110)$[16]
$Rh_2(CO)_3$ bridge	1818	Al_2O_3[31]
$Rh_2(CO)_3$ linear	1987	Al_2O_3[31]

$Rh(CO)_2$ (ν_{sym})	2108 (2112)	Al_2O_3[14,18-21], SiO_2[15-17], $TiO_2(110)$[30]
$Rh(CO)_2$ (ν_{asym})	2040 (2030)	Al_2O_3[14,18-21], SiO_2[15-17], $TiO_2(110)$[30]
$Rh(NO)^+$	1910-1930	Al_2O_3[14,18-21], SiO_2[15-17], $TiO_2(110)$[30]
$Rh(NO)_2$ (ν_{sym})	1820-1830	Al_2O_3[14,18,21], SiO_2[17]
$Rh(NO)_2$ (ν_{asym})	1740	Al_2O_3[14,19,21], SiO_2[17]
Rh(NO)(CO) (ν_{CO})	2101	Al_2O_3[14,19,20]
Rh(NO)(CO) (ν_{NO})	1755	Al_2O_3[14,19,20]
Rh(NO)	1830	Al_2O_3[14,17,21]
$Rh(NO)^-$	1770-1710	Al_2O_3[14,19-22], SiO_2[15,16]
$Rh_2(NO)$ bridge	1630, 1560-1710	Rh(111)[26], Rh(110)[24]
$Rh_3(NO)$ hollow sites	1644-1690	Theory[28]
(NCO)	2260, 2235	Al_2O_3[14,19-22], SiO_2[15]
N_2O	2225	Al_2O_3[14,19], SiO_2[15]
CO_3^{2-}	1385, 1440, 1580	Al_2O_3[20]
NO_2^- or NO_3^-	1550	Al_2O_3[30], SiO_2[17]

Table 4.1 Transmission Infrared Frequencies for rhodium carbonyl and nitrosyl species on both high area and single crystal systems.

4.2 Reaction of $[Rh(CO)_2Cl]_2$ Supported on TiO_2 and Al_2O_3 with NO followed by CO, at Room Temperature

4.2.1 DRIFTS Study of Reaction of $[Rh(CO)_2Cl]_2$ Supported on TiO_2 and Al_2O_3 with NO followed by CO, at Room Temperature

$[Rh(CO)_2Cl]_2$ was supported on partially dehydroxylated titania with a 5% metal loading, by MOCVD (method described in sections 2.6 and 3.7). Following this, a difference DRIFTS spectrum was acquired, using hydroxylated titania as a background, figure 4.1(a). A discussion of the assignments of the infrared bands in the

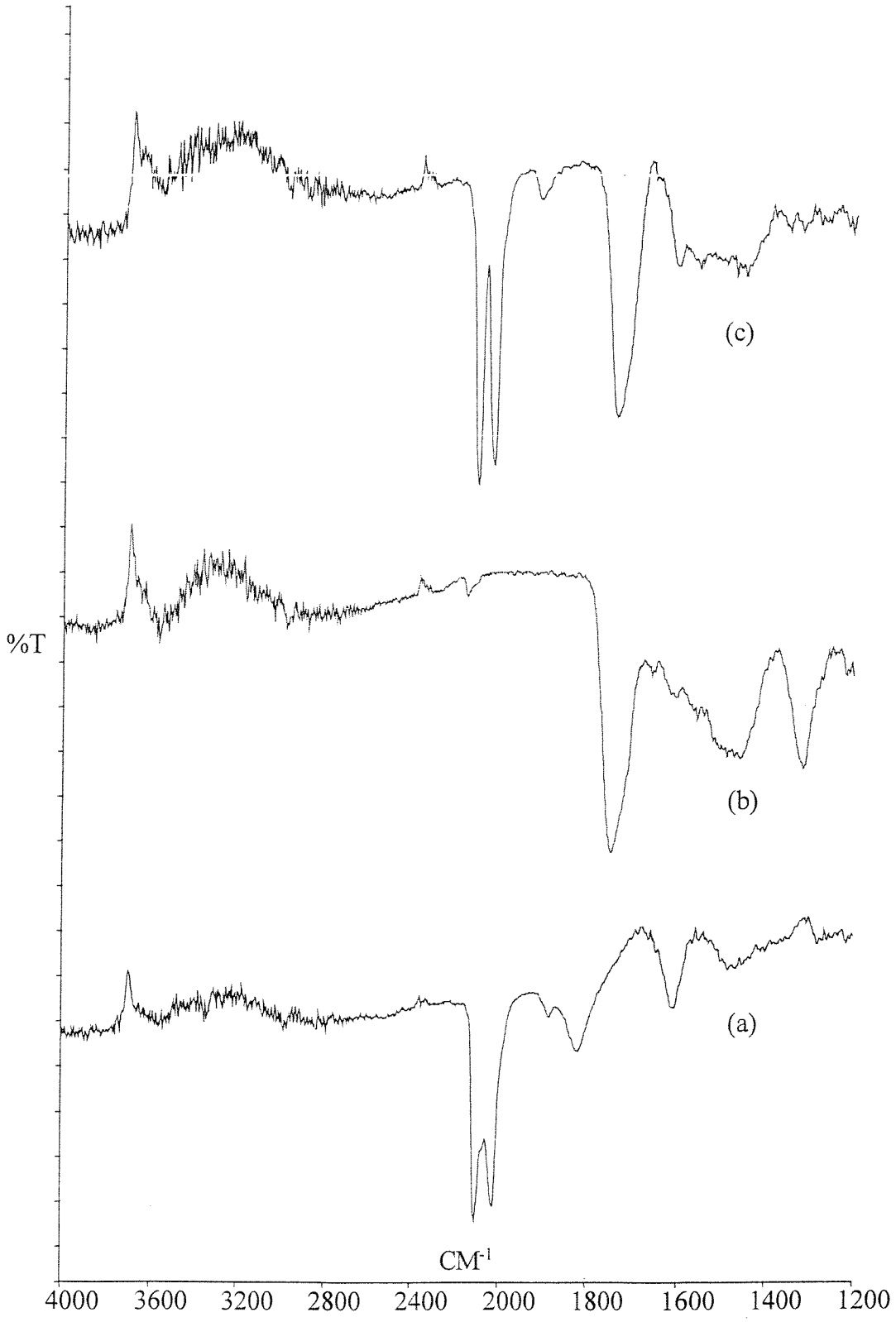

Figure 4.1 DRIFTS difference spectra of reaction of $[Rh(CO)_2Cl]_2$ supported on TiO_2 with NO and CO at room temp: (a) Before exposure to NO, (b) After reaction with NO for 30 mins, (c) After reaction with CO for 2 hrs.

spectrum is found in section 3.2.1. In addition to the *gem* dicarbonyl species present there also appears to be bridging rhodium carbonyl species $Rh_2(CO)_3$ present at 1840cm^{-1}, and a surface carbonate species (and possibly surface water) at 1600cm^{-1}. These may arise from slight reduction of the rhodium *gem* dicarbonyl species, and have been observed in differing degrees in the starting spectra of several analogous experiments. Their presence has not been observed to affect the subsequent reaction of the *gem* dicarbonyl species with NO, discussed below.

The supported sample was loaded into the DRIFTS cell under an inert atmosphere, and was exposed to 1 bar of NO at a flow rate of 5 ml/min for a period of 20 minutes, at room temperature. Following this, the DRIFTS cell was flushed with helium for 5 minutes to remove any gaseous products and unreacted NO. The resulting spectrum acquired is shown in figure 4.1(b). The spectrum shows a strong, broad band at 1742cm^{-1}, which is assigned to a $Rh(NO)^-$ species. There is another small peak at 2145cm^{-1}, which is possibly an [O]Rh(NO)(CO)(Cl) species (Cl and surface O ligands included for completeness). The shape of this feature shows two components. This can be interpreted as being due to two possible isomers. In one isomer the NO species is trans to the surface oxygen, and in the other the NO is trans to the Cl, with the higher frequency component being due to the latter situation. Peaks at 1458cm^{-1} and 1313cm^{-1} are assigned to surface nitrate/nitrite species, i.e. interaction of NO with surface alumina sites. Refer to Table 1 for infrared assignments. There is no evidence of the prevalence of the rhodium *gem* dicarbonyl species after exposure to NO, and indeed the band was observed to diminish in intensity as spectra were acquired during exposure to NO. The conclusion drawn from this experiment is that substitution of the rhodium *gem* dicarbonyl species for a $Rh(NO^-)$ species, and a Rh(NO)(CO) species has occurred. There is no evidence for the formation of a $Rh(NO)^+$ species, which has been observed in an analogous experiment performed on both TiO_2 powder and single crystal, under UHV conditions[29]. There is also no evidence for the formation of a $Rh(NO)_2$ species, as the symmetry and frequency of the second band at 2145cm^{-1} is inconsistent with this (the symmetric and asymmetric bands are at 1825cm^{-1} and 1740cm^{-1} respectively). DRIFTS spectroscopy offers no clues as to whether the chlorine remains attached to the rhodium centre, or if there is any change in the bonding of the rhodium to the TiO_2 surface. Changes in the coordination around the rhodium are to be expected due to the

need to satisfy the 16-electron rule required for square planar complexes (see chapter 5 for a more substantial discussion of geometry of Rh complexes). Spectrum 4.1(b) shows an increase in the hydroxyl region (3000-3500cm^{-1}), indicating consumption of these species during the NO reaction. This may be a result of the formation of nitrate/nitrite species on free areas of alumina discussed above. EXAFS spectroscopy will be more helpful in understanding the coordination around the rhodium centre.

Following this, the sample was exposed to CO, at room temperature, at a pressure of 1 bar and a flow rate of 5ml/min, for 2 hours. Following exposure to CO. the DRIFTS cell was flushed with helium and the spectrum was acquired. The spectrum illustrates a 95% return of the rhodium *gem* dicarbonyl bands at 2103cm^{-1} and 2028cm^{-1} (the same frequencies as the starting species) and the appearance of a weak band at 1909cm^{-1}, which can be attributed to a $Rh(NO)^+$ species. However, there is little decrease in the intensity of the Rh(NO)- band at 1733cm^{-1} (frequency decrease of 10cm^{-1}). The weak band at 2145cm^{-1} produced after exposure to NO, disappears completely after exposure to CO. The surface nitrate species at 1458cm^{-1} and 1313cm^{-1} are also removed during exposure to CO. A possible conclusion from this experiment is that substitution of the rhodium NO^- ligand for the *gem* dicarbonyl ligand has occurred. However, there is no explanation for the persistence of the band at 1732cm^{-1}. The change of frequency may suggest that the ligand has migrated to the TiO_2 surface, with a small amount of $Rh(NO)^+$ being formed. However, exposure of NO to TiO_2 revealed no infrared frequencies in this region. Again, it is hoped that EXAFS spectroscopy will reveal the coordination around the rhodium atom after exposure to CO.

This experiment was repeated using Al_2O_3 as a support, as this would enable direct comparison with results obtained by EDE (TiO_2 could not be used as a support for this experiment, section 3.2). The results obtained from this experiment are almost identical to those from the TiO_2 analogue, figure 4.2. Initial substitution of the *gem* dicarbonyl band for $Rh(NO)^-$, 1736cm^{-1} and Rh(NO)(CO), 2150cm^{-1}, occurs. The latter band has a greater intensity here than in the TiO_2 analogue. Re-substitution of the *gem* dicarbonyl occurs on exposure to CO, with a larger $Rh(NO)^+$ band produced and persistence of the $Rh(NO)^-$ band at a lower frequency of 1723cm^{-1}. The

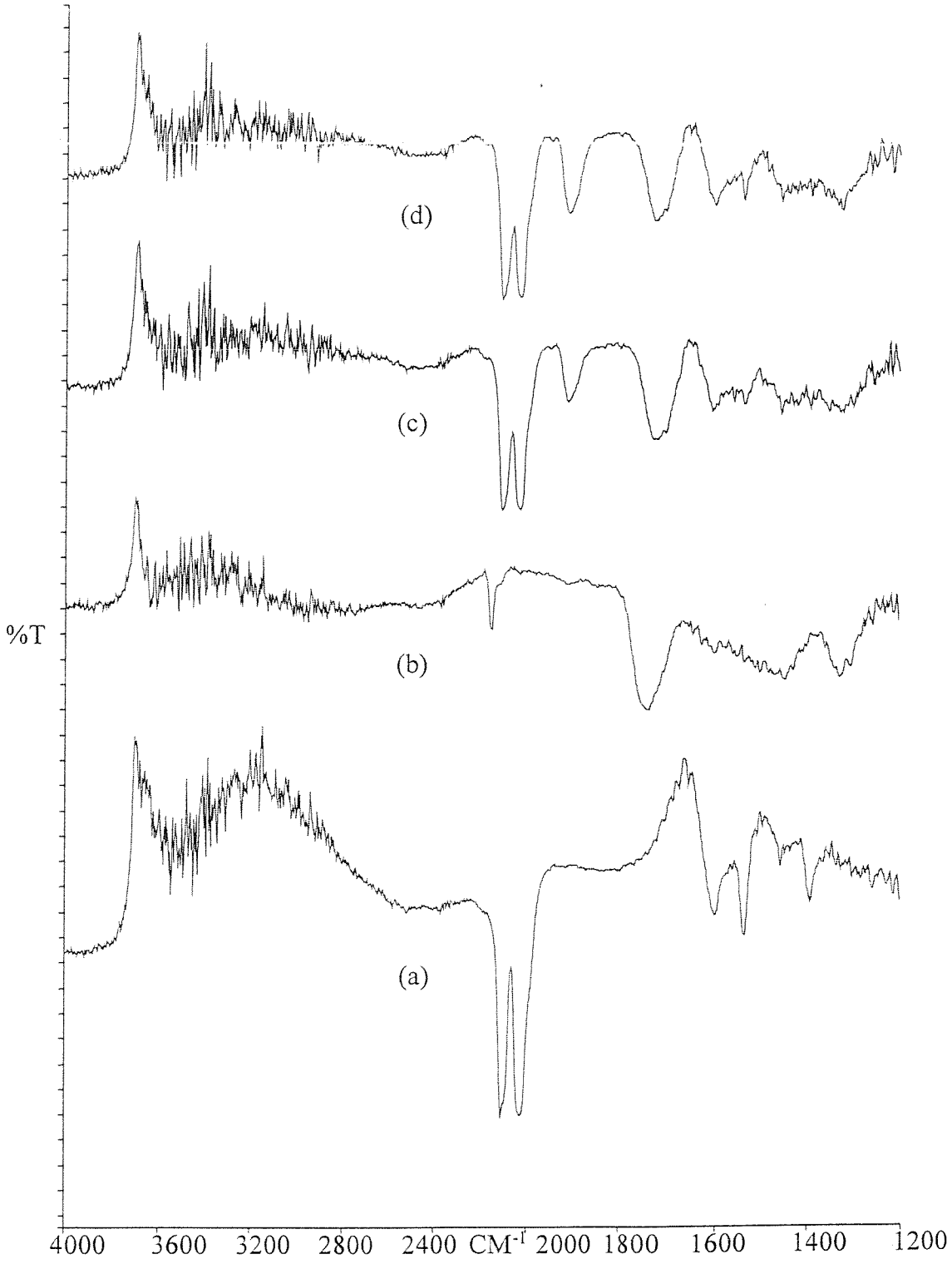

Figure 4.2 DRIFTS difference spectra of reaction of $[Rh(CO)_2Cl]_2$ supported on Al_2O_3 with NO and CO at room temp: (a) Before reaction with NO, (b) After reaction with NO for 30 mins, (c) After reaction with CO for 1 hr, (d) After reaction with CO for 2 hrs.

conclusion of this experiment is that there is identical chemistry for the two supports used for the NO/CO reaction.

4.2.2 EXAFS Study of Reaction of $[Rh(CO)_2Cl]_2$ Supported on TiO_2 and Al_2O_3 with NO followed by CO, at Room Temperature

The Rh K-edge Energy Dispersive EXAFS experiment for the reaction of $[Rh(CO)_2Cl]_2$ supported on partially dehydroxylated alumina with NO and CO, was performed at the ESRF in Grenoble at station ID24. The starting spectrum shows the [Al-O]$Rh(CO)_2Cl$ species, figure 4.3. The spectrum is an average of 100 scans, each lasting 19 ms (19 frames at 1ms), resulting in a total acquisition time of 1.9s. The rationale behind the assignments of this species is given in section 3.2.2.

The sample was then exposed to NO at a pressure of 1 bar and a flow rate of 5ml/min, at room temperature. After an exposure time of 10 minutes, the cell was flushed with helium for 5 minutes and a spectrum was acquired, figure 4.4. The acquisition time of the spectrum is 1.8s. There is a significant change in the shape of the EXAFS and the Fourier transform spectra. The EXAFS has changed from having three main peaks for the surface gem dicarbonyl species, to two in the nitrosyl species. There is also a phase shift in the peak positions during the reaction. This is reflected in the Fourier transform, which shows three main peaks, but at different distances and relative intensities than for the surface gem dicarbonyl species. The first peak is at ≈1.80Å, and is assigned to contributions from the Rh-N bond (1.80Å) and the Rh-O(surface) bond (1.95Å). The second peak in the Fourier transform is due to contributions from another Rh-O(surface) bond at 2.12Å and a Rh-Cl bond at 2.40Å. The third peak at 2.87Å, is due to the Rh-O (nitrosyl) bond. A variety of possible models were attempted to fit the data to. The best, and most consistent across a series of spectra from repeats of the reaction, however, involved a bent (135°) Rh-N-O species, with two surface oxygen bonds, and a single chlorine bond. The orientation and bond distances of the nitrosyl species are in agreement with literature values for a

Figure 4.3 Rh K-Edge EXAFS and Fourier transform of $[Rh(CO)_2Cl]_2$ supported on Al_2O_3

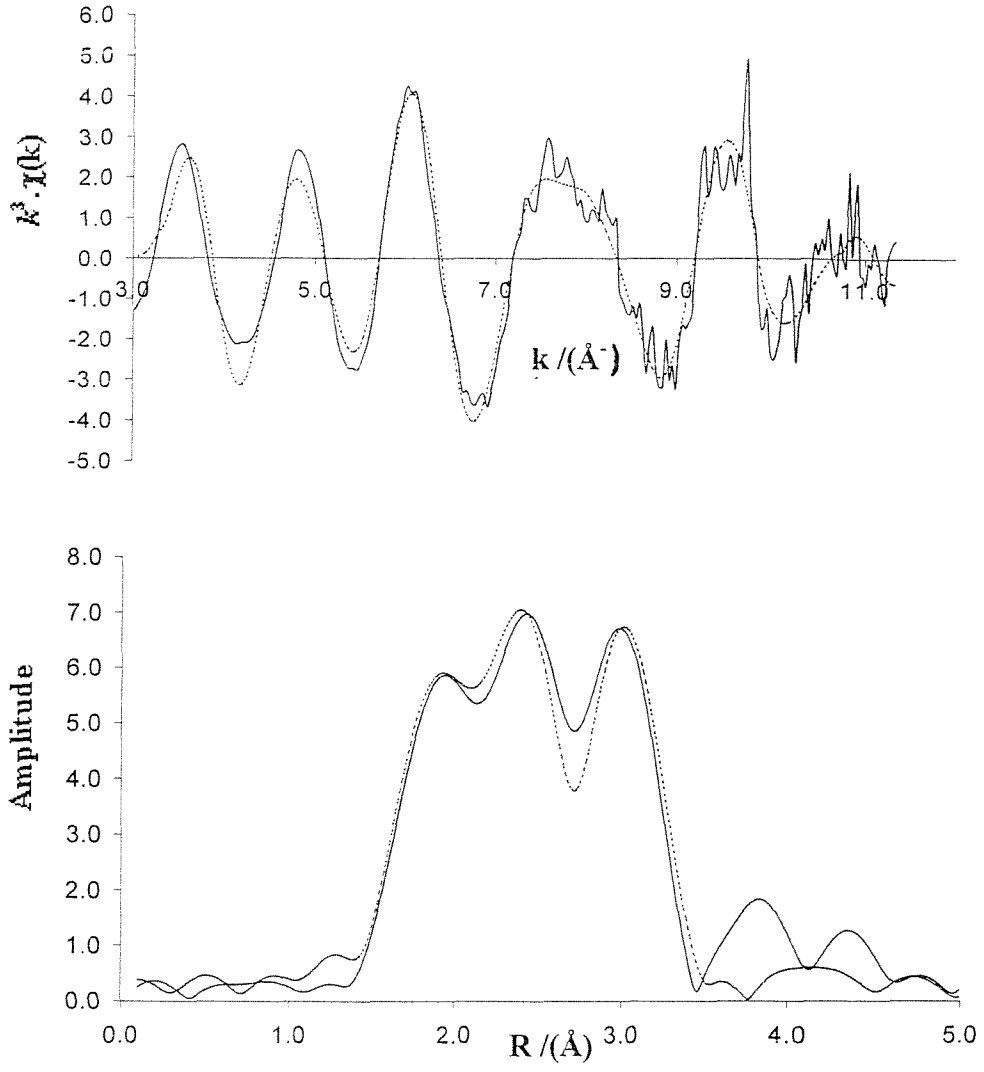

Atom	C.N.	r/Å	$2\sigma^2$ / Å^2
C	2(0.1)	1.897(2)	0.002(1)
O	1(0.1)	2.132(4)	0.004(2)
Cl	1(0.2)	2.382(3)	0.004(2)
O	2(0.2)	2.988(4)	0.007(3)
Al	1(0.3)	3.575(5)	0.012(4)

R = 33.30 %
Ef = -0.36 eV

Figure 4.4 Rh K-Edge EXAFS and Fourier transform of $[Rh(CO)_2Cl]_2$ supported on Al_2O_3 after reaction with NO for 10 mins

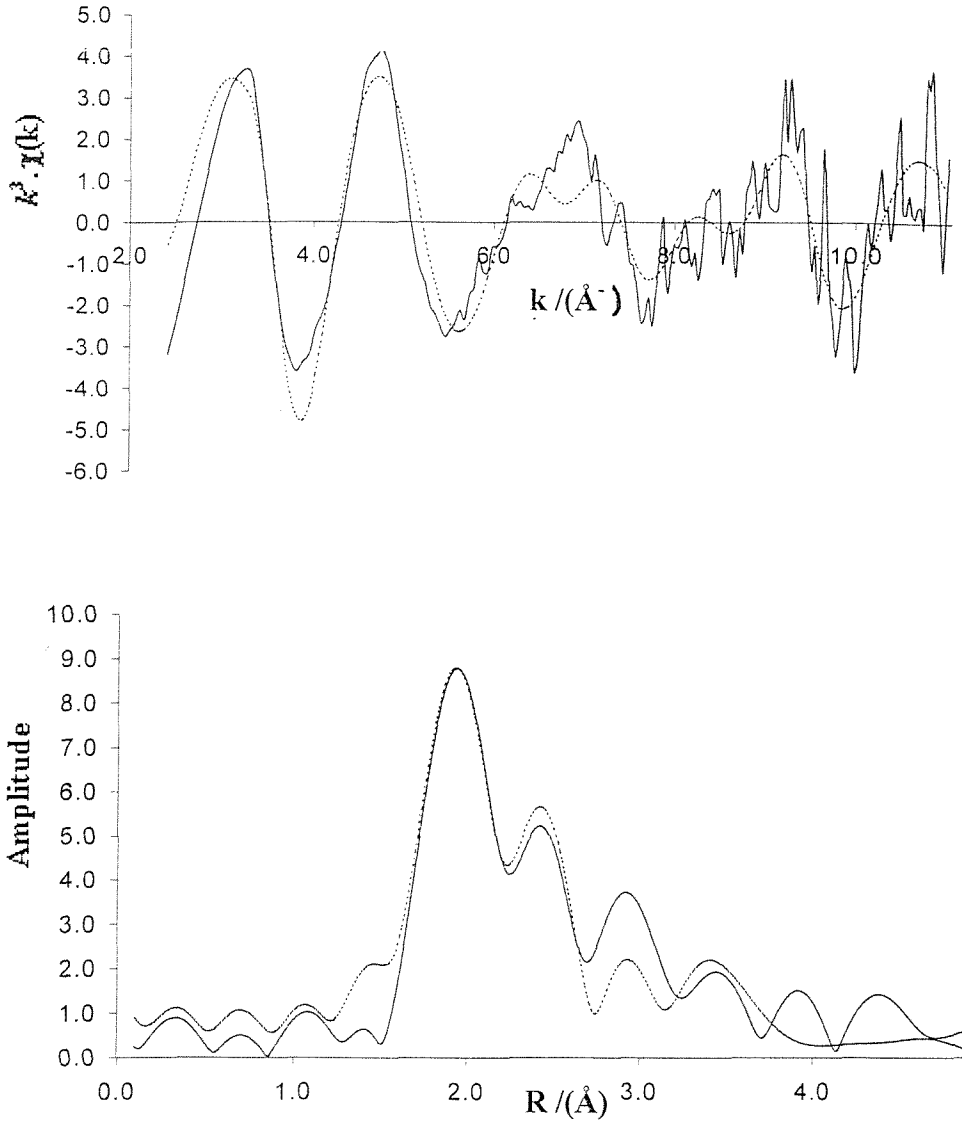

Atom	C.N.	r/Å	$2\sigma^2$ / Å^2
N	1(0.1)	1.803(2)	0.003(1)
O	1(0.1)	2.120(4)	0.003(1)
O	1(0.2)	1.951(3)	0.002(1)
Cl	1(0.2)	2.406(3)	0.006(3)
O	1(0.2)	2.875(4)	0.010(1)

R = 53.32 %
Ef = 0.51 eV

bent inorganic nitrosyl (Rh-NO$^-$) species[32,33]. The differing distances of the surface oxygen species may be due to differing types of bonding (one standard surface oxygen bond and one surface hydroxyl group). The second oxygen atom could also originate from dissociation of NO. The two different Rh-O bondlengths could also originate from the NO ligand being trans to either the Cl ligand or a surface O, in the $[O]_2Rh(NO)(Cl)$ isomers described in 4.2.1. The inclusion of multiple scattering improved the quality of the fit from R=58% to 53%. The conclusion from this experiment is that exposure to NO results in substitution of the gem dicarbonyl ligands for a single NO$^-$ ligand and an additional surface oxygen bond. There are no previous EXAFS investigations of this reaction to compare results with, but the results obtained are in agreement with those of the DRIFTS reaction. The DRIFTS experiment also indicated the formation of a mixed Rh(CO)(NO) species, which could not be fitted in the EXAFS experiment. It is probable that only a small quantity of this species is formed, whilst the majority of the rhodium *gem* dicarbonyl reacts to form the Rh(NO)$^-$ species. A stacked plot of this reaction is shown in figure 4.5. This clearly illustrates the shifts in the profile of the EXAFS during the transition from the rhodium *gem*-dicarbonyl to the nitrosyl species.

The sample was then exposed to CO for 1 hour at room temperature at a pressure of 1 bar and a flow rate of 5ml/min. The EXAFS and Fourier transform acquired during this experiment are illustrated in figure 4.6. The shape of the EXAFS and Fourier transform spectra resemble that of the rhodium *gem* dicarbonyl species. A variety of models were attempted to fit the data to, including mixed carbonyl and nitrosyl species and varying the number of surface oxygen atoms. The best model however, is the rhodium *gem* dicarbonyl species. The bond distances closely resemble those of the starting species, although the shape and relative intensities of the Fourier transform are not quite the same. The results of this experiment and the DRIFTS experiment suggest that the reverse reaction proceeds at a considerably slower rate than the forward one. The EXAFS data suggests that the majority if not all the rhodium nitrosyl species has been converted back to the *gem* dicarbonyl species after one hour. The shape of the EXAFS and the DRIFTS spectra suggest that some of the Rh(NO)$^-$ species still persists after this time however. Attempts to fit spectra obtained during the course of re-exposure to CO, thus offering the opportunity to study reaction

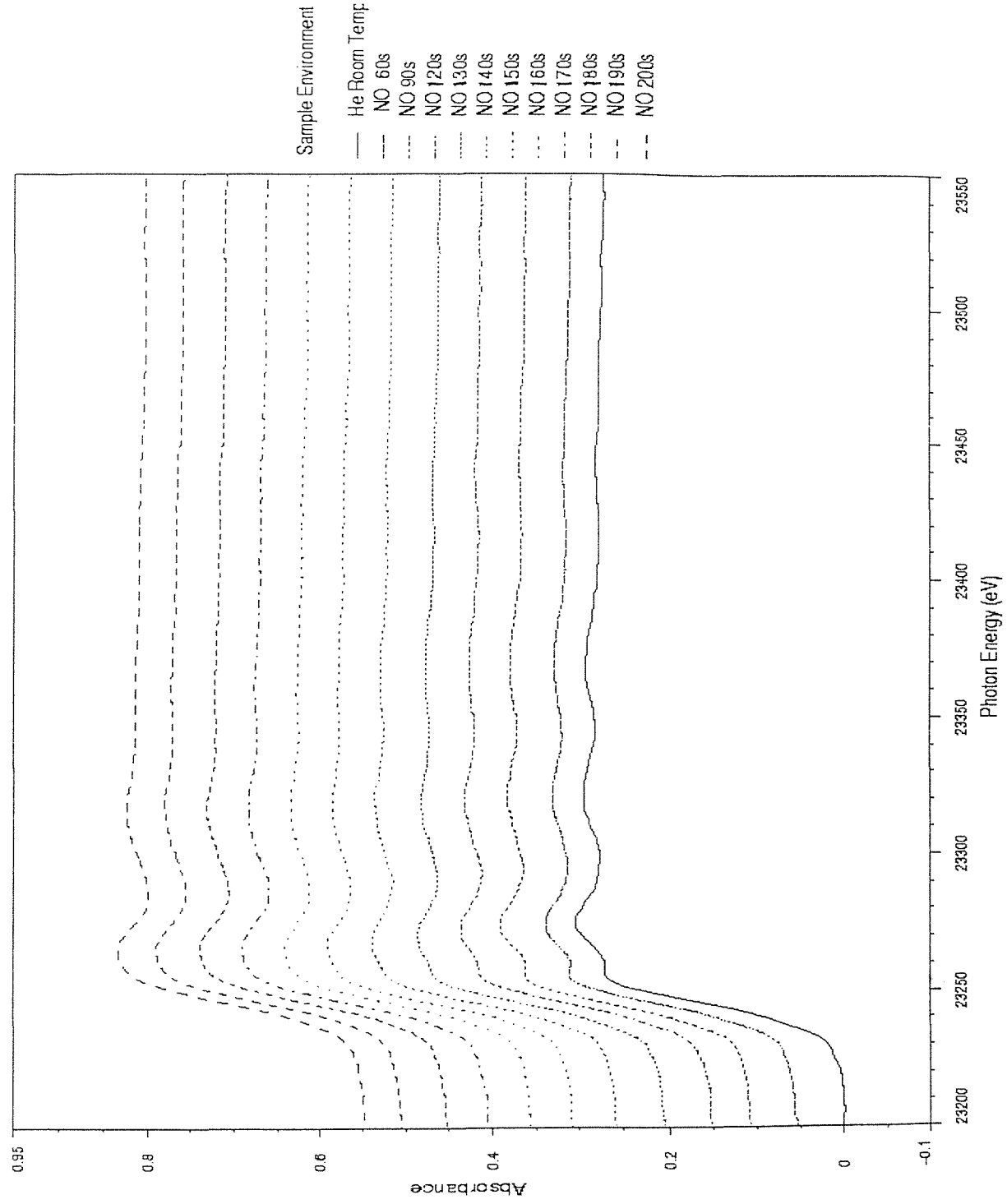

Figure 4.5 Energy dispersive X-ray absorption spectra recorded during reaction of $[Rh(CO)_2Cl]_2$ supported on Al_2O_3 with NO at room temperature. Acquisition time of each spectrum is 0.4s. Recorded in time resolved mode.

Figure 4.6 Rh K-Edge EXAFS and Fourier transform of $[Rh(CO)_2Cl]_2$ supported on Al_2O_3 after reaction with NO for 30 mins and CO for 1 hr, at room temp.

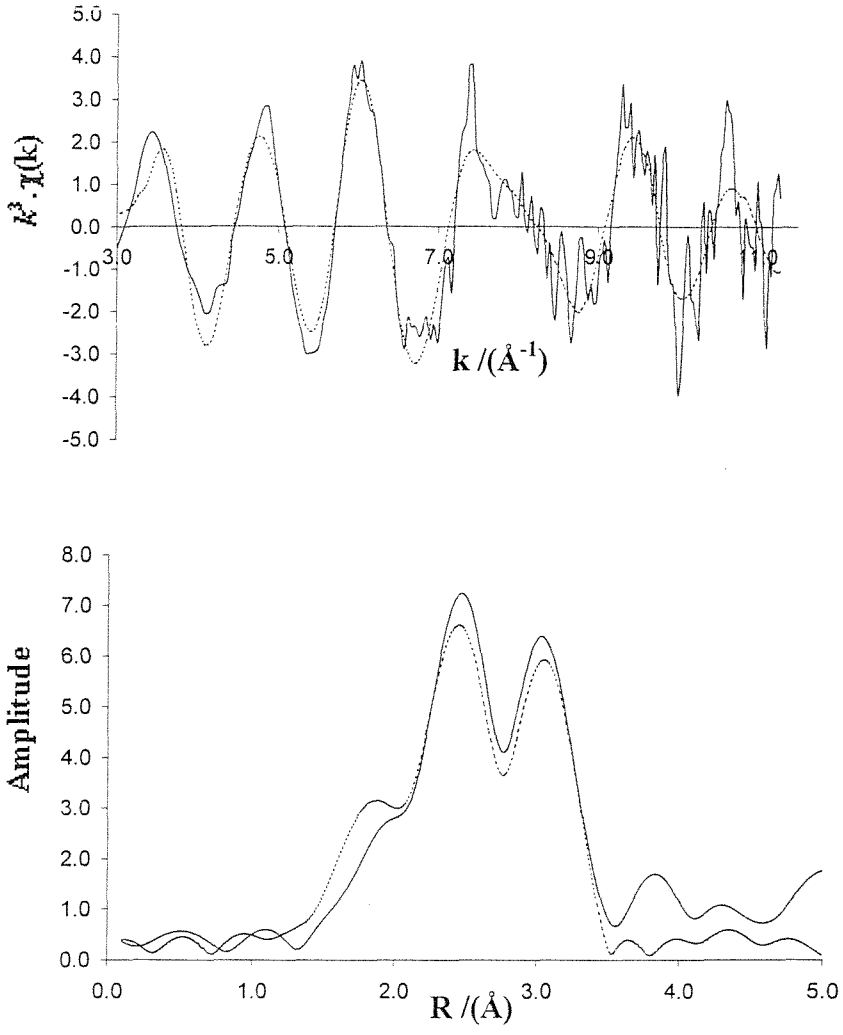

Atom	C.N.	r/Å	$2\sigma^2$ / Å^2
C	2(0.1)	1.868(2)	0.003(1)
O	1(0.1)	2.161(4)	0.004(2)
Cl	1(0.2)	2.377(3)	0.004(2)
O	2(0.2)	3.017(3)	0.007(3)
Al	1(0.3)	3.583(5)	0.012(4)

R = 46.58 %
Ef = -1.56 eV

intermediates, were unsuccessful. These experiments were performed in time resolved mode, with each spectrum being acquired in 0.4s. Even with an average of 10 spectra, the signal to noise ratio was too high to identify a reaction intermediate. A stacked plot of this reaction is shown in figure 4.7. This clearly illustrates the changes in the profile of the EXAFS during the transition from the rhodium nitrosyl species back to the *gem* dicarbonyl species.

The sample was again exposed to NO for 30 mins under the same conditions as before. The EXAFS and Fourier transform are shown in figure 4.8. The spectrum was acquired in 1.8 seconds. The spectrum has identical features to that of the initial NO exposure experiment. There are three main peaks in the Fourier transform, their assignments the same as before. The quality of the fit is superior with an R factor of 40%, and demonstrates that the NO/CO/NO reaction is reversible. It can also be concluded that the rhodium remains monodispersed during the course of these reactions, as no rhodium-rhodium coordination could be detected. A stacked plot of this reaction is shown in figure 4.9 illustrating the changes in the profile of the EXAFS during the transition from the rhodium gem-dicarbonyl to the nitrosyl species.

These data illustrate the reversibility of this reaction at room temperature though they do not fully reveal the extent of *gem*-carbonyl regeneration, which is better evidenced by DRIFTS spectroscopy. Indeed it would seem that there are a mixture of carbonyl and nitrosyl species upon re-exposure to CO at room temperature.

4.3 Re-Exposure to CO at Variable Temperature After Reaction with NO

This reaction was performed at the ESRF using Energy Dispersive EXAFS on 5% weight $[Rh(CO)_2Cl]_2$ supported on Al_2O_3 prepared according to the standard method (section 2.6 and 3.7). In each experiment, the sample was exposed to NO for 30 minutes before exposure to CO for 1 hour at various temperatures. The aim of this

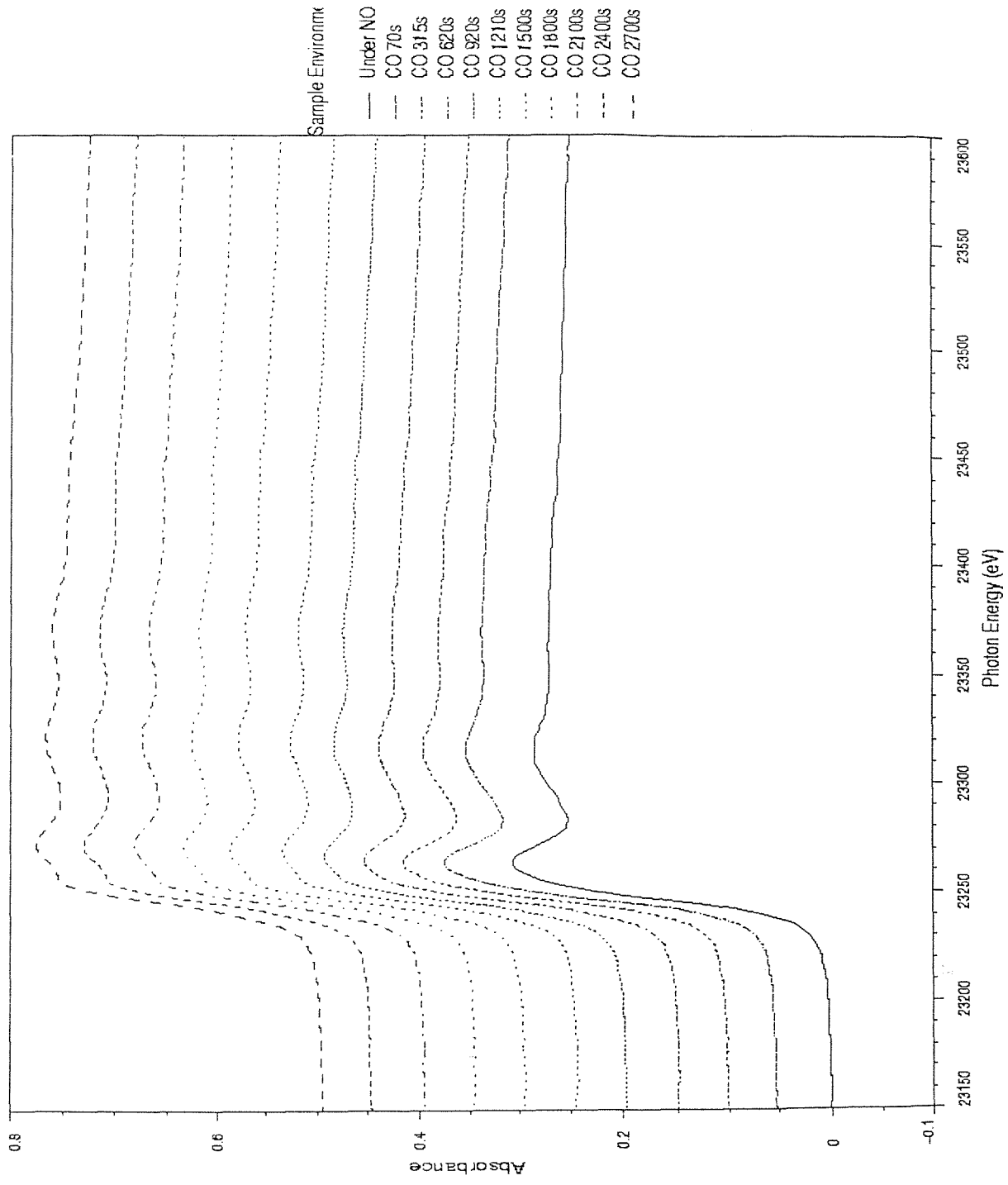

Figure 4.7 Energy dispersive X-ray absorption spectra recorded during reaction of $[Rh(CO)_2Cl]_2$ supported on Al_2O_3 with CO after reaction with NO, at room temperature. Acquisition time of each spectrum is 0.4s. Recorded in time resolved mode.

Figure 4.8 Rh K-Edge EXAFS and Fourier transform of $[Rh(CO)_2Cl]2$ supported on Al_2O_3 after reaction with NO (30 mins), CO (2 hrs) and NO (30 mins)

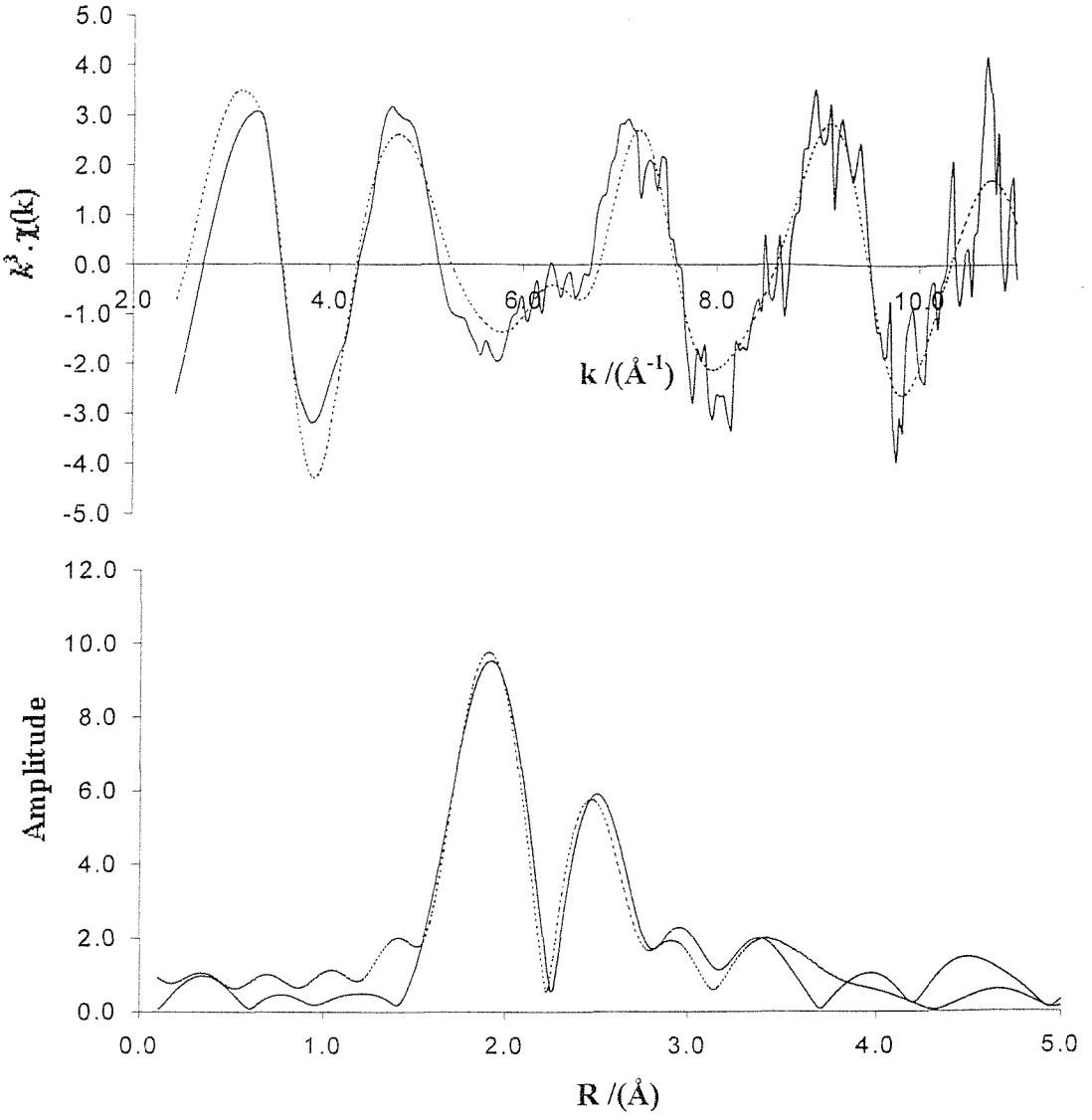

Atom	C.N.	r/Å	$2\sigma^2$ / Å^2
N	1(0.1)	1.791(2)	0.002(1)
O	1(0.1)	2.140(4)	0.002(1)
O	1(0.2)	1.968(3)	0.002(1)
Cl	1(0.2)	2.400(3)	0.007(3)
O	1(0.2)	2.893(4)	0.012(1)

R = 40.03 %
Ef = 0.84 eV

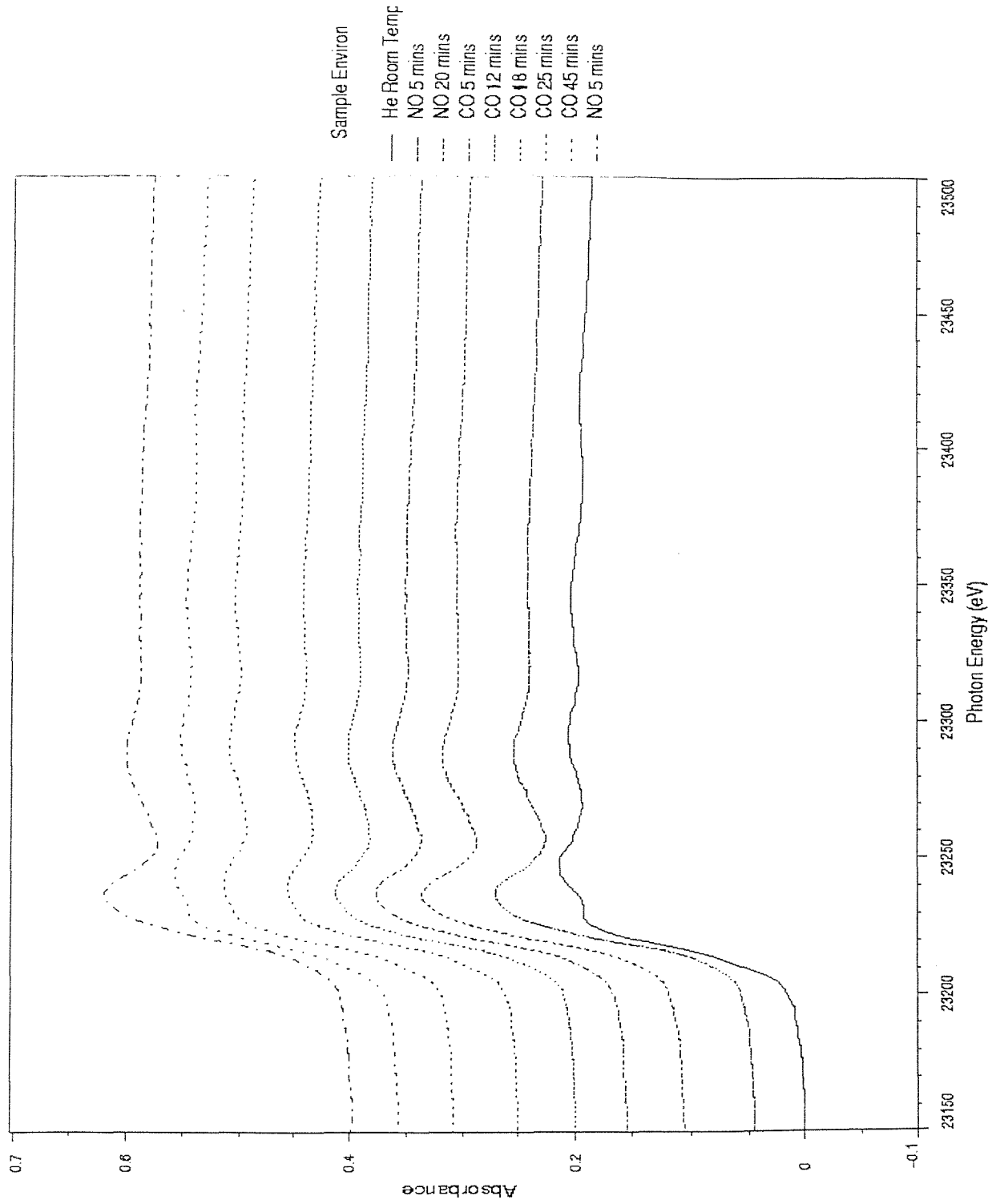

Figure 4.9 Energy dispersive X-ray absorption spectra recorded during reaction of $[Rh(CO)_2Cl]_2$ supported on Al_2O_3 with NO, CO and NO, at room temperature. Acquisition time of each spectrum is 0.4s. Recorded in time resolved mode.

experiment was to investigate the temperature dependence of the regeneration of the *gem*-carbonyl species, in order to extract kinetic data about the reaction. This would potentially further the limits of the uses of EDE. The regeneration temperature was raised from room temperature in 10°C increments up to 65°C. The spectra of the nitrosyl species are not shown here as this reaction has been shown by DRIFTS and EDE to proceed to completion at room temperature.

Figure 4.10 shows the species after re-exposure to CO for 1 hour at 35°C. This spectrum and all others recorded in this section were acquired in 1.9s. The spectrum resembles that for the *gem*-carbonyl species much more closely than that of the room temperature regeneration (fig 4.6). The bond distances are also more realistic for a $Rh(CO)_2(Cl)(O)$ species and the statistical errors smaller. The three peaks in the Fourier transform are more visibly defined and it can be inferred that a greater degree of regeneration has occurred relative to the room temperature experiment.

Figure 4.11 shows the spectrum acquired after re-exposure to CO for 1 hour at 45°C. The Fourier transform resembles that observed for a standard $Rh(CO)_2(O)(Cl)$ species (fig 4.3) even more closely than that for the species regenerated at 35°C. The statistical errors for the fit and the R factor are lower than those for the 35°C species too. There are three distinct peaks in the Fourier transform at distances that are diagnostic of the rhodium *gem*-carbonyl species. This suggests that the regeneration of the *gem*-carbonyl species is very nearly or totally complete at this temperature.

The spectrum for the species re-exposed to CO at 55°C is shown in figure 4.12. The quality of the data obtained in this experiment is poorer than that of the previous two samples. However, the Fourier transform has the shape and bond distances, which are strongly diagnostic of the rhodium *gem*-carbonyl species.

Figure 4.13 shows the spectrum acquired after re-exposure to CO for 1 hour at 65°C. The shape of the Fourier transform and the bond distances observed are virtually identical to those observed for the rhodium *gem*-carbonyl species (figure 4.3). The fit is of high quality, with low statistical errors and R factor. This result

Figure 4.10 Rh K-Edge EXAFS and Fourier transform of $[Rh(CO)_2Cl]_2$ supported on Al_2O_3 after reaction with NO for 30 mins and CO for 1 hr, at 35°C

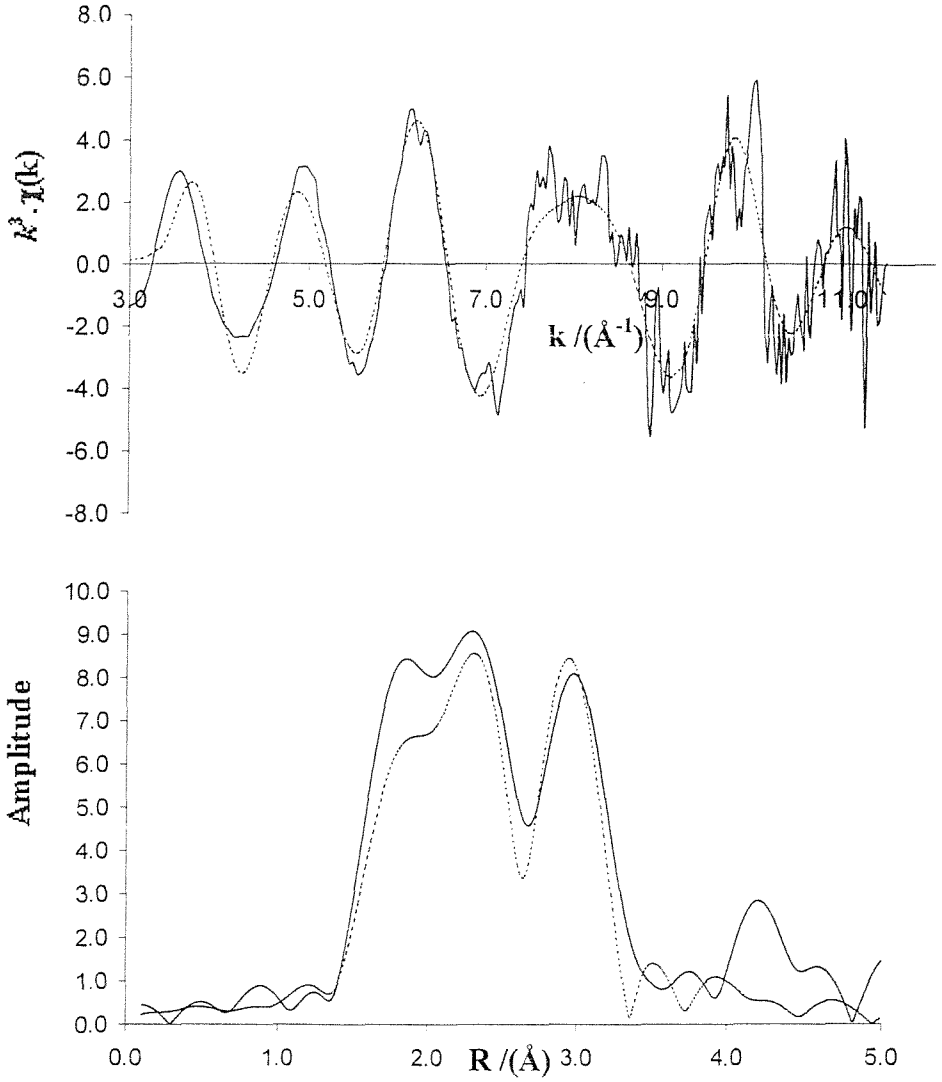

Atom	C.N.	r/Å	$2\sigma^2$ / Å^2
C	2(0.1)	1.892(2)	0.003(1)
O	1(0.1)	2.140(4)	0.001(2)
Cl	1(0.2)	2.357(3)	0.006(2)
O	2(0.2)	3.014(3)	0.007(3)
Al	1(0.3)	3.603(5)	0.012(4)

R = 44.05 %
Ef = 0.90 eV

Figure 4.11 Rh K-Edge EXAFS and Fourier transform of $[Rh(CO)_2Cl]_2$ supported on Al_2O_3 after reaction with NO for 30 mins and CO for 1 hr, at 45°C

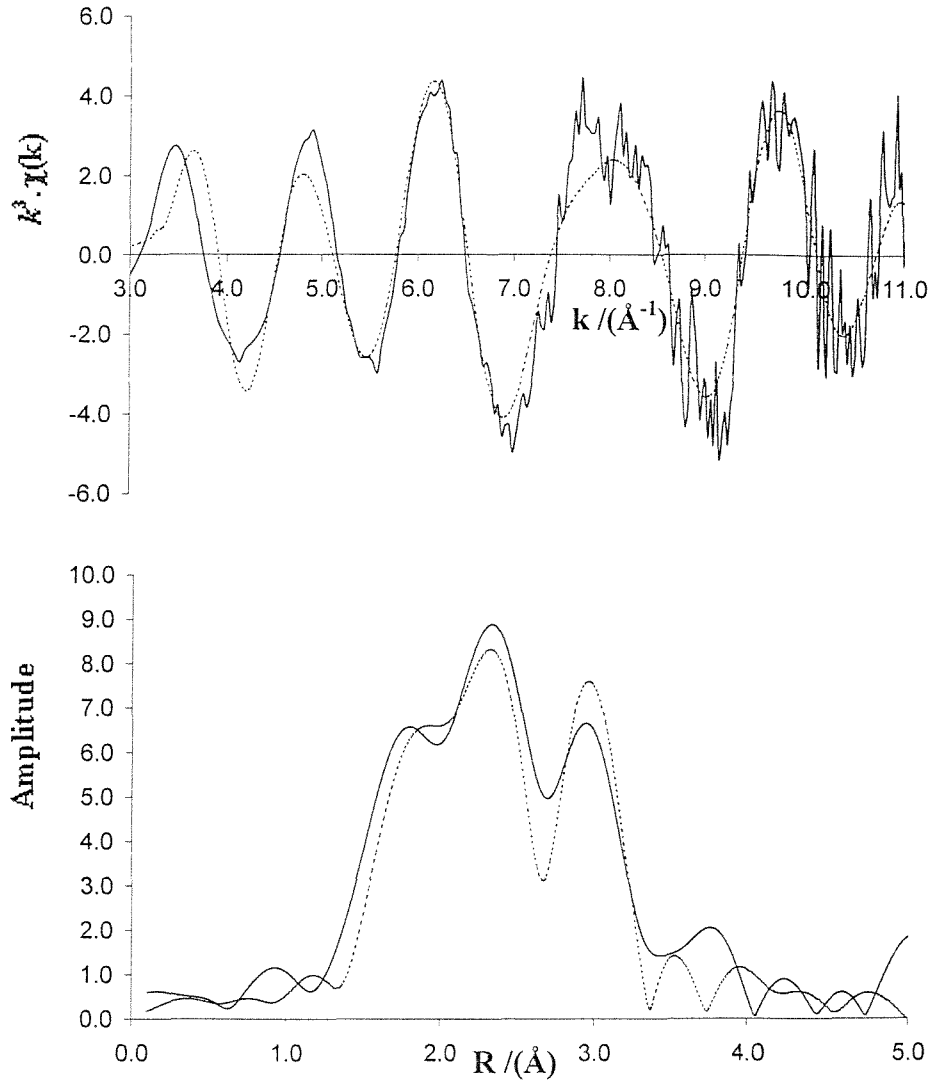

Atom	C.N.	r/Å	$2\sigma^2$ / Å^2
C	2(0.1)	1.884(2)	0.003(1)
O	1(0.1)	2.124(3)	0.002(2)
Cl	1(0.2)	2.353(2)	0.003(2)
O	2(0.2)	3.020(3)	0.007(3)
Al	1(0.3)	3.610(5)	0.015(4)

R = 37.45 %
Ef = -0.80 eV

Figure 4.12 Rh K-Edge EXAFS and Fourier transform of $[Rh(CO)_2Cl]_2$ supported on Al_2O_3 after reaction with NO for 30 mins and CO for 1 hr, at 55°C

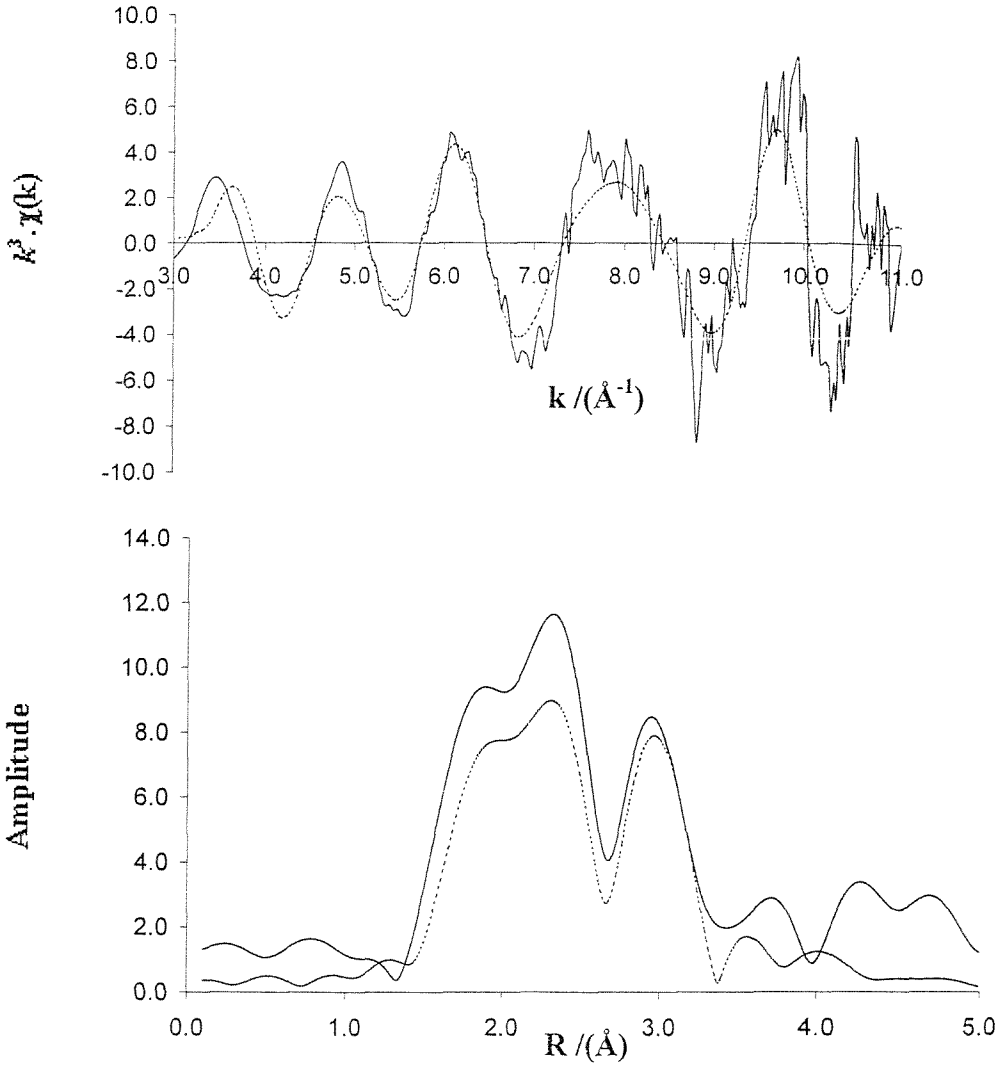

Atom	C.N.	r/Å	$2\sigma^2$ / Å^2
C	2(0.1)	1.908(3)	0.002(1)
O	1(0.1)	2.126(2)	0.002(2)
Cl	1(0.2)	2.351(3)	0.004(2)
O	2(0.2)	3.002(3)	0.009(3)
Al	1(0.3)	3.613(6)	0.012(4)

R = 49.26 %
Ef = -2.40 eV

Figure 4.13 Rh K-Edge EXAFS and Fourier transform of $[Rh(CO)_2Cl]_2$ supported on Al_2O_3 after reaction with NO for 30 mins and CO for 1 hr, at 65°C

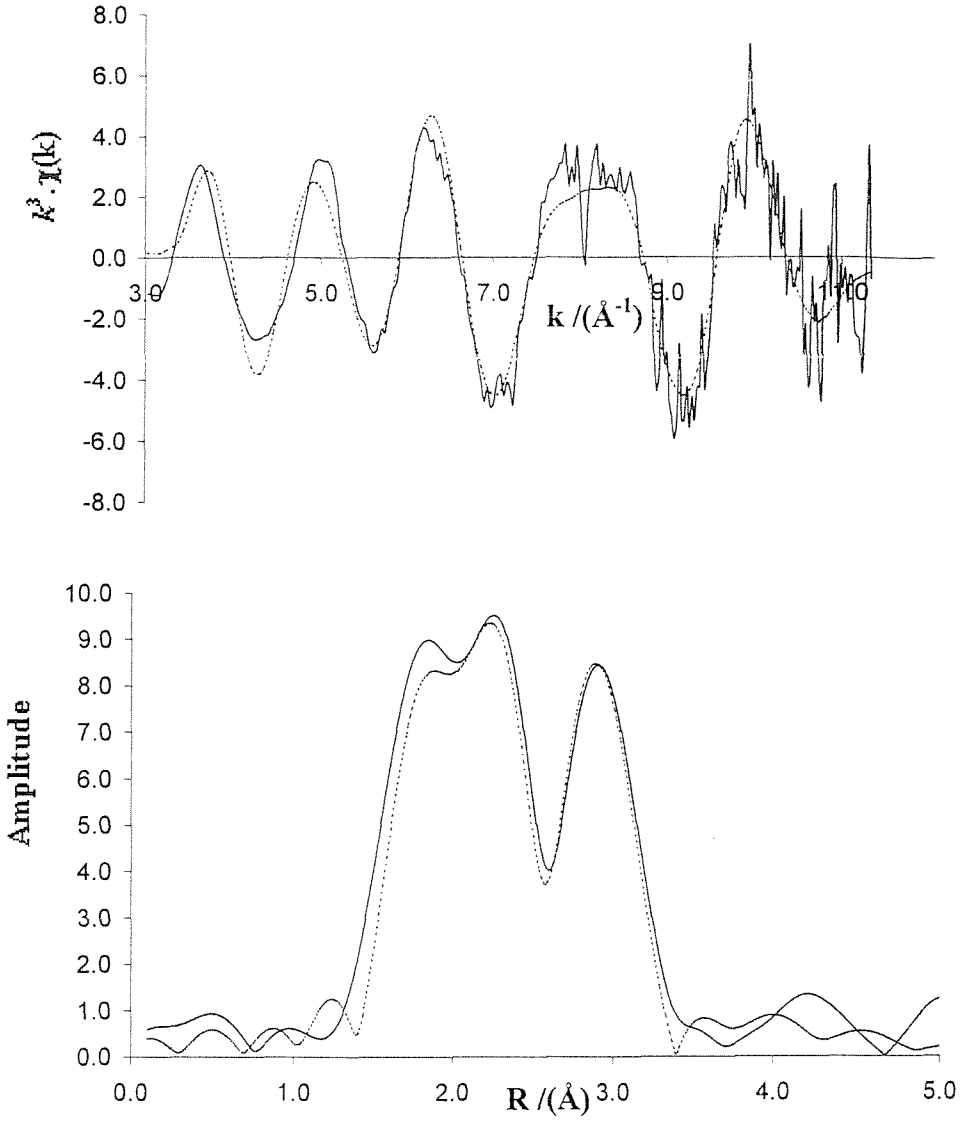

Atom	C.N.	r/Å	$2\sigma^2$ / Å^2
C	2(0.1)	1.889(2)	0.003(1)
O	1(0.1)	2.132(3)	0.001(2)
Cl	1(0.2)	2.360(2)	0.006(2)
O	2(0.2)	3.008(4)	0.006(3)
Al	1(0.3)	3.612(6)	0.016(4)

R = 41.42 %
Ef = 3.85 eV

suggests that complete regeneration of the *gem*-carbonyl species has occurred. There is no evidence of any remaining nitrosyl species as fits including linear and bent NO species were attempted.

4.4 Thermolysis of Rhodium Nitrosyl Species

The helium thermolysis (inert atmosphere) of the rhodium nitrosyl species, generated by exposure of the rhodium *gem*-carbonyl species to NO for 30 minutes, was performed at the ESRF using EDE spectroscopy. The first spectrum shown in figure 4.14 was taken after heating to 120°C. This spectrum and all others recorded in this section were acquired in 1.8s. The spectrum shows no significant change from the room temperature $Rh(NO^-)(O)_2(Cl)$ species (figure 4.4). This finding supports the idea that the Rh-NO^- bond is stronger than the Rh-CO bond, which is broken at this temperature.

The spectrum of the species after heating to 180°C is shown in figure 4.15. This spectrum illustrates partial decomposition to small rhodium clusters of the rhodium nitrosyl species. The degree of decomposition is slight at this temperature and the surface is still likely to be populated with the starting species. This result again suggests that the Rh-NO^- bond is stronger than the Rh-CO bond. At this temperature, the rhodium *gem*-carbonyl species had been reduced to small rhodium clusters.

The spectrum shown in figure 4.16 shows the sample after heating to 220°C. Analysis of the spectrum, involving attempting to fit a variety of models, suggests that further reduction to rhodium clusters had occurred, though there remained some $Rh(NO^-)(O)_2(Cl)$ on the surface.

Figure 4.14 Rh K-Edge EXAFS and Fourier transform of $[Rh(CO)_2Cl]_2$ supported on Al_2O_3 after reaction with NO for 30 mins and subsequent thermolysis in helium to 120°C

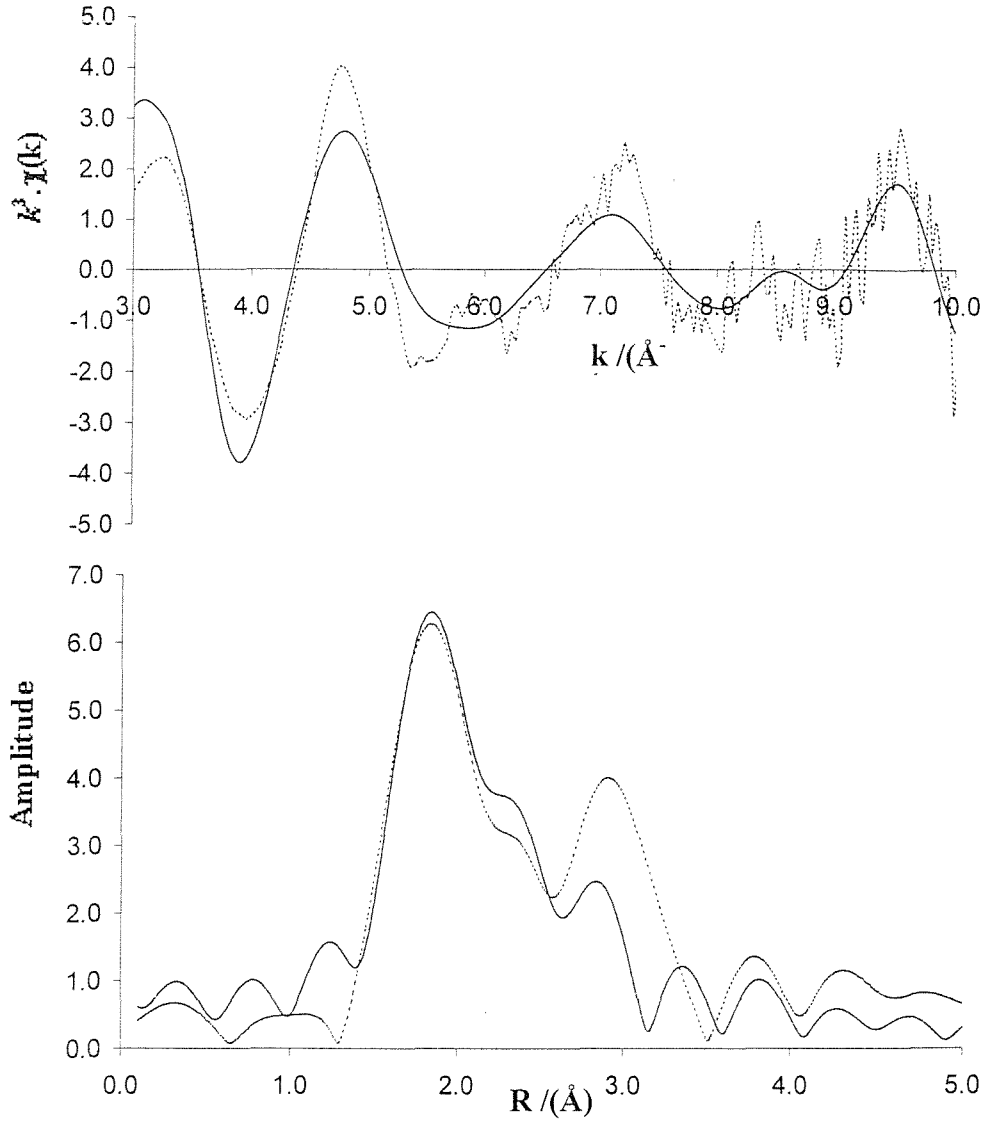

Atom	C.N.	r/Å	$2\sigma^2$ / Å^2
N	1(0.1)	1.802(2)	0.003(1)
O	1(0.1)	2.123(4)	0.001(1)
O	1(0.2)	1.987(3)	0.003(1)
Cl	1(0.2)	2.386(3)	0.004(3)
O	1(0.2)	2.903(4)	0.010(1)

R = 40.03 %
Ef = 0.84 eV

Figure 4.15 Rh K-Edge EXAFS and Fourier transform of $[Rh(CO)_2Cl]_2$ supported on Al_2O_3 after reaction with NO for 30 mins and subsequent thermolysis in helium to 180°C

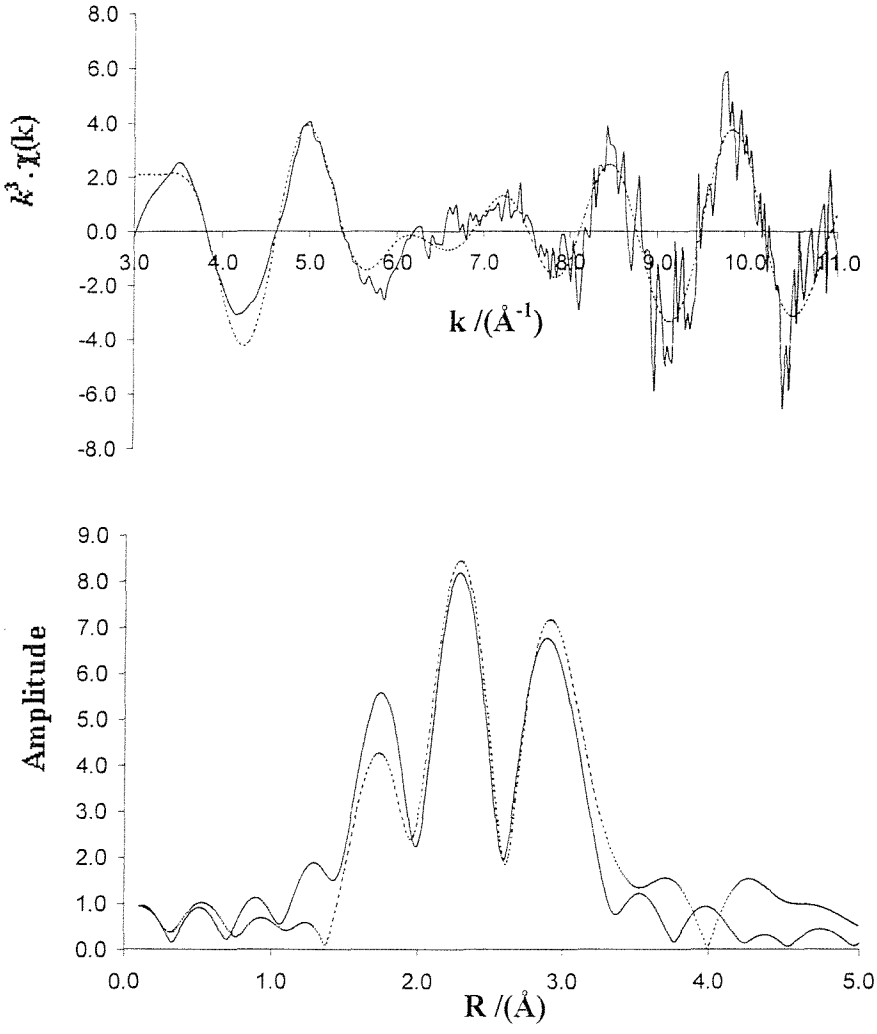

Atom	C.N.	r/Å	$2\sigma^2$ / Å^2
N	1(0.1)	1.804(2)	0.003(1)
O	1(0.1)	2.112(3)	0.001(1)
O	1(0.2)	1.991(4)	0.003(1)
Cl	1(0.2)	2.376(2)	0.004(3)
Rh	4(1.3)	2.751(3)	0.017(4)
O	1(0.2)	2.903(4)	0.018(1)

R = 47.21 %
Ef = 2.54 eV

Figure 4.16 Rh K-Edge EXAFS and Fourier transform of $[Rh(CO)_2Cl]_2$ supported on Al_2O_3 after reaction with NO for 30 mins and subsequent thermolysis in helium to 220°C

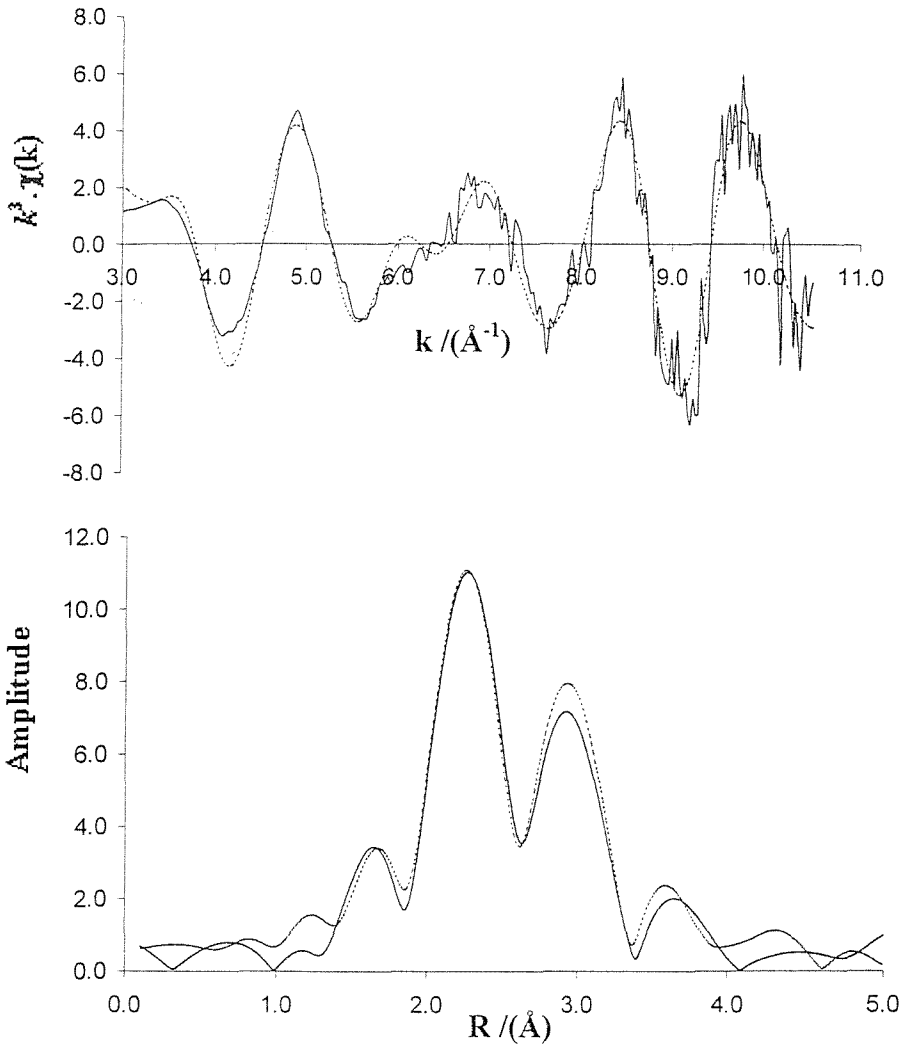

Atom	C.N.	r/Å	$2\sigma^2$ / Å^2
N	1(0.1)	1.800(3)	0.002(1)
O	1(0.1)	2.125(4)	0.001(1)
O	1(0.2)	1.989(4)	0.003(1)
Cl	1(0.2)	2.380(3)	0.004(3)
Rh	5(1.3)	2.751(3)	0.017(4)
O	1(0.2)	2.903(4)	0.010(1)
Rh	2(0.6)	3.842(5)	0.020(5)

R = 32.04 %
Ef = 1.18 eV

The sample was subsequently heated to 300°C. The spectrum is shown in figure 4.17, and illustrates the presence of small rhodium clusters on the alumina surface. This happens at 150°C higher than for the rhodium *gem*-carbonyl species.

This experiment has served to confirm the greater strength and thermal stability of the Rh-NO bond relative to the Rh-CO bond.

4.5 NO/CO Reaction of $[Rh(CO)_2Cl]_2$ with Variable Surface Pre-treatment of TiO_2 and Al_2O_3

The effect of the pre-treatment of the oxide surface upon the NO/CO reaction of supported $[Rh(CO)_2Cl]_2$ was investigated by DRIFTS spectroscopy. Typically, in supported systems studies in this thesis, the oxide support is heated to 220°C under vacuum for 6 hours prior to MOCVD. Brønsted acidity derives from the inherent acidity of surface OH groups present on an oxide. In samples pre-treated as above, the surface remains largely hydroxylated and should therefore show little Lewis acidity. Varying the pre-treatment of the surface necessarily alters the concentration of hydroxyl groups and thus the reactivity of the surface. In this case removal of hydroxyl groups ($2OH \rightarrow H_2O + O$) will result in one oxygen deficient site per hydroxyl. This will show Lewis acidity and may be capable of stabilising electron rich species. As the temperature is raised during pre-treatment, the Brønsted acidity is reduced, and Lewis acid functionalities emerge. In the case of pre-treating TiO_2 at 700°C under an H_2 atmosphere, there is conversion of the anatase polymorph to rutile, evidenced by XRD by T. Campbell at Southampton University. There is also a net reduction of the TiO_2 surface, promoting the formation of point defects and increasing Lewis acidity.

The first study involves preparing alumina at 550°C under vacuum, prior to MOCVD, which occurs according to the procedure detailed in section 2.6. The reaction with NO occurs at room temperature and the spectra are shown in figure 4.18. The peak at $2145cm^{-1}$ is much more prominent than for the sample prepared

Figure 4.17 Rh K-Edge EXAFS and Fourier transform of $[Rh(CO)_2Cl]_2$ supported on Al_2O_3 after reaction with NO for 30 mins and subsequent thermolysis in helium to 300°C

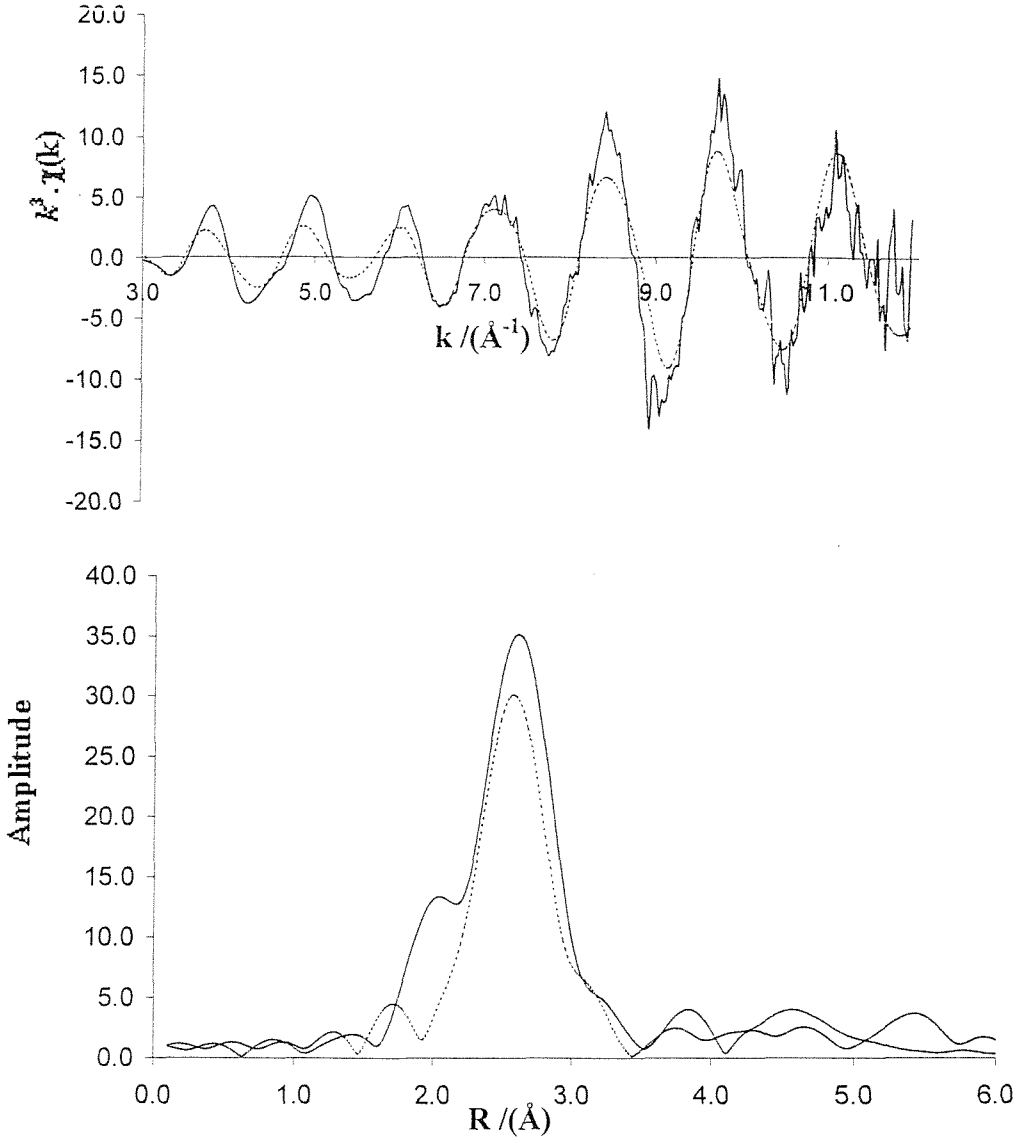

Atom	C.N.	r/Å	$2\sigma^2$ / Å^2
Rh	4(1.3)	2.751(2)	0.009(4)
Rh	3(1.1)	3.833(4)	0.010(1)
Rh	3(1.7)	4.654(5)	0.017(5)

R = 41.14 %
Ef = 2.38 eV

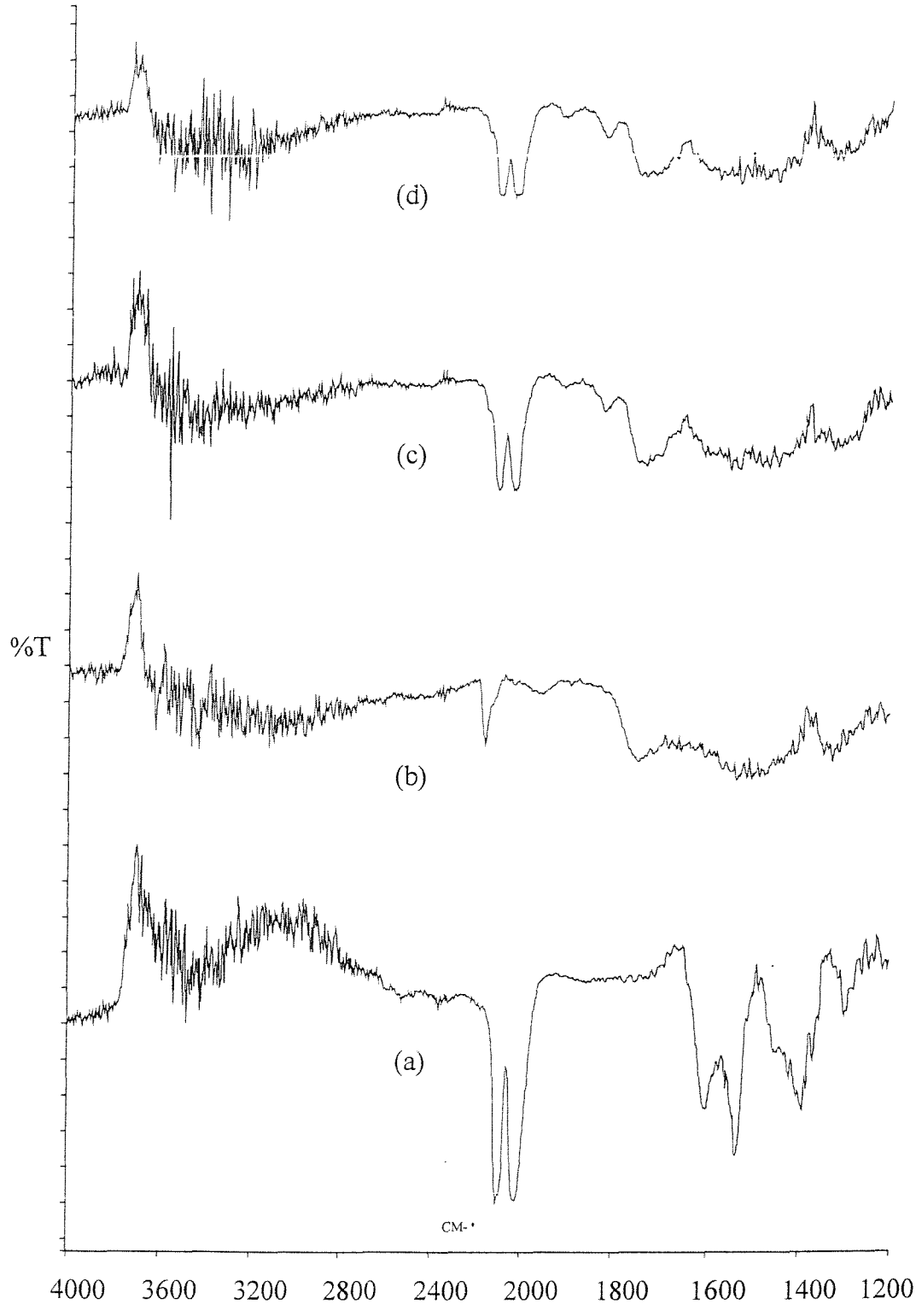

Figure 4.18 DRIFTS difference spectra of reaction of $[Rh(CO)_2Cl]_2$ supported on Al_2O_3 (Dehydroxylated at 550°C) with NO and CO: (a) Before exposure to NO, (b) After reaction with NO for 30 mins, (c) After reaction with CO for 1 hr, (d) After reaction with CO for 2 hrs.

according to general procedure (figure 4.2). This peak has been attributed to a Rh-(NO)(CO) species. The NO^- peak at 1742cm^{-1} is weaker and broader than in the previous case. There is also a weak band at 1920cm^{-1}, which is attributed to a linear Rh-NO^+ species. This is the species, which is commonly observed in analogous UHV systems upon exposure to NO[29]. The greater level of dehydroxylation of such systems supports this proposal. The features present in the spectrum between 1200cm^{-1} and 1600cm^{-1} are attributed to surface nitrate/nitrite and carbonate species (see table 4.1), as well as possible surface water. Re-exposure to CO results in 70% regeneration of the *gem*-dicarbonyl species, and complete removal of the Rh-(NO)(CO) band. The Rh-NO^- and Rh-NO^+ bands are unchanged in intensity, even after 2 hours.

This result is even more pronounced for a sample in which the alumina is heated to 700°C under vacuum for 6 hours prior to MOCVD (figure 4.19). The Rh-CO band has greater intensity than in the previous sample. Again, there is evidence of a weak Rh-NO^+ band at 1920cm^{-1}. Re-exposure to CO shows exactly the same results as the previous example. Again the results show greater similarity to those obtained under UHV conditions when prepared in a similar way.

Figure 4.20 shows the spectra obtained for the NO/CO reaction for alumina pre-treated under a hydrogen atmosphere at 700°C for 6 hours prior to MOCVD. This resulted in an extremely dehydroxylated surface. Although there is a strong Rh-(NO)(CO) band at 2140cm^{-1}, there is no evidence of the Rh-NO^+ species in addition to the broad Rh-NO^- species at 1742cm^{-1}. Re-exposure to CO for 2 hours results in 70% regeneration of the *gem*-dicarbonyl species, a bridging carbonyl species at 1840cm^{-1}, and a band at 1915cm^{-1}, which is attributed to Rh-NO^+.

This experiment was also performed on titania, pre-treated at higher temperatures. Figure 4.21 shows the spectra obtained for the NO/CO reaction for titania pre-treated under H_2 at 700°C for 6 hours prior to MOCVD. The results are very similar to those obtained by pre-treating alumina at the same temperature. The sharp peak at 2140cm^{-1} is again believed to be a Rh-(NO)(CO) species. The broad peak at 1740cm^{-1} is diagnosed as the Rh-NO^- species. There is again a weak band at 1920cm^{-1}, which is believed to be the Rh-NO^+ species. Again, it is believed that the

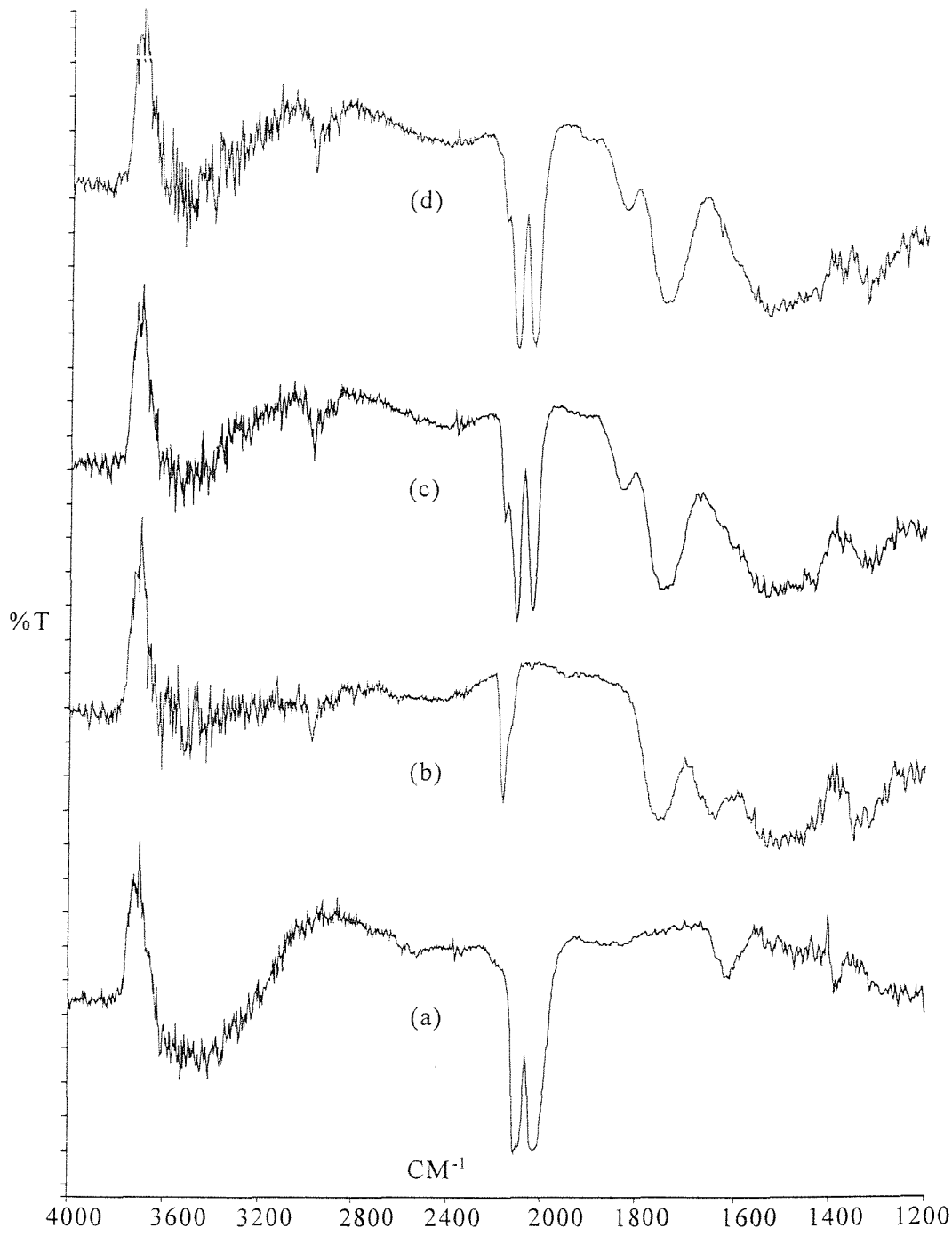

Figure 4.19 DRIFTS difference spectra of reaction of $[Rh(CO)_2Cl]_2$ supported on Al_2O_3 (Dehydroxylated at 550°C) with NO and CO: (a) Before exposure to NO, (b) After reaction with NO for 30 mins, (c) After reaction with CO for 1 hr (d) After reaction with CO for 2 hrs.

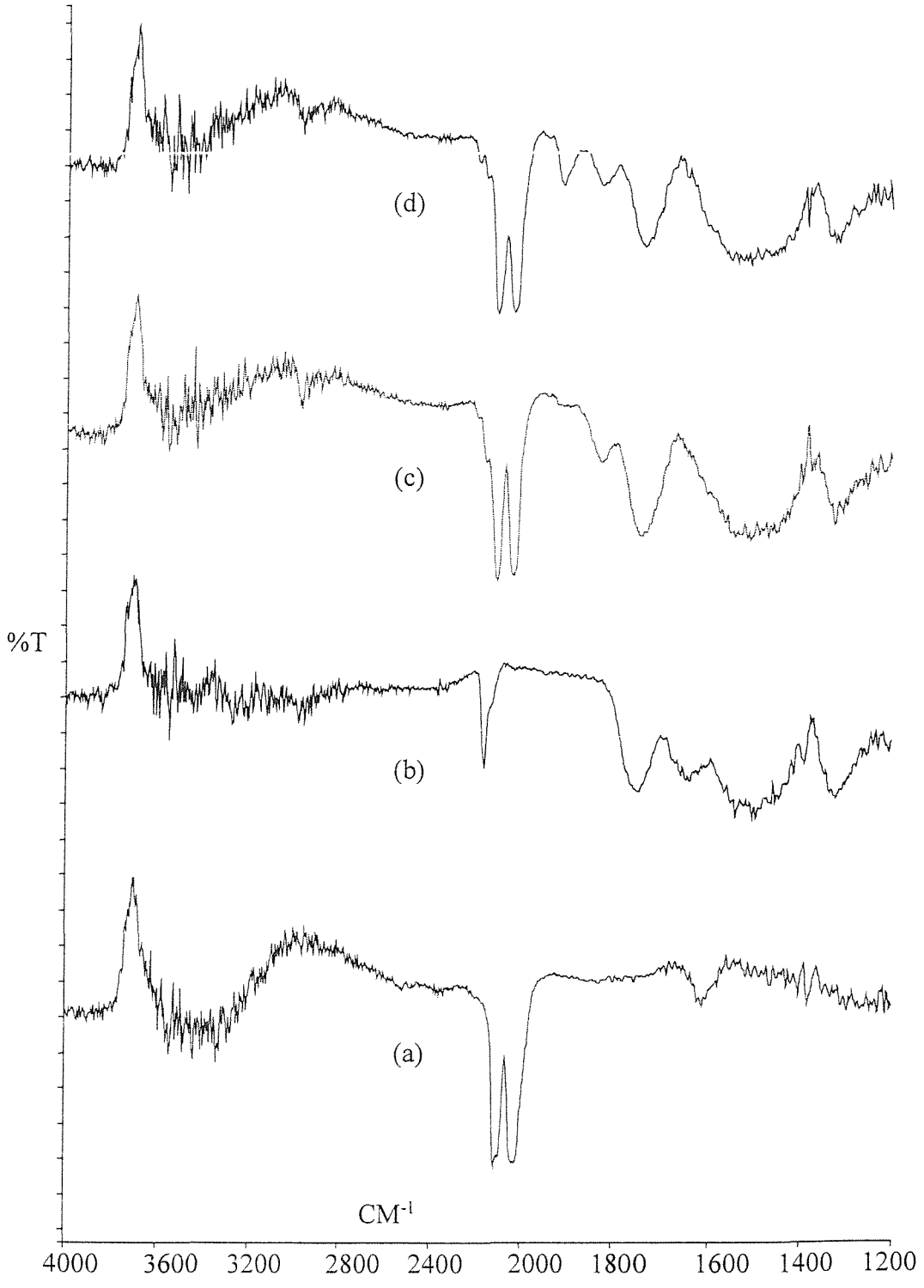

Figure 4.20 DRIFTS difference spectra of reaction of $[Rh(CO)_2Cl]_2$ supported on Al_2O_3 (dehydroxylated at 700°C in H_2) with NO and CO: (a) Before exposure to NO, (b) After reaction with NO for 30 mins, (c) After reaction with CO for 1 hr (d) After reaction with CO for 2 hrs.

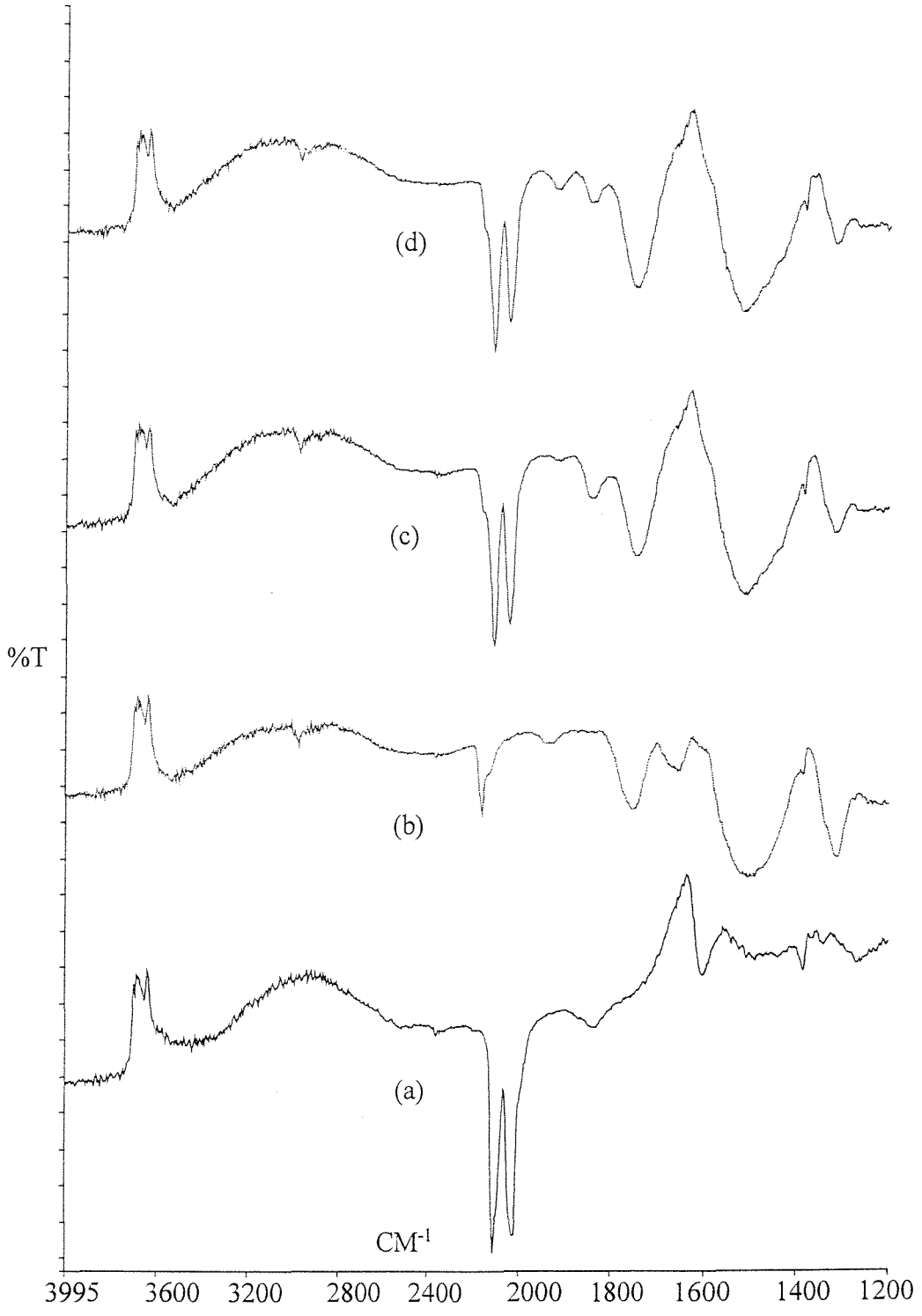

Figure 4.21 DRIFTS difference spectra of reaction of $[Rh(CO)_2Cl]_2$ supported on TiO_2 (Reduced at 700°C Under H_2) with NO and CO: (a) Before exposure to NO, (b) After reaction with NO for 30 mins, (c) After reaction with CO for 1 hr, (d) After reaction with CO for 2 hrs.

greater dehydroxylation of the surface is related to the nature of the nitrosyl species formed. In UHV studies performed at Southampton[29], the surfaces are strongly reduced and Rh-NO^+ species are observed after exposure of titania supported $[Rh(CO)_2Cl]_2$. Re-exposure to CO for 2 hours results in 80% regeneration of the gem dicarbonyl species. There is also a bridging carbonyl band at 1830cm^{-1}. There is however, little attenuation of the NO^- band.

It is possible that the apparent preference for the Rh(CO)(NO) species to form on the surfaces pre-treated at higher temperatures, is due to the fact that the extra electron from the NO can be transferred into the Lewis acid sites (present at higher temperatures). A 16 electron count will apply to the Rh(I) centre and the electron deficient Lewis may have been filled.

4.6 Conclusions

DRIFTS and EDE studies have shown that exposure of titania or alumina supported $[Rh(CO)_2Cl]_2$ to NO for 30 minutes results in a substitution reaction with the *gem*-dicarbonyl ligands and the formation of a Rh-NO^- nitrosyl species and a mixed Rh(NO)(CO) species (indicated by DRIFTS only). EXAFS studies indicates the surface species exists as a $[O]_2Rh(NO)^-(Cl)$ unit. This nitrosyl species is characterised by an infrared stretch at 1742cm^{-1}, and as a bent ligand in EXAFS analysis. This surface nitrosyl species is more stable than the *gem*-dicarbonyl species, and the reverse reaction to reform the *gem*-dicarbonyl species does not proceed to completion at room temperature. Raising the temperature to 65°C upon re-exposure to CO ensures that the regeneration of the *gem*-dicarbonyl species proceeds to completion. Thermolysis of the surface nitrosyl species under a helium atmosphere, results in the formation of small rhodium clusters on the alumina surface at 300°C. This experiment confirms the greater strength of the Rh-NO^- bond relative to the Rh-CO bond. Greater reduction of the surfaces of titania and alumina prior to MOCVD (by heating at greater temperatures and under a hydrogen atmosphere), results in changes in the species formed upon exposure of supported $[Rh(CO)_2Cl]_2$ to NO.

There is a strengthening in the intensity of the Rh-(NO)(CO) species formed at for the more dehydroxylated surfaces (with an exception for alumina reduced under hydrogen at 700∘C), and the appearance of a Rh-NO^+ band at 1920cm^{-1}. These results bear greater resemblance to analogous experiments performed in UHV systems[29], in which the surfaces are highly reduced prior to MOCVD. Many of the experiments in this study require further study, particularly the persistence of the Rh-NO^- ligand after CO regeneration in DRIFTS studies, and variable reduction of the surfaces prior to MOCVD.

4.7 Experimental

Refer to section 3.8 for details of preparation of $[Rh(CO)_2Cl]_2$ and surface supported species.

4.8 References

1. M Funabiki, T. Yamada and K. Kayano, *Catal. Today*, 1981, **10**, 33.

2. S. W. Briggs, *Applied Ind. Catal.*, Ed B. E. Leach, Vol. 3, Academic Press, New York, 1984.

3. B. J. Cooper, W. D. Evans and B. Harrison, *Catalysis and Automotive Pollution Control*, Ed A. Cruq, Vol 30, Elsevier, New York, 1987, p117.

4. S. H. Oh, G. B. Fisher, J. E. Carpenter and D. W. Goodman, *J. Catal.*, 1986, **100**, 360.

5. T. Hahn and G. H.Lintz, *Surf. Sci.*, 1988, **211**, 1030.

6. R. J. Farrauto, R. M. Heck and B. K Speronello, *Chem Eng. News*, 1992, 7, 42.

7. K. C. Taylor, *Catal. Rev.Sci. Eng.*, 1993, **35**, 457.

8. Platinum 1993, Johnson Matthey, London.

9. B. E. Nieuwenhuys, J. Siera, K. Tanaka and H. Hirano, *ACS Symp. Ser.*, 1994, **V552**, pp114-39.

10. K. C. Taylor, *Automotive Catalytic Converters*, Springer Verlag, Berlin, 1984.

11. C. D. Meyer and R. Eisenberger, *J. Am. Chem. Soc.*, 1976, **98**, 1364.

12. H. C. Yao, Y. F. Yu-Yao and K. Otto, *J. Catal.*, 1979, **56**, 21.

13. S. E. Oh and C. C. Eickel, *J. Catal.*, 1991, **128**, 526.

14. F. Solymosi, T. Bansagi and E. Novak, *J. Catal.*, 1988, **112**, 183.

15. G. Srinivas, S. S. C. Chang and S. Debnath, *J. Catal.*, 1994, **148**, 748.

16. E. Novak, D. Sprinceana and F. Solymosi, *Appl. Catal. A*, 1997, **149**, 89.

17. K. C. Cannon, S. K. Ho and J. M. White, *J. Am. Chem. Soc.*, 1989, **111**, 5064.

18. F. Solymosi and J. Sarkany, *Appl. Surf. Sci.*, 1979, **3**, 68.

19. E. A. Hyde and R. Rudham, *J. Chem. Soc. Faraday Trans.*, 1984, **80**, 531.

20. H. Arai and H. Tominaga, *J. Catal.*, 1976, **43**, 131.

21. J. Liang, H. P. Wang and L. P. Spicer, *J. Phys. Chem.*, 1985, **89**, 5840.

22. R. Dictor, *J. Catal.*, 1988, **109**, 89.

23. T. W. Root, G. B. Fisher and L. D. Schmidt, *J. Chem. Phys.*, 1986, **85**, 4879.

24. G. Cautero, C. Astaldi, P. Rudolf, M. Kishkinova and R. Rosei, *Surf Sci.*, 1991, **258**, 44.

25. J. S. Villarubia and W. Ho, *J. Phys. Chem.*, 1987, **87**, 750.

26. H. J. Borg, J. F. C. Reijerse, R. A. Van Santen and J. W. Niemantsverdriet, , *J. Chem. Phys.*, 1994, **101**, 10052.

27. Y. J. Kim, S. Thevuthasen, G. S. Herman, C. H. F. Peden, S. A. Chambers, D. H. Belton and H. Permana, *Surf Sci.*, 1996, **359**, 269.

28. D. J. Loffreda, D. Simon and P. Saudet, *Chem. Phys. Lett.*, 1998, **291**, 15.

29. B. E. Hayden, A. King, M. A. Newton and N. Yoshikawa, *J. Phys. Chem.*, Submitted.

30. P. Bsau, T. H. Ballinger and J. T. Yates Jr, *Rev. Sci. Instr.*, 1988, **59**, 1321.

31. J. C. S. Wong and J. T. Yates Jr, *J. Phys. Chem.*, 1995, **99**, 12640.

32. J. M. R. Galas, M. B. Hursthouse, D. S. Moore and S. D. Robinson, *Inorg. Chem. Acta.*, 1983, **77**, 135.

33. S. Z. Goldberg, C. Kubiak, C. D. Meyer and R. D. Eisenberg, *Inorg. Chem..*, 1975, **14**, 1650.

Chapter 5

The Surface Organometallic Chemistry of $Rh(CO)_2(acac)$ Supported on Titania and Alumina

5.1 Introduction

The organometallic $Rh(CO)_2(acac)$ is a monermeric, air stable compound. It sublimes at ambient temperatures without decomposition, and is thus an ideal precursor for MOCVD. One of the possible advantages of using $Rh(CO)_2(acac)$ as a precursor instead of $[Rh(CO)_2Cl]_2$ is that the acac ligand is unlikely to affect the properties of the surface unlike the chlorine in $[Rh(CO)_2Cl]_2$ is understood to do[1]. However, the surface organometallic chemistry of $Rh(CO)_2(acac)$ has not been as widely investigated as that of $[Rh(CO)_2Cl]_2$, and is therefore not as well understood.

The reaction of $Rh(CO)_2(acac)$ with partially dehydroxylated titania has been investigated by Rudkin and Williams[2,3]. Samples were supported on the oxide surface by MOCVD in those investigations, and therefore offer results that can be compared with those from this study. EXAFS spectroscopy indicated that the surface organometallic species has no observable change in coordination around the metal centre[3]. The use of CP-MAS ^{13}C NMR has also shown the acac ligand to be retained on the surface after adsorption[3]. Rh XPS indicated that the $Rh(CO)_2(acac)$ remained unaltered when adsorbed on silica, and after use as a carbon monoxide hydrogenation catalyst, rhodium metal was formed[4]. $Rh(CO)_2(acac)$ has also been attached to phosphine functionalised polymers, with the evolution of one equivalent on CO[5,6].

A DRIFTS study of $Rh(CO)_2(acac)$ supported on partially dehydroxylated titania was conducted by Williams[2]. It was observed that surface hydroxyl groups were consumed during the adsorption process, and the organometallic molecule was bound to the surface intact.

Studies by Tearle on the adsorption of $Rh(CO)_2(acac)$ onto aluminophosphates $AlPO_4$-5 and $AlPO_4$-11 again showed no change in the coordination around the rhodium upon adsorption onto $AlPO_4$-5, though the presence of two coordinated surface oxygen atoms could be observed from EXAFS studies of $Rh(CO)_2(acac)$

adsorbed onto $AlPO_4$-11[7]. It was again observed, however, that there was no change in the coordination of the carbonyl or the acac ligand on reaction with either of the supports.

Studies by Özin et al. of $Rh(CO)_2(acac)$ supported into Na-Y Zeolite by wet impregnation, caused the carbonyl bands of the precursor, observed at 2084cm^{-1} and 2015cm^{-1} to shift to 2103cm^{-1} and 2039cm^{-1}. Photolysis of this sample was considered to lead to the formation of the *gem* dicarbonyl species, which had infrared bands at 2098cm^{-1} and 2021cm^{-1}, accompanied by the formation of Na(acac). The proposed reaction is:

$$NaY + Rh(CO)_2(acac) \rightarrow Na(acac) + ZO\text{-}Rh(CO)_2$$

EXAFS studies of the thermolysis of the surface supported species by Rudkin[3] have shown all ligand coordination to be lost upon heating to 473K under an inert atmosphere. Further heating of the sample caused continual growth in the size of the metal particles. Subsequent exposure to CO caused disruption of these particles, but formation of any surface supported rhodium carbonyl species was insufficient to be detected by EXAFS spectroscopy. Reaction of the surface species with hydrogen at 473K caused loss all organometallic ligands and growth of small metal particles. Exposure to CO was seen to cause a growth in size of the metal particles.

Thermolysis studies using DRIFTS spectroscopy, by Williams[2], have shown a gradual loss in intensity for both CO groups and acac ligand, accompanied by the growth of a band at 2060cm^{-1} occurring at 475K, which was assigned to a linear carbonyl species adsorbed on metal particles. Loss of the carbonyl signal was complete by 573K. Re-exposure of the surface to CO regenerated the *gem* dicarbonyl species, which indicated that the rhodium was highly dispersed.

DRIFTS studies by Tearle[7] on the thermolysis of $Rh(CO)_2(acac)$ supported on $AlPO_4$-5 again showed a reduction in the intensity of the *gem* dicarbonyl band and the development of a linear carbonyl species at 2060cm^{-1}. EXAFS studies of this system

have shown the formation of small metal particles, with a first shell coordination number of 4 to become apparent by 423K, with the coordination to two surface atoms and two carbonyl groups to the rhodium also being observed at this temperature. By 573K, the size of the metal particles had grown, accompanied by the loss of coordination to the carbonyl groups and surface species. Comparative studies of the thermolysis of $Rh(CO)_2(acac)$ supported on $AlPO_4$-11, showed no intermediate carbonyl species during the transition to metal clusters. At 423K the EXAFS spectrum showed coordination to 2 surface oxygen atoms, and 6 rhodium atoms.

Studies by Jackson et al. of the hydrogenation of CO performed by silica supported rhodium catalysts found the specific activity to be proportional to the amount of hydrocarbon residue per active site[4]. Variation in selectivity was attributed to variations in the available site geometries on the metal crystallites. It was found that the catalyst prepared from $[Rh(CO)_2Cl]_2$ showed higher activity than that prepared from $Rh(CO)_2(acac)$. The latter system did however have the highest selectivity to ethanal production of all catalysts involved in this study.

Serp *et al*[9] investigated the reaction of $Rh(CO)_2(acac)$ supported on SiO_2 with hydrogen. This supported system was prepared using MOCVD and is thus comparable to the systems under investigation in this thesis. They suggested that the acac group may be hydrogenated to form 2-4-pentanedione under an H_2 stream.

5.2 Adsorption of $Rh(CO)_2(acac)$ onto TiO_2 and Al_2O_3

5.2.1 DRIFTS Study of Adsorption of $Rh(CO)_2(acac)$ onto TiO_2

An infrared spectrum of $Rh(CO)_2(acac)$ is shown in figure 5.1. The spectrum was acquired using a KBr disc of the organometallic. The infrared bands observed are due to the vibrations of the carbonyl and acetylacetonato (acac) ligands of $Rh(CO)_2(acac)$. Assignments were made by comparison with a single crystal IR

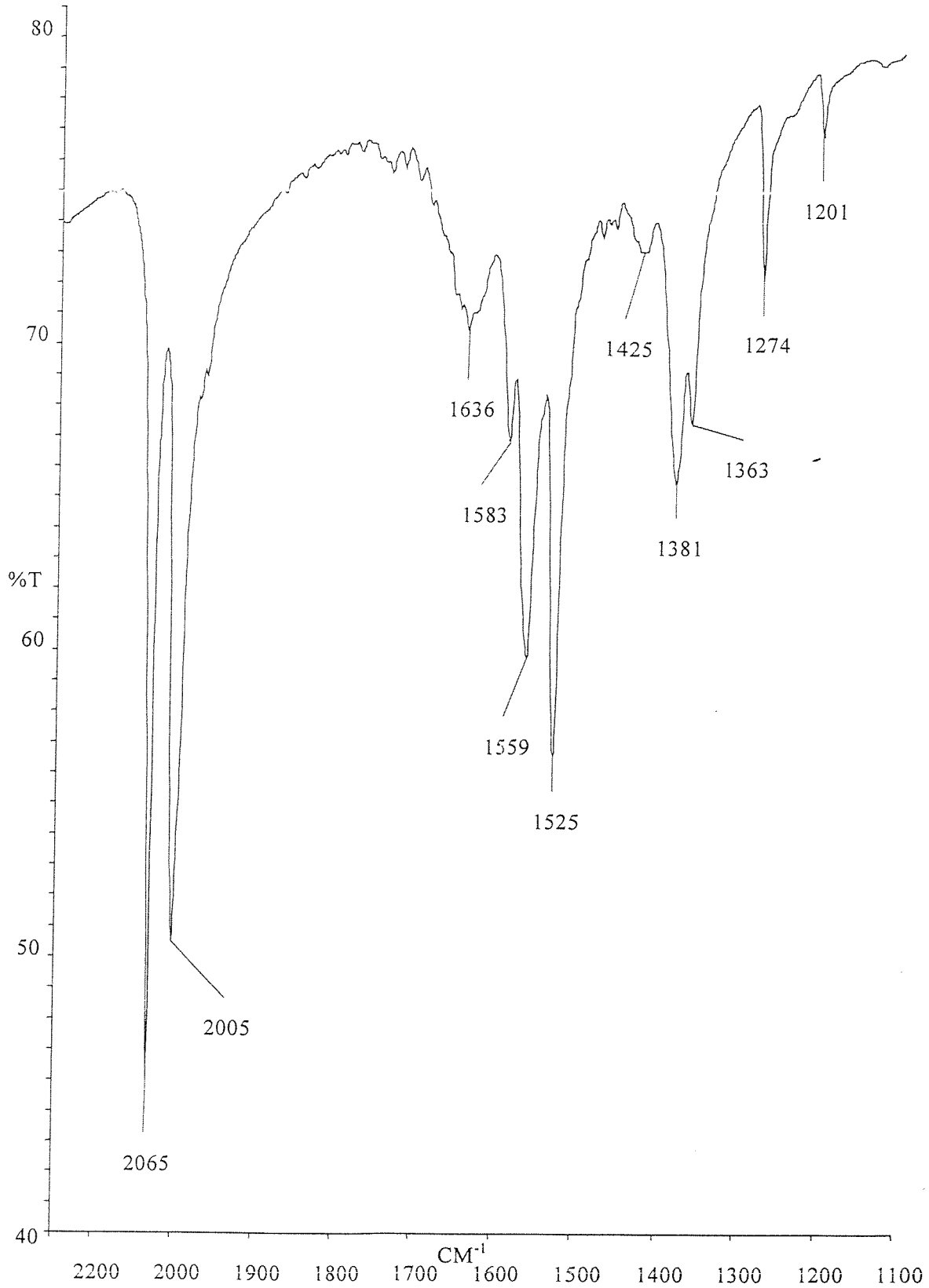

Figure 5.1 Infrared (KBr) Spectrum of $Rh(CO)_2(acac)$

investigation of $Rh(CO)_2(acac)$[10], and comparison with the IR frequencies of the well studied $Fe(acac)_3$ and $Cu(acac)_2$ complexes (table 5.1).

$Rh(CO)_2(acac)$ was supported on partially dehydroxylated titania by MOCVD and a difference DRIFTS spectrum was taken, using untreated titania as the background. The spectrum is shown in figure 5.2. There is a slight change in the $\nu(CO)$ region of the $Rh(CO)_2(acac)$ on adsorption, with the high frequency band being shifted from $2083cm^{-1}$ to $2090cm^{-1}$, whilst the lower frequency band remains unchanged at $2012cm^{-1}$. This slight increase in frequency of the carbonyl bands suggests a possible slight weakening of the Rh-C bond due to less backbonding from the carbonyl ligand to the metal. This may be due to a modification of the electronic environment of the rhodium upon adsorption to the surface. These carbonyl frequencies are almost identical to those observed in the $[Rh(CO)_2Cl]_2$ system post thermolysis, and after exposure to CO (3.4.1). In this case the removal of the chlorine ligands was responsible for the increase in backbonding into the CO antibonding orbitals, thus reducing the frequency from $2105cm^{-1}$ and $2025cm^{-1}$, to $2090cm^{-1}$ and $2018cm^{-1}$. EXAFS studies will illustrate this change more clearly and allow inferences about the nature of the adsorption of the organometallic to the surface to be made. The broad, positive band from $3000cm^{-1}$ to $3500cm^{-1}$ suggests that the $Rh(CO)_2(acac)$ has reacted with surface hydroxyl groups upon adsorption to the titania surface. The acac region of the spectrum is seen to undergo some changes upon adsorption to the titania surface. There is a significant modification of the band at $1435cm^{-1}$, which is assigned to $\delta(CH)$ or $\nu(C\text{-}C)$. The two precursor bands at $1579cm^{-1}$ and $1552cm^{-1}$, merge to form one band at $1582cm^{-1}$. The precursor band at $1379cm^{-1}$, which is associated with $\delta(CH_3)$, becomes much broader in the surface species. The precursor band at $1272cm^{-1}$, which is attributed to $\upsilon(C\text{-}CH_3)$, shifts to $1279cm^{-1}$ upon adsorption. These changes are insufficient to suggest a change in the coordination of the acac ligand to the rhodium centre, or the structure of the ligand itself.

$Rh(CO)_2(acac)$ was also supported on $\gamma\text{-}Al_2O_3$ prior to EDE studies at the ESRF, as titania could not be used as a support for such studies (see section 3.2). A difference DRIFTS spectrum was recorded (figure 5.3), and shows no significant

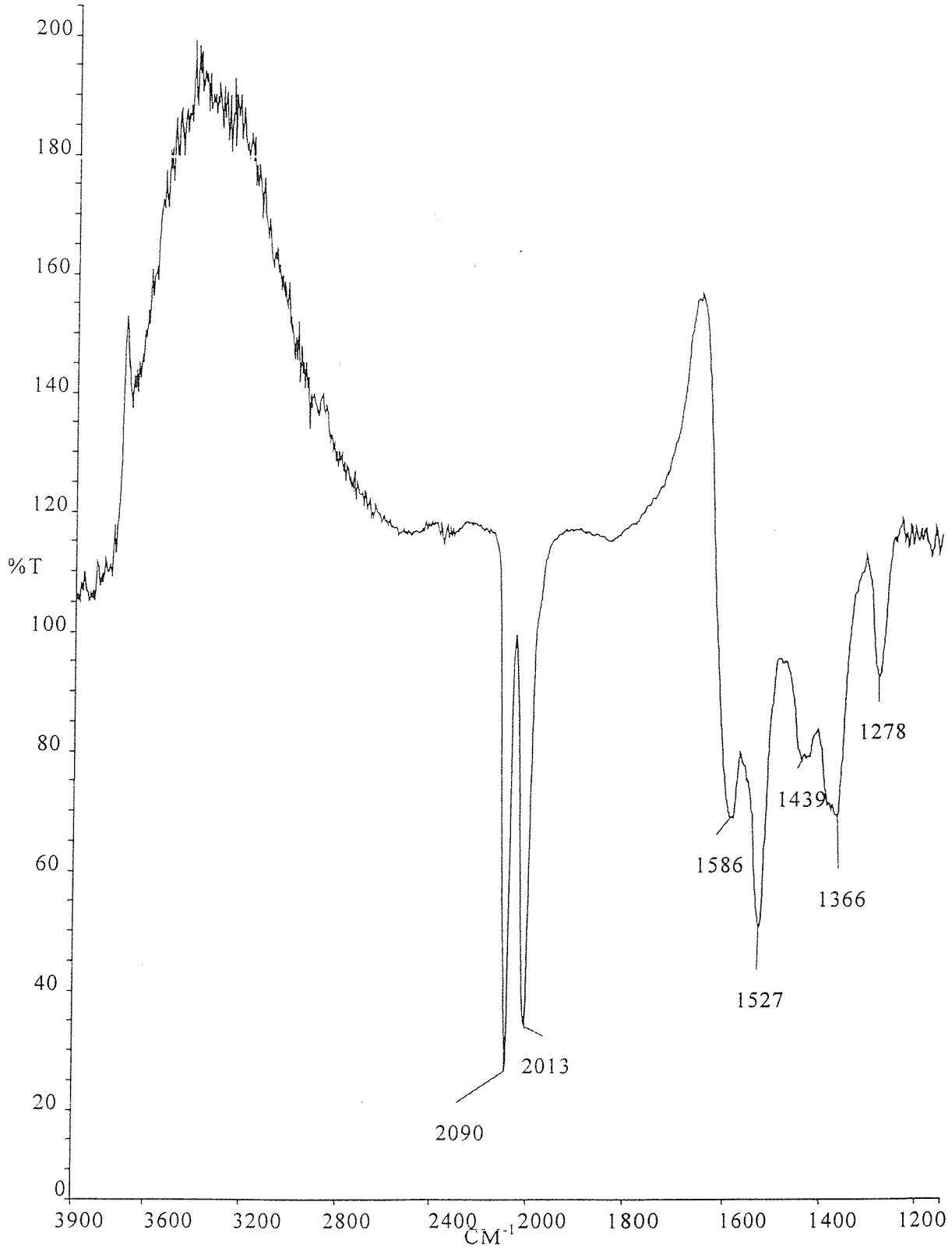

Figure 5.2 DRIFTS difference spectrum of $Rh(CO)_2(acac)$ supported on TiO_2

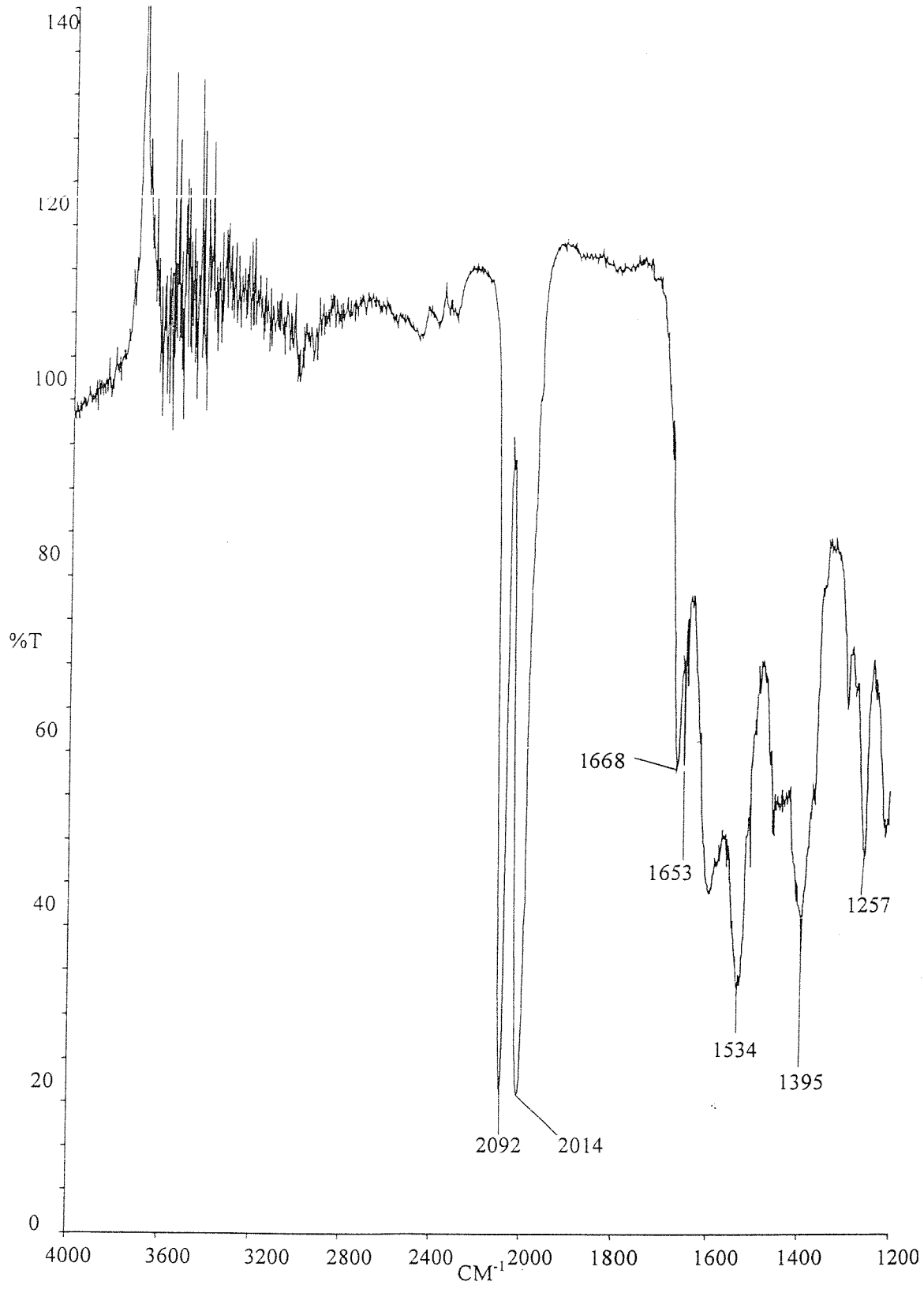

Figure 5.3 DRIFTS difference spectrum of $Rh(CO)_2(acac)$ supported on partially dehydroxylated Al_2O_3

differences in carbonyl and acac intensities or frequencies from the titania supported sample. It can be concluded that the organometallic is physisorbed intact to the surface, and has occurred with the consumption of surface hydroxyl groups. This may be via a reaction of the surface hydroxyl groups and the delocalised π electrons and oxygen of the acac ligand.

The data quality of the alumina supported $Rh(CO)_2(acac)$ is poorer than the titania analogue, because alumina has a more poorly reflecting surface than titania. Therefore results from titania studies only are subsequently presented, as the mode of surface adsorption appears to be identical.

$Cu(acac)_2$	$Fe(acac)_3$	$Rh(CO)_2(acac)_2$	$Rh(CO)_2(acac)_2/ TiO_2$	Assignment
1577	1570	1579	1587	ν(C-O)
1549		1552		combination
1529	1525	1525	1528	ν(C-C)
1461	1445	1435	1440	δ(CH) + ν(C-C)
1413	1425			δ_d(CH)
1353	1385, 1360	1379	1366	δ_s(CH)
1274	1274		1279	ν(C-CH_3)

Table 5.1 Frequencies and assignments of acetylacetonato complexes in the 1700-1200cm^{-1} region[2].

5.2.2 EXAFS Study of Adsorption of $Rh(CO)_2(acac)$ onto TiO_2

The Rh K-Edge EXAFS and Fourier transform for $Rh(CO)_2(acac)$ supported on partially dehydroxylated titania (section 5.9 for method) are shown in figure 5.4.

Figure 5.4 Rh K-Edge EXAFS and Fourier transform of $Rh(CO)_2(acac)$ supported on TiO_2

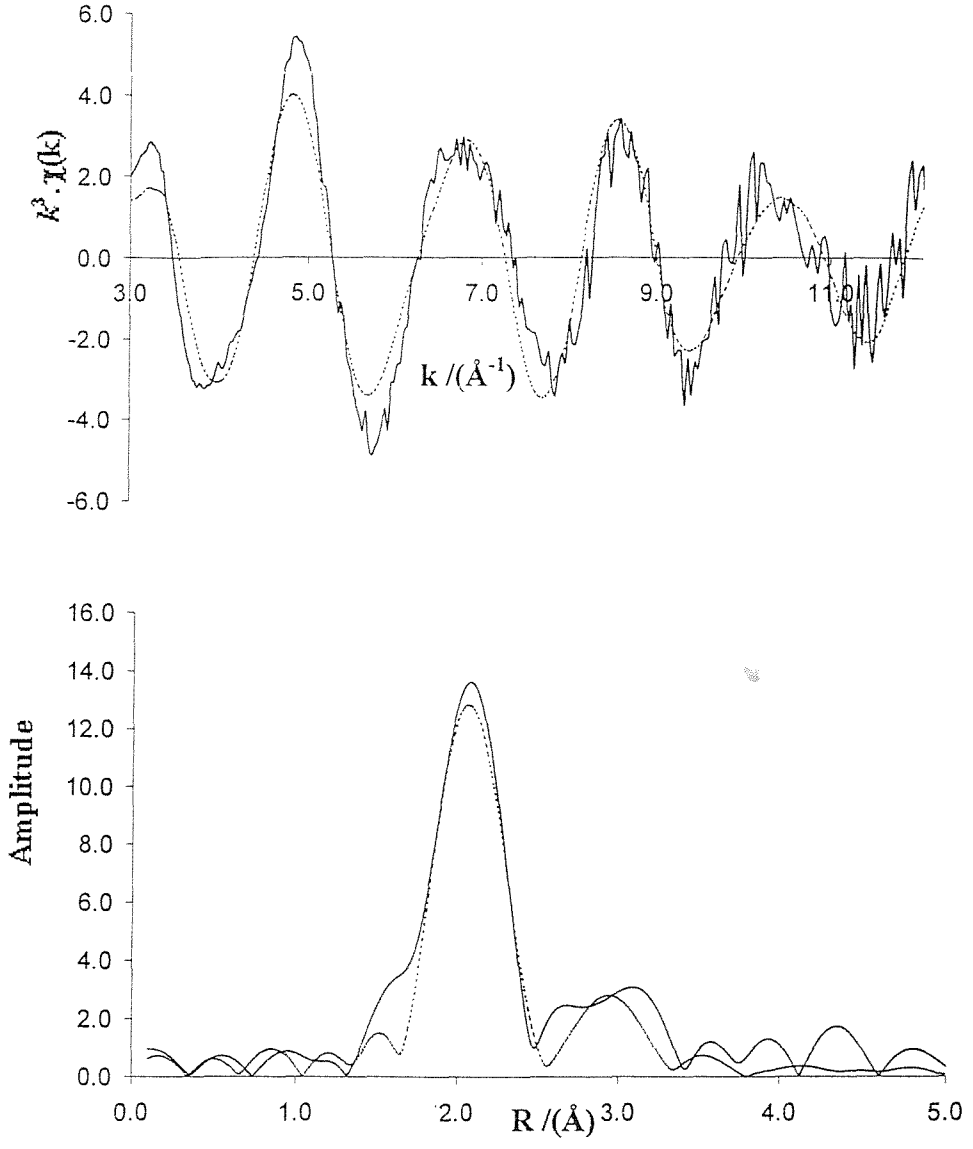

Atom	C.N.	r/Å	$2\sigma^2$ / Å^2
O	2(0.2)	2.058(6)	0.002(1)
C	2(0.1)	2.074(5)	0.003(1)
C	2(0.3)	3.035(5)	0.006(2)
O	2(0.2)	3.131(7)	0.012(3)

R = 34.22 %
Ef = -1.00 eV

The spectrum was acquired at the SRS at Daresbury using the *in situ* EXAFS cell. Three spectra were averaged to improve the signal to noise ratio. Inclusion of multiple scattering calculations for the carbonyl group and the acac ligand gave a fit with structural parameters close to those obtained for $Rh(CO)_2(acac)$ in crystal structure in crystal structure determinations, and by EXAFS spectroscopy, see table 5.2.

Parameter	$Rh(CO)_2(acac)$ X-Ray[11]	$Rh(CO)_2(acac)$ EXAFS[3]	$Rh(CO)_2(acac)/TiO_2$, EXAFS	$Rh(CO)_2(acac)/Al_2O_3$, EDE
Rh-C	1.831 Å	1.857(4) Å	2.058(6) Å	2.069(5) Å
Rh-O	2.042 Å	2.024(4) Å	2.074(5) Å	2.090(4) Å
Rh-O	2.986 Å	2.995(5) Å	3.131(7) Å	3.125(7) Å
Rh-C	2.973 Å	3.028(11) Å	3.031(7) Å	3.052(4) Å
∠ Rh-C-O	179°		180°	180°
∠ Rh-O-C	125°		125°	125°

Table 5.2 A comparison of structural parameters for $Rh(CO)_2(acac)$ both as a free organometallic, and supported on oxide surfaces

There is one large peak at ≈ 2.1Å in the Fourier transform spectrum as well as a smaller peak at ≈ 3.1Å. The former is attributed to the Rh-C and Rh-O shells from the carbonyl and acac groups respectively. The latter peak is attributed to the Rh-O and Rh-C distances, also respectively from the carbonyl and acac groups. The lengthening of the rhodium-carbonyl distances upon supporting the organometallic onto titania suggests a weakening of the carbonyl bond. This could be due to bonding of the rhodium centre to a surface oxygen, either by chemisorption or physisorption. Alternatively, the lengthening of the Rh-C bond could be due to too much correlation with Rh-O (acac).The DRIFTS spectra also indicates a slight weakening of the rhodium carbonyl bond upon adsorption to the TiO_2 surface (an increase in the frequency of the carbonyl bands), and indicate the consumption of surface hydroxyl groups upon absorption. However, the inclusion of a surface oxygen atom in the

coordination sphere, did not give a significant improvement in the quality of the fit. The EXAFS data, in conjunction with the DRIFTS results, therefore suggests that $Rh(CO)_2(acac)$ is physisorbed on the titania surface.

The Rh K-edge Energy Dispersive EXAFS (EDE) spectrum and its Fourier transform for $Rh(CO)_2(acac)$ supported on partially dehydroxylated alumina, are shown in figure 5.5. The spectrum was acquired at the ESRF at Grenoble using the catalytic microreactor with the sample maintained under a flow of helium (5ml/min). The spectrum is an average of 100 scans, each lasting 19 ms (19 frames at 1ms), resulting in a total acquisition time of 1.9s.

The Fourier transform shows the presence of two coordination shells, the first main peak is at ≈ 2.1Å, as well as another large peak at ≈ 3.1Å. The former is attributed to the Rh-C and Rh-O shells from the carbonyl and acac groups respectively. The latter peak is attributed to the Rh-O and Rh-C distances, also respectively from the carbonyl and acac groups. Inclusion of multiple scattering calculations for the carbonyl group and the acac ligand improved the fit of the data. Though the intensities of the peaks are slightly different to the titania supported sample, the bonding rationale is believed to be the same. Again, no surface oxygen bond was observed, and the organometallic is believed to be physisorbed to the alumina surface, possibly via hydrogen bonding from Al-OH with the acac ligand.

5.3 Thermolysis of $Rh(CO)_2(acac)$ onto TiO_2 and Al_2O_3

5.3.1 DRIFTS Study of Thermolysis of $Rh(CO)_2(acac)$ onto TiO_2 and Al_2O_3

The thermolysis experiment was carried out *ex-situ* under a helium atmosphere, where samples were heated to the stated temperature for 10 minutes and transferred to the DRIFTS cell. Spectra were collected at 100 scans, using

Figure 5.5 Rh K-Edge EXAFS and Fourier transform of $Rh(CO)_2(acac)$ supported on Al_2O_3

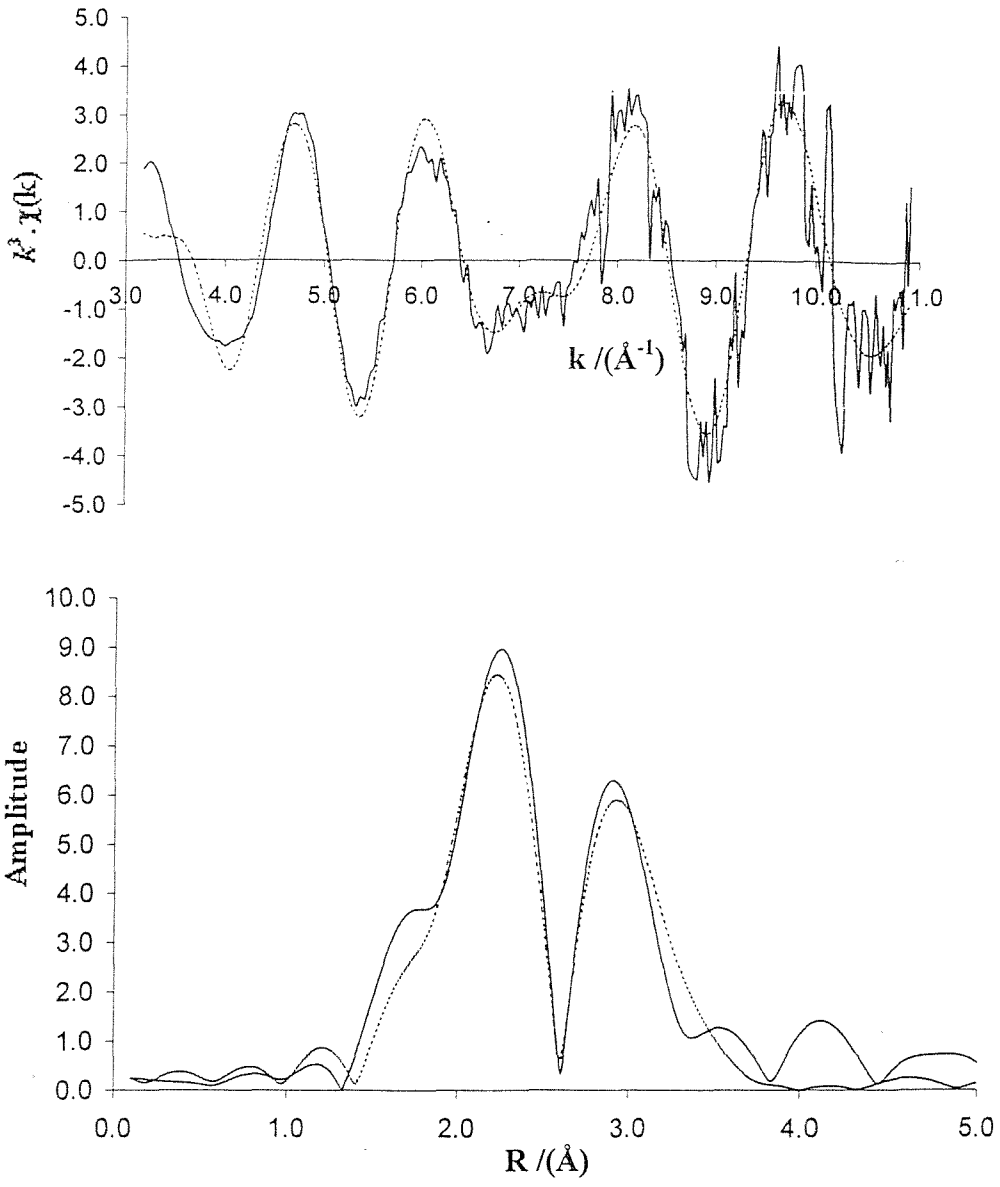

Atom	C.N.	r/Å	$2\sigma^2$ / Å^2
C	2(0.3)	2.069(5)	0.002(1)
O	2(0.2)	2.090(4)	0.003(1)
C	2(0.2)	3.052(4)	0.006(2)
O	2(0.3)	3.125(7)	0.012(3)

R = 36.28 %
Ef = -0.26 eV

hydroxylated titania as a background.

A stacked plot of the DRIFTS spectra from the thermolysis experiment is shown in figure 5.6. The assignments for the starting room temperature spectrum are given in table 5.1. At 100°C, the intensity of the carbonyl ligands had reduced to 70% of their original value, though their frequencies remained unchanged. The overall intensity of the acac region was unchanged, though there were changes in the intensities of the individual bands. The υ(C-O) band at 1580cm^{-1} had decreased slightly in intensity, and the υ(C-C) band at 1528cm^{-1} had sharpened. The bands at 1433cm^{-1} and 1386cm^{-1} had merged to form a broad feature, and the band at 1272cm^{-1} remained unchanged. By 130°C, the carbonyl intensities had reduced to 40% of their original intensity, though again the frequencies were unchanged. The trends in the acac region had continued, with the two main features being the sharp band at 1528cm^{-1} and the broad band in the 1400-1430cm^{-1} region. There was also a weakening in the intensity of the band at 1272cm^{-1}. At 160°C, the carbonyl intensities had reduced to 20% of their original intensity, and the development of a linear carbonyl band at 2070cm^{-1} had begun. The acac region is identical to that at 130°C. By 190°C, the carbonyl features have disappeared, and the acac region consists of two peaks at 1528cm^{-1} and 1440cm^{-1}. The acac features gradually decrease in intensity as the temperature is raised, until they disappear completely at 310°C. Again, their frequencies remained unchanged during this process.

The nature of the removal of the carbonyl ligands in this experiment seems quite different to that of the $[Rh(CO)_2Cl]_2$ analogue (3.4.1). The carbonyl ligands in the latter system persist until higher temperatures (≈200°C) and pass through a distinct linear carbonyl species. In the acac system, there is much less of the transitional linear species present, and the carbonyl ligands disappear at around 170°C.

There appears to be considerable transformation of the acac ligands between 130°C and 280°C, before complete their complete removal by 310°C. It is possible

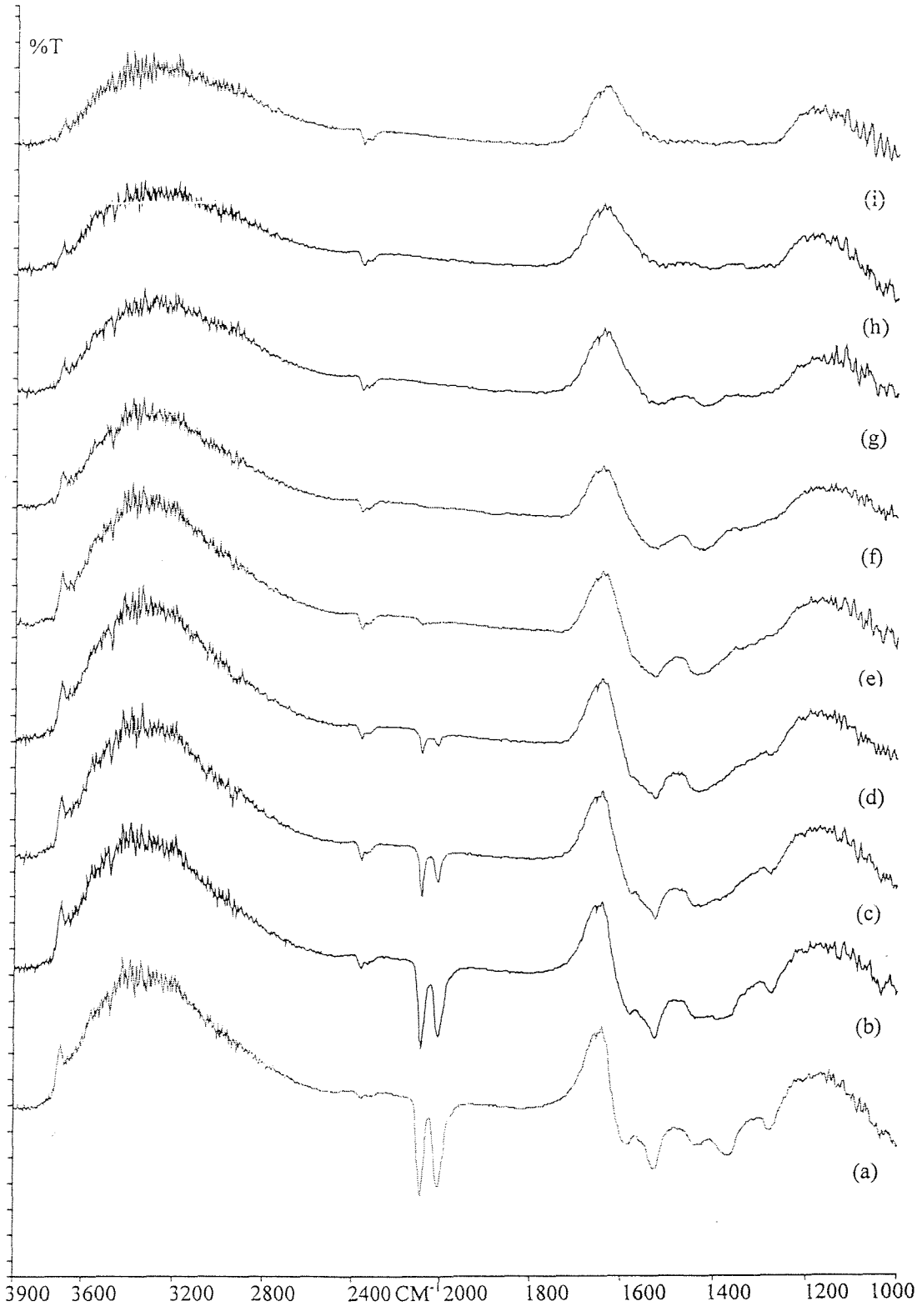

Figure 5.6 DRIFTS difference spectra of $Rh(CO)_2(acac)$ supported on TiO_2 during helium thermolysis: (a) Room temp, (b) 100°C, (c) 130°C, (d) 160°C, (e) 190°C, (f) 220°C, (g) 250°C, (h) 280°C, (i) 310°C

that some dehydrogenation of the CH_3 ligands occurs followed by cleavage of the C-O ligands. The C-C backbone seems to remain intact until higher temperatures before removal by 330°C. A deeper understanding of the mechanism could be found from TPD results, which would monitor the gas phase during the thermolysis, indicating fragments of the acac ligand desorbed during the experiment.

5.3.2 Energy Dispersive EXAFS Study of Thermolysis of $Rh(CO)_2(acac)$ Supported on TiO_2 and Al_2O_3

The Rh K-edge Energy Dispersive EXAFS experiment for the helium thermolysis of $Rh(CO)_2(acac)$ supported on partially dehydroxylated alumina was performed at the ESRF in Grenoble, at station ID24. The samples were heated at a rate of 5°C per minute, under a flow of 5ml/min of helium. The experiment was time resolved, with 150 spectra being collected as the temperature was raised from 30°C to 400°C, with each individual spectrum acquired in 0.6 seconds.

The starting spectrum has been illustrated in figure 5.5, showing the surface supported $Rh(CO)_2(acac)$ species. No significant changes in the spectrum were apparent until a temperature of 180°C (apart from the change in the size of the edge jump-see next paragraph) had been reached, figure 5.7. The shape of the EXAFS is different to that of the starting species, in that there is greater intensity at higher energies, which is diagnostic of the presence of heavy backscatterering atoms such as rhodium. The Fourier transform has the basic shape of that of the $Rh(CO)_2(acac)$ species, but with greater intensity in the first and second peaks, corresponding to the distances of the first and second rhodium shells in a rhodium cluster. Several models were used to try and fit to the data, including a linear carbonyl species and metal clusters. The best fit came from a model with a mixture of the $Rh(CO)_2(acac)$ species and three partially filled shells of rhodium. The bond lengths of the $Rh(CO)_2(acac)$ species are consistent with those found on the previous spectra in this experiment. The rhodium distances are at 2.69, 3.73, and 4.64Å, which are consistent with the distances found in the bulk metal.

Figure 5.7 Rh K-Edge EXAFS and Fourier transform of $Rh(CO)_2(acac)$ supported on Al_2O_3 after reaction with helium at 180°C

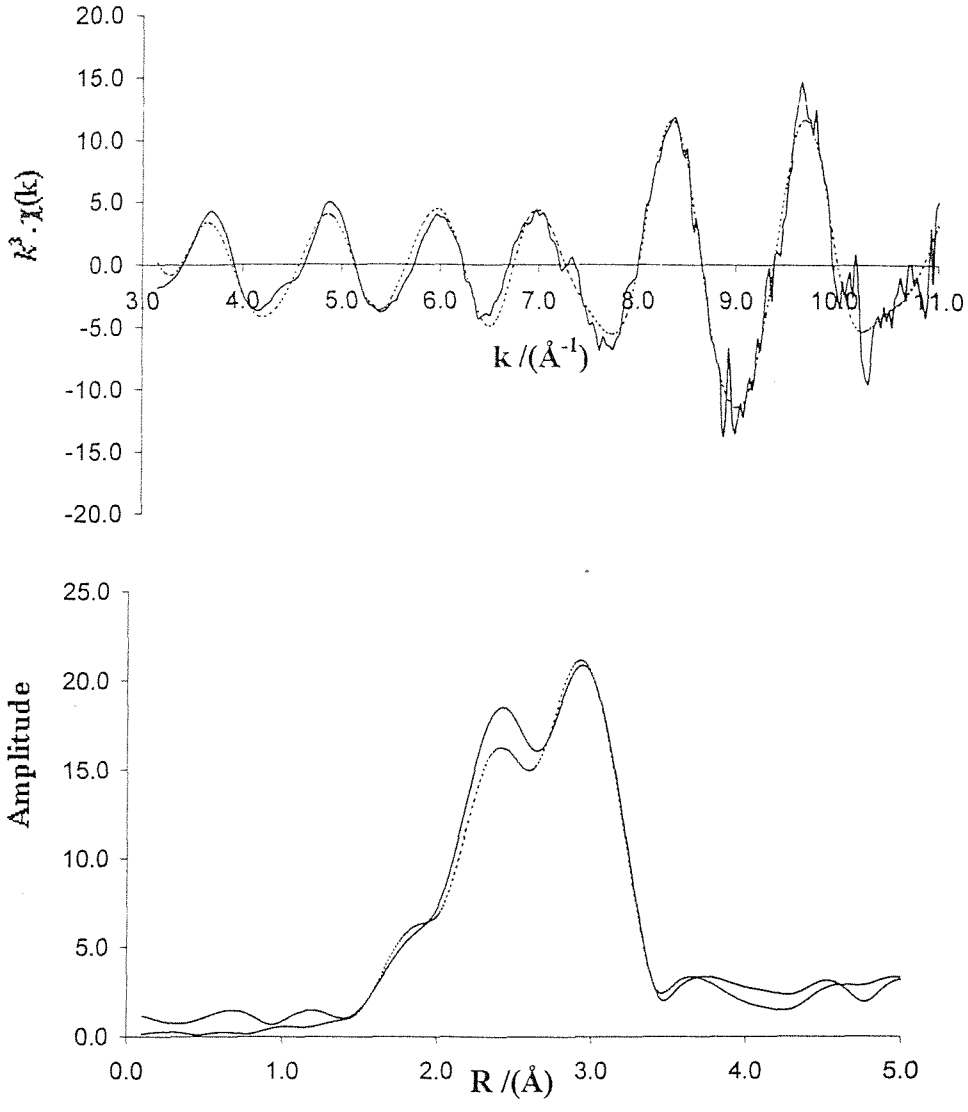

Atom	C.N.	r/Å	$2\sigma^2$ / Å^2
C	2(0.2)	1.878(2)	0.002(1)
O	2(0.2)	2.122(3)	0.001(1)
Rh	8(1.3)	2.691(3)	0.009(1)
O	2(0.3)	3.019(4)	0.005(3)
Rh	5(1.1)	3.734(5)	0.021(3)
Rh	6(1.4)	4.685(5)	0.024(2)

R = 34.00 %
Ef = 2.69 eV

The data quality of subsequent spectra, illustrated the growth of bulk rhodium clusters on the alumina surface. The data quality is poor however due to the rapid acquisition time, and coordination numbers for the clusters have large error values. The hydrogen thermolysis of $Rh(CO)_2(acac)$ produced data of superior quality, and the results for this experiment are shown in section 5.5.2.

The final spectrum of the sample after heating to 400°C in helium, is shown in figure 5.8. There are five peaks in the Fourier transform, the first of which is much more intense than the other four. A rhodium cluster model was applied to these data, and the coordination number was refined. The results indicate that the thermolyisis experiment has generated large clusters of rhodium, as the coordination numbers for the five shells resemble those of bulk metal. The bond distances also match those found in bulk rhodium, with deviations no greater than 0.05Å.

The results of these experiments agree well with those for the DRIFTS study of the same reaction in terms of the removal of the carbonyl and acac species and the formation of rhodium clusters on the alumina surface. The temperature at which the transition takes place is consistent in both experiments. The differences in results between the DRIFTS and EDE studies can be explained in terms of the varying sensitivities of the two techniques. Infrared spectroscopy is particularly sensitive to the intense bands caused by the C-O stretch, while it will not observe any signal for metal particles. Conversely, EXAFS spectroscopy is sensitive to large backscattering atoms such as rhodium. Since EXAFS observes an average signal from all absorbing atoms, the presence of small metal particles will swamp the signal for any residual carbonyl groups, which would still be detectable by infrared spectroscopy. This probably explains why it was impossible to fit a linear carbonyl species to any of the spectra obtained in this study, as the onset of this species was coincident with the formation of rhodium clusters.

Figure 5.9. shows a stack plot for the helium thermolysis. The spectra clearly illustrate the onset of oscillations at higher energies between 180 and 200°C. These oscillations are indicative of the presence of heavier backscattering atoms, which

Figure 5.8 Rh K-Edge EXAFS and Fourier transform of $Rh(CO)_2(acac)$ supported on Al_2O_3 after reaction with helium at 400°C

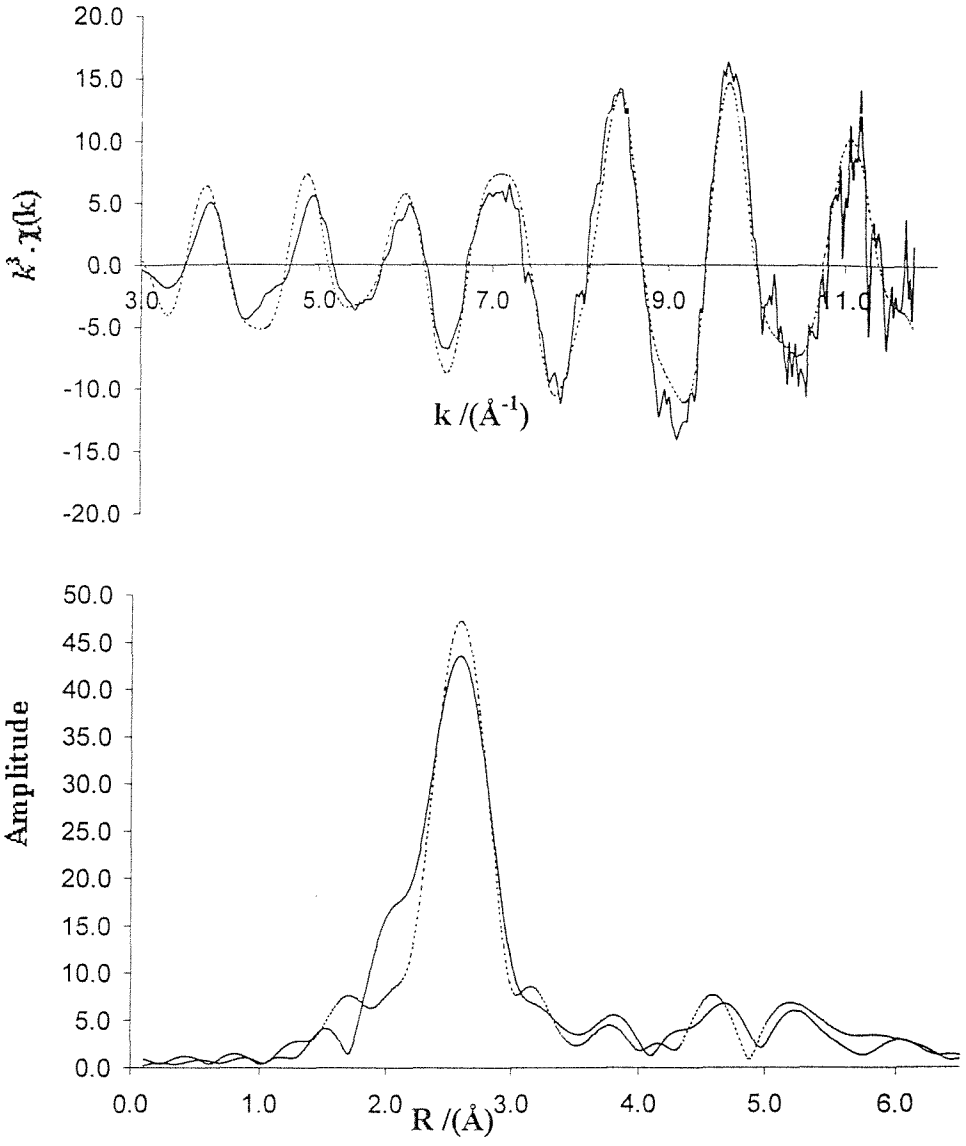

Atom	C.N.	r/Å	$2\sigma^2$ / Å^2
Rh	12(1.3)	2.671(2)	0.012(1)
Rh	6(1.1)	3.710(2)	0.018(1)
Rh	20(2.3)	4.672(4)	0.019(2)
Rh	9(1.2)	5.268(4)	0.019(3)
Rh	15(1.5)	6.018(4)	0.020(6)

R = 30.53 %
Ef = 2.29 eV

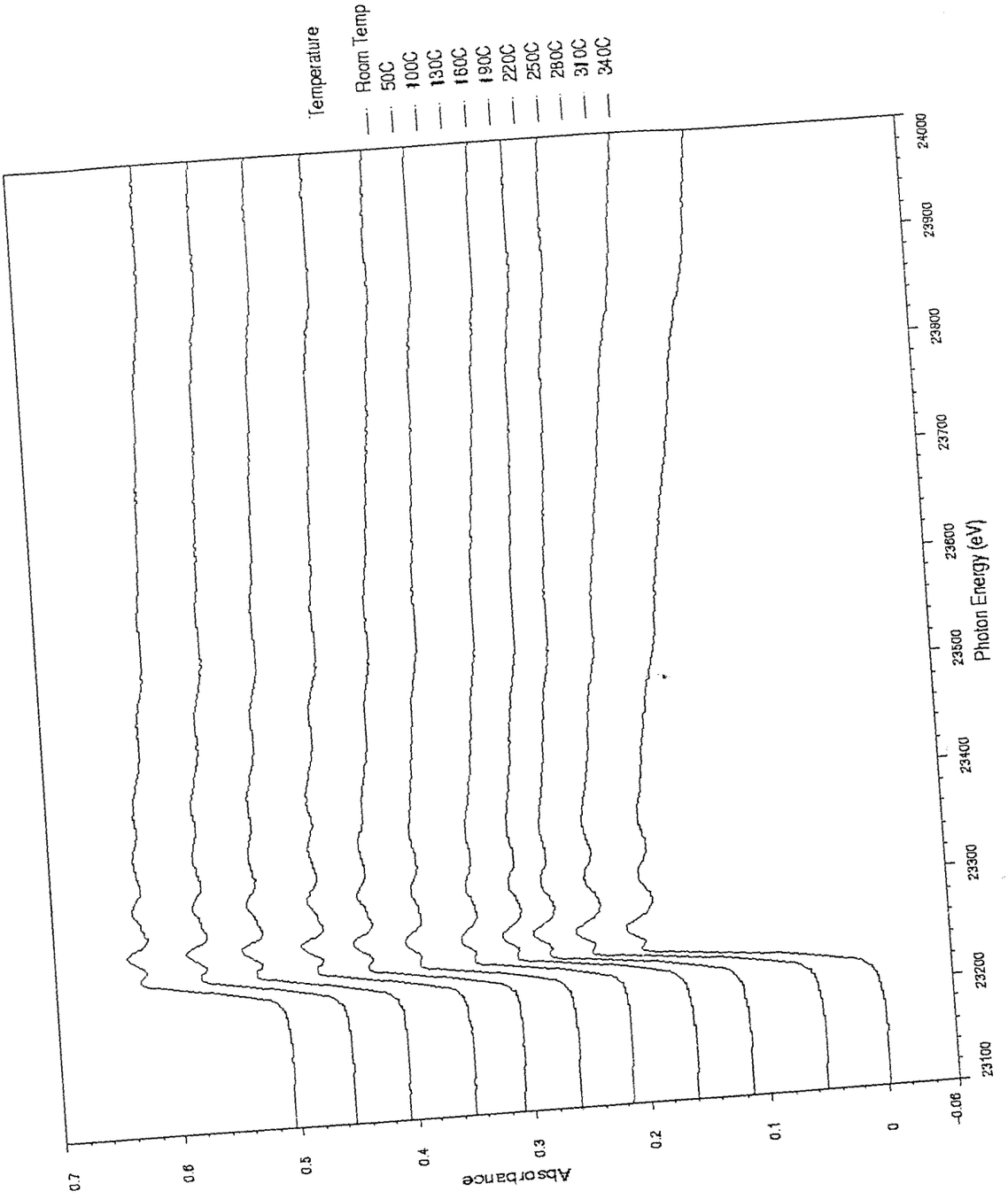

Figure 5.9 Energy Dispersive X-Ray absorption spectra recorded during heating of $Rh(CO)_2(acac)/Al_2O_3$ in helium from room temperature to 340∘C.

indicate the onset of formation of rhodium clusters on the alumina surface. Also there is a significant (60%) drop in the size of the edge jump at 160°C. This is almost certainly due to the removal of weakly physisorbed surface species. This observation corresponds well with the idea that $Rh(CO)_2(acac)$ is physisorbed onto the TiO_2 surface, but raises the question of whether the remaining species are simply more strongly physisorbed or chemisorbed. Certainly the size of the edge jump does not change again up to 340°C, suggesting two types of surface bond formed.

5.3.3 EXAFS Study of Thermolysis of $Rh(CO)_2(acac)$ Supported on TiO_2

This experiment was performed using standard EXAFS at the SRS at Daresbury. A sample of $Rh(CO)_2(acac)$ supported on partially dehydroxylated titania was heated to 150°C in helium for 5 minutes using the *in situ* EXAFS cell. A spectrum of the EXAFS and Fourier transform after heating are shown in figure 5.10. Analysis of the spectrum indicates that the carbonyl and acac functionalities are still present at this temperature. This result is in agreement with DRIFTS studies, although the carbonyl stretches had shown some attenuation at this temperature.

A spectrum of the EXAFS and Fourier transform after heating to 200°C is shown in figure 5.11. The spectrum suggests that the carbonyl functionality has been removed whilst the acac functionality still remains at this temperature. There is also evidence of bonding to two surface oxygen atoms. The distances are in agreement with rhodium- surface oxygen distances observed in chapters 3 and 7. This result is also in agreement with results observed in the DRIFTS study.

Figure 5.10 Rh K-Edge EXAFS and Fourier transform of $Rh(CO)_2(acac)$ supported on TiO_2 After heating in helium to 150°C

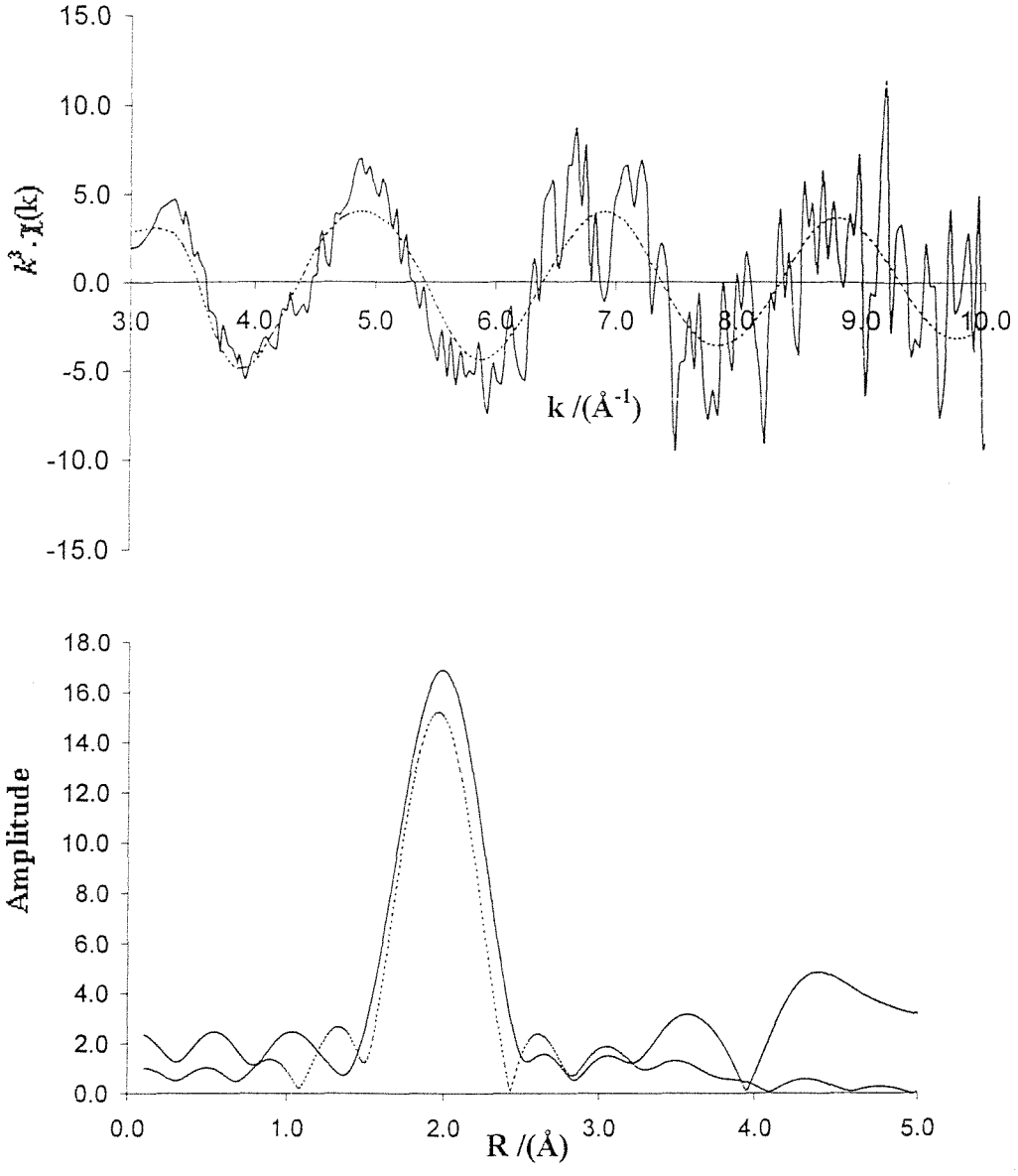

Atom	C.N.	r/Å	$2\sigma^2$ / Å^2
O	2(0.3)	1.977(5)	0.002(1)
O	2(0.2)	2.047(4)	0.003(1)
C	2(0.2)	2.996(4)	0.006(2)

R = 54.21 %
Ef = 2.17 eV

Figure 5.11 Rh K-Edge EXAFS and Fourier transform for $Rh(CO)_2(acac)$ supported on TiO_2 after reaction with H_2 at 200°C

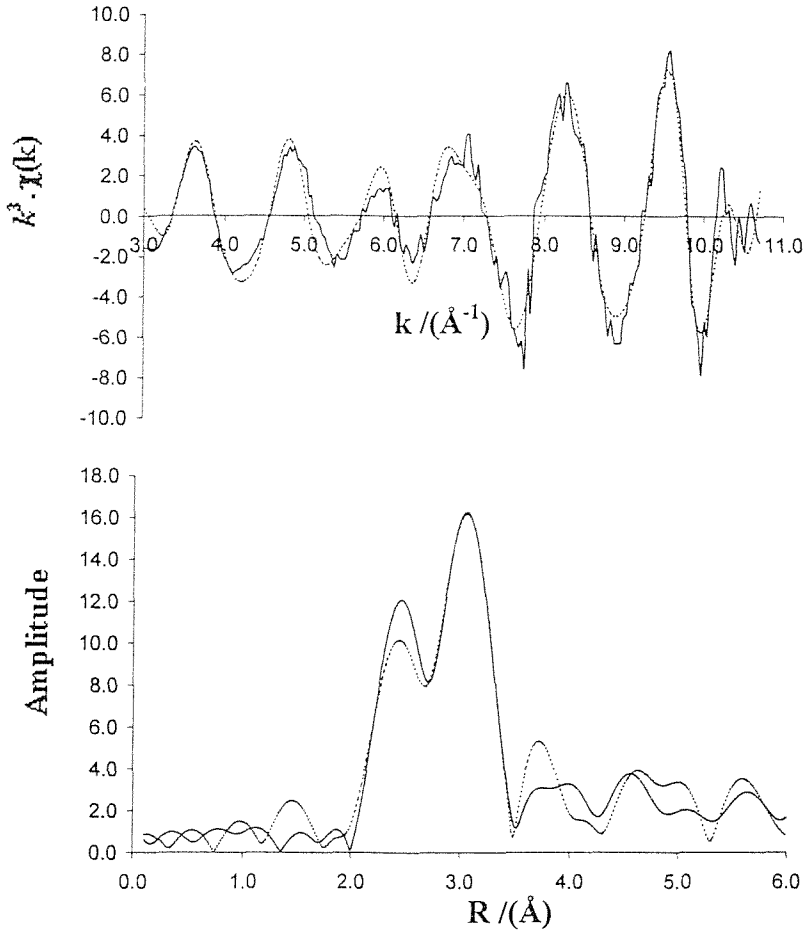

Atom	C.N.	r/Å	$2\sigma^2$ / Å^2
C	2(0.2)	1.894(3)	0.003(1)
O	2(0.2)	2.117(4)	0.002(1)
Rh	9(1.0)	2.727(2)	0.010(1)
O	2(0.3)	3.056(4)	0.007(3)
Rh	3(1.2)	3.782(4)	0.017(3)
Rh	9(0.8)	4.718(5)	0.015(2)

R = 31.26 %
Ef = 0.02 eV

5.4 CO Regeneration of Thermolysed $Rh(CO)_2(acac)$ Supported on TiO_2

5.4.1 DRIFTS Study of CO Regeneration

Two separate studies were conducted regarding CO regeneration on this system. The first was re-exposure to CO after removal of the carbonyl ligands only, and the second after removal of both carbonyl and acac ligands.

The first experiment involved heating the sample *in situ* to 130°C under a helium atmosphere prior to exposing the sample to 1 bar of CO at room temperature for 1 hour, at a flow rate of 5ml/min. Two main bands are observed after CO exposure, at 2058cm^{-1}, and a broad band at 1892cm^{-1}, shown in figure 5.12. The band at 2058cm^{-1} is attributed to a linear rhodium mono-carbonyl species. This band has shoulders at 2087cm^{-1} and 2012cm^{-1}, which are attributed to the rhodium *gem* dicarbonyl species. The intensity of this band is 50% of that of the original *gem* dicarbonyl band. The second band is at 1892cm^{-1} and is attributed to a bridging carbonyl species. The intensity of this band is about 40% of that of the original *gem* dicarbonyl band. The acac region of the spectrum is unaffected by the CO exposure. A further hour of exposure to CO under the same conditions results in a 5% increase in the intensity of the bands described above. These results can be interpreted in two ways. Firstly, the thermolysis experiment removes the *gem* dicarbonyl ligands, with the acac ligands migrating onto the titania surface. This generates a range of small rhodium clusters of varying size. Exposure to CO results in generation in a mixture of *gem* dicarbonyl, linear carbonyl and bridging carbonyl species, reflecting the range of sizes of rhodium clusters produced. The other interpretation is that the acac ligand remains bound to the rhodium as the carbonyl ligands are removed thermolytically. A few rhodium clusters are produced during the thermolysis, which explains the linear and bridging carbonyl species produced upon re-exposure to CO in addition to the gem dicarbonyl species which are reformed on rhodium with the acac intact. The frequencies of the carbonyl bands are identical to those of the initially adsorbed

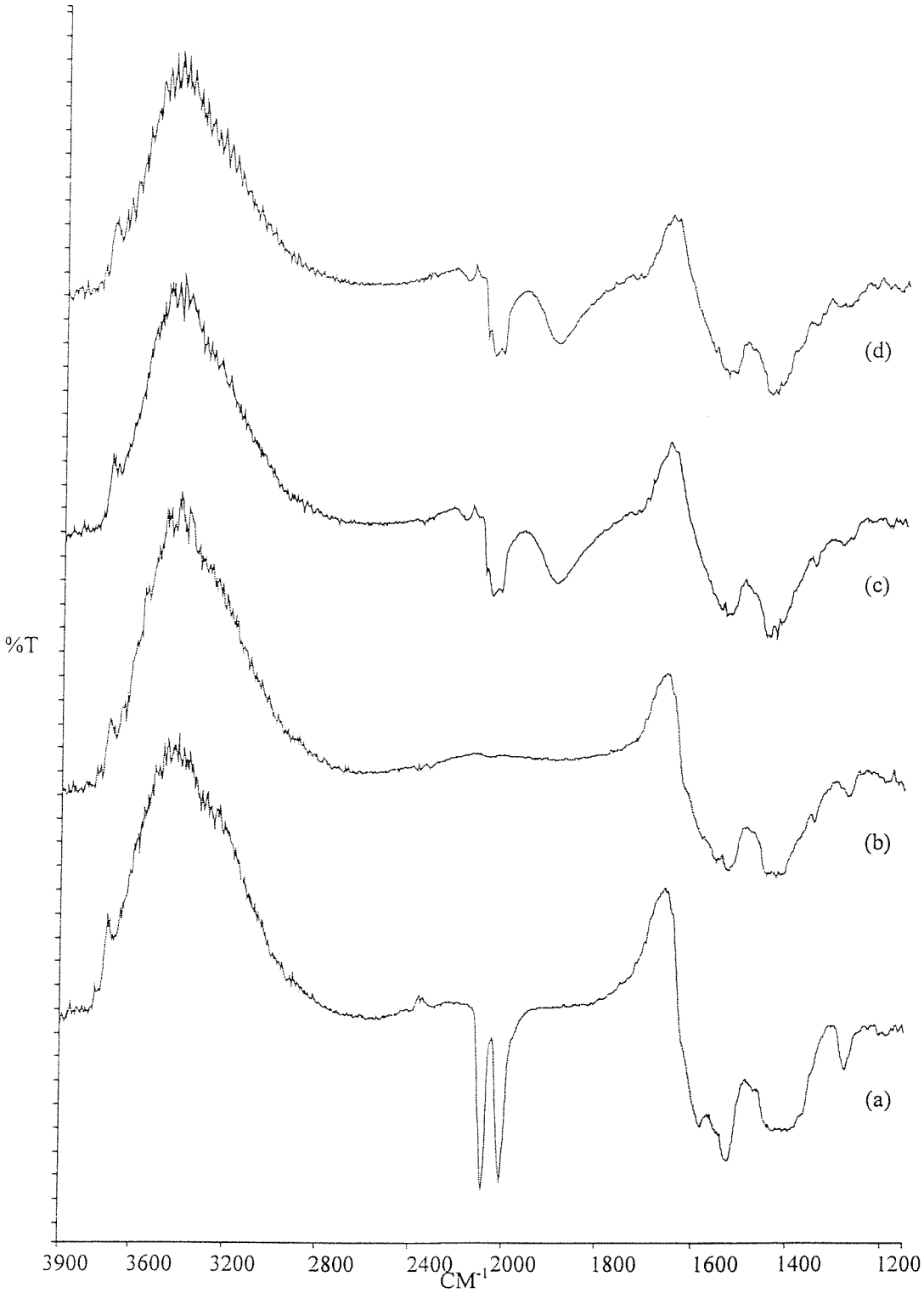

Figure 5.12 DRIFTS difference spectra of $Rh(CO)_2(acac)$ supported on TiO_2 during CO regeneration After helium thermolysis of carbonyl functionality: (a) Room temp, (b) Heated to 190°C, (c) 1hr CO exposure, (d) 2hrs CO exposure.

species, suggesting that the acac ligand is still bound to the rhodium centre. This is supported by the observation in the analogous experiment using $[Rh(CO)_2Cl]_2$ (3.4.1), in which the frequencies of the carbonyl bands shifted downfield on exposure to CO post thermolysis, due to the removal of the electron withdrawing Cl ligand.

The second experiment involves heating the surface supported $Rh(CO)_2(acac)$ to 310°C in a helium atmosphere, prior to exposure to 1 bar of CO at room temperature for one hour at a flow rate of 5ml/min. This experiment produces a broad *gem* dicarbonyl band at 2090cm^{-1} and 2023cm^{-1}, and a broad band at 1806cm^{-1}, shown in figure 5.13. The intensities of these bands are 50% of those of the original gem dicarbonyl bands of the $Rh(CO)_2(acac)$. The broadness of the *gem* dicarbonyl band suggests that there is also a linear monocarbonyl species present. There is no change in the acac region of the spectrum upon exposure to CO. These results suggest that the thermolysis experiment produces small rhodium clusters of varying size. The smaller clusters probably result in the generation of *gem* dicarbonyl units upon exposure to CO, whereas the larger clusters result in the formation of linear and bridging carbonyl species. Prolonged exposure to CO caused only very slight increases in the intensities of the respective carbonyl species. The shift to slightly higher frequencies (≈5cm^{-1}) of the carbonyl bands in this experiment confirms the removal of the acac ligands and a resultant change in the electronic environment of the rhodium centres.

5.4.1 EXAFS Study of CO Regeneration

This experiment was performed using standard EXAFS at station 9.2 at the SRS. A sample of $Rh(CO)_2(acac)$ supported on partially dehydroxylated titania was heated to 150°C in helium for 5 minutes using the *in situ* EXAFS cell. A spectrum of the EXAFS and Fourier transform after heating is shown in figure 5.10. The spectrum suggests that the carbonyl functionality has been removed whilst the acac functionality still remains at this temperature. There is also evidence of bonding to two surface oxygen atoms. The distances are in agreement with rhodium- surface oxygen distances observed in chapters 3 and 4. This result is also in agreement with

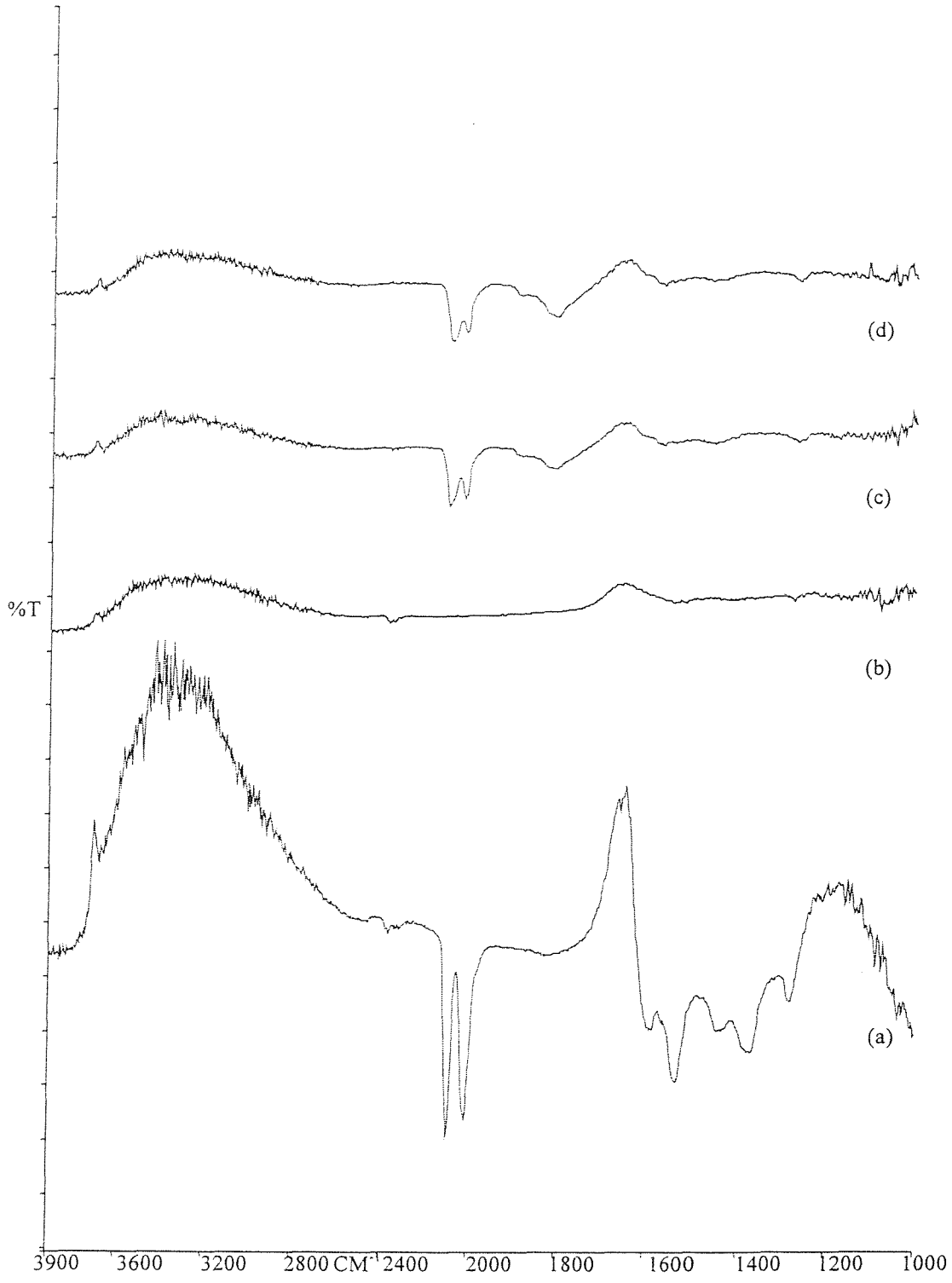

Figure 5.13 DRIFTS difference spectra of $Rh(CO)_2(acac)$ supported on TiO_2 during CO regeneration after helium thermolysis (to 310°C) of carbonyl and acac functionalities: (a) Room temp, (b) Post thermolysis, (c) After 1 hr CO exposure, (d) After 2hrs CO exposure.

results observed in the DRIFTS study.

The sample was then exposed to CO for 30 minutes at room temperature. The resulting EXAFS and Fourier transform are shown in figure 5.14. A variety of models were used to fit the data. The best model, however, is one, which suggests regeneration of the *gem* dicarbonyl species occurs in a substitution reaction with the surface oxygen atoms (acac ligands are retained). The bond distances are in agreement with those observed in the sample before the thermolysis experiment. This result is again in agreement with that observed in the corresponding DRIFTS experiment.

5.5 Hydrogen Thermolysis of $Rh(CO)_2(acac)$ Supported on TiO_2 and Al_2O_3

5.5.1 DRIFTS Study of Hydrogen Thermolysis of $Rh(CO)_2(acac)$ Supported on TiO_2 and Al_2O_3

The thermolysis experiment was carried out *ex-situ* under a hydrogen atmosphere, where samples were heated to the stated temperature for 10 minutes under a flow of hydrogen, and transferred to the DRIFTS cell. Spectra were collected at 100 scans, with a resolution of $4cm^{-1}$, using hydroxylated titania as a background. A stacked plot of the DRIFTS spectra collected is shown in figure 5.15. The assignments for the starting room temperature spectrum are given in table 5.1. Room temperature exposure of the supported system to hydrogen for 10 minutes, resulted in a 20% reduction in the intensity of the *gem* dicarbonyl ligands, with no change in their frequency. A 50% reduction in the *gem* dicarbonyl intensity is observed after 1 hour, again with no change in frequency. At 60°C, there is the development of linear monocarbonyl species and bridging carbonyl species at $2060cm^{-1}$ and $1844cm^{-1}$ respectively, in addition to the *gem* dicarbonyl species. By 80°C, only the linear and bridging species are present, at $2060cm^{-1}$ and $1836cm^{-1}$. At 110°C there are no observable rhodium carbonyl species present on the surface. The overall intensity of

Figure 5.14 Rh K-Edge EXAFS and Fourier transform of $Rh(CO)_2(acac)$ after heating in helium to 150°C and subsequent exposure to CO for 30 mins

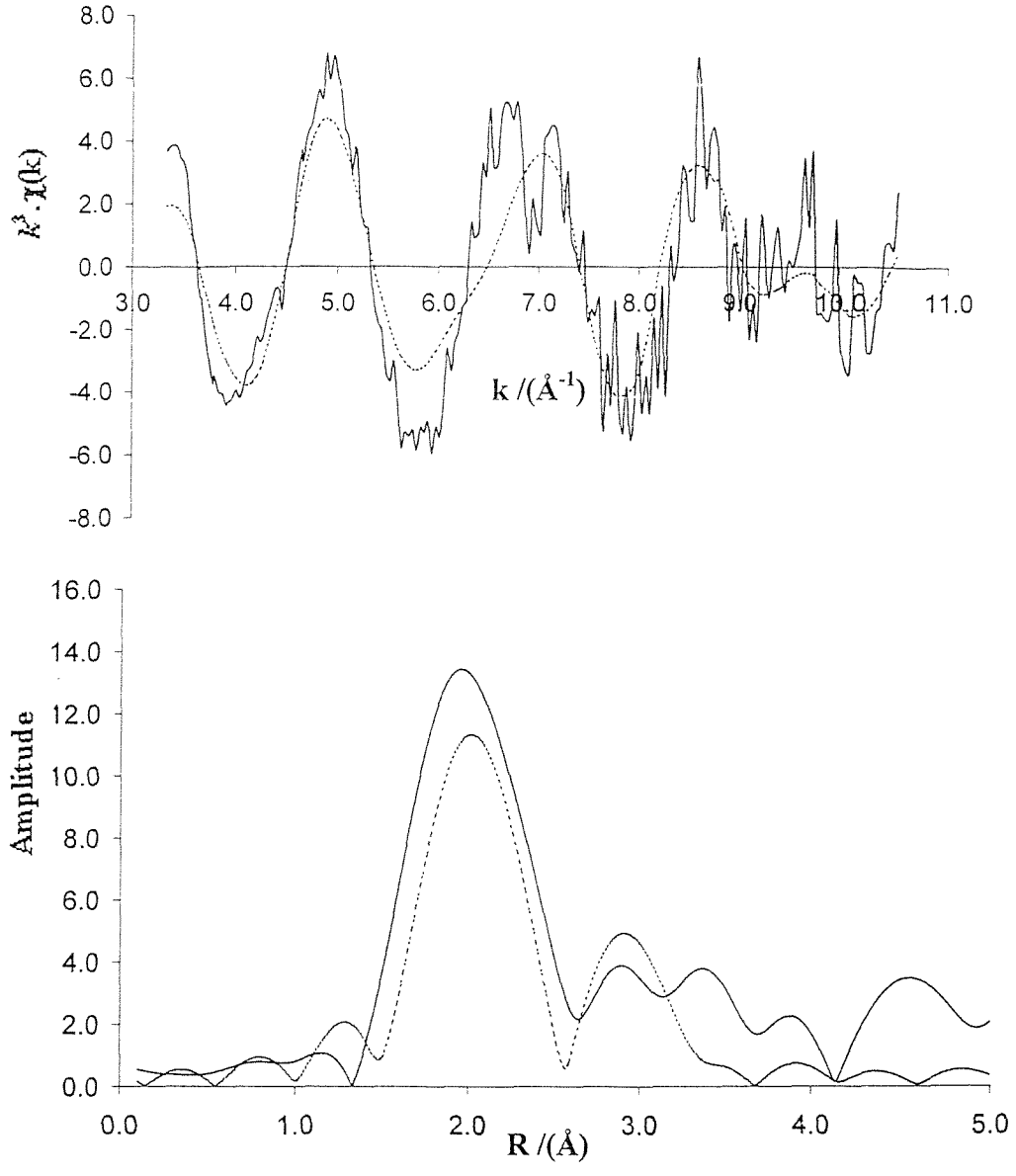

Atom	C.N.	r/Å	$2\sigma^2$ / Å^2
C	2(0.3)	2.069(5)	0.002(1)
O	2(0.2)	2.090(4)	0.003(1)
C	2(0.2)	3.052(4)	0.006(2)
O	2(0.3)	3.125(7)	0.012(3)

R = 47.09 %
Ef = 2.77 eV

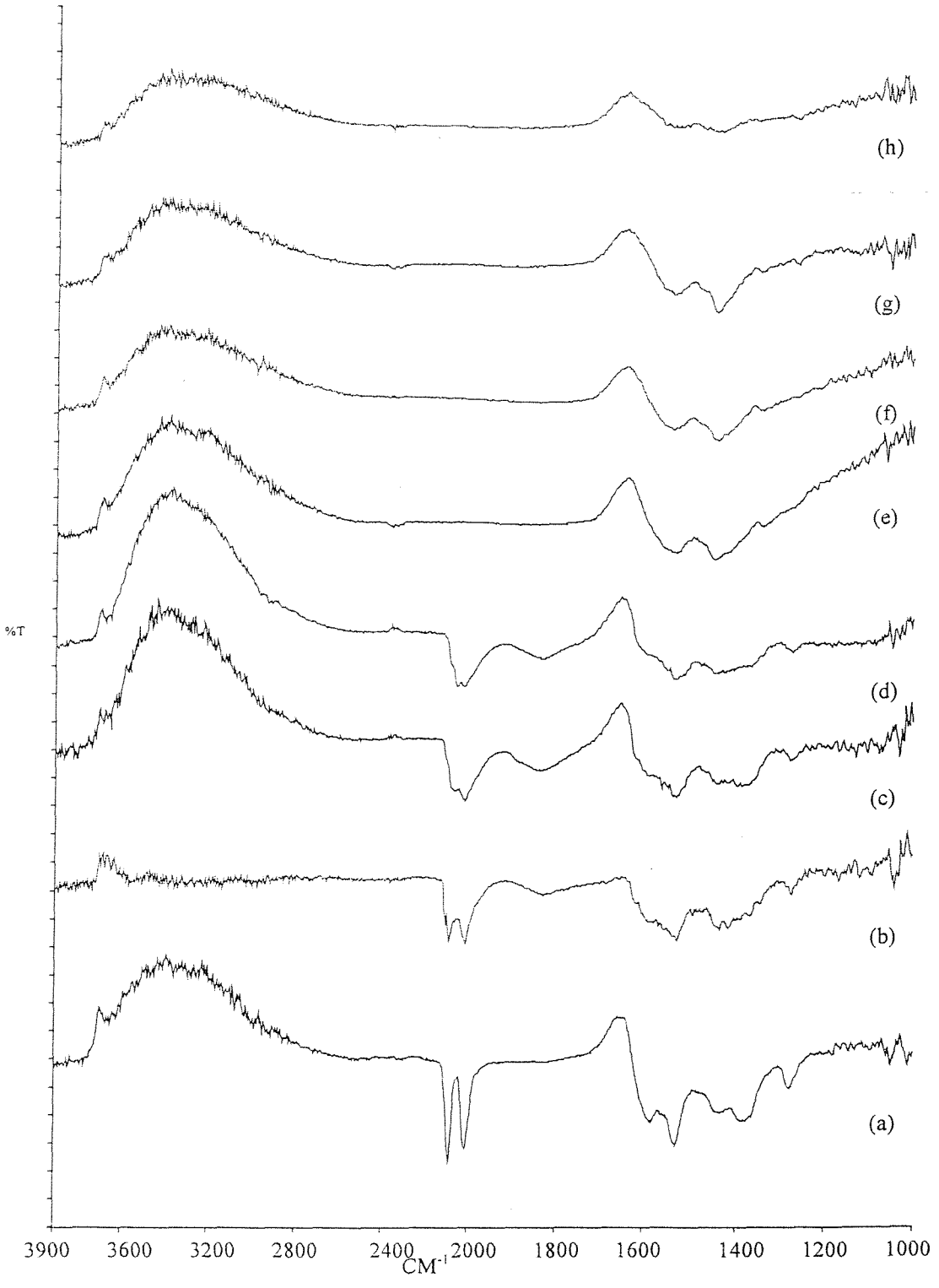

Figure 5.15 DRIFTS difference spectra of hydrogen thermolysis of $Rh(CO)_2(acac)$ supported on TiO_2: (a) Room temp under He, (b) Room temp under H_2 for 10 mins, (c) Room temp under H_2 for 1 hr (d) 60°C, (e) 80°C, (f) 110°C, (g) 170°C, (h) 240°C

the acac region was unchanged at 110°C, though there were changes in the intensities of the individual bands. The υ(C-O) band at 1580cm^{-1} had decreased slightly in intensity, and the υ(C-C) band at 1528cm^{-1} had sharpened. The bands at 1433cm^{-1} and 1386cm^{-1} had merged to form a broad feature, and the band at 1272cm^{-1} remained unchanged. As the temperature was increased up to 170°C, the trends in the acac region continued, with the two main features being the sharp band at 1528cm^{-1} and the broad band in the 1400-1430cm^{-1} region. There was also a weakening in the intensity of the band at 1272cm^{-1}. These intensities weakened together as the temperature was further increased, and by 240°C, the acac bands had completely disappeared.

Again, the nature of the removal of the carbonyl ligands in this experiment seems quite different to that of the $[Rh(CO)_2Cl]_2$ analogue (3.4.1). The carbonyl ligands in the latter system persist until higher temperatures (≈85°C) and pass through a distinct linear carbonyl species. In the acac system, there is much less of the transitional linear species present, and the carbonyl ligands disappear at around 70°C. The presence of the acac ligand still bound to the rhodium may inhibit the formation of the linear carbonyl species. EDE studies should make identification of intermediate species simpler.

5.5.2 EDE Study of Hydrogen Thermolysis of $Rh(CO)_2(acac)$ Supported on TiO_2 and Al_2O_3

The Rh K-edge Energy Dispersive EXAFS experiment for the hydrogen thermolysis of $Rh(CO)_2(acac)$ supported on partially dehydroxylated alumina was performed at the ESRF in Grenoble, at station ID24. The samples were heated at a rate of 5°C per minute, under a flow of 5ml/min of hydrogen. The experiment was time resolved, with 150 spectra being collected as the temperature was raised from 30°C to 295°C, with each individual spectrum acquired in 0.8 seconds.

The starting spectrum, shown in figure 5.16, illustrates the $Rh(CO)_2(acac)$ surface species at room temperature. The EXAFS and Fourier transform are very similar to the previous spectrum of $Rh(CO)_2(acac)$ supported on alumina, shown in figure 5.4. The bond distances are also identical to within 0.03Å, though the data quality is slightly poorer because of the more rapid acquisition time.

Figure 5.17 shows the EXAFS and Fourier transform of the sample after exposure to hydrogen at 90°C. The shape of the EXAFS is different to that of the starting species, in that there is greater intensity at higher energies, which is diagnostic of the presence of heavy backscatterering atoms such as rhodium. The Fourier transform has the basic shape of that of the $Rh(CO)_2(acac)$ species, but with greater intensity in the first and second peaks, corresponding to the distances of the first and second rhodium shells in a rhodium cluster. Several models were used to try and fit to the data, including a linear carbonyl species and metal clusters. The best fit came from a model with a mixture of the $Rh(CO)_2(acac)$ species and three partially filled shells of rhodium. The bond lengths of the $Rh(CO)_2(acac)$ species are consistent with those found on the previous spectra in this experiment. The rhodium distances are at 2.74, 3.73 and 4.64Å, which are consistent with the distances found in the bulk metal.

Figure 5.18 shows the EXAFS and Fourier transform of the sample after heating to 110°C. It can be seen that the EXAFS has changed considerably from before in that the greatest intensity is at larger k values, suggesting the presence of heavier backscattering atoms such as rhodium. The Fourier transform also has a very different shape to that of the $Rh(CO)_2(acac)$ species. Such a shape in the Fourier transform is diagnostic of a rhodium cluster. Several models were again attempted to fit the data, the best being a rhodium cluster with four shells. The coordination number was refined and the result was a series of four partially filled shells. The bond distances are in close agreement with the values found for a rhodium cluster to within 0.05Å.

Figure 5.19 shows the EXAFS and Fourier transform of the sample after heating in hydrogen to 140°C. This spectrum was acquired in 1.3 seconds. The

Figure 5.16 Rh K-Edge EXAFS and Fourier transform of $Rh(CO)_2(acac)$ supported on Al_2O_3

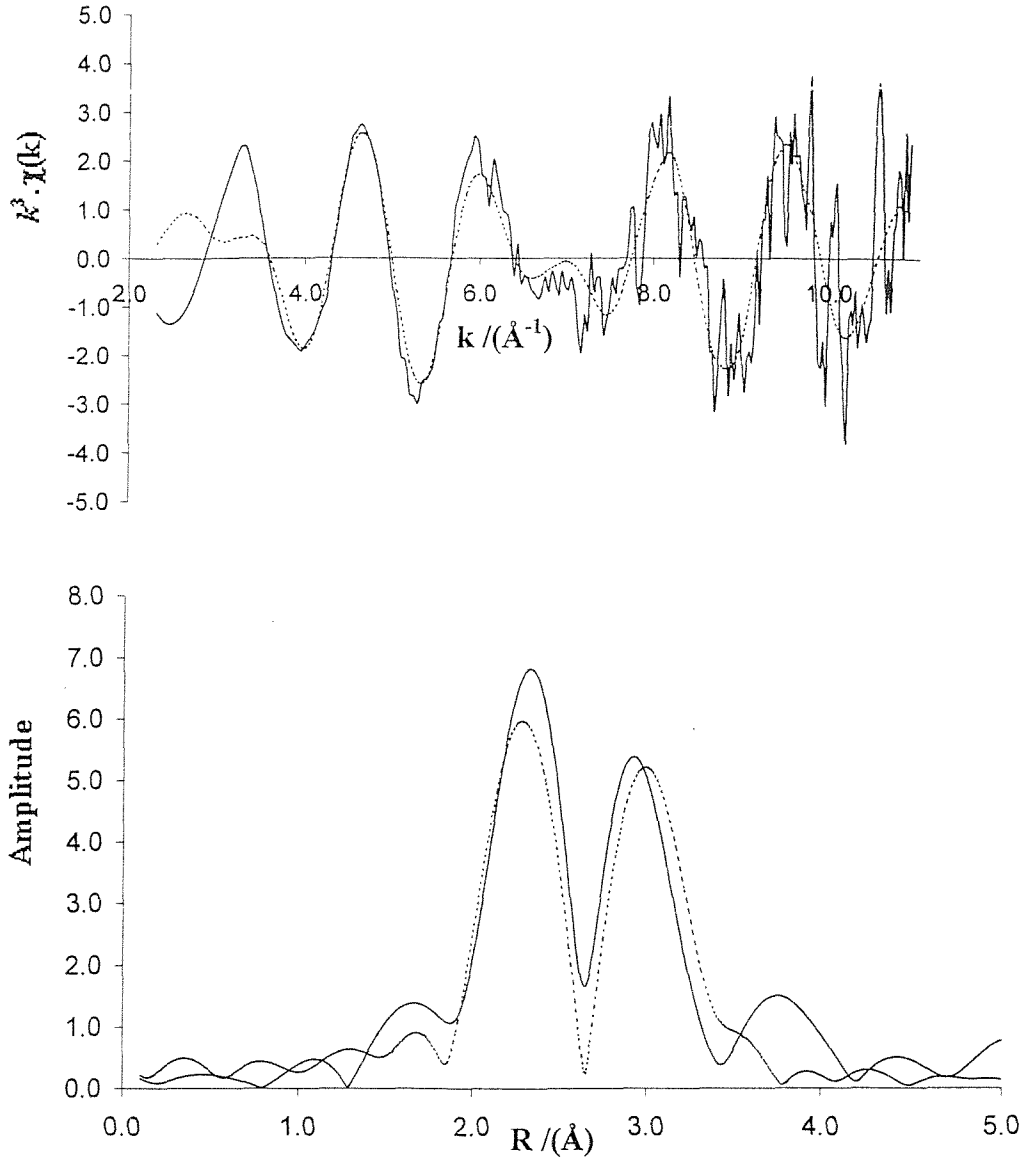

Atom	C.N.	r/Å	$2\sigma^2$ / Å^2
C	2(0.3)	2.038(3)	0.002(1)
O	2(0.2)	2.074(4)	0.007(1)
C	2(0.2)	3.035(4)	0.004(2)
O	2(0.3)	3.112(7)	0.016(3)

R = 51.18 %
Ef = -0.55 eV

Figure 5.17 Rh K-Edge EXAFS and Fourier transform of $Rh(CO)_2(acac)$ supported on Al_2O_3 After Reaction with H_2 at 90°C

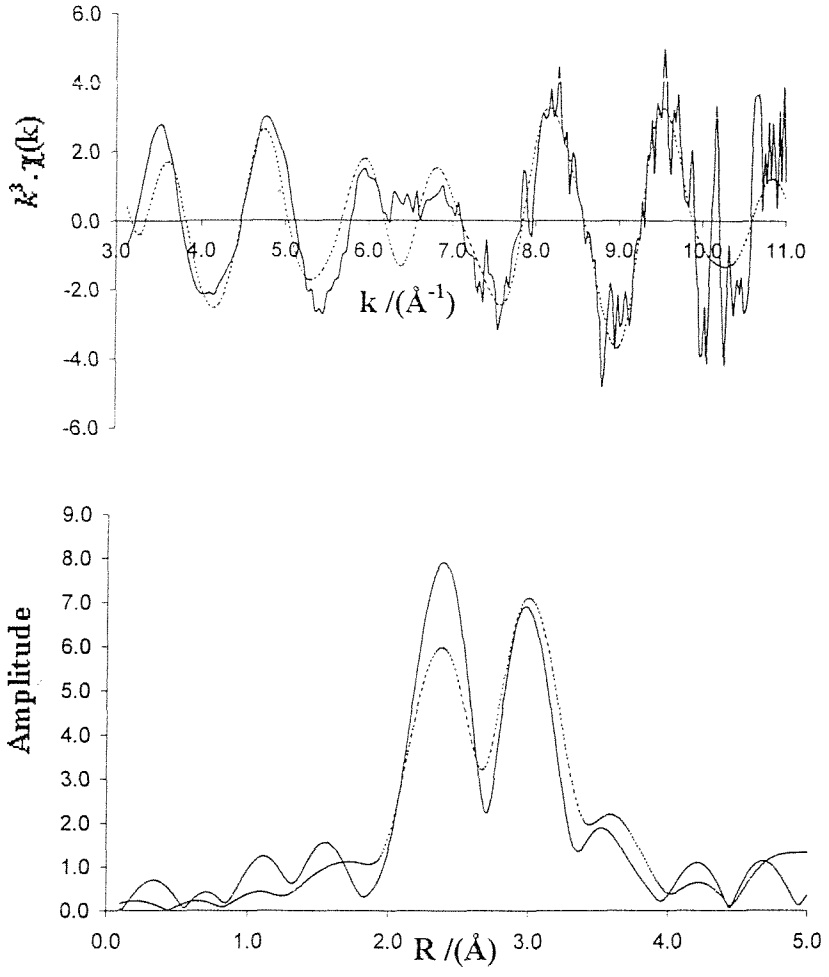

Atom	C.N.	r/Å	$2\sigma^2$ / Å^2
C	2(0.2)	1.923(3)	0.003(1)
O	2(0.2)	2.128(4)	0.003(1)
Rh	8(1.0)	2.732(2)	0.010(1)
O	2(0.3)	3.028(4)	0.007(3)
Rh	3(1.2)	3.738(4)	0.020(3)
Rh	7(1.2)	4.704(5)	0.019(2)

R = 50.44 %
Ef = -1.85 eV

Figure 5.18 Rh K-Edge EXAFS and Fourier transform of $Rh(CO)_2(acac)$ supported on Al_2O_3 After reaction with H_2 at 110°C

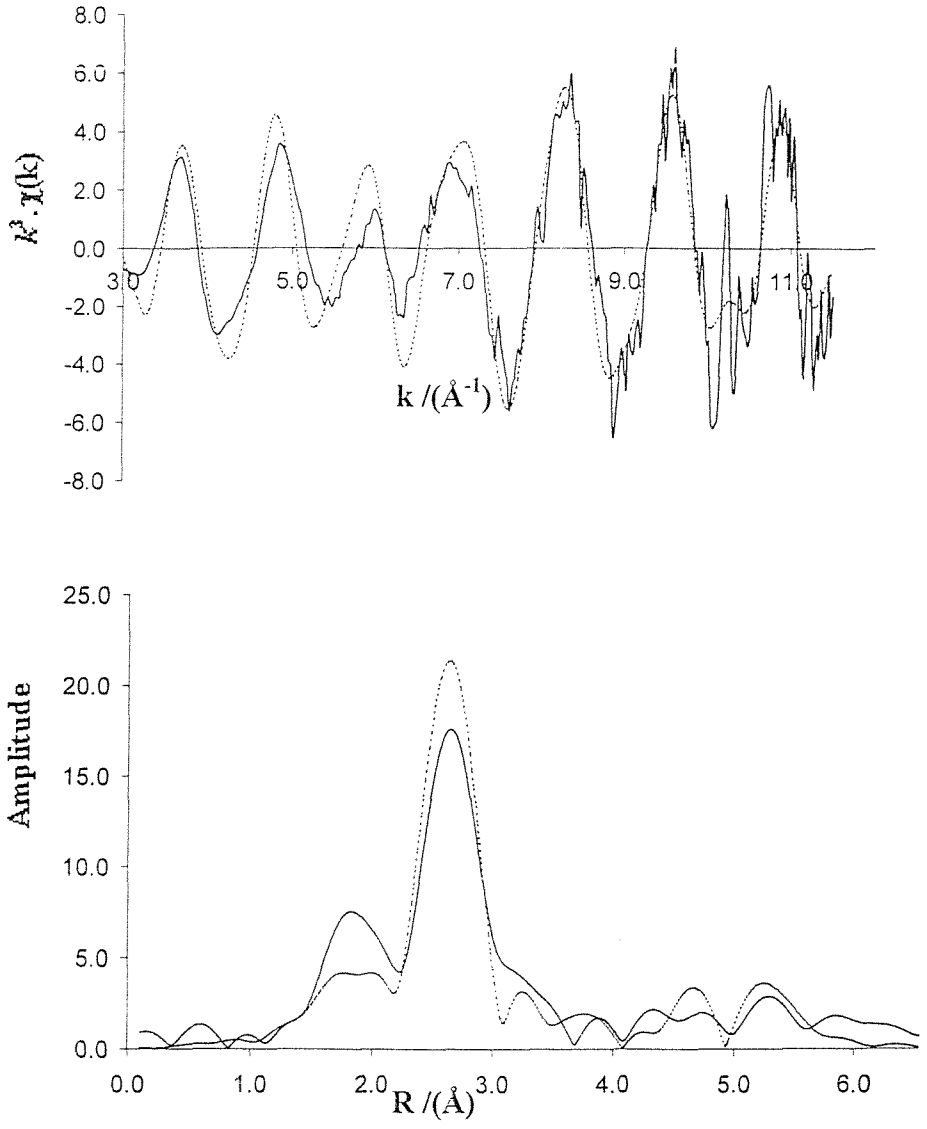

Atom	C.N.	r/Å	$2\sigma^2$ / Å^2
Rh	9(0.6)	2.691(3)	0.012(1)
Rh	3(1.1)	3.771(2)	0.020(1)
Rh	8(1.5)	4.658(5)	0.021(2)
Rh	6(0.9)	5.267(3)	0.019(3)

R = 47.48 %
Ef = 0.74 eV

Figure 5.19 Rh K-Edge EXAFS and Fourier transform of $Rh(CO)_2(acac)$ supported on Al_2O_3 after reaction with H_2 at 140°C

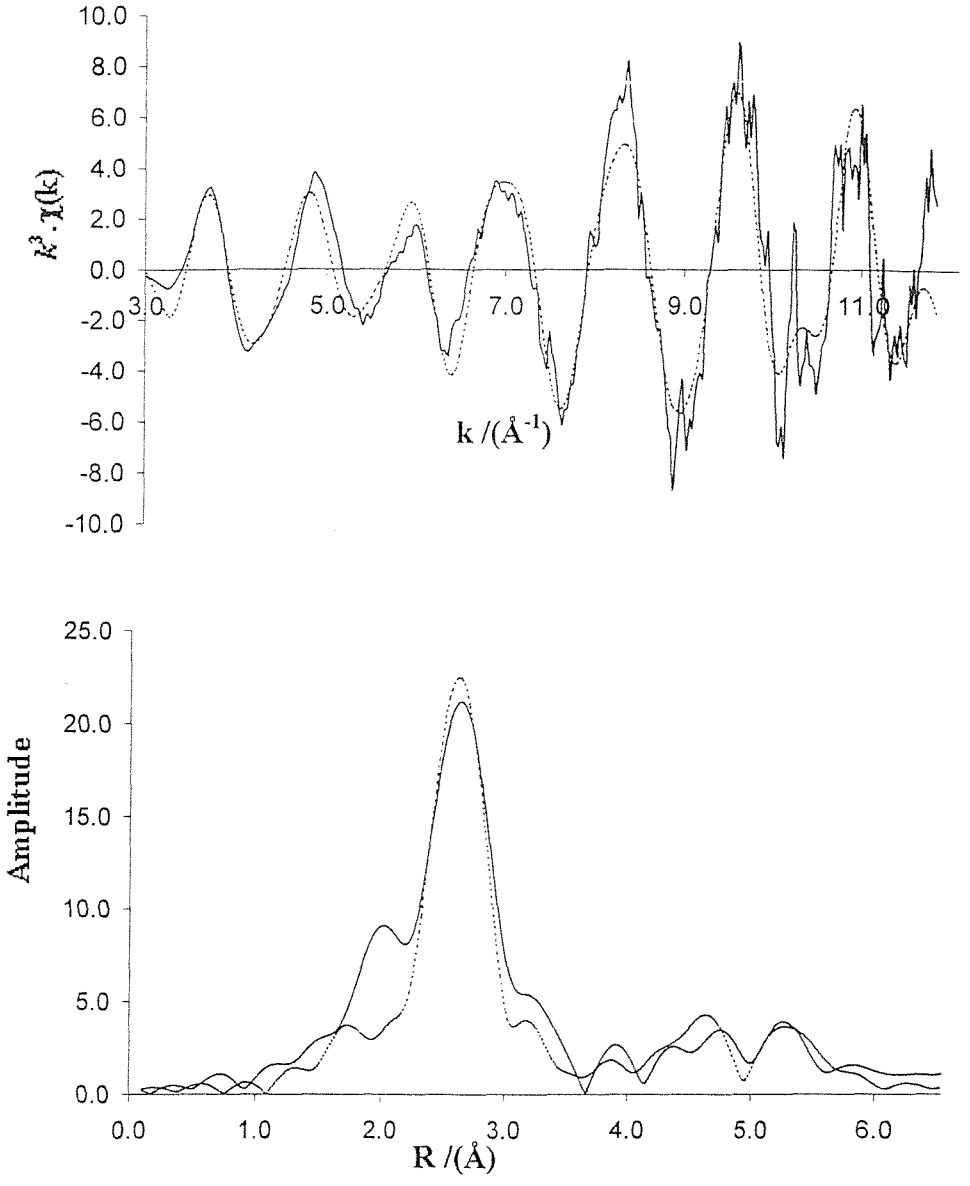

Atom	C.N.	r/Å	$2\sigma^2$ / Å^2
Rh	11(0.8)	2.709(4)	0.012(1)
Rh	5(1.1)	3.734(2)	0.016(1)
Rh	9(1.5)	4.684(5)	0.012(2)
Rh	6(0.9)	5.276(4)	0.009(3)

R = 39.77 %
Ef = 1.50 eV

EXAFS and Fourier transform are very similar in shape to that of the sample after heating to 110°C. A rhodium cluster model was employed and the coordination number was refined. The results of this show the rhodium clusters to have grown in size by a small amount relative to the previous experiment. The first two shells have eleven and five rhodium atoms respectively, which is the same number as that for bulk rhodium metal. The third shell has a coordination number of nine, and the fourth has a coordination number of six, relative to twelve for bulk metal. It can be seen that the coordination number has only increased for the first two shells relative to the sample heated to 110°C.

The final spectrum was acquired after heating to 220°C. The EXAFS and Fourier transform for this sample is shown in figure 5.20. There are five peaks in the Fourier transform, the first of which is much more intense than the other four. A rhodium cluster model was applied to these data, and the coordination number was refined. The results indicate that the thermolysis experiment has generated large clusters of rhodium, as the coordination numbers for the five shells resemble those of bulk metal. The bond distances also match those found in bulk rhodium, with deviations no greater than 0.05Å. The results of these experiments agree well with those for the DRIFTS study of the same reaction in terms of the removal of the carbonyl and acac species and the formation of rhodium clusters on the alumina surface. The temperature at which the transition takes place is consistent in both experiments. The differences in results between the DRIFTS and EDE studies can be explained in terms of the varying sensitivities of the two techniques. Infrared spectroscopy is particularly sensitive to the intense bands caused by the C-O stretch, while it will not observe any signal for metal particles. Conversely, EXAFS spectroscopy is sensitive to large backscattering atoms such as rhodium. Since EXAFS observes an average signal from all absorbing atoms, the presence of small metal particles will swamp the signal for any residual carbonyl groups, which would still be detectable by infrared spectroscopy. This probably explains why it was impossible to fit a linear carbonyl species to any of the spectra obtained in this study, as the onset of this species was coincident with the formation of rhodium clusters.

Figure 5.20 Rh K-Edge EXAFS and Fourier transform of $Rh(CO)_2(acac)$ supported on Al_2O_3 after reaction with H_2 at 220°C

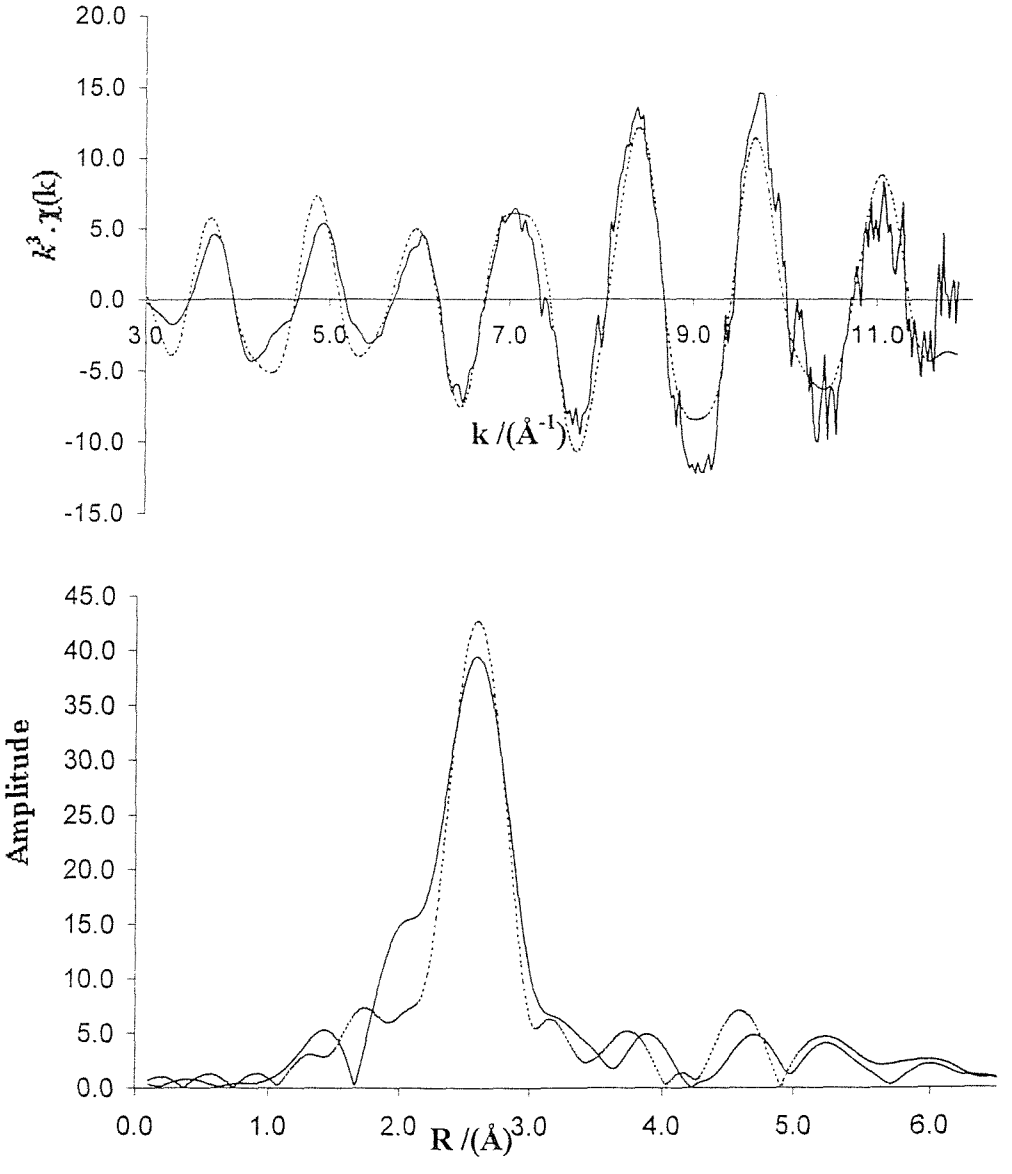

Atom	C.N.	r/Å	$2\sigma^2$ / Å^2
Rh	12(1.1)	2.691(3)	0.012(1)
Rh	6(0.9)	3.771(2)	0.020(1)
Rh	20(2.1)	4.658(5)	0.021(2)
Rh	6(0.7)	5.267(3)	0.019(3)
Rh	10(1.4)	5.995(4)	0.020(6)

R = 35.70 %
Ef = 1.37 eV

Figure 5.21 shows a stack plot for the hydrogen thermolysis. The spectra clearly illustrate the onset of oscillations at higher energies between 80 and 100°C. These oscillations are indicative of the presence of heavier backscattering atoms, which indicate the onset of formation of rhodium clusters on the alumina surface.

5.6 CO Regeneration of Hydrogen Thermolysed $Rh(CO)_2(acac)$ Supported on TiO_2

5.6.1 DRIFTS Study of CO Regeneration of Hydrogen Thermolysed $Rh(CO)_2(acac)$ Supported on TiO_2

Two separate studies were conducted regarding CO regeneration on this system. The first was re-exposure to CO after removal of the carbonyl ligands only, and the second after removal of both carbonyl and acac ligands.

The first experiment involved heating the sample *in situ* to 110°C under a hydrogen atmosphere prior to exposing the sample to 1bar of CO at room temperature for 1 hour, at a flow rate of 5ml/min. Bands appeared at 2086cm^{-1}, 2057cm^{-1}, 2020cm^{-1} and a broad band at 1893cm^{-1}, shown in figure 5.22. These are attributed to a mixture of *gem*-dicarbonyl, linear and bridging carbonyl species respectively. They are present in approximately equal proportions. Subsequent exposure to CO under the same conditions for one and two hours resulted in a 5% increase in the intensity of all these carbonyl bands. The acac region of the spectrum is unaffected by the CO exposure. Again these results can be interpreted in two ways. Firstly, the thermolysis experiment removes the *gem* dicarbonyl ligands, with the acac ligands migrating onto the titania surface. This generates a range of small rhodium clusters of varying size. Exposure to CO results in generation in a mixture of *gem* dicarbonyl, linear carbonyl and bridging carbonyl species, reflecting the range of sizes of rhodium clusters produced. The second interpretation is that the acac ligand remains bound to the rhodium as the

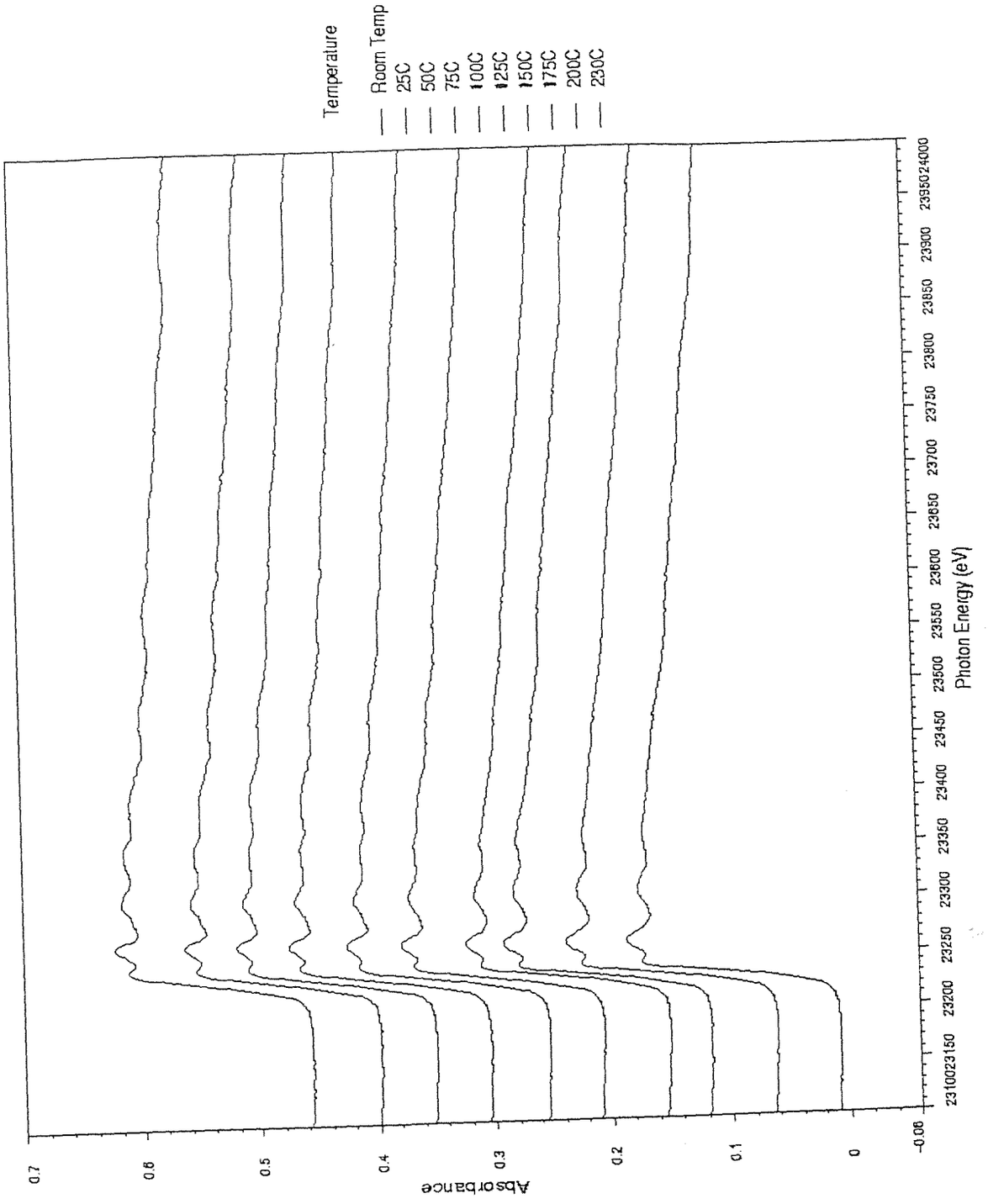

Figure 5.21 Energy Dispersive X-Ray absorption spectra recorded during hydrogen thermolysis of $Rh(CO)_2(acac)/Al_2O_3$ from room temperature to 220°C.

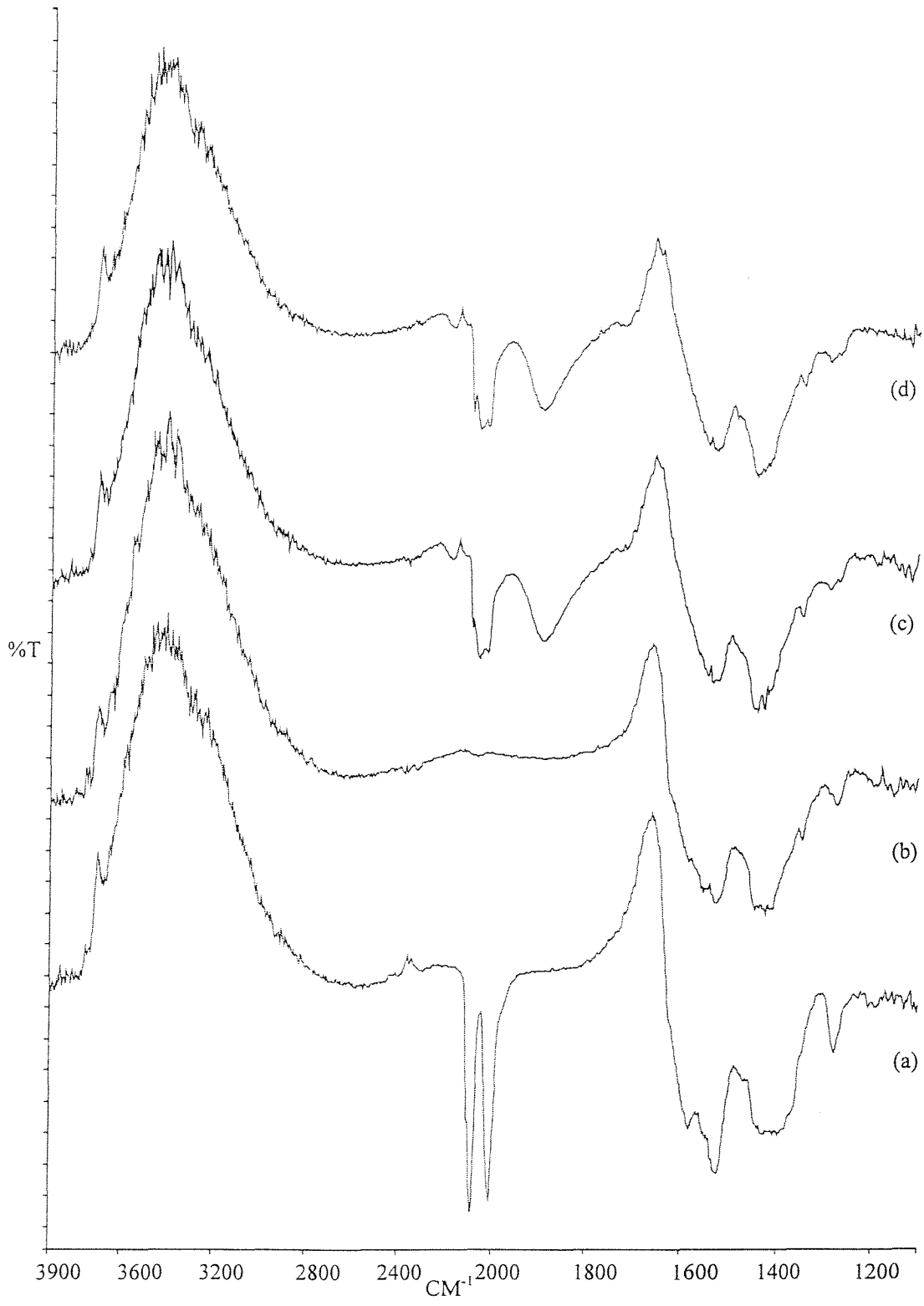

Figure 5.22 DRIFTS difference spectra of $Rh(CO)_2(acac)$ supported on TiO_2 during CO regeneration After hydrogen thermolysis of carbonyl functionality: (a) Room temp, (b) Heated to 130°C in H_2, (c) 1 hr CO exposure, (d) 2 hrs CO exposure.

carbonyl ligands are removed thermolytically. A few rhodium clusters are produced during the thermolysis, which explains the linear and bridging carbonyl species produced upon re-exposure to CO in addition to the gem dicarbonyl species which are reformed on rhodium with the acac intact. Again, the fact that there is no significant change in the carbonyl frequency relative to the initially adsorbed species, suggests that the electronic environment has not changed, and the acac ligand remains bound to the rhodium centre (c.f change in carbonyl frequency in post thermolysis exposure to CO in $[Rh(CO)_2Cl]_2$ analogue, 3.4.1). The results of this experiment are very similar to the helium analogue, 5.4.1, indicating that hydrogen simply lowers the temperature at which reduction of the rhodium occurs. See section 5.4.1 also for a comparison with analogous experiment performed on TiO_2 supported $[Rh(CO)_2Cl]_2$.

The second experiment involves heating the surface supported $Rh(CO)_2(acac)$ to 225°C in a hydrogen atmosphere, prior to exposure to 1 bar of CO at room temperature for one hour at a flow rate of 5ml/min. This experiment produces bands at 2106cm^{-1}, 2092cm^{-1}, a weak band at 2060cm^{-1}, 2012cm^{-1} and 1811cm^{-1}, shown in figure 5.23. These peaks can be attributed to a mixture of *gem*-dicarbonyl, linear and bridging carbonyl species respectively. The band at 2092cm^{-1} may be a gem dicarbonyl band or a high frequency linear carbonyl band. There is a greater proportion of the gem dicarbonyl (and possibly linear carbonyl) species than the bridging carbonyl. What can be said with certainty, is that there are rhodium clusters of varying sizes created by the thermolysis experiment, and a variety of rhodium carbonyl species are generated on exposure to CO at room temperature. The acac region remains unchanged during the exposure to CO. This experiment, like the helium anologue, indicates complete removal of the acac ligands during the thermolysis stage, evidenced by the lowering of the frequencies of the regenerated *gem*-dicarbonyl ligands relative to the starting species. These results are very similar to those observed in the $[Rh(CO)_2Cl]_2$ analogue, 3.4.1), but show the *gem*-dicarbonyl ligands at much higher frequencies than the helium analogue (5.4.1). This may be due to formation of carbonyl species on different size clusters, or on different surface planes. There could also be a difference in the quantity of *gem*-dicarbonyl produced.

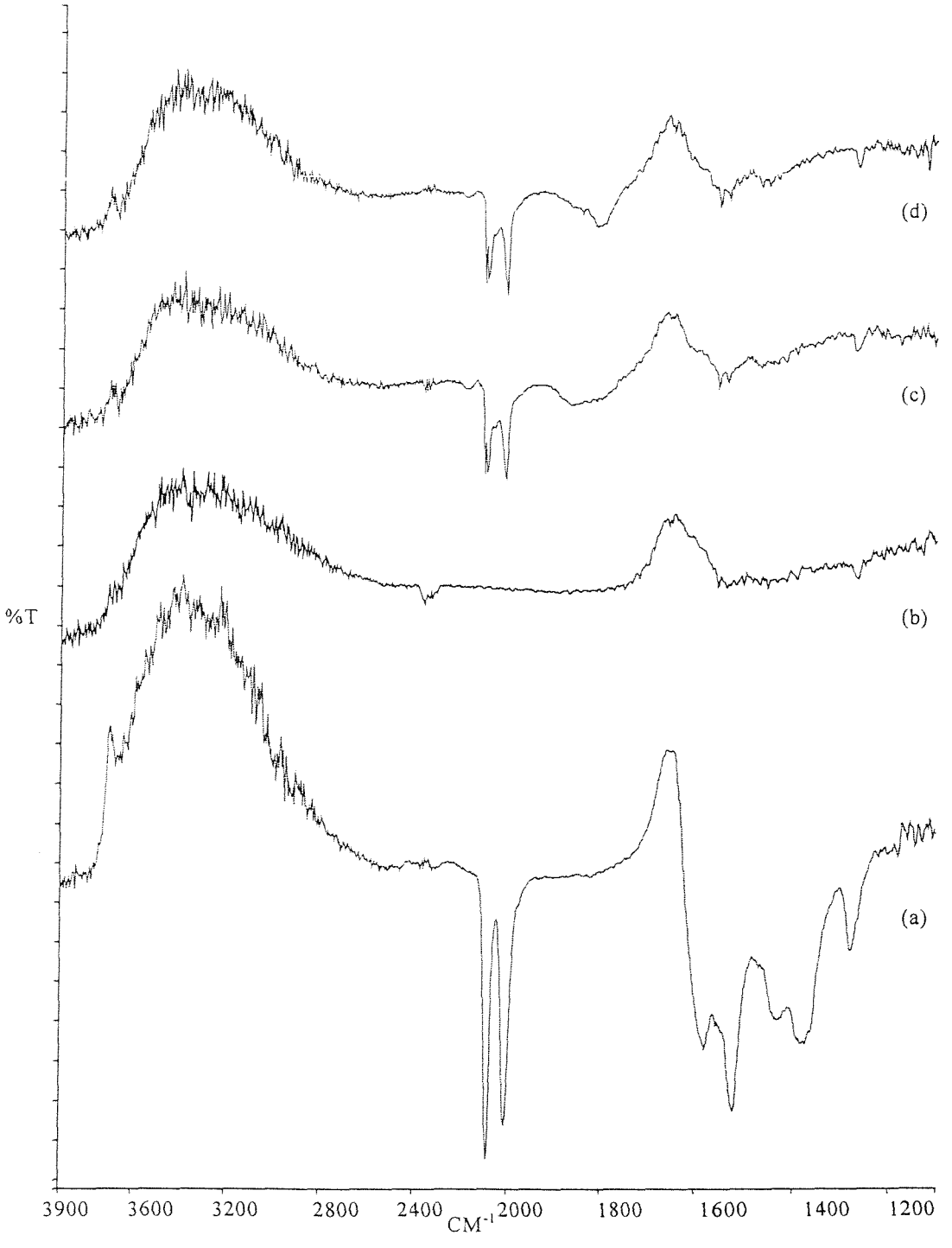

Figure 5.23 DRIFTS difference spectra of $Rh(CO)_2(acac)$ supported on TiO_2 during CO regeneration After hydrogen thermolysis of both carbonyl and acac functionalities: (a) Room Temp, (b) Heated to 220°C in H_2, (c) 1 hr CO exposure, (d) 2 hrs CO exposure.

5.6.2 EXAFS Study of CO Regeneration of Hydrogen Thermolysed $Rh(CO)_2(acac)$ Supported on Titania

This experiment was performed using standard EXAFS at the SRS at Daresbury. A sample of $Rh(CO)_2(acac)$ supported on partially dehydroxylated titania was heated to 100°C in hydrogen for 5 minutes using the *in situ* EXAFS cell. A spectrum of the EXAFS and Fourier transform after heating is shown in figure 5.24. The spectrum clearly illustrates the presence of small rhodium clusters on the titania surface. The coordination number has been refined, indicating the presence of two partially filled rhodium shells. The bond distances are consistent with those for a rhodium foil.

The sample was then exposed to CO for 30 minutes at room temperature. The resulting EXAFS and Fourier transform are shown in figure 5.25. A variety of models were used to fit the data to. The best model, however, consists of a mixture of a rhodium *gem* dicarbonyl species bonded to two surface oxygen atoms, and small rhodium clusters.

5.7 Reaction of $Rh(CO)_2(acac)$ Supported on Titania with NO

5.7.1 DRIFTS Study of Reaction of $Rh(CO)_2(acac)$ Supported on Titania with NO

A sample of $Rh(CO)_2(acac)$ supported on titania was reacted with 1 atmosphere of NO at room temperature for 20 minutes. The reaction was performed *in situ* with a flow rate of 5ml/min.

The room temperature spectrum of $Rh(CO)_2(acac)$ supported on titania, figure

Figure 5.24 Rh K-Edge EXAFS and Fourier transform of $Rh(CO)_2(acac)$ after heating in H_2 to 200°C

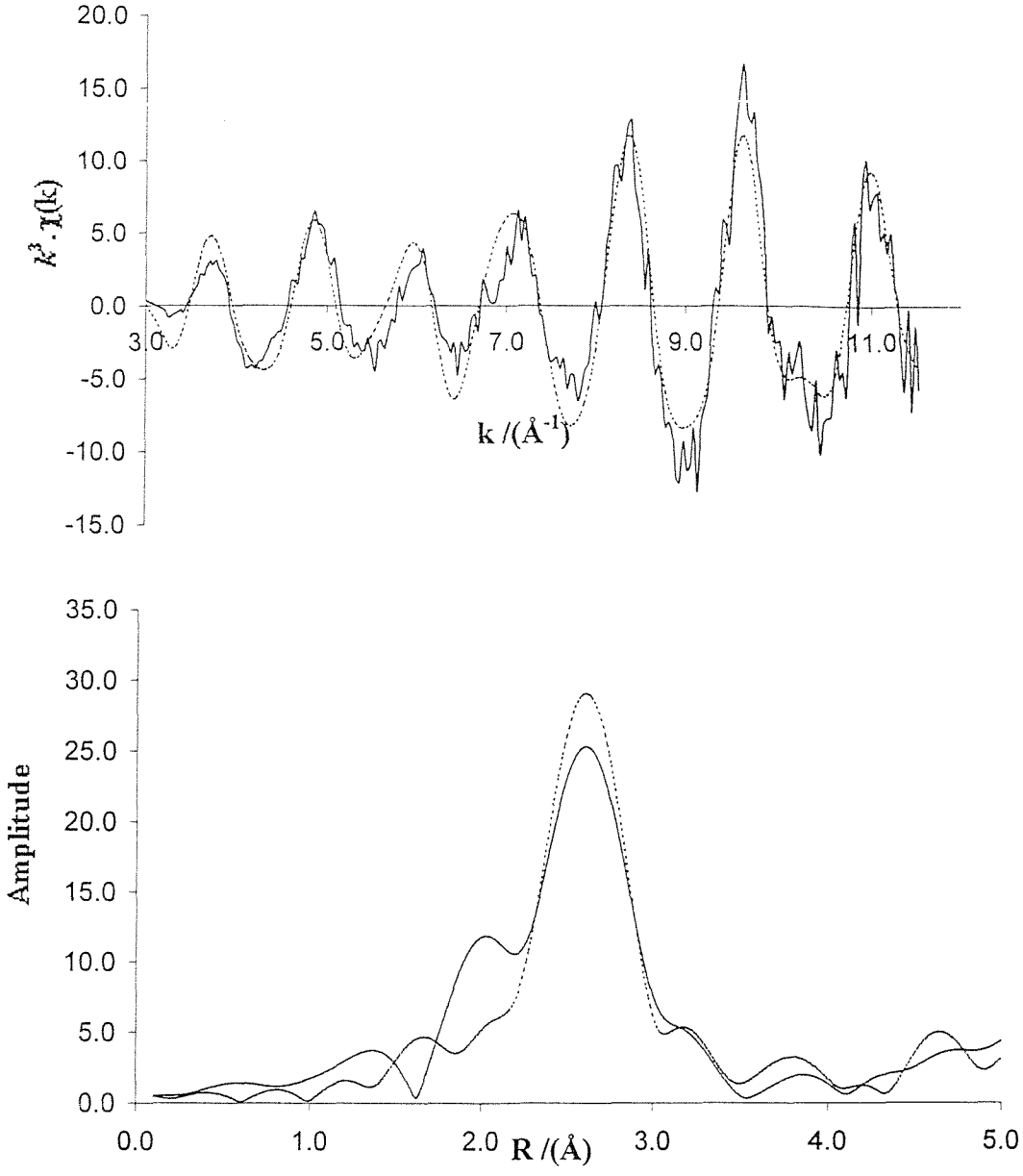

Atom	C.N.	r/Å	$2\sigma^2$ / Å^2
Rh	12(0.6)	2.727(3)	0.012(1)
Rh	4(1.1)	3.837(2)	0.017(1)
Rh	13(3.2)	4.734(3)	0.019(3)
Rh	11(1.5)	5.354(6)	0.012(2)

R = 42.57%
Ef = 1.45 eV

Figure 5.25 Rh K-Edge EXAFS and Fourier transform of $Rh(CO)_2(acac)$ after heating in H_2 to 200°C and subsequent exposure to CO for 30 mins

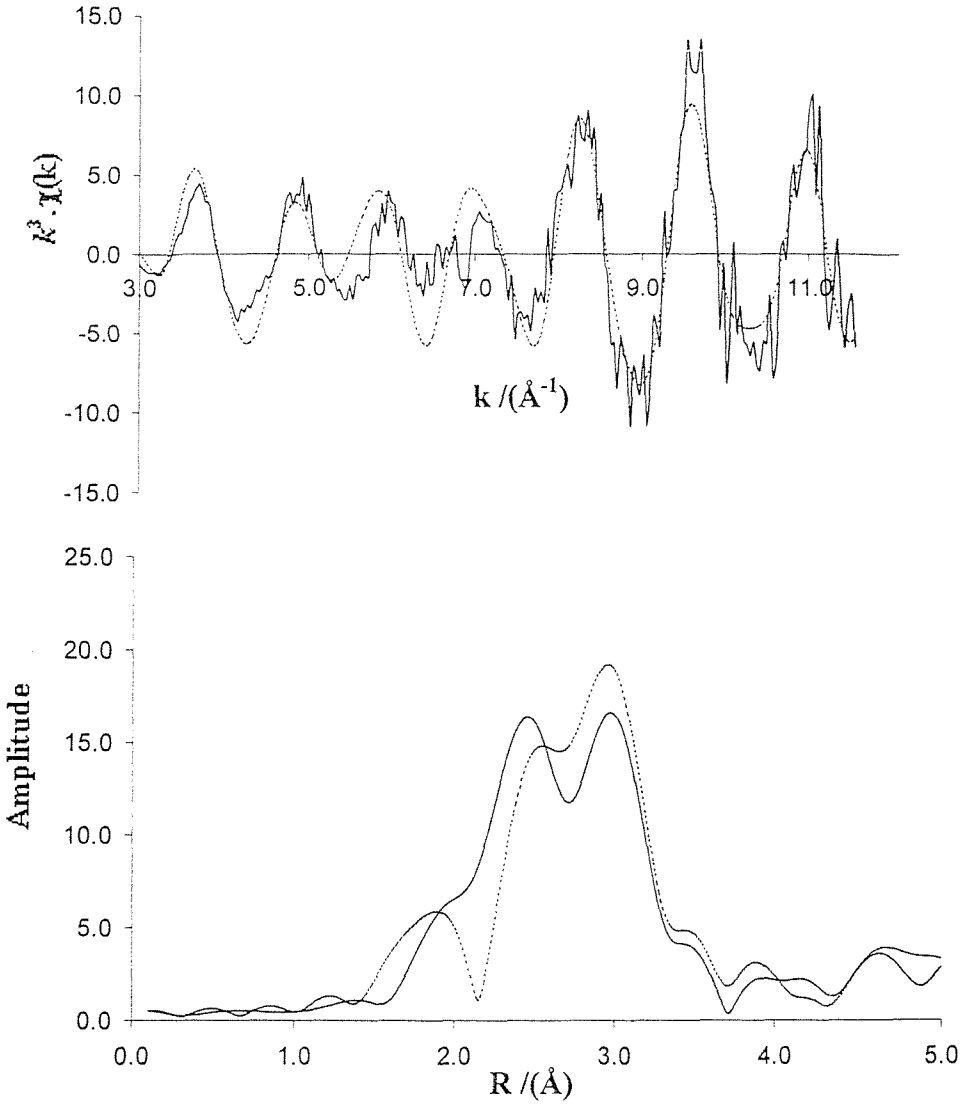

Atom	C.N.	r/Å	$2\sigma^2$ / Å^2
C	2(0.3)	2.069(5)	0.002(1)
Rh	12(1.3)	2.714(3)	0.005(2)
O	2(0.2)	2.090(4)	0.003(1)
Rh	4(1.0)	3.798(4)	0.010(2)
Rh	2(1.1)	4.656(3)	0.013(3)

R = 48.48 %
Ef = 1.92 eV

5.26, shows the characteristic carbonyl peaks at 2088cm^{-1} and 2012cm^{-1}, and acac peaks at 1585cm^{-1}, 1528cm^{-1}, 1431cm^{-1}, 1381cm^{-1}, 1366cm^{-1} and 1276cm^{-1}, in addition to a broad positive band in the hydroxyl region of the spectrum (3000-3500cm^{-1}).

After exposure to NO for 20 minutes, the cell was flushed with helium to remove gaseous NO and other reaction products. The spectrum acquired shows a broad sharp band at 1698cm^{-1}, which is attributed to a Rh-NO^{-} species[12-16]. This is at a frequency 40cm^{-1} lower than the than the Rh(NO)$^{-}$ species formed in the $[Rh(CO)_2Cl]_2$ analogue (4.2). There is also no evidence of a stretch at 2145cm^{-1}, which is also found in the $[Rh(CO)_2Cl]_2$ analogue. This stretch is attributed to a CO stretch is an Rh(NO)(CO) species. This species is therefore not present in this case. There are also changes in the acac region of the spectrum. The peak at 1586cm^{-1} has attenuated. The peak at 1528cm^{-1} has lost some intensity and shifted to 1520cm^{-1}. The peak at 1431cm^{-1} has disappeared, and a new, intense peak appears at 1455cm^{-1}. This peak may be attributed to a [Ti-O]-NO_2 species. The peak at 1381cm^{-1} has disappeared, and the peak at 1276cm^{-1} has shifted up to 1318cm^{-1}. A possible explanation for these findings is that exposure to NO causes the removal of the carbonyl ligands as gaseous CO. The acac ligand is also removed from the metal centre, and is subsequently bound to the titania support via a reaction of the surface hydroxyl groups and the delocalised π electrons and oxygen of the acac liagnd. This results in the formation of a Rh(NO)$^{-}$ species, in agreement with the literature assignments of a nitrosyl band at this frequency[12-16]. The lower frequency relative to the $[Rh(CO)_2Cl]_2$ analogue (4.2) is likely to be due to the absence of the strongly electron withdrawing Cl ligand. The rhodium centre (Rh(I) has 8 valence electrons) is likely to be bound to three surface oxygen atoms, and is also possibly still partially bound to the acac ligand. There is no need for a Rh(I) complex to satisfy the 18 electron rule, as a stable square planar arrangement is favoured on crystal field grounds, thus requiring 16 electrons. A square planar arrangement is also preferred over a tetrahedral geometry on crystal field grounds. There is insufficient evidence from the DRIFTS experiment to be certain of the coordination around the metal centre, although most of the literature examples of inorganic nitrosyl complexes are 5-coordinate rather than 4[12-16].

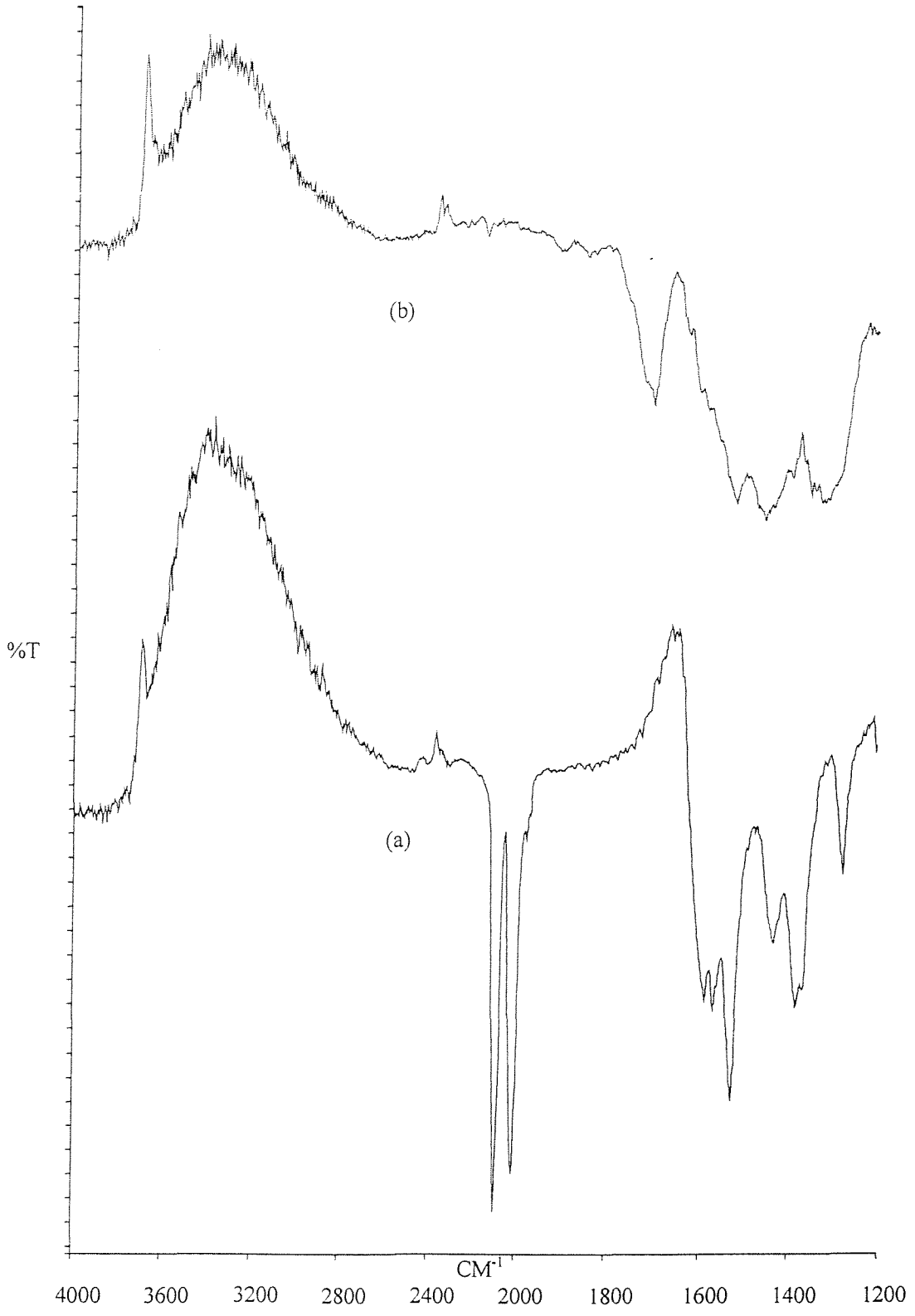

Figure 5.26 DRIFTS difference spectrum showing reaction of $Rh(CO)_2(acac)$ supported on TiO_2 with NO: (a) Before exposure to NO, (b) After reaction with NO for 30 mins.

5.7.2 Post NO Reaction Exposure to CO of $Rh(CO)_2(acac)$ Supported on TiO_2

Following exposure of $Rh(CO)_2(acac)$ supported on titania to NO for 20 minutes, the sample was exposed to 1 atmosphere of CO for 2 hours at room temperature, at a flow rate of 5ml/min. The reaction was conducted *in situ*, and is illustrated in figure 5.27.

After 2 hours of exposure to CO, there is the appearance of a band at 2134cm^{-1}. It is possible that CO causes reduction of the NO, producing N_2 and oxidised rhodium. It is possible that the Rh-NO^- reacts to form a Rh(CO)(NO) species, as the observed carbonyl frequency is too high to be due to CO adsorbed upon Rh metal particles. There is also a slight shift in position of the NO^- band to 1705cm^{-1} during exposure to CO, suggesting a change in the electronic environment, brought about by the Rh-CO bond formed. There is no obvious attenuation of the Rh-NO^- band after further exposure, and it is thus inferred that the Rh-NO^- species prevails. The species formed is very similar to that formed when $[Rh(CO)_2Cl]_2$ is exposed to NO (4.2), and is likely to be a Rh(CO)(NO) surface species. The acac region of the spectrum is unchanged during and after exposure to CO.

5.8 Conclusions

DRIFTS and EXAFS spectroscopies indicate that $Rh(CO)_2(acac)$ is adsorbed intact onto the partially dehydroxylated surfaces of TiO_2 and Al_2O_3. DRIFTS spectroscopy indicates that surface hydroxyl groups are consumed upon adsorption to both surfaces, though EXAFS indicates that there is no coordination to surface atoms. It is possible that hydrogen bonds are formed between the surface hydroxyl groups and the acac ligands. Thermolysis under a helium atmosphere results in removal firstly of the carbonyl ligands at 160°C, and the acac ligands at approximately 300°C. There is no evidence from DRIFTS or EXAFS spectroscopy of a linear carbonyl

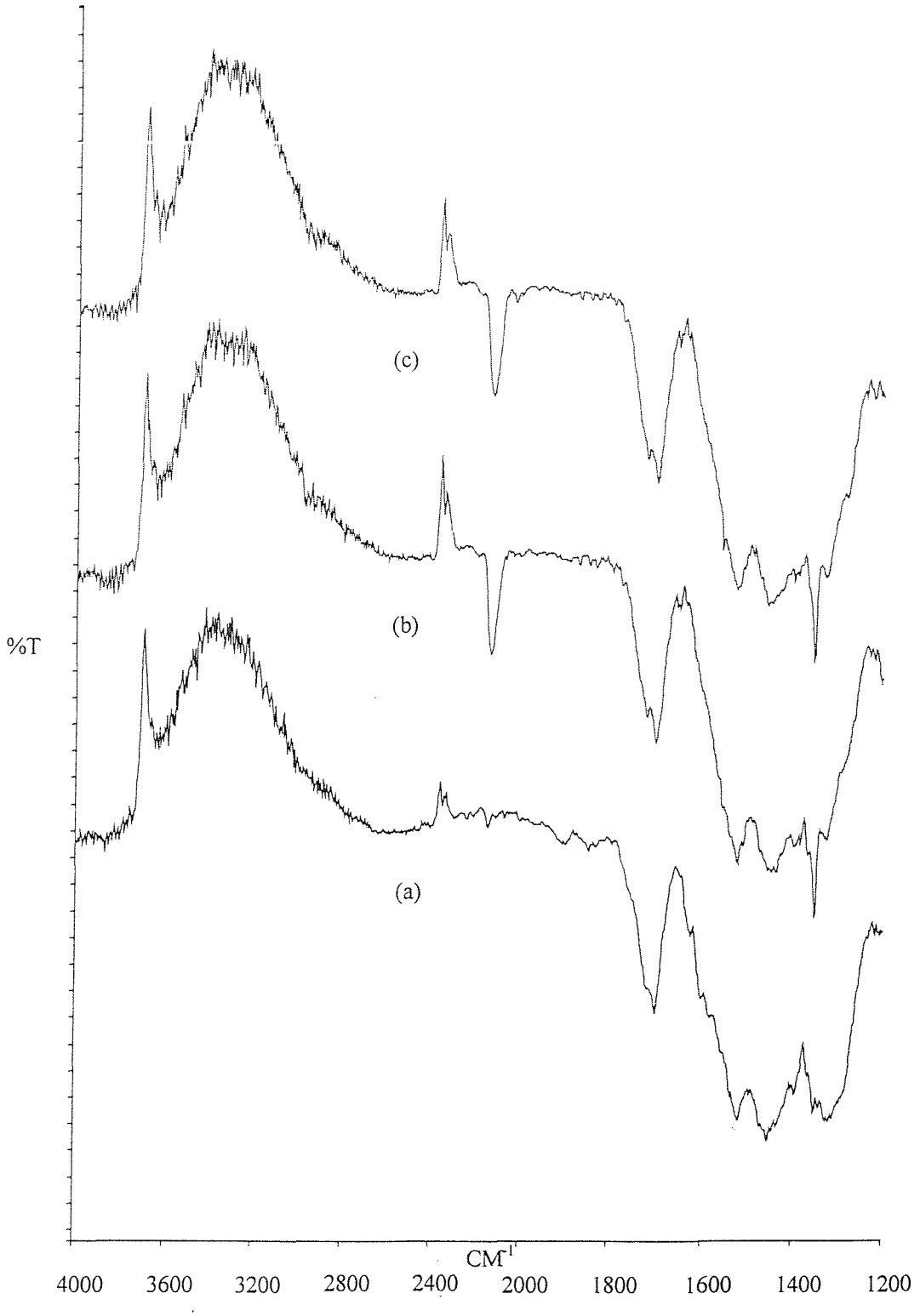

Figure 5.27 DRIFTS difference spectra showing reaction of $Rh(CO)_2(acac)$ supported on TiO_2 with NO and CO: (a) After reaction with NO for 30 mins, (b) After reaction with CO for 1 hour, (c) After reaction with CO for 2 hours.

species being formed during decomposition of the carbonyl ligands. EDE spectroscopy indicates the development of rhodium coodination during thermolysis, and the presence of small clusters on the surface at 320°C. The mode of acac decomposition is not understood, though TPD experiments would offer some clues to this. Re-exposure to CO after thermolysis to 190°C results in the regeneration of a mixture of gem-carbonyl, linear and bridging carbonyl species. The acac ligand is believed to be retained by most of the rhodium atoms during this experiment. The linear and bridging carbonyl species are possibly formed on rhodium atoms which have also lost the acac ligand, and formed small clusters at this temperature. It is possible that a disproportionation reaction takes place during the thermolysis process:

$3Rh^{I}(acac) \rightarrow Rh^{III}(acac)_3 + 2Rh^{O}$

Exposure to CO of species which have been thermolysed to 300°C, again results in the formation of a mixture of the above three carbonyl species. Thermolysis under a hydrogen atmosphere results in identical results to that of the helium analogue, except the carbonyl ligands are removed at 90°C, and the acac ligands at 240°C. There is however, evidence from the DRIFTS experiment of a linear carbonyl intermediate during the carbonyl decomposition in this experiment. EXAFS indicates the formation of small rhodium clusters during this experiment. Re-exposure to CO produces identical results to the helium thermolysis analogue. The reaction of $Rh(CO)_2(acac)$ supported on TiO_2 with NO at room temperature was investigated by DRIFTS spectroscopy. The carbonyl ligands were exchanged for a $Rh(NO)^{-}$ ligand, and there were changes in the acac region of the spectrum. The coordination around the rhodium atom would be better understood by the use of EXAFS spectroscopy, and details of gaseous species evolved by temperature programmed desorption. Re-exposure to CO for 30 minutes at room temperature results in the appearance of a band at 2134cm^{-1}, indicating the possible formation of a Rh(CO)(NO) species. There is no attenuation of the NO^{-} ligand, or change in the acac region during this reaction.

5.9 Experimental

Though $Rh(CO)_2(acac)$ was first prepared by Bonati and Wilkinson[17], this study has employed the subsequent simpler method of Varshavskii and Cherkasova[18]. Acetylacetone (4ml) was added to a solution of $RhCl_3.nH_2O$ (1g) in DMF (20ml). The solution was boiled for 30 minutes to cause a colour change to orange/brown. The solution was allowed to cool before adding water to cause precipitation of the product. After separating the product by filtration, it was washed with ethanol and ether before recrystallising from hexane. The product was characterised by NMR spectroscopy: ^1H 2.05 (CH_3), 5.62 (CH); ^{13}C 27.11 (CH_3), 101.8 (CH), 187.4 (CO), and infrared spectroscopy (see section 5.2.1).

Preparation of the surface supported organometallic species species for DRIFTS and EXAFS studies, by MOCVD was conducted according to the general procedure, given in section 2.7. $Rh(CO)_2(acac)$ (60mg) was deposited onto partailly dehydroxylated titania (Degussa P25,0.5g) or γ alumina (Degussa, 0.5g), by heating the organometallic at 50-60°C for three hours. This gave a 5% weight metal loading on the support. During the deposition of the organometallic the titania turned a pale green colour, and the alumina a yellow-green colour. The sample was treated as air sensitive as was thus stored in a Schlenk tube under an argon atmosphere, and refrigerated until used.

5.10 References

1. S. Kawi, Z. Xu and B. C. Gates, *Inorg. Chem.*, 1994, **33**, 503.
2. N. A. Williams, PhD Thesis, University of Southampton, 1992.
3. C. J. Rudkin, PhD Thesis, University of Southampton, 1997.
4. S. D. Jackson, B. J. Brandreth and D. Winstanley, *J. Chem. Soc. Faraday Trans. I*, 1988, **84**, 1741.
5. K. G. Allum, R. D. Hancock, I. V. Howell, S. C. McKensie, R. C. Pitkethly and P. J. Robinson, *J. Organomet. Chem.*, 1975, **87**, 203.
6. F. R. Hartley, S. G. Murray and P. N. Nicholson, *J. Mol. Catal.*,1982, **16**, 363.
7. K. M. Tearle, PhD Thesis, University of Southampton, 1995.
8. G. A. Ozin, D. M. Haddleton, and C. J. Gil, *J. Phys. Chem.*, 1989, **93**, 6710.
9. P. Serp, R. Feurer, R. Morancho and P. Kalck, *J. Catal.*, 1995, **101**, 107.
10. D. M. Adams and W. R. Trumble, *J. Chem. Soc. Dalton. Trans.*, 1974, 690.
11. F. Huq and A.C. Skapski, *J. Cryst. Mol. Struct.*, 1974, **4**, 411.
12. F. Solymosi, T. Bansagi and E. Novak, *J. Catal.*, 1988, **112**, 183.
13. E. A. Hyde and R. Rudham, *J. Chem. Soc. Faraday Trans.*, 1984, **80**, 531.
14. H. Arai and H. Tominaga, *J. Catal.*, 1976, **43**, 131.
15. J. Liang, H. P. Wang and L. P. Spicer, *J. Phys. Chem.*, 1985, **89**, 5840.
16. R. Dictor, *J. Catal.*, 1988, **109**, 89.
17. F. Bonati and G. Wilkinson, *J. Chem. Soc.*, 1964, 3156.
18. Y. S. Varshavskii and T. G. Cherkasova, *Russ. J. Inorg. Chem.*, 1967, **12**, 899.

Chapter 6

The Surface Organometallic Chemistry of $Pd(acac)_2$ Supported on Titania

6.1 Introduction

Metal β-diketonates can be used as precursors for the thermal and photochemical production of homogeneous and heterogeneous catalysts, and thin films[1]. $Pd(acac)_2$ is an ideal precursor for MOCVD as it is air stable and volatile. The structure of $Pd(acac)_2$ has been determined by single crystal X-ray diffraction, and has been found to have a square planar symmetry[2].

$Pd(acac)_2$ is used as a homogeneous catalyst for the decarboxylation-hydrogenolysis of propargyl formates which have internal acetylenic bonds. The Pd(0) catalyst is prepared from $Pd(acac)_2$ and n-Bu_3P in a 1:1 mixture, and affords disubstituted acetylenes in high yield with a high selectivity[3].

A 1:1:1 mixture of $Pd(acac)_2$: PPh_3: BF_3OEt_2 catalyses the oligomerisation of styrenes[4]. Styrene conversion at optimum conditions (Temp 70°C, B/Pd = 7, P/Pd = 2) was as high as 75000 mol of C_8H_8 per mole of Pd in 7 hours, with a selectivity to dimers, mostly diphenylbut-1-ene, up to 93%.

The surface organometallic chemistry of $Pd(acac)_2$ supported on high area silica and alumina has been studied by several groups[5,6,7]. One of the possible advantages of using $Pd(acac)_2$ as a precursor instead of $PdCl_2$ is that the acac ligand is unlikely to affect the properties of the surface unlike the chlorine is understood to do[8]. Pd-VO_x/ γAl_2O_3 catalysts prepared from $Pd(acac)_2$ and $V(acac)_3$ have been shown to be active for the reduction of NO to N_2[8].

$Pt(acac)_2$, which is a close analogue of $Pd(acac)_2$, adsorbs undecomposed on high surface area silica. The fourfold coordinated Pt(II) cannot form additional coordinations to the surface; only the delocalised π electrons of the acetyl acetonate ligands and free electron pairs of the ligand oxygens may form hydrogen bridges with the surface silanol groups. Therefore, it is assumed that the metal acetyl acetonates interact via hydrogen bridges with silanol groups of the silica surface[9]. On alumina

$Pt(acac)_2$ is partly decomposed by the catalytic action of the acidic and basic sites of the support surface. The surface reaction involves the split of acetyl acetonate ligands, which adsorb on Al^{3+} sites in their enolate form, and possibly the further conversion to acetone and acetic acid strongly adsorbed on Al^{3+} sites. In consecutive reaction steps carbon oxides originating from decomposition form surface carbonates.

A study by Krishankutty *et al*[10], discusses the importance of the pretreatment conditions in the preparation of carbon supported Pd catalysts with clean and active Pd crystallites capable of chemisorption and hydrogen adsorption. Carbon from the $Pd(acac)_2$ precursor contaminated both the bulk and surface of Pd crystallites in Pd/C and Pd/SiO_2 catalysts during a standard hydrogen reduction pretreatment at 573K, but this carbon was removed by calcination in oxygen. Additional contamination of the surface and bulk of Pd crystallites by carbon atoms from the support occurred during a subsequent reduction-evacuation period at 573K for Pd catalysts supported on high surface area turbostratic carbon black. This contamination can be prevented by a chemisorbed layer of oxygen on the Pd surface obtained by cooling the catalyst in oxygen to 300K after calcination and conducting subsequent exposures to hydrogen at a lower temperature of 373K.

The Heck reaction of acrylonitrile with iodobenzene takes place on 5% Pd supported on Al_2O_3 and MgO, prepared from $Pd(acac)_2$[11]. Cinnamonitrile is the major product in the CH_3CN medium with $Pd(acac)_2$ and Pd/MgO catalysts in impregnated and reduced forms. 3,3-diphenyl acrylonitrile is formed as a minor product in the consecutive reaction of the cinnamonitrile with iodobenzene.

The thermochemical behaviour of $Pd(acac)_2$ adsorbed onto differently pre-treated magnesium oxides have been studies by means of the TPRD (temperature-programmed reductive decomposition) technique coupled to mass spectrometry[12]. The thermal profiles of the different decomposition products, including acetone and isopropanol, have been rationalised in terms of chemical interactions with the support, and then correlated with the catalytic properties in the dehydrocyclisation reaction of n-heptane.

6.2 Adsorption of $Pd(acac)_2$ onto Titania

6.2.1 DRIFTS Study of Adsorption of $Pd(acac)_2$ onto Titania

An infrared spectrum of $Pd(acac)_2$ is shown in figure 6.1. The spectrum was acquired by preparing a KBr disk of $Pd(acac)_2$, and was acquired in transmission mode with 100 scans. The infrared bands observed are due to the vibrations of the acetylacetonato (acac) ligands of $Pd(acac)_2$. Assignments were made by comparison with a single crystal IR investigation of $Pd(acac)_2$, and comparison with the IR frequencies of $Fe(acac)_3$ and $Cu(acac)_2$ complexes[13,14].

$Pd(acac)_2$ was supported on partially dehydroxylated titania by MOCVD and a difference DRIFTS spectrum was taken, using untreated titania as the background, illustrated in figure 6.2. The broad, positive band from $3000cm^{-1}$ to $3500cm^{-1}$ suggests that $Pd(acac)_2$ has reacted with the surface via possible formation of hydrogen bonds between the acac ligands and the surface hydroxyl groups. The acac region of the spectrum is seen to undergo some changes upon adsorption to the titania surface. The two precursor bands at $1569cm^{-1}$ and $1550cm^{-1}$, which are attributed to ν(C-O) stretches, merge to form one band at $1592cm^{-1}$. The band at $1527cm^{-1}$, which is attributed to ν(C-C), remains unchanged. There is the development of a new band at $1435cm^{-1}$ in the supported species, which is assigned to δ(CH) or ν(C-C). The precursor band at $1397cm^{-1}$, which is associated with $\delta(CH_3)$, becomes broader and less sharp in the surface supported species. The precursor band at $1357cm^{-1}$, which is attributed to $\delta(CH_3)$, shifts to $1366cm^{-1}$ in the supported species. The precursor band at $1272cm^{-1}$, which is attributed to $\upsilon(C\text{-}CH_3)$, shifts to $1279cm^{-1}$ upon adsorption. Though there are several differences between the spectra of the unsupported and supported species, these are insufficient to suggest a change in the coordination of the acac ligand to the palladium centre, or the structure of the ligand itself. The conclusion which can be best made from this study is that the $Pd(acac)_2$ is physisorbed intact to the surface, and has occurred with the consumption of surface hydroxyl groups. This may be via a reaction of the surface hydroxyl groups and the delocalised π electrons and oxygen of the acac ligands.

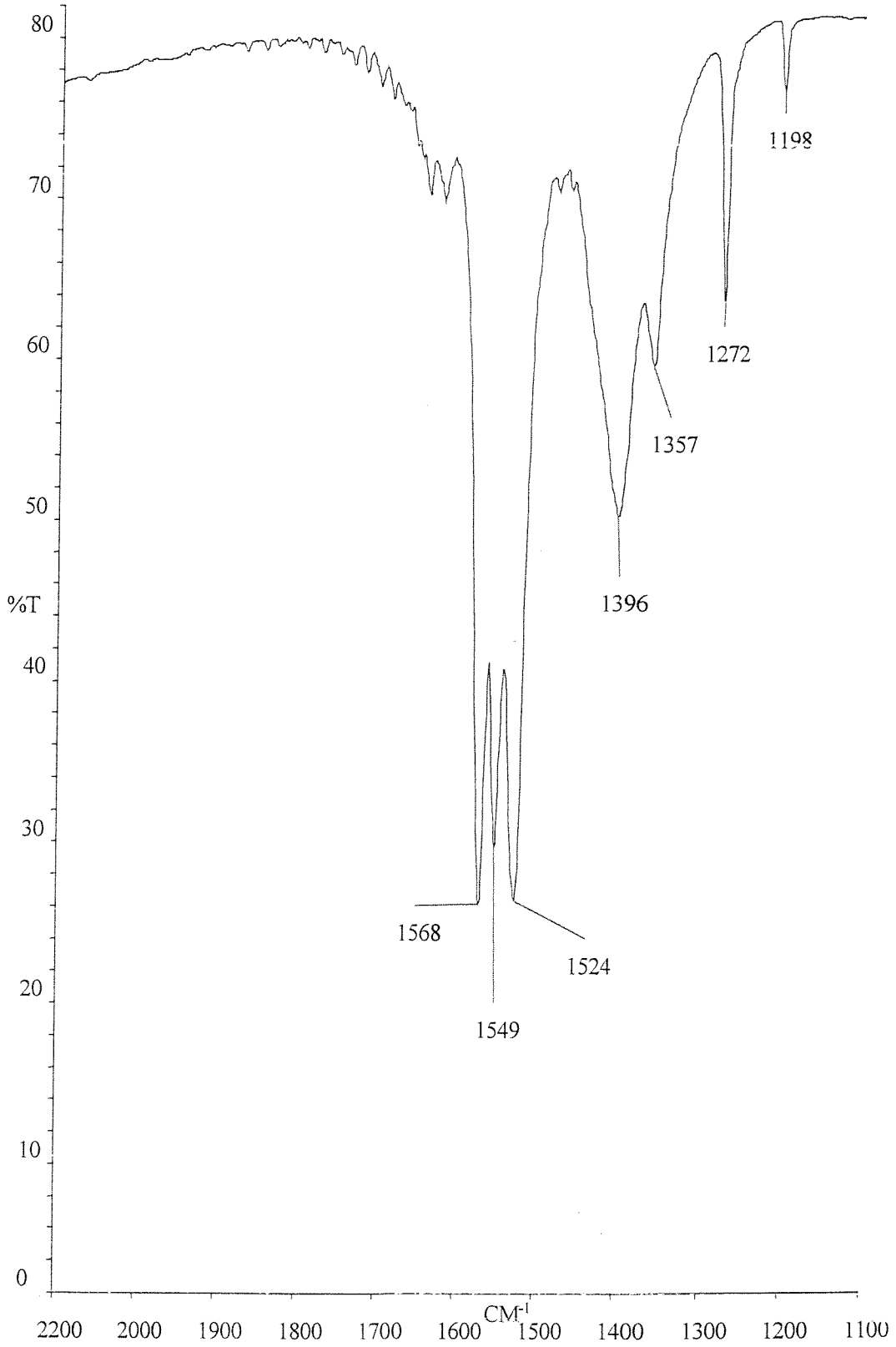

Figure 6.1 Infrared (KBr) Spectrum of $Pd(acac)_2$

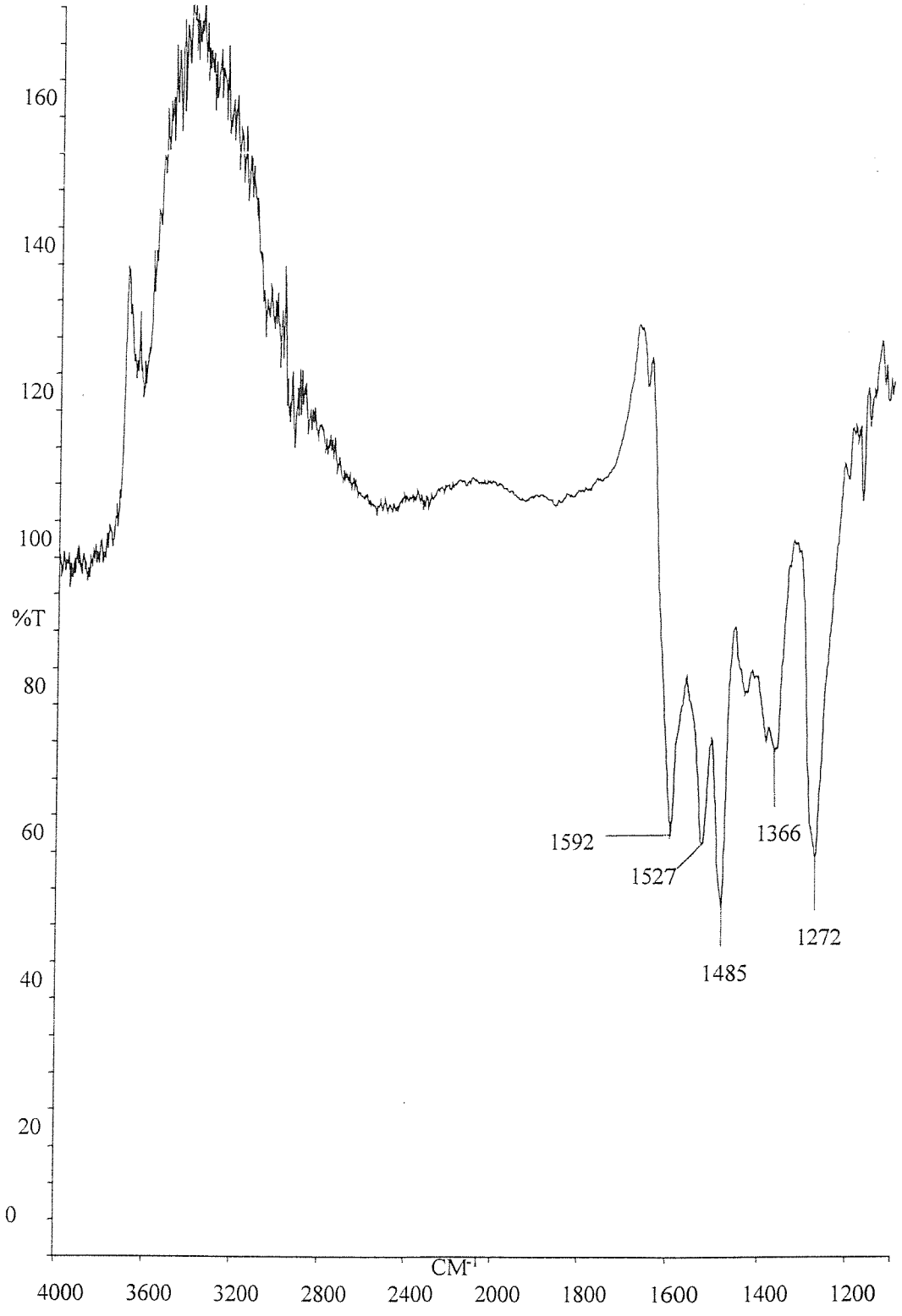

Figure 6.2 Difference DRIFTS Spectrum of $Pd(acac)_2$ Supported on Partially Dehydroxylated TiO_2

$Cu(acac)_2$	$Fe(acac)_3$	Assignment	$Pd(acac)_2$	$Pd(acac)_2/TiO_2$
1577	1570	ν(C-O)	1569	1592
1549		Combination	1549	
1529	1525	ν(C-C)	1524	1527
1461	1445	δ(CH) + ν(C-C)		1485
1413	1425	$\delta_d(CH_3)$	1396	1396
1353	1385, 1360	$\delta_s(CH_3)$	1357	1366
1274	1274	$\nu(C\text{-}CH_3)$	1272	1272

Table 6.1. A comparison of infrared frequencies (cm^{-1}) from various acatylacetonato compounds[13].

6.2.2 EXAFS Study of Adsorption of $Pd(acac)_2$ onto Titania

The Pd K-Edge EXAFS and Fourier Transform for $Pd(acac)_2$ is shown in figure 6.3. The spectrum was acquired in transmission mode at the SRS in Daresbury, at station 9.2, using the EXAFS sample holder. The organometallic was ground up in boron nitride to give a metal loading of 5% weight. Three spectra were averaged to improve the signal to noise ratio. Inclusion of multiple scattering calculations for the acac ligand gave a fit with structural parameters close to those obtained for $Pd(acac)_2$ in crystal structure determinations (see table 6.2). There is one main peak in the Fourier transform at ≈2Å, corresponding to the Pd-O distance. The second, smaller peak at ≈3Å, corresponds to the Pd-C distance. The fit was not improved by attempting to fit subsequent carbon atoms at greater distances.

The Pd K-Edge EXAFS and Fourier transform for $Pd(acac)_2$ supported on partially dehydroxylated titania (see section 6. for method) is shown in figure 6.4. The spectrum was again acquired at station 9.2 at the SRS, using the *in situ* EXAFS cell. Three spectra were averaged to improve the signal to noise ratio. Inclusion of multiple scattering calculations for the acac ligand gave a fit with structural parameters close to those obtained for $Pd(acac)_2$ in crystal structure determinations. The bond distances are greater than in the pure organometallic by ≈0.05Å. This may be due to a weakening of the bonding of the palladium to the acetylacetonate group due to

Figure 6.3 Pd K-Edge EXAFS and Fourier transform of $Pd(acac)_2$

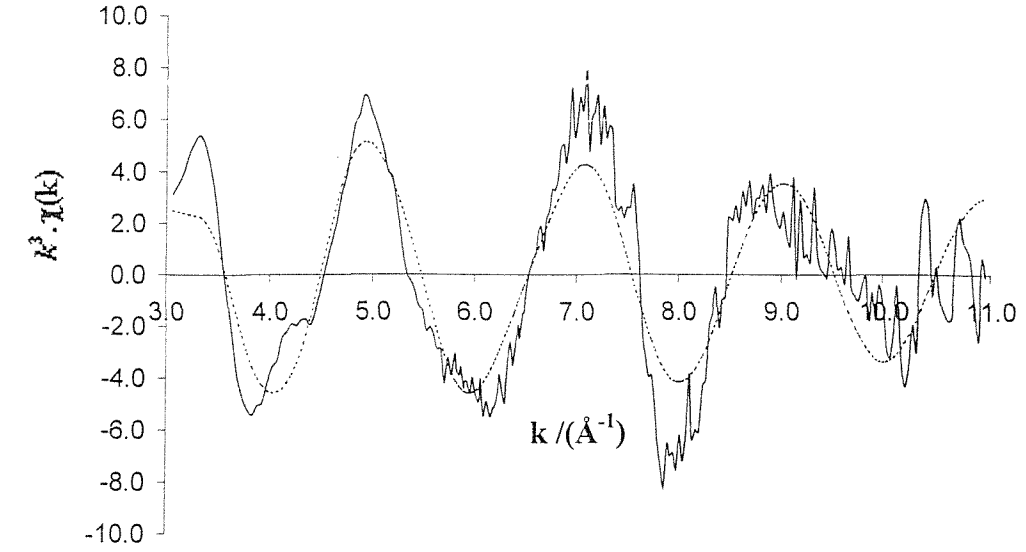

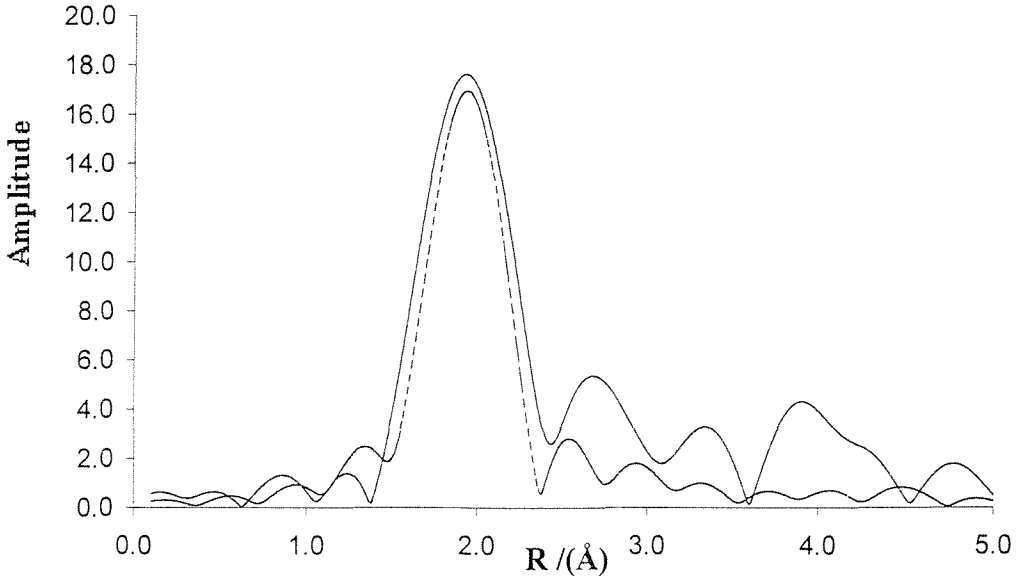

Atom	C.N.	r/Å	$2\sigma^2$ / Å^2
O	4(0.1)	2.031(2)	0.004(1)
C	4(0.1)	3.056(4)	0.008(1)

R = 37.85
Ef –2.31eV

Figure 6.4 Pd K-Edge EXAFS and Fourier transform of $Pd(acac)_2$ supported on TiO_2

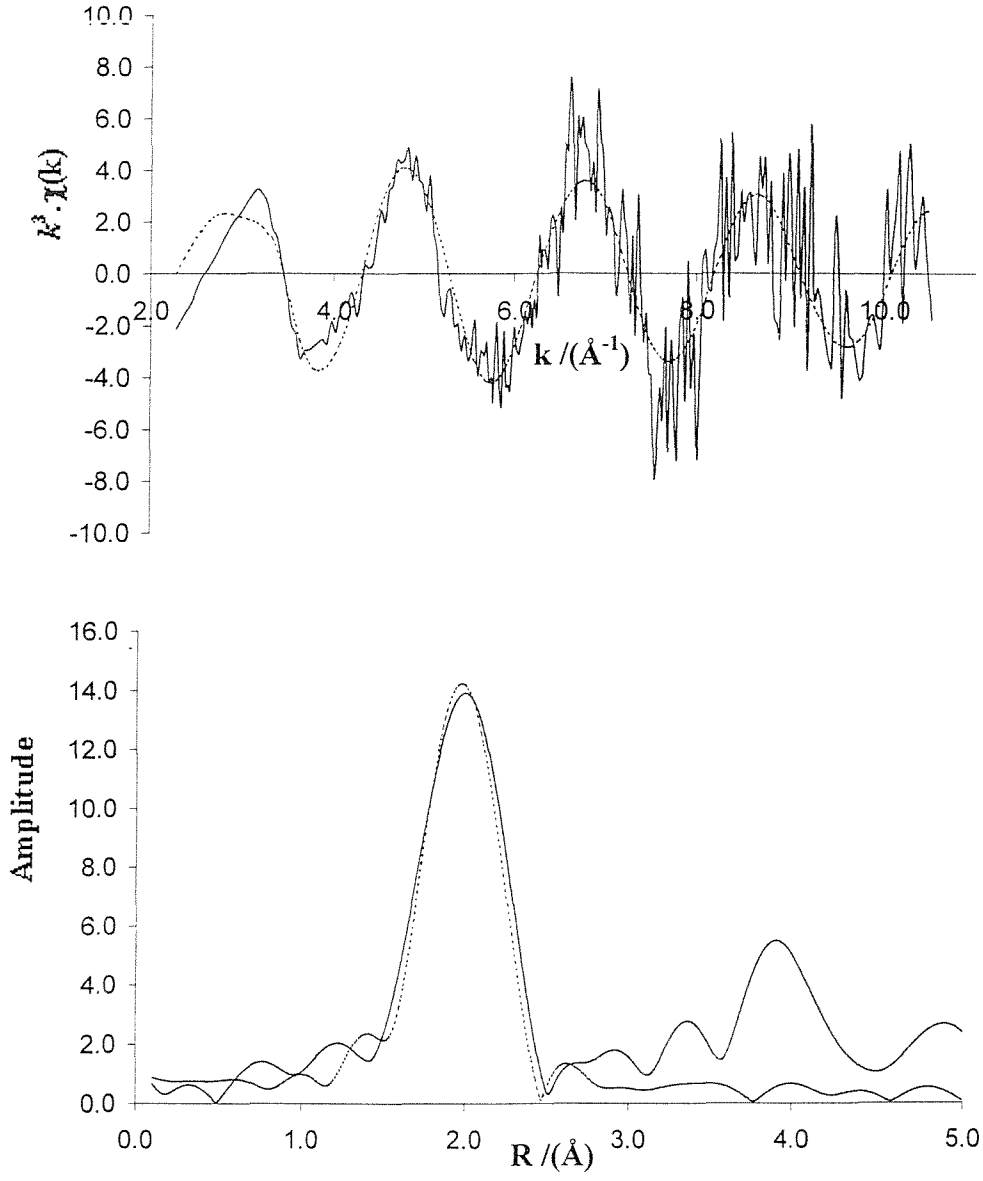

Atom	C.N.	r/Å	$2\sigma^2$ / Å^2
O	4(0.1)	2.038(4)	0.008(1)
C	4(0.2)	3.061(6)	0.010(1)

R = 47.67
Ef =1.89eV

bonding to the TiO_2 surface. No Pd-O(surface) shell could be fitted to the data, indicating that the $Pd(acac)_2$ is physisorbed intact to the TiO_2 surface. This is in agreement with the results from the DRIFTS experiment. There is also a peak at ≈4Å in the spectrum, which could possibly be due to Pd-Pd interactions in the physisorbed layer. However, any attempts to fit a Pd shell to the data were unsuccessful.

Parameter	$Pd(acac)_2$ X-Ray[2]	$Pd(acac)_2$, EXAFS	$Pd(acac)_2$/ TiO_2, EXAFS
Pd-O	1.976 Å	2.031(2) Å	2.038(4) Å
Pd-C	2.916 Å	3.056(4) Å	3.061(6) Å
∠ Pd-O-C	125°	125°	125°

Table 6.2. A comparison of structural parameters for $Pd(acac)_2$ both as a free organometallic, and supported on oxide surfaces

6.3 Thermolysis of $Pd(acac)_2$ Supported on TiO_2

6.3.1 DRIFTS Study of Thermolysis of $Pd(acac)_2$ Supported on Titania

The thermolysis experiment was carried out *ex-situ* under a helium atmosphere, where samples were heated to the stated temperature for 10 minutes and transferred to the DRIFTS cell. Spectra were collected at 100 scans, using hydroxylated titania as a background. The spectra acquired during this experiment are shown in figure 6.5.

By 100°C, there is very little change in the acac region of the spectrum. The only change is a reduction in intensity of the peaks at 1396cm^{-1} and 1366cm^{-1}, which have been attributed to $\delta_d(CH_3)$ and $\delta_s(CH_3)$ respectively.

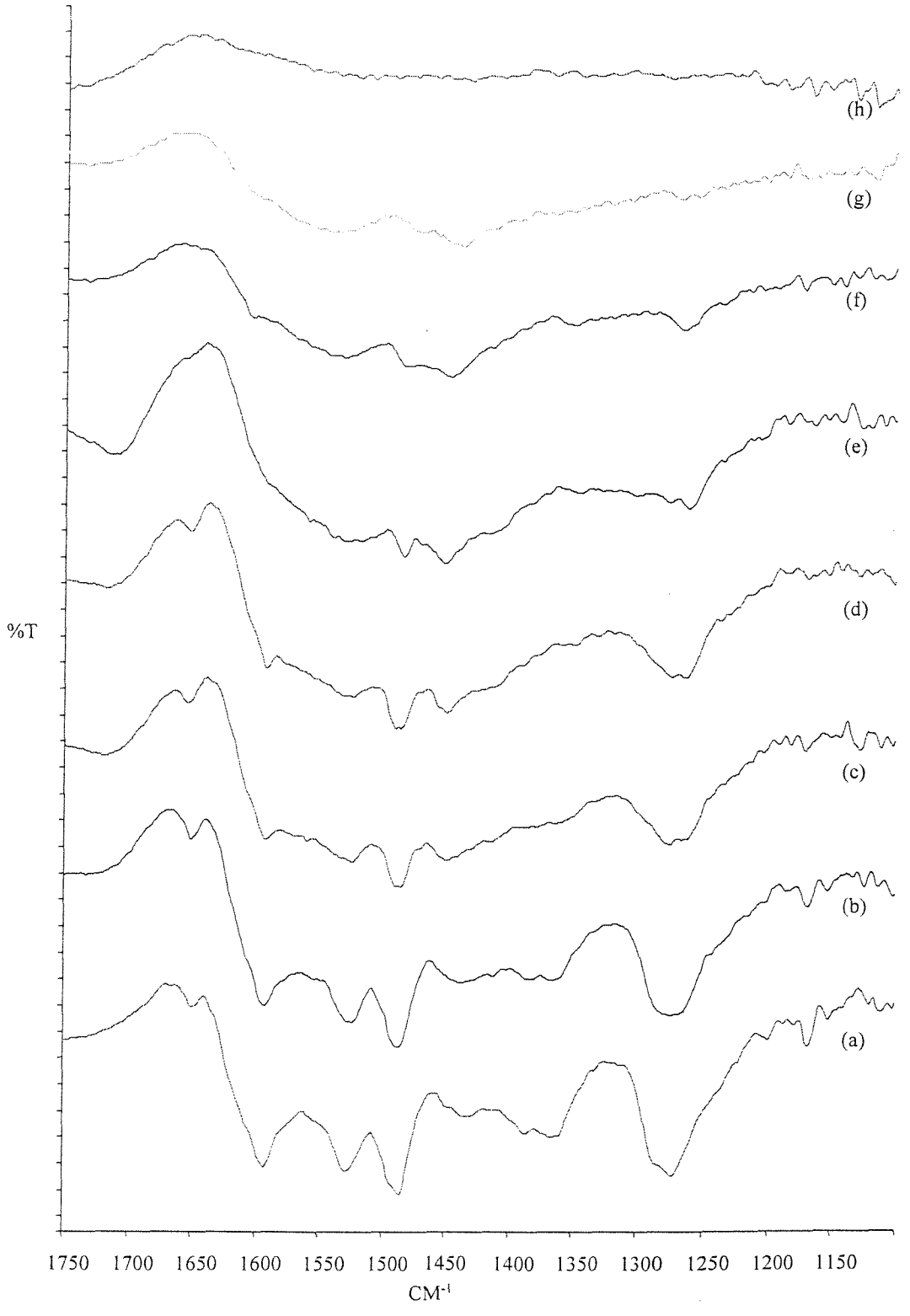

Figure 6.5 DRIFTS difference spectra of $Pd(acac)_2$ supported on TiO_2 during helium thermolysis: (a) Room temp, (b) 100°C, (c) 130°C, (d) 160°C, (e) 190°C, (f)220°C, (g)280°C, (h) 330°C.

At 130°C, there is a reduction in intensity of the bands at 1592cm^{-1} and 1523cm^{-1}. These observations suggest possible dehydrogenation and subsequent C-C and C-O bond cleavage of within the acac ligand, though no reaction mechanism can be inferred from the data. The bands at 1396cm^{-1} and 1366cm^{-1} have almost disappeared at this temperature. There is very little change in the spectrum between 130°C and 160°C. At 190°C, the peak at 1591cm^{-1} has almost disappeared (C-O). The peaks at 1396cm^{-1} and 1366cm^{-1} have disappeared at this temperature. At 220°C, the main remaining peaks at 1527cm^{-1}, 1483cm^{-1}, 1450cm^{-1} and 1262cm^{-1} have reduced in intensity slightly. At 250°C, the peak at 1483cm^{-1} has almost disappeared, whilst the others are relatively unchanged from 220°C. At 280°C, the only discernible peaks are observable at 1538cm^{-1} (C-C), and 1441cm^{-1}, (C-H). These two peaks are also observable at 310°C, and at 330°C, there are no observable peaks. It can be concluded that at this temperature, there are palladium metal clusters of varying size on the titania surface. Though the DRIFTS experiment carefully monitors the progress of the thermolysis experiment, it is difficult to deduce the reaction mechanism with certainty from these data. There appears to be considerable transformation of the acac ligands between 130°C and 280°C, before complete their complete removal by 330°C. It is possible that some dehydrogenation of the CH_3 ligands occurs followed by cleavage of the C-O ligands. The C-C backbone seems to remain intact until higher temperatures before removal by 330°C. A deeper understanding of the mechanism could be found from TPD results, which would monitor the gas phase during the thermolysis, indicating fragments of the acac ligand desorbed during the experiment. EDE would also monitor the environment of the palladium during the thermolysis experiment. Changes in the acac coordination, and the palladium clustering process could be observed using this technique.

6.3.2 EXAFS Study of Thermolysis of $Pd(acac)_2$ Supported on Titania

A sample of $Pd(acac)_2$ supported on TiO_2, was heated to 330°C in helium, using the *in situ* EXAFS cell. The EXAFS and Fourier transform are shown in figure 6.6. After cooling the XAS spectrum was acquired. Three spectra were acquired and

Figure 6.6 Pd K-Edge EXAFS and Fourier transform of $Pd(acac)_2$ supported on TiO_2 after heating to 200°C in He

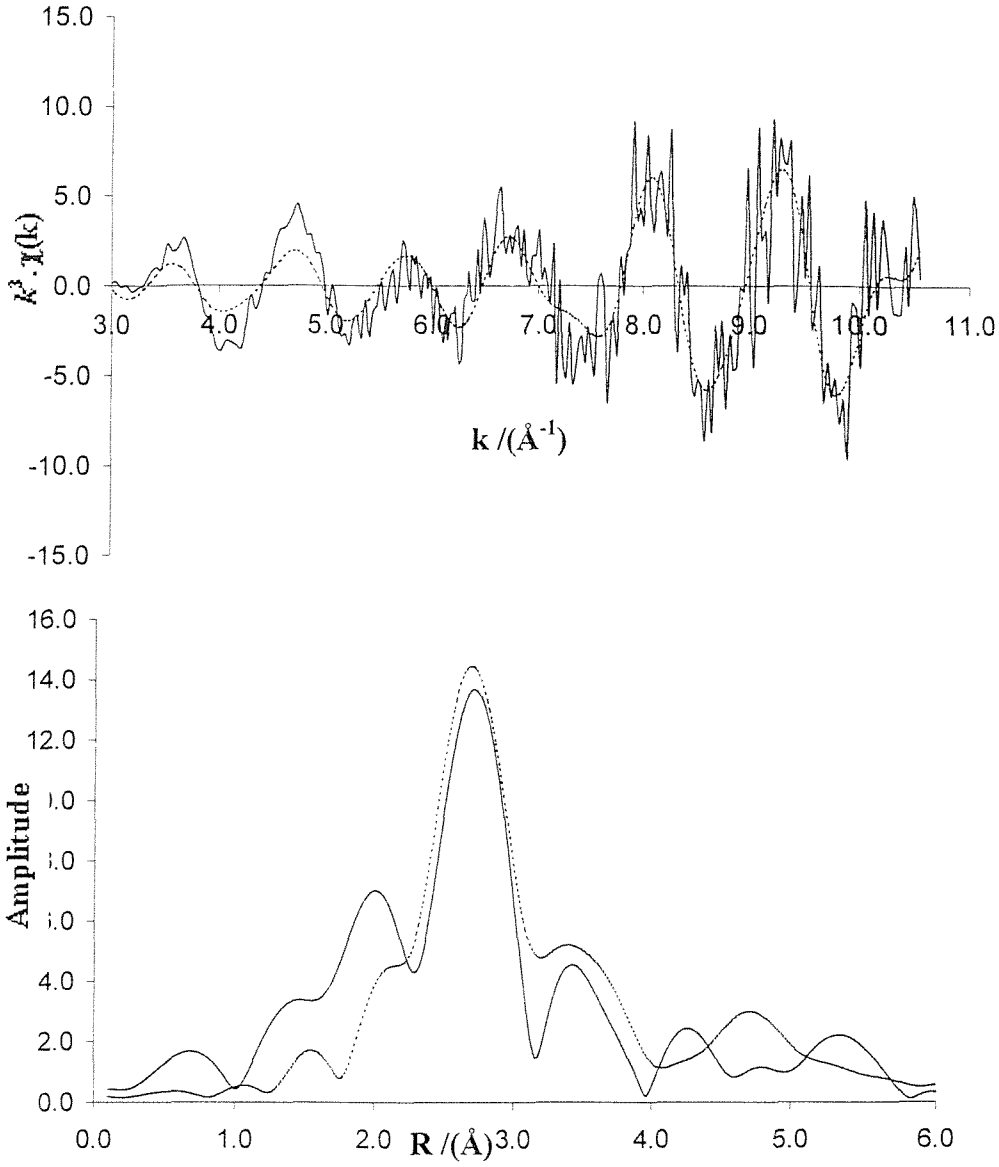

Atom	C.N.	r/Å	$2\sigma^2$ / Å^2
Pd	4(0.6)	2.751(3)	0.010(2)
Pd	3(1.1)	3.813(2)	0.010(3)
Pd	3(3.2)	4.729(3)	0.008(3)

R = 55.63 %
Ef = 2.40 eV

averaged in order to improve the signal to noise ratio. There are three peaks in the Fourier transform. The first is the main peak at 2.75Å, which corresponds to the first shell of four palladium atoms. The second shell at 3.81Å, corresponds to the second shell of three palladium atoms. The third shell is observed at 4.72Å, and contains 3 palladium atoms. The bond distances are in close agreement with those observed for a palladium foil with an FCC structure[15]. These results indicate that the thermolysis experiment has caused removal of the acac ligands, resulting in the formation of small palladium clusters. These clusters are smaller in size than those produced from analogous thermolysis experiments using $[Rh(CO)_2Cl]_2$ and $Rh(CO)_2(acac)$ supported on TiO_2 (chapters 3 and 5). This could be due to the fact that the acac ligand has greater thermal stability that the CO ligand, and clustering is limited until all the acac ligands are removed, whereas the process can commence earlier in the other systems.

6.4 CO Adsorption onto Thermolysed $Pd(acac)_2$ Supported on Titania

6.4.1 DRIFTS Study of CO Adsorption

Following the thermolysis experiment in which the acac ligands were removed thermolytically under an inert atmosphere, the sample was exposed to one atmosphere of CO for two hours at room temperature. The CO was exposed at a pressure of 1 bar and at a flow rate of 5ml/min. This experiment serves as a probe for investigation of the size of the palladium clusters formed from the thermolysis experiment, as the type of palladium carbonyl species formed is indicative of the cluster size, as well as the surface planes present in the small metal particles[16]. The spectra acquired for this experiment are shown in figure 6.7.

After one hour there are peaks observable at $2090cm^{-1}$, $1815cm^{-1}$ and a broad band at $1900\text{-}1960cm^{-1}$. These are attributed to a linear Pd-CO species, a three fold bridging carbonyl species and a two fold bridging carbonyl species respectively. The two fold bridging carbonyl species is present in greater abundance than the others at

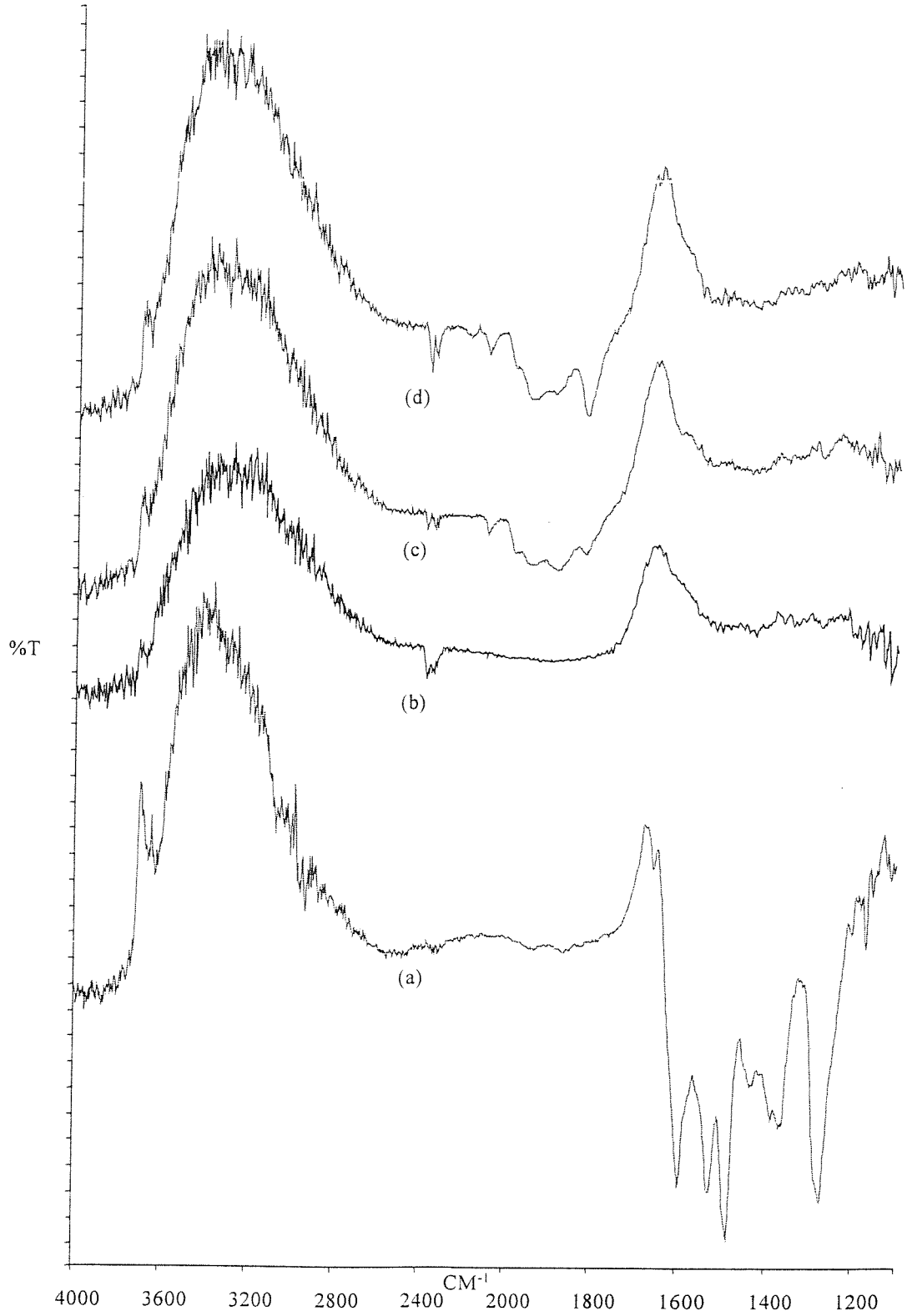

Figure 6.7 DRIFTS difference spectra of $Pd(acac)_2$ supported on TiO_2 during CO regeneration After helium thermolysis to 330°C: (a) Room temp, (b) Heated to 330°C, (c) 1 hr CO exposure, (d) 2 hrs CO exposure.

this stage of the experiment are. The width of this band and the presence of other palladium carbonyl species indicates that there are clusters of widely varying size on the surface, as well as a variety of surface planes exposed. The linear carbonyl species are likely to be present on smaller palladium clusters, whereas the bridging carbonyl species are indicative of larger clusters. After two hours of exposure to CO at room temperature, all the described carbonyl species increase in intensity. The linear carbonyl species stretch intensity doubles, as does the intensity of the two fold bridging carbonyl species. The intensity of the three fold bridging carbonyl species increased by a factor of four and is easily the most intense of the carbonyl species present on the surface.

6.4.2 EXAFS Study of CO Adsorption

A sample of $Pd(acac)_2$ supported on TiO_2 was first heated to 330°C in helium, before exposure to CO for 30 minutes, using the *in situ* EXAFS cell. The EXAFS and Fourier transform, are shown in figure 6.8. There are three peaks corresponding to palladium shells in the Fourier transform. The coordination numbers are virtually unchanged within the limits of error. Although some carbonylation may have occurred, the EXAFS signal is likely to be swamped by the heavy palladium atoms, and is thus unnoticeable.

6.5 Hydrogen Thermolysis of $Pd(acac)_2$ Supported on TiO_2

6.5.1 DRIFTS Study of Hydrogen Thermolysis of $Pd(acac)_2$ Supported on TiO_2

The hydrogen thermolysis experiment was carried out *ex-situ* under a hydrogen atmosphere, where samples were heated to the stated temperature for 10 minutes and transferred to the DRIFTS cell. Spectra were collected at 100 scans,

Figure 6.8 Pd K-Edge EXAFS and Fourier transform of $Pd(acac)_2$ supported on TiO_2 heated to 200°C in He and subsequently exposed to CO for 30 mins

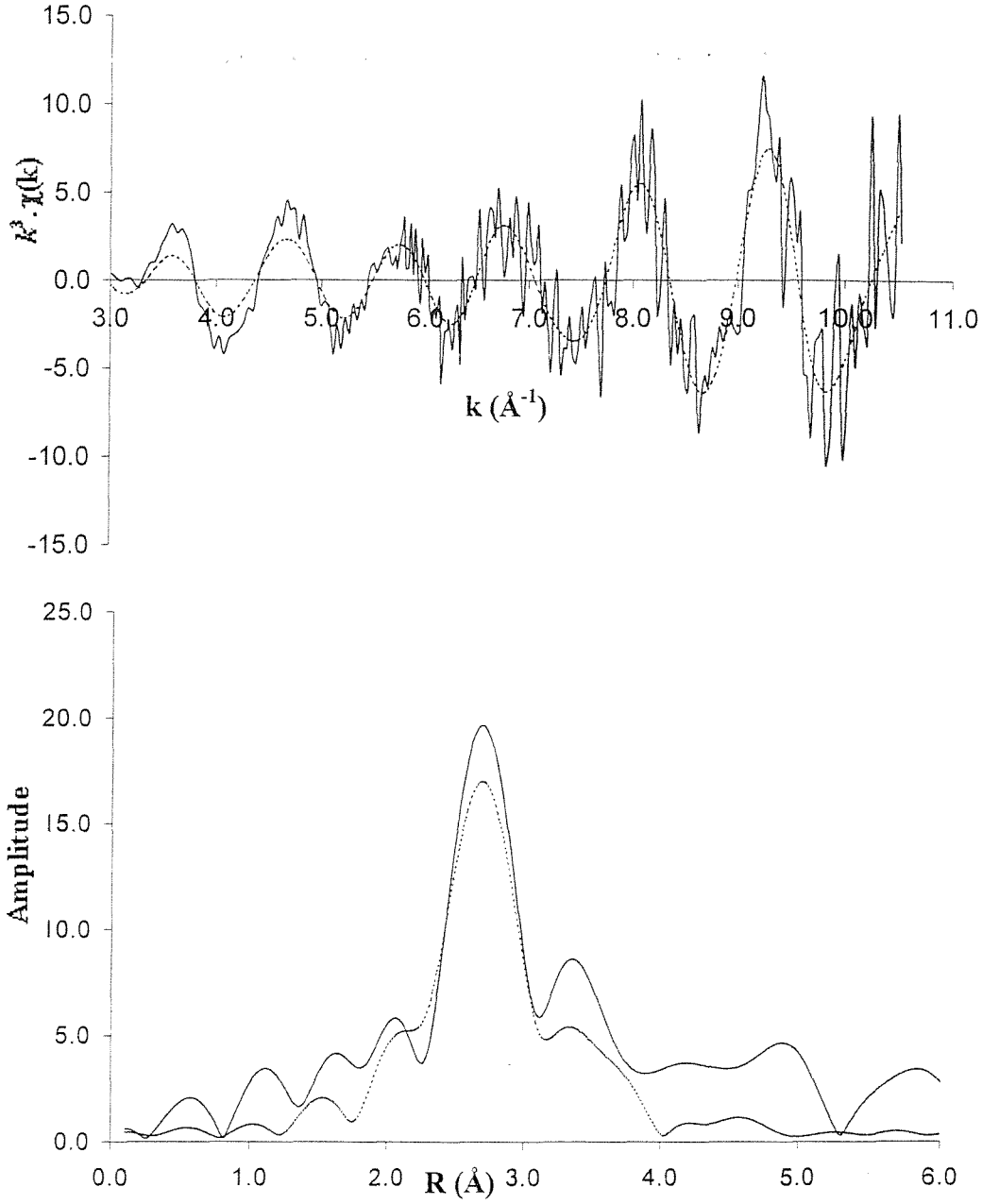

Atom	C.N	r/Å	$2\sigma^2$ / Å^2
Pd	5(0.6)	2.751(3)	0.010(2)
Pd	2(1.1)	3.813(2)	0.010(3)
Pd	1(3.2)	4.729(3)	0.008(3)

R = 56.34 %
Ef = 2.82 eV

using hydroxylated titania as a background. The spectra acquired during this experiment are shown in figure 6.9.

The room temperature spectrum shows the characteristic infrared stretches associated with $Pd(acac)_2$ supported on titania, with stretches at 1592cm^{-1}, 1529cm^{-1}, 1485cm^{-1}, 1396cm^{-1}, 1366cm^{-1} and 1272cm^{-1}, in addition to a broad positive band in the hydroxyl region of the spectrum (3000-3500cm^{-1}).

Exposure to a stream of hydrogen at a pressure of 1 bar for 10 minutes at room temperature, results in a 30% reduction in the intensity of the acac region of the spectrum, with no change in the frequencies or relative intensities of the bands. After 40 minutes at room temperature the intensity of the acac region has reduced to 50% of the original intensity. There is a reduction in intensity of the peaks at 1396cm^{-1} and 1366cm^{-1}, which have been attributed to $\delta_d(CH_3)$ and $\delta_s(CH_3)$ respectively.

After heating to 100°C, there is a significant change in the intensity of the acac region of the spectrum. The peaks at 1592cm^{-1} and 1525cm^{-1} are significantly attenuated. The peaks at 1396cm^{-1} and 1366cm^{-1} have also disappeared. The remaining peaks are at 1488cm^{-1} and 1272cm^{-1}. There is also an increase in the relative intensity of the peak at 1448cm^{-1}. Upon heating to 140°C, the band at 1527cm^{-1} has weakened and broadened, and the band at 1448cm^{-1} has relatively (to that at 1488cm^{-1}) intensified. At 180°C the peaks at 1483cm^{-1} and 1272cm^{-1} have almost disappeared, leaving peaks at 1518cm^{-1} and 1457cm^{-1}. At 200°C, the peaks at 1518cm^{-1} and 1457cm^{-1}, shift to 1538cm^{-1} and 1440cm^{-1}. They also appear sharper and are weaker in intensity than at 180°C. All peaks in the acac region of the spectrum have disappeared after heating to 220°C in hydrogen. The progress of the decomposition of the acac ligands is very similar to that of the helium thermolysis experiment (6.3), except the reaction proceeds at substantially lower temperature due to the reductive environment created by the hydrogen. The interpretation of the results is therefore the same, and the discussion is found in 6.3.1. This result is again similar to analogous results found using supported rhodium organometallics (chapters 3 and 5), in that reduction of the supported organometallic to metallic clusters occurs at significantly lower temperatures under a hydrogen atmosphere.

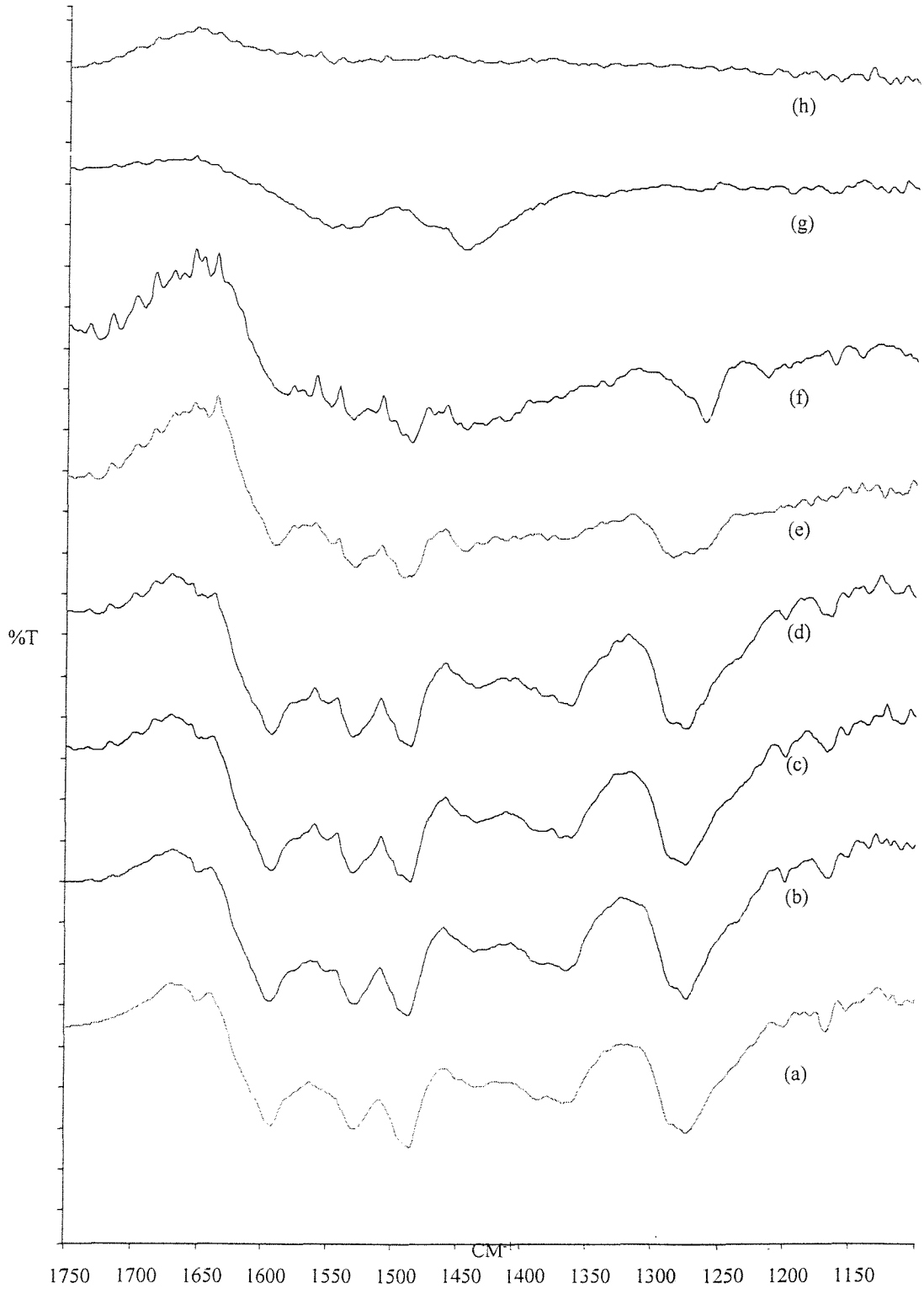

Figure 6.9 DRIFTS difference spectra of $Pd(acac)_2$ supported on TiO_2 during hydrogen thermolysis: (a) Room temp, (b) H_2 Room temp 10 mins, (c) H_2 Room temp 30 mins, (d) 100°C, (e) 140°C, (f)180°C, (g) 200°C, (h) 220°C.

6.5.2 EXAFS Study of Hydrogen Thermolysis of $Pd(acac)_2$ Supported on TiO_2

A sample of $Pd(acac)_2$ supported on TiO_2, was heated to 220°C in hydrogen, using the *in situ* EXAFS cell. After cooling the XAS spectrum was acquired. Three spectra were acquired and averaged in order to improve the signal to noise ratio. The EXAFS and Fourier transform are shown in figure 6.10. There are four peaks in the Fourier transform. These correspond to successive palladium shells. The bond distances are in close agreement with those observed for a palladium foil with an FCC structure[13]. The clusters generated are larger than those formed from the corresponding helium thermolysis experiment. This is due to the reducing nature of the hydrogen atmosphere under which the thermolysis was conducted. Again though, the clusters formed are smaller than those formed under analogous conditions using rhodium organometallics (chapters 3 and 5). A discussion of the possible reasons for this is found in 6.3.2.

6.6 CO Adsorption onto Hydrogen Thermolysed $Pd(acac)_2$ Supported on Titania

6.6.1 DRIFTS Study of CO Adsorption onto Hydrogen Thermolysed $Pd(acac)_2$ Supported on Titania

Following the hydrogen thermolysis experiment in which the acac ligands were removed, the sample was exposed to 1 atmosphere of CO at room temperature for two hours. Results obtained have shown that the hydrogen thermolysis results in the creation of palladium clusters. The nature and distribution of sizes of these clusters can be probed by exposure to CO at room temperature. The types of carbonyl ligand formed are indicative of the size of the palladium clusters that have been formed, as well as the surface planes present[16]. CO was exposed to the thermolysed sample *in situ* at a flow rate of 5ml/min. The spectra acquired from this experiment are shown in figure 6.11.

Figure 6.10 Pd K-Edge EXAFS and Fourier transform of $Pd(acac)_2$ supported on TiO_2 heated to 200°C in H_2

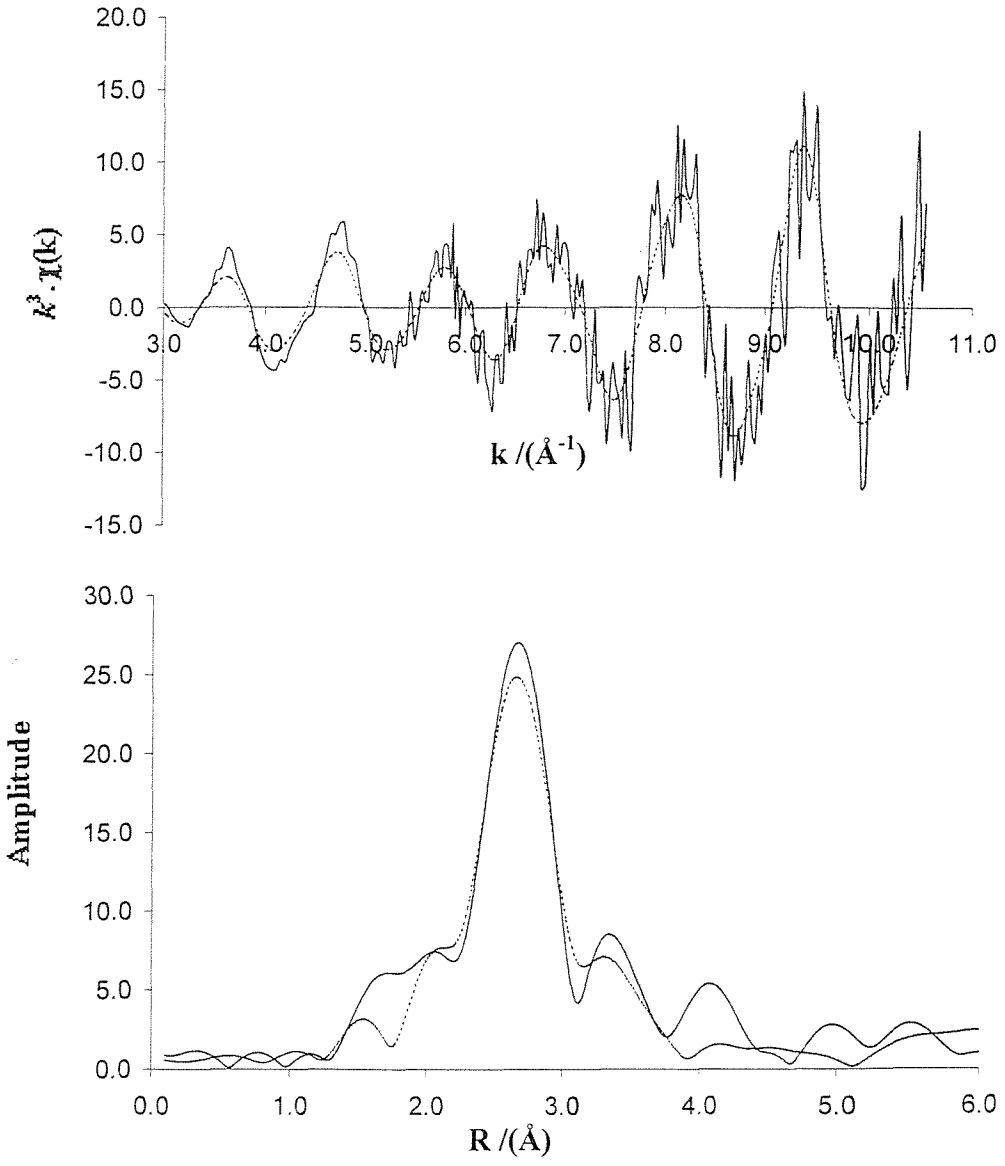

Atom	C.N.	r/Å	$2\sigma^2$ / Å^2
Pd	7(0.6)	2.751(3)	0.010(2)
Pd	2(1.1)	3.813(2)	0.010(3)
Pd	4(1.2)	4.729(3)	0.008(3)
Pd	2(0.8)	5.303(4)	0.013(2)

R = 46.20 %
Ef = 2.41 eV

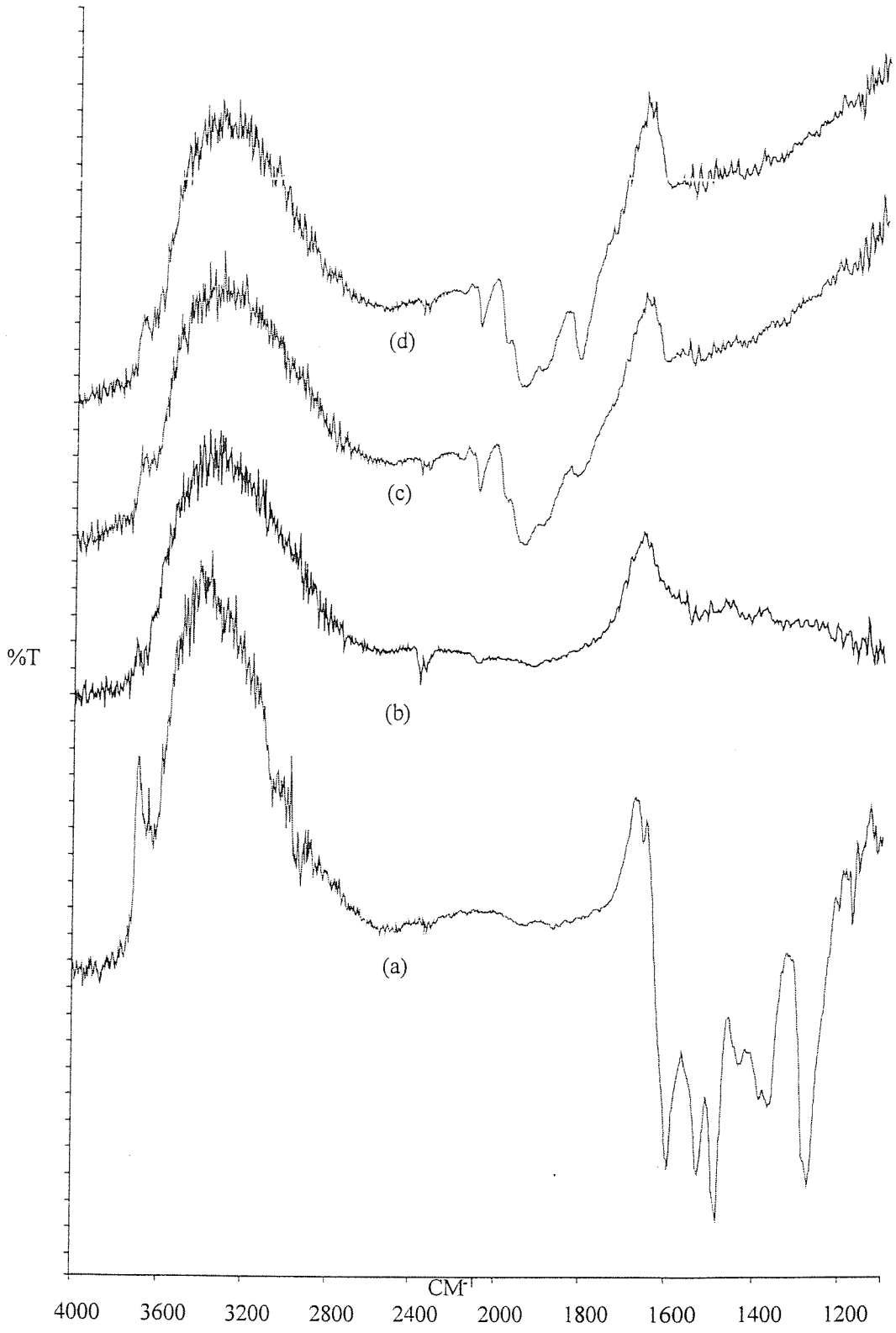

Figure 6.11 DRIFTS difference spectra of $Pd(acac)_2$ supported on TiO_2 during CO exposure after hydrogen thermolysis to 220°C: (a) Room temp, (b) Heated to 220°C, (c) 1 hr CO Exposure, (d) 2 hrs CO exposure.

After 1 hour, there has been the development of three peaks in the carbonyl region of the spectrum. The most intense peak is at 1811cm^{-1}, which is attributed to a three fold bridging carbonyl species. This is indicative of CO reacting with large clusters of palladium. The next most intense peak is a broad band at 1944cm^{-1}, which is attributed to a two fold bridging carbonyl species. The breadth of this band suggests that there are a variety of palladium surfaces exposed upon which the two fold bridging species is forming. The weakest peak is a sharper stretch at 2090cm^{-1}, which is attributed to a linear carbonyl species. Such species are believed to form on monodispersed palladium or very small palladium clusters. A further hour of exposure to CO under the same reaction conditions results in very little change in the spectrum. The intensities of the linear and three-fold bridging sites remain unchanged. There is a change in the two-fold bridging band, with the most prominent peak now at 1879cm^{-1}. The acac region of the spectrum remains unchanged during this experiment. These results suggest that the hydrogen thermolysis experiment has generated palladium clusters with a variety of sizes, with a variety of surface planes exposed. The results also indicate that most of the regeneration has occurred within the first hour of exposure to CO.

The results of the experiment are very similar to that where CO is exposed to the He thermolysed species. There appears to be a greater proportion of the three-fold bridging carbonyl species in this experiment, suggesting that larger palladium clusters have been formed. This is in agreement with results obtained in an analogous experiment performed on a single crystal[16]. These results agree with the EXAFS results obtained in 6.4.2, which indicate the formation of larger Pd clusters under the more reductive hydrogen atmosphere.

6.6.2 EXAFS Study of CO Regeneration of Hydrogen Thermolysed $Pd(acac)_2$ Supported on Titania

A sample of $Pd(acac)_2$ supported on TiO_2 was first heated to 220°C in hydrogen, before exposure to CO for 30 minutes, using the *in situ* EXAFS cell. The

Figure 6.12 Pd K-Edge EXAFS and Fourier transform of $Pd(acac)_2$ supported on TiO_2 heated to 200°C in H_2 and subsequently exposed to CO for 30 mins

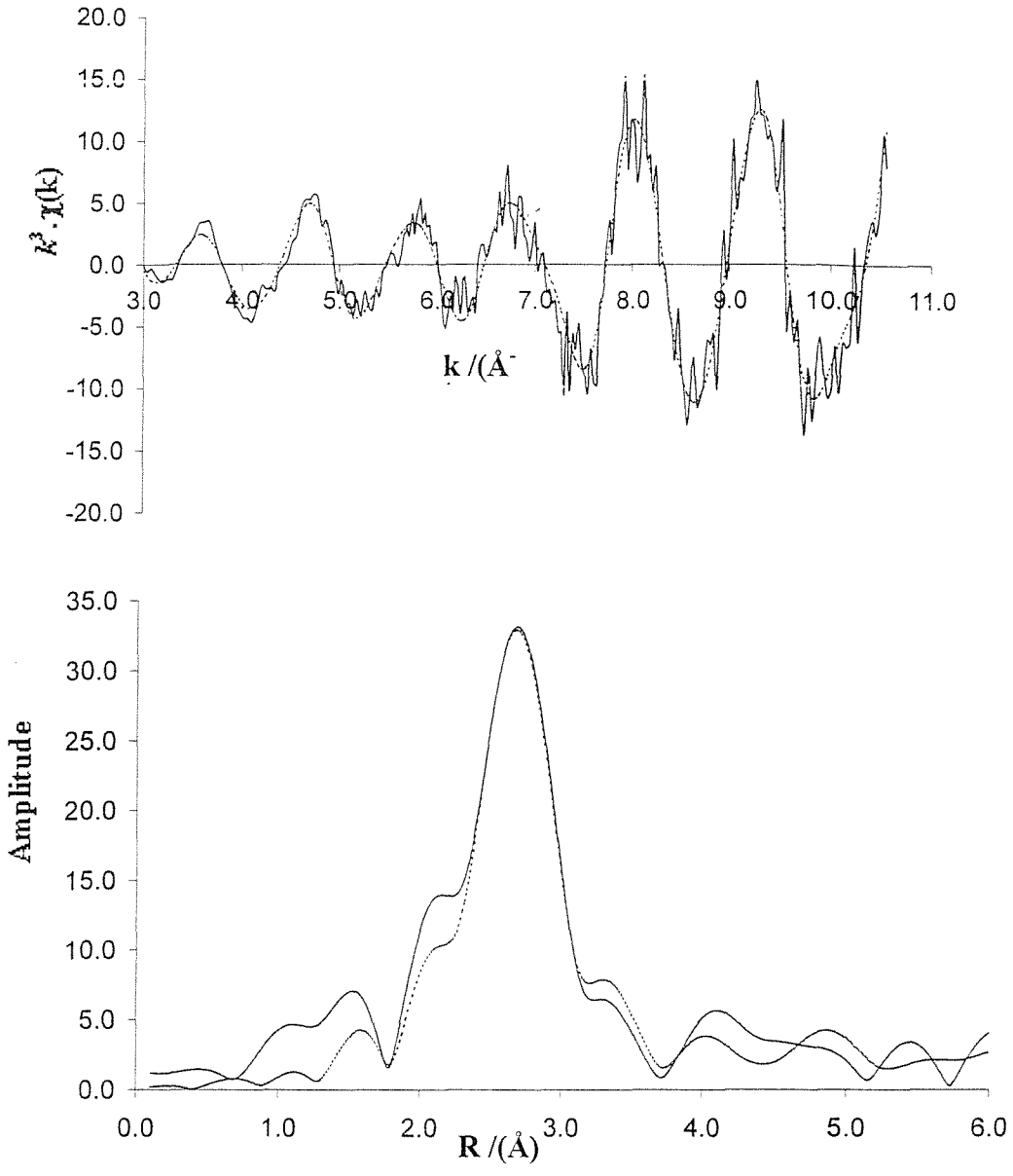

Atom	C.N.	r/Å	$2\sigma^2$ / Å^2
Pd	9(0.8)	2.748(3)	0.010(2)
Pd	3(0.9)	3.810(2)	0.011(3)
Pd	5(1.4)	4.729(3)	0.010(3)
Pd	3(1.1)	5.292(3)	0.014(2)

R = 30.53 %
Ef = 2.28eV

EXAFS and Fourier transform are shown in figure 6.12. There are four peaks corresponding to palladium shells in the Fourier transform. The effect of the CO is observed to have caused a slight growth in the size of the clusters. Again, some carbonylation may have occurred, but the EXAFS signal of any carbonyl groups is likely to be swamped by heavy palladium backscatterers.

6.7 Reaction of $Pd(acac)_2$ Supported on TiO_2 with NO

6.7.1 DRIFTS Study of Reaction of $Pd(acac)_2$ Supported on TiO_2 with NO

A sample of $Pd(acac)_2$ supported on titania was reacted with 1 atmosphere of NO at room temperature for 20 minutes. The reaction was performed *in situ* with a flow rate of 5ml/min.

The room temperature spectrum of $Pd(acac)_2$ supported on titania, figure 6.13, shows the characteristic acac peaks at $1587cm^{-1}$, $1523cm^{-1}$, $1435cm^{-1}$, $1386cm^{-1}$, $1366cm^{-1}$ and $1276cm^{-1}$, in addition to a broad positive band in the hydroxyl region of the spectrum ($3000\text{-}3500cm^{-1}$).

After exposure to NO for 20 minutes, the cell was flushed with helium to remove gaseous NO and other reaction products. The spectrum acquired shows a broad sharp band at $1718cm^{-1}$, which is attributed to a $Pd\text{-}NO^-$ species[17]. There are also changes in the acac region of the spectrum. The peak at $1586cm^{-1}$ has attenuated and shifted to $1568cm^{-1}$. The peak at $1523cm^{-1}$ has lost almost all its intensity. The peak at $1435cm^{-1}$ has shifted to $1446cm^{-1}$. Two sharp peaks at $1378cm^{-1}$ and $1351cm^{-1}$ have replaced the peak at $1386cm^{-1}$, and the peak at $1276cm^{-1}$ has moved to $1294cm^{-1}$. A possible explanation for these findings is that exposure to NO causes the removal of one or both of the acac ligands which may subsequently be bound to the titania support via a reaction of the surface hydroxyl groups and the delocalised π electrons and oxygen of the acac liagnd. This results in the formation of a $Pd(NO)^-$ species, in

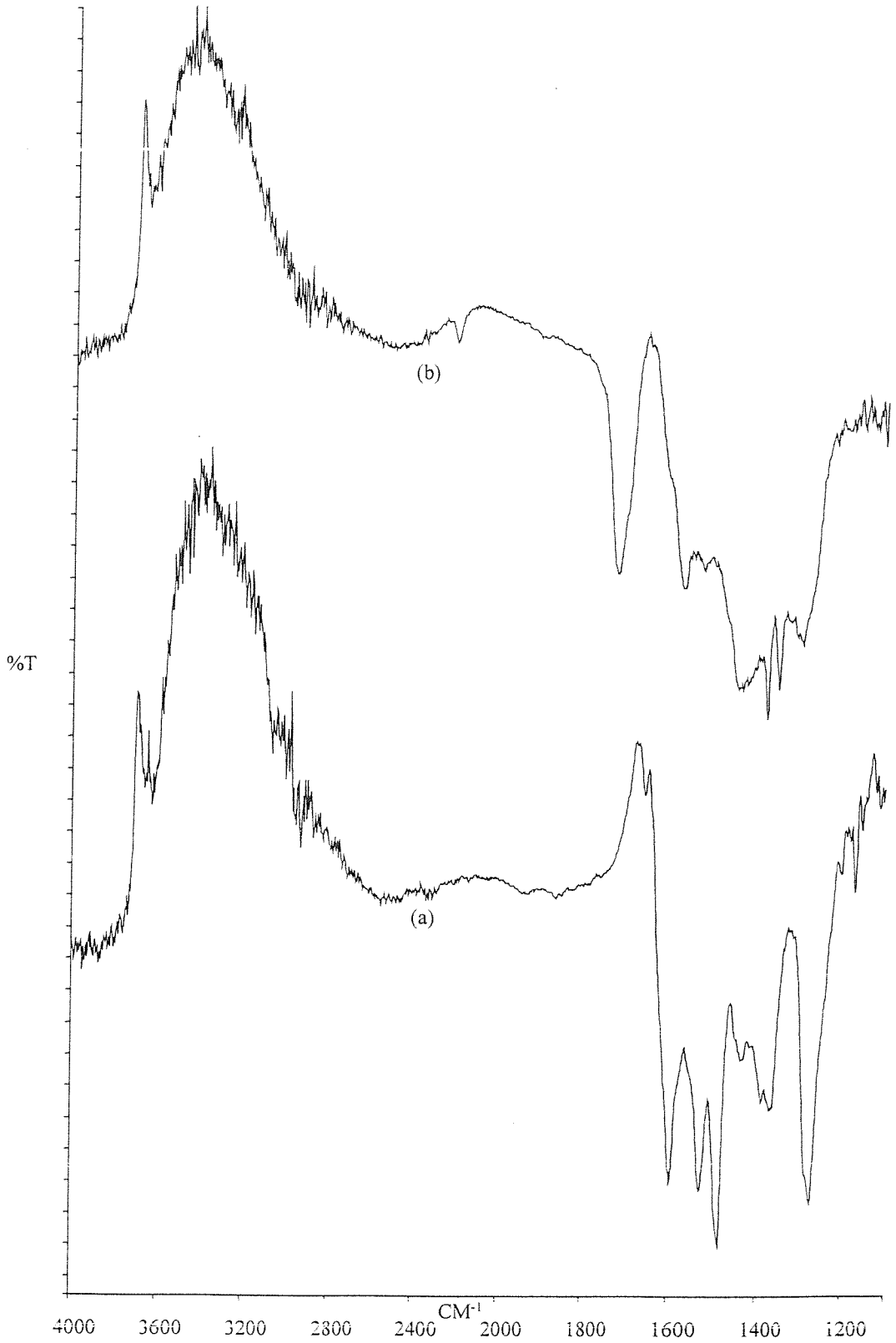

Figure 6.13 DRIFTS difference spectra of $Pd(acac)_2$ supported on TiO_2: (a) Before exposure to NO & (b) After exposure to NO for 30 mins at room temperature.

agreement with the literature assignments of a nitrosyl band at this frequency[17].

In order to satisfy the requirement for an 18 electron metal centre, the palladium centre (Pd(II) has 8 valance electrons) is likely to be bound to three surface oxygen atoms, and is also possibly still partially bound to one or both of the acac ligands. This is under the assumption that the palladium remains monodispersed during the process. The 18 electron rule would of course not be relevant if the surface species is square planar. The geometry of the molecule could be deduced by EXAFS analysis, and would be a valuable future experiment on this system. There is insufficient evidence from the DRIFTS experiment to be certain of the coordination around the metal centre.

6.7.2 Post NO Reaction Exposure to CO of $Pd(acac)_2$ Supported on TiO_2

Following exposure of $Pd(acac)_2$ supported on titania to NO for 20 minutes, the sample was exposed to 1 atmosphere of CO for 2 hours at room temperature, at a flow rate of 5ml/min. The reaction was conducted *in situ*, and is illustrated in figure 6.14.

After 1 hour, there is the development of a weak band at 1970cm^{-1}, which is attributed to a two-fold bridging palladium carbonyl species. There is a slight attenuation of the Pd-NO^- peak at 1718cm^{-1} and a shift to 1724cm^{-1}. There is very little change in the acac region of the spectrum, with a slight intensification of the peak at 1377cm^{-1}. After a further hour of exposure to CO, there is a slight intensification of the peak at 1970cm^{-1} and attenuation of the peak at 1723cm^{-1}, which shifts again to 1728cm^{-1}. These findings can be rationalised by the conclusion that a slow or partial substitution reaction takes place between the Pd-NO^- and Pd_2-CO species. The role of the acac ligand in this reaction is not yet understood. The results obtained suggest that the Pd-NO^- species is easily formed and is chemically stable.

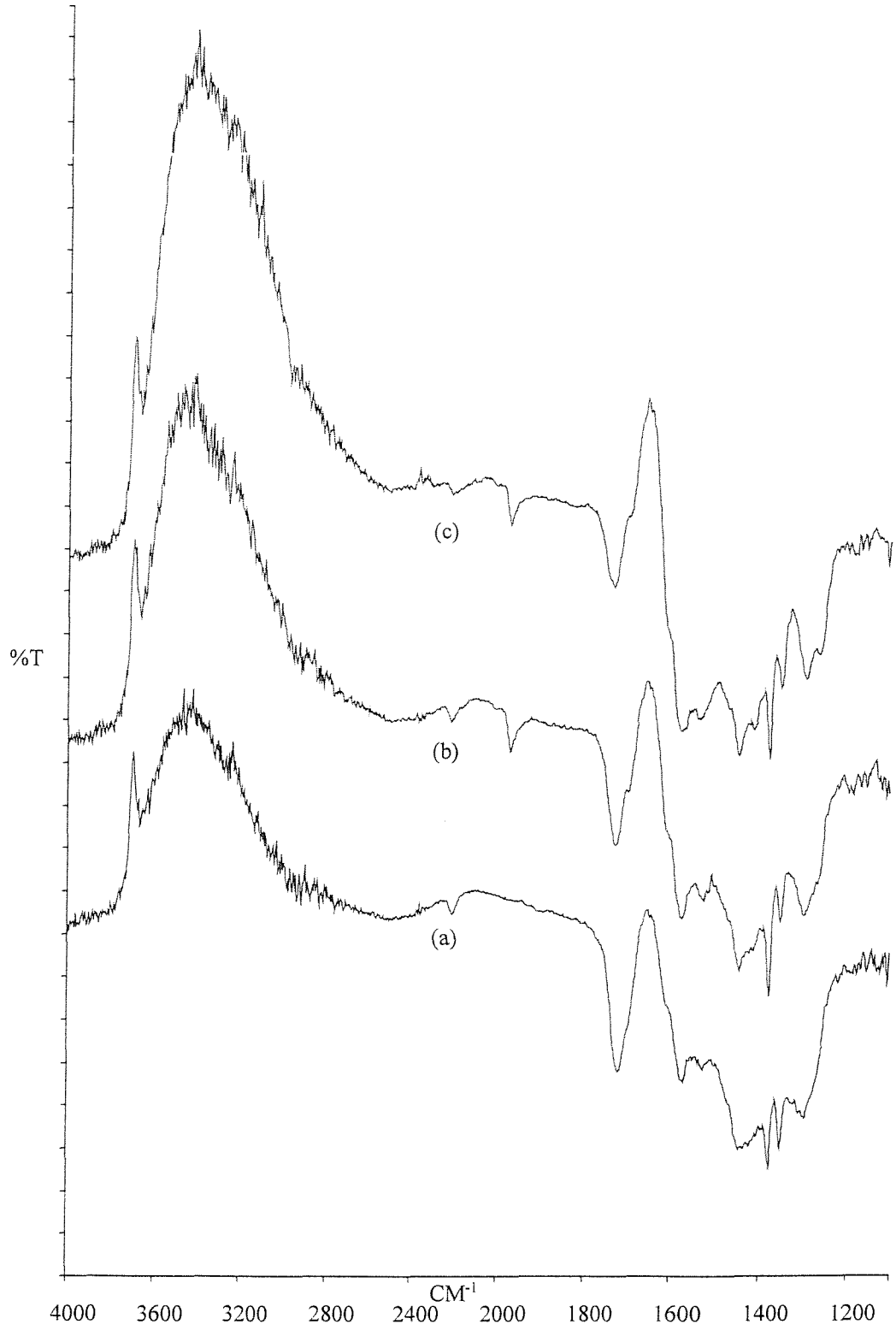

Figure 6.14 DRIFTS difference spectra of $Pd(acac)_2$ supported on TiO_2: (a) After exposure to NO for 30 mins, (b) After exposure to CO for 1 hour, (c) After exposure to CO for 2 hours.

6.8 Conclusions

DRIFTS and EXAFS spectroscopy indicate that the MOCVD of $Pd(acac)_2$ onto partially dehydroxylated TiO_2 results in the organometallic being adsorbed intact, with the consumption of surface hydroxyl groups upon adsorption. The thermolysis of the supported organometallic under an inert atmosphere results in removal of the acac ligands by 330°C, though the process of reduction begins at around 150°C. The mechanism of the removal of the ligands is not understood, though temperature programmed desorption and energy dispersive EXAFS spectroscopy may offer some clues to this. EXAFS spectroscopy indicates the formation of small rhodium clusters occurs by 200°C during the thermolysis experiment. Re-exposure to CO after thermolysis results in the formation of linear and bridging carbonyl species, evidenced by DRIFTS spectroscopy. The results of thermolysis under a hydrogen atmosphere result in total removal of the acac ligands by 220°C, evidenced by DRIFTS and EXAFS spectroscopy. EXAFS indicates the formation of small rhodium clusters at this temperature. DRIFTS, again indicates regeneration of linear and bridging carbonyl species upon exposure to CO, post thermolysis. Exposure to NO at room temperature resulted in the formation of a $Pd(NO)^{\cdot}$ species. The coordination of the acac ligand was observed to change, though the bonding to the palladium is not understood. EXAFS spectroscopy would assist in understanding the nature of the reaction with NO. Re-exposure to CO results in a very small development of a bridging carbonyl species, though the NO and acac regions are hardly attenuated by the exposure to CO.

6.9 Experimental

$Pd(acac)_2$ was purchased from Aldrich. It exists as a yellow powder and is characterised by infrared spectroscopy (figure 6.1 and table 6.1).

Preparation of the surface supported organometallic species for DRIFTS and EXAFS studies, by MOCVD involves deposition of $Pd(acac)_2$ (80mg) onto partially

dehydroxylated titania (Degussa 0.5g), according to the general procedure given in section 2.7. Heating the organometallic sample to 70°C for 3 hours caused sublimation, resulting in the titania becoming a yellow colour.

6.10 References

1. F. D. Lewis, G. D. Salvi, D. R. Kanis and M. A. Ratner, *Inorg. Chem.*, 1993, **32**, 1251-1258
2. A. N. Knyazena, E. A. Shugam and L. M. Schkolnikova, *Zh. Struct. Khim.*, 1970, **11**, 938.
3. T. Mandai, T. Matsumoto, M. Kawada and J. Tsuji, *Tetraherdron Letters*, 1993, **34**, 2161-2164.
4. V. S. Tkach, G. Myagmarsuran, M. Mesyef and F. K. Schmidt, *Reaction Kin. Cat. Lett.*, 1999, **66**, 281-287.
5. A. J. Renouprez, J. F. Trillat, B. Moraweck, J. Massardier and G. Bergerat, *J. Catal.*, 1998, **179**, 390-399.
6. C. Methiveir, B. Benguin, M. Brun, J. Massardier and J. C. Bertolini, *J. Catal.*, 1998, **173**, 374-382.
7. M. Kita and M. Nonoyama, *Polyhedron*, 1993, **12**, 1027-1030.
8. C. Neyertz and M. Volpe, *Colloids and Surfaces*, 1997, **136**, 136-139.
9. S. Kohler, M. Reiche, C. Frobel and M. Baerns, *Prep. Catalysts*, 1995, 1009-1016.
10. N. Krishankutty, J. Li and M. A. Vannice, *Applied Cat. A. General*, 1998, **173**, 137-144.
11. A. Wali, S. M. Pillai, V. Kaushik, S. Satish, *Applied Cat. A. General*, 1996, **135**, 83-93.
12. C. Dossi, R. Psaro, A. Fusi, S. Recchia, V. D. Santo and L. Sordelli, *Thermochimica Acta*, 1998, **317**, 157-164.
13. N. A. Williams, PhD Thesis, University of Southampton, 1992
14. D. W. Adams and D. W. Trumble, *J. Chem. Soc. Dalton Trans.*, 1974, 690.
15. C. J. Rudkin, PhD Thesis, University of Southampton, 1997.
16. J. Evans, B. E. Hayden and G. Lu, , *J. Chem. Soc. Farad. Trans.*, 1996, **92**, 2963
17. H. Arai and H. Tominaga, *J. Catal.*, 1976, **43**, 131.

Chapter 7

The Surface Organometallic Chemistry of Rh(sulphos)(cod) and Rh(sulphos)$(CO)_2$ Supported on Silica

7.1 Introduction

Organometallic compounds have been widely studied in order to prepare metal sites with well defined composition on inorganic supports and to elucidate catalytic reaction mechanisms at a molecular level.

The surface chemistry of rhodium has been deeply investigated[1], however the reactivity of isolated Rh(I) surface sites during catalytic conditions is still an open question[2].

The new ligand $NaO_3S(C_6H_4)CH_2C(CH_2\text{-}PPh_2)_3$(sulphos) has been synthesised by Bianchini *et al*[3]. The application of zwitterionic Rh(I) complexes Rh(sulphos)(cod) and Rh(sulphos)$(CO)_2$ in liquid biphasic catalysis has been demonstrated for the hydrogenation of styrene and the hydroformylation of 1-hexene respectively[3]. The latter reaction gives C_7 alcohols in an alcohol/hydrocarbon system and C_7 aldehydes in an alcohol-water/hydrocarbon system. All rhodium is recovered in the polar phase at the end of the catalytic reactions. Rh(sulphos)(cod) is also an efficient liquid-biphase catalyst precursor for the hydrogenation and hydrogenolysis of benzo[b]thiophene to 2,3-dihydrobenzothiophene and 2-ethylthiophenol, respectively[4]. In all these biphasic reactions, the rhodium complexes remain in the polar phase. The catalyst recycling and/or separation for eventual reactivation procedures, however, require a tedious and somewhat demanding manipulation under an inert atmosphere.

Sulphos makes its metal complexes exclusively soluble in light alcohols, which have very low miscibility in hydrocarbons at room temperature. This ligand offers the advantage of a low steric hindrance on the donor atoms giving stable complexes with many transition metals in different oxidation states. The hydrophilic sulphonated tail, other than making the complex soluble in polar solvents, offers the possibility of grafting the complex onto an inorganic support. The heterogenisation of Rh(sulphos)(cod) and Rh(sulphos)$(CO)_2$ is anticipated as a viable technique to

facilitate the recycling of the expensive Rh catalysts as well as widen their range of application to catalysis.

It is hypothesised that the organometallic precursors can be grafted onto high surface area silica with an immobilisation procedure based uniquely on the capability of the sulphonate tail of the sulphos to link the silanol groups of the support via hydrogen bonding. Catalysts obtained by this technique are denoted supported hydrogen bonded (SHB) catalysts. A similar heterogenisation strategy has previously been employed for the preparation of supported transition metal oxide catalysts as well as supported aqueous phase (SAP) catalysts[5]. These latter, however, involve the immobilisation of water-soluble complexes into a thin surface water film[6].

This study comprises of EXAFS and ^{31}P CP-MAS NMR experiments on various rhodium organometallic compounds, both as pure compounds and supported species. Particular attention is paid to Rh(sulphos)(cod) grafted to silica and various associated gas reactions.

EXAFS experiments were conducted at Station 9.2 at the SRS, Daresbury. All spectra were recorded at the Rh K-edge. All pure organometallic samples were ground up with boron nitride prior to recording the spectra, in order to give a metal content in them of approximately 10%. The silica supported organometallic samples were loaded 'neat' into the EXAFS cell, as the metal loading was approximately 5%. Three scans were acquired for each sample to improve the signal to noise ratio of the acquired data. On all the plots displayed, the EXAFS is k^3 weighted. Solid lines represent experimental data, while the dashed lines show the phaseshift corrected theoretical model.

Solid State NMR experiments were recorded at room temperature on a Bruker AM 300 spectrometer equipped with a 4mm BB-CP MAS probe working at a frequency of 121.50MHz at the both at the University of Southampton, and the University of Milan, in Italy.

7.2 EXAFS Study of Rhodium Foil

Figure 7.1 shows the EXAFS and Fourier transform and derived structural parameters for rhodium foil obtained by scanning EXAFS on Station 9.2 at Daresbury laboratory. Two scans of the foil were acquired and then averaged to improve the signal to noise ratio. The bond lengths obtained for rhodium metal by X-ray crystallography are also shown. The spectrum shows coordination numbers expected for an FCC structure, up to the fifth shell, which shows a coordination of 12 rather than the expected fifth shell value of 24. It is only with the fourth coordination shell that the bond length shows any appreciable disagreement with the X-ray value. The inclusion of multiple scattering had no effect on the quality of the fit of the data to the proposed model. Crystallographic values were obtained from the CDS database using CCDL.

7.3 $RhCl(PPh_3)_3$; Wilkinson's Catalyst

An XAS spectrum of Wilkinson's catalyst, $RhCl(PPh_3)_3$, was acquired to provide a standard approximation for distances from a rhodium centre bonded to three triphenylphosphine groups, which are characteristic of the systems under investigation in this study.

The Fourier transform of the EXAFS spectrum shown in figure 7.2 indicates the presence of three coordination shells, two of which have low intensity. The first shell is fitted to both the Rh-P and Rh-Cl ligand groups. The Rh-P and Rh-Cl bond lengths are in close agreement with the crystal structure data[7,8,9,10]. The second and third Fourier transform shells are fitted to carbon atoms from the phosphine phenyl groups. The number of carbon atoms quoted is the 'best fit' value, whereby the coordination number was refined and validated with reference to the crystal structure.

Figure 7.1 Rh K-Edge EXAFS and Fourier transform for rhodium foil. (Solid lines show actual spectra, dotted lines show theoretical spectra)

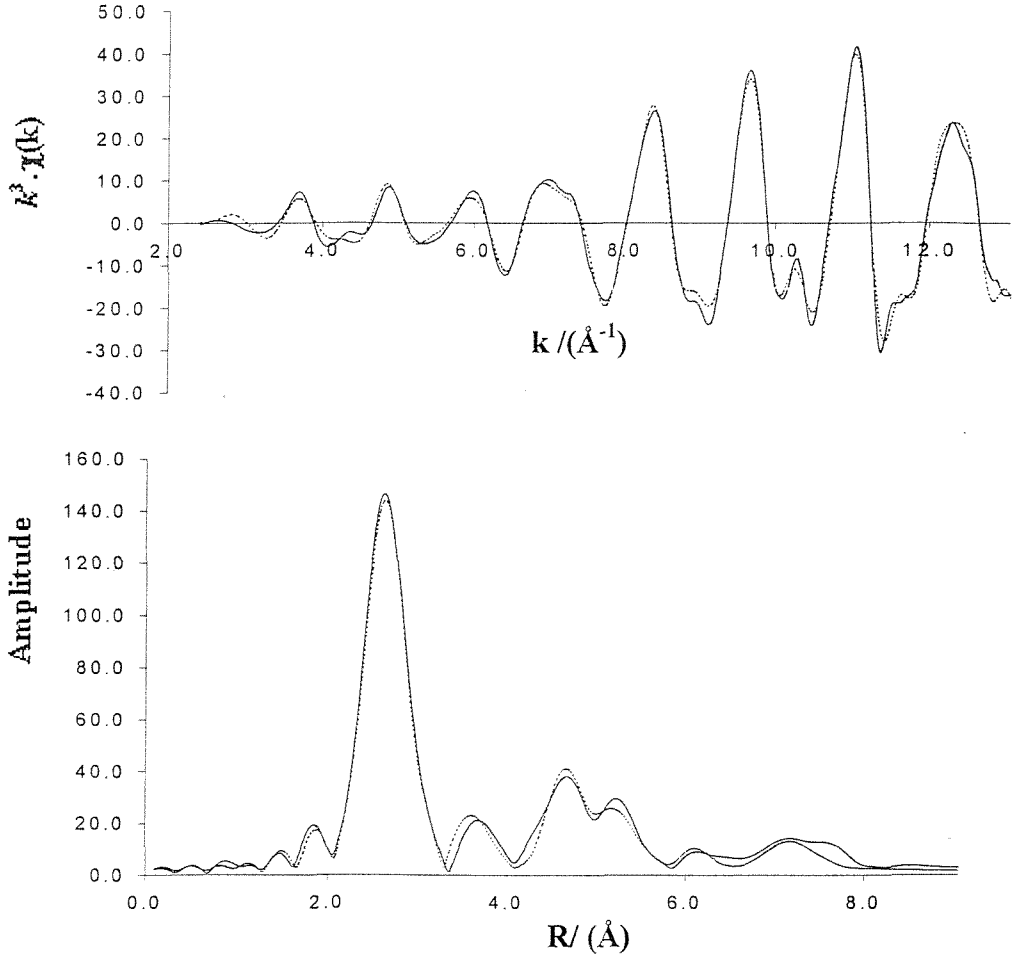

Atom	C.N.	r/Å	X-Ray Bond Length / Å	$2\sigma^2$ / Å^2 (D.W)
Rh	12	2.676(1)	2.69	0.007(1)
Rh	6	3.784(4)	3.80	0.011(1)
Rh	24	4.652(3)	4.66	0.012(1)
Rh	12	5.262(3)	5.38	0.004(1)
Rh	24	5.999(9)	6.01	0.019(2)
Rh	12	7.157(4)	7.17	0.001(1)

R= 15.93%

Ef= 1.57 eV

Figure 7.2 Rh K-Edge EXAFS and Fourier transform for Wilkinson's catalyst. $RhCl(PPh_3)_3$

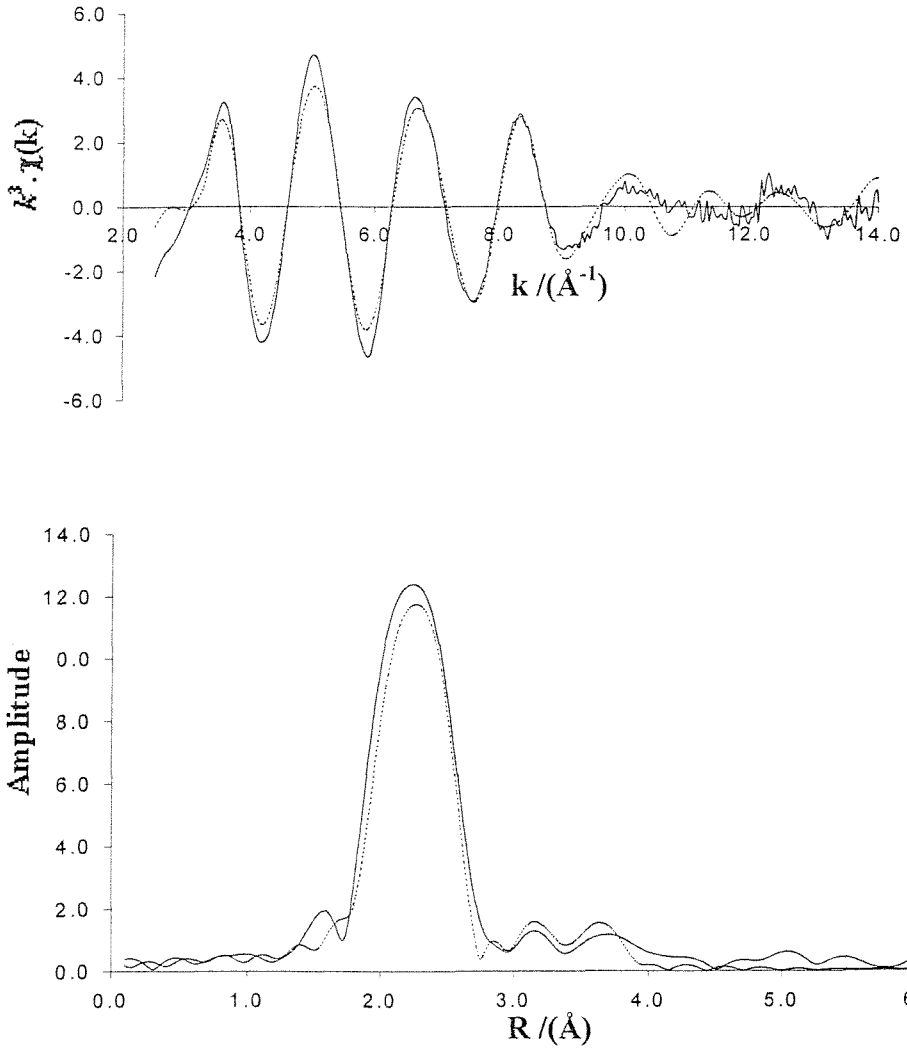

Atom	C.N.	r/Å	X-Ray Bond Length / Å	$2\sigma^2$ / Å^2
P	3	2.262(2)	2.310	0.007(4)
Cl	1	2.366(2)	2.377	0.001(4)
C	4	3.322(1)	≈3.300	0.015(3)
C	5	3.654(2)	≈3.650	0.022(5)

R= 23.73%

Ef= 0.04 eV.

7.4 $[RhCl(cod)]_2$

An XAS spectrum of this organometallic was acquired to provide a reference for the distances of the carbon atoms in the (cod) group from the rhodium centre in a system similar to those being investigated. The crystal structure is well established and distances can be compared to those obtained in the XAS experiment.

Figure 7.3 indicates that there are four coordination shells in the Fourier transform, the first two of much greater intensity than the last two. The first shell is fitted to the first four carbon atoms of the cyclo-octadiene (cod) group at 2.11Å. The second shell is fitted to the two bridging chlorine atoms at 2.40Å. The second equidistant group of four carbons from the (cod) group, account for the third shell at 3.05Å. Further afield is the other rhodium atom from this dimeric compound. The Fourier transform peak is observable at about 3.52Å. The data obtained agree well with the crystal data obtained for this molecule[11,12,13].

7.5 Rh(sulphos)(cod)

7.5.1 EXAFS Study of Rh(sulphos)(cod)

An XAS spectrum of Rh(sulphos)(cod) was acquired in order to provide a comparison with that of the silica supported species.

Figure 7.4 indicates that the main peak in the Fourier transform comprises of four equidistant carbon atoms from the (cod) group and the three phosphorus atoms. The carbon atoms of the (cod) group are about 0.2Å further away from the Rh than in $[RhCl(cod)]_2$, consistent with the greater *trans* influence of the P donors as compared with μ-Cl as well as the fact that, in the zwitterionic complex, the positive charge is localised on the Rh atom. The phosphorus atoms are the only atoms from the sulphos group, which can clearly be assigned. The Rh-P distances are quite consistent with those (2.367Å) obtained by X-ray methods for $[Rh(tripod)(cod)]BPh_4$ where tripod is

Figure 7.3 Rh K-Edge EXAFS and Fourier transform for $[RhCl(cod)]_2$

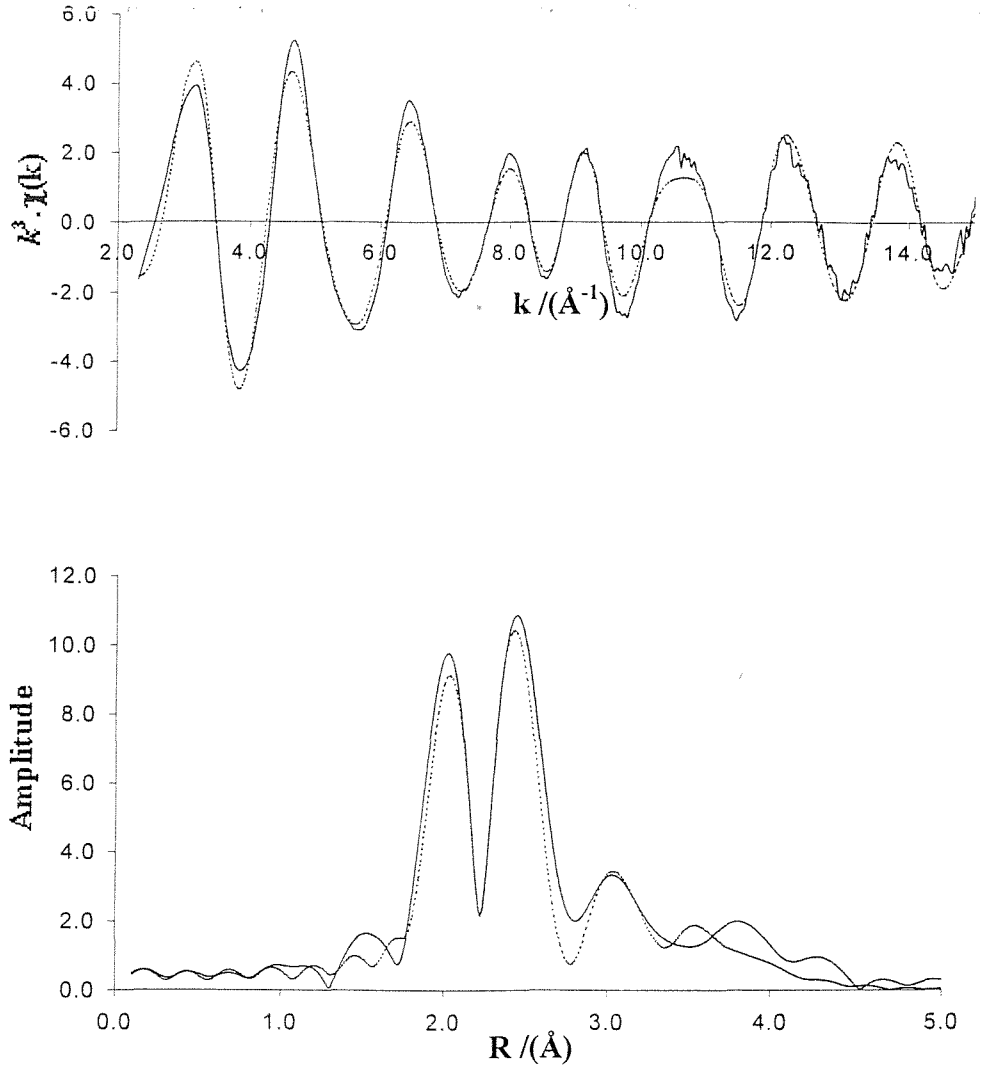

Atom	C.N.	r/Å	X-Ray Bond Length / Å	$2\sigma^2$ / Å^2
C	4	2.105(1)	2.106	0.006(2)
Cl	2	2.403(1)	2.399	0.008(2)
C	4	3.049(4)	3.051	0.010(9)
Rh	1	3.516(5)	3.509	0.014(9)

R= 19.25%

Ef= -2.20 eV

Figure 7.4 Rh K-Edge EXAFS and Fourier transform for Rh(sulphos)(cod)

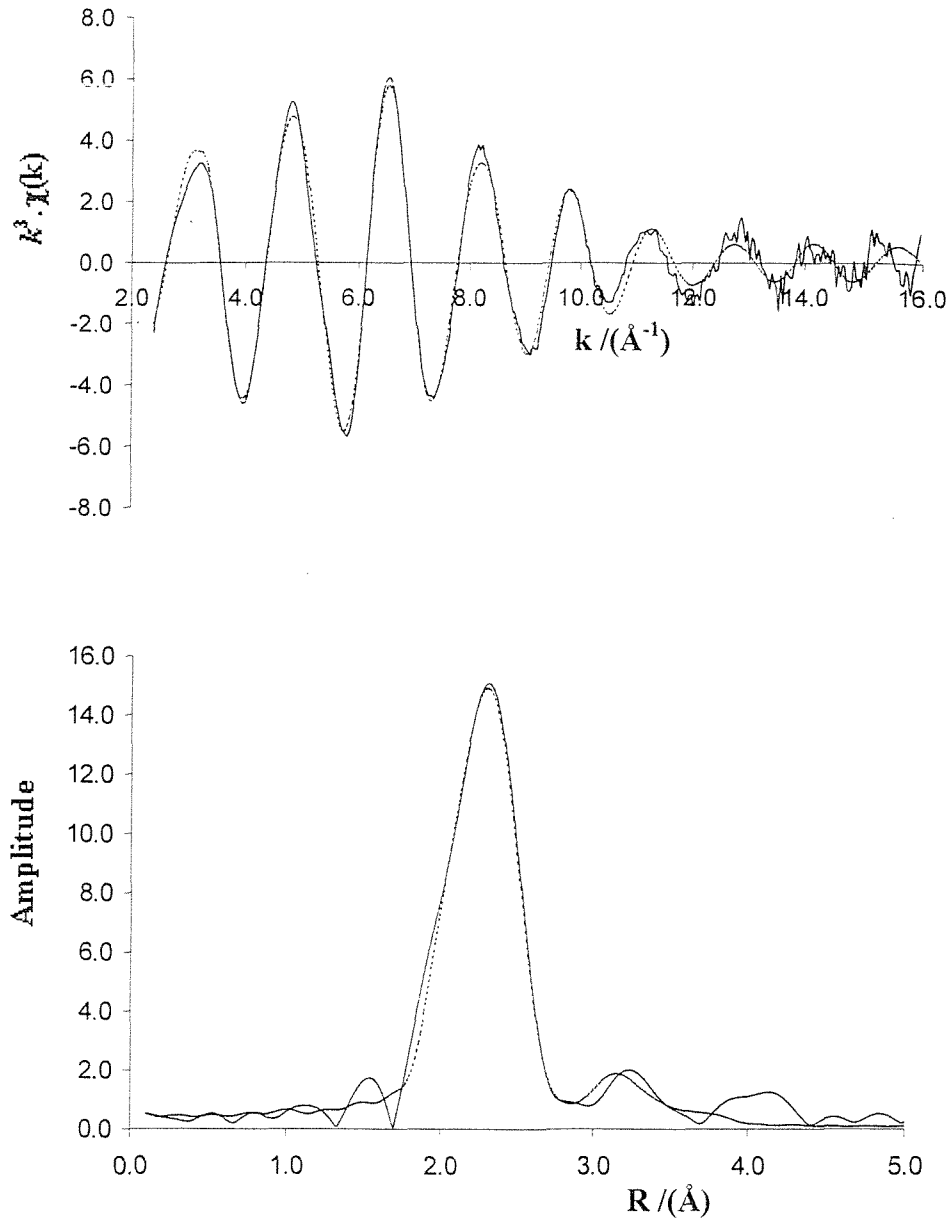

Atom	C.N.	r/Å	$2\sigma^2$ / Å^2
C	4	2.135	0.011
P	3	2.363	0.010
C	4	3.141	0.021
C	5	3.561	0.018

R= 18.27%

Ef= 1.17 eV

the tripodal ligand $PhCH_2C(CH_2PPh_2)_3$, differing from sulphos only for having a benzyl substituent in place of the sulphonated-benzylic tail[14]. It is possible to assign variable numbers of carbon atoms from the phenyl groups. The number of phenyl carbons which gave the best fit whilst having a sensible Debye-Waller factor was five. No single crystal data is available for this compound. The molecule Rh(sulphos)(cod) is illustrated below:

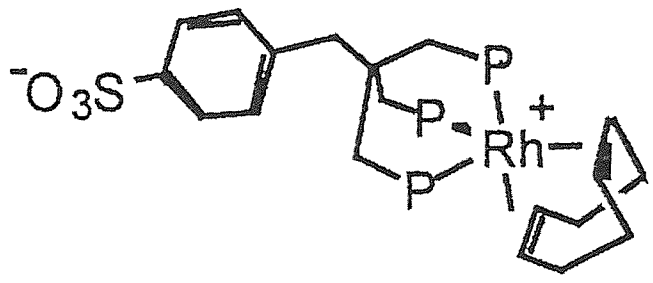

Figure 7.5 Rh(sulphos)(cod)

7.5.2 Solid State NMR Study of Rh(sulphos)(cod)

A solid state ^{31}P NMR spectrum of Rh(sulphos)(cod) was recorded using the cross polarisation sequence under magic angle spinning at a spinning rate of 10KHz at room temperature. The 90° pulse was 3.9μs and the contact pulse was 1ms. The spectrum was collected after 80 scans using a recycle time of 10s.

The spectrum contains three phosphorus resonances at δ 23.8, 0.5 and –3.5 for an δ_{av} of ca. 6.9 not too far from the solution shift (δ 5.8) given the sensitivity of the ^{31}P shifts to solvent and temperature. Variable temperature solution $^{31}P\{^1H\}$NMR spectra indicate a fast rearrangement between a square pyramidal and trigonal-bipyramidal structure[15]. Due to the geometrical constraints of the tripodal ligand, no five-coordinate metal complex with triphos can assume a perfect square pyramidal or trigonal-bipyramidal structure in the solid state. The complexes invariably adopt more

or less distorted geometries depending on the co-ligands. A distorted trigonal-bipyramidal structure has been determined for the iridium derivative Ir(sulphos)(cod), which has been characterised by X-ray diffraction methods[16]. On the basis of the CP-MAS ^{31}P NMR spectrum, Rh(sulphos)(cod) may be tentatively assigned to a structure closer to a square pyramid than to a trigonal bipyramid. In square pyramidal geometry, the peak at lowest field (δ 23.8) can be assigned to the axial P atom which has no *trans* olefinic ligands.

7.6 Rh(sulphos)$(CO)_2$

An XAS spectrum of Rh(sulphos)$(CO)_2$ was acquired in order to provide a comparison with that of the silica supported species.

There are three characteristic peaks in the Fourier transform of the EXAFS spectrum, shown in figure 7.6. The first is assigned to the two carbon atoms belonging to the carbonyl groups at 1.87Å. The second peak at 2.35Å is assigned to the three phosphorus atoms. The third peak, at 3.00Å, is assigned to the two oxygen atoms of the carbonyl groups. Multiple scattering is employed here to the carbonyl groups, with an optimised bond angle of 180° between the rhodium, carbon and oxygen atoms. Multiple scattering significantly improves the quality of the fit of the data to the Rh(sulphos)$(CO)_2$ model. No single crystal data has been found for this compound. The molecule Rh(sulphos)$(CO)_2$ is illustrated below:

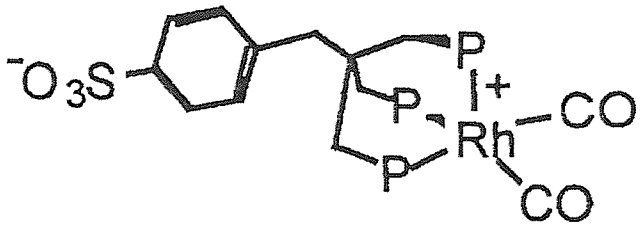

Figure 7.6 Rh(sulphos)$(CO)_2$

Figure 7.7 Rh K_Edge EXAFS and Fourier transform for Rh(sulphos)$(CO)_2$

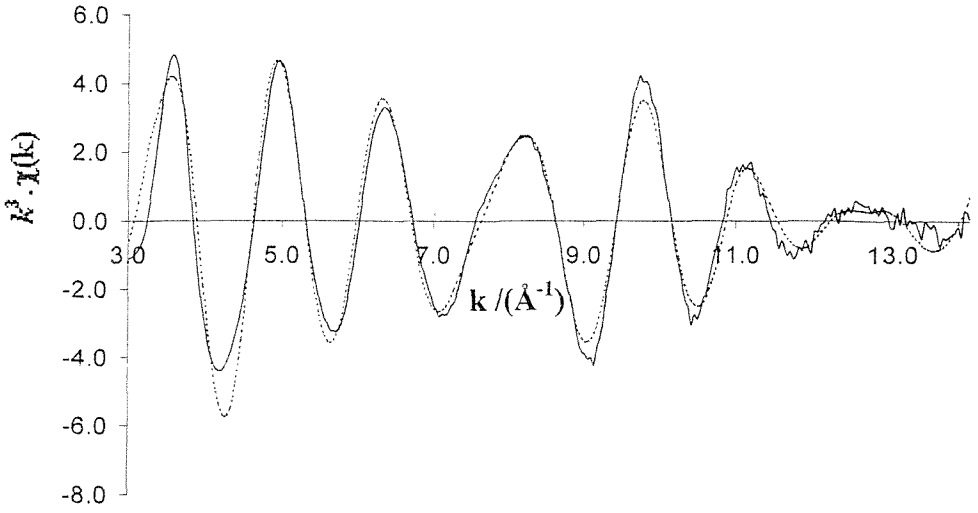

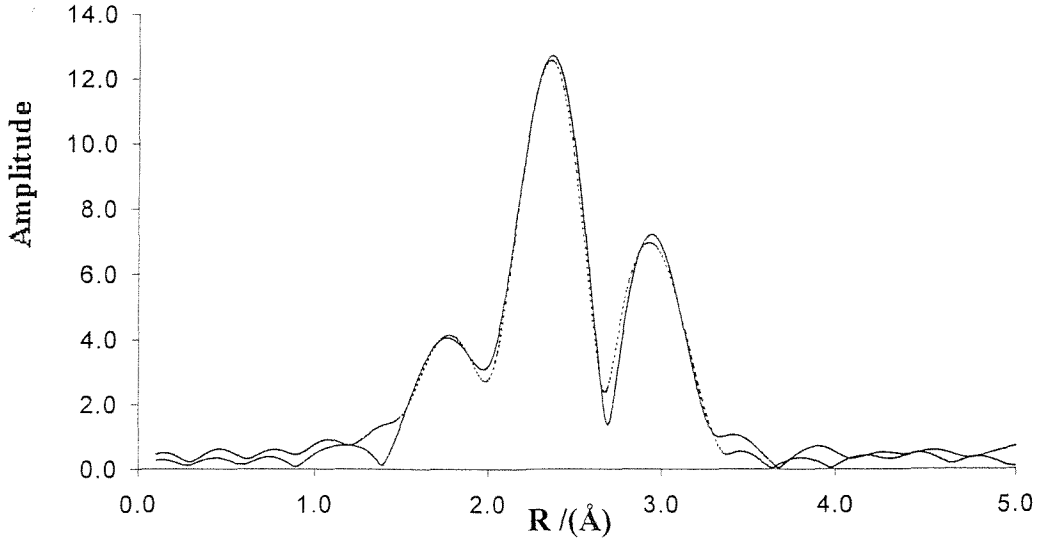

Atom	C.N.	r/Å	$2\sigma^2$ / Å^2
C	2	1.867(2)	0.013(3)
P	3	2.351(2)	0.010(4)
O	2	2.995(4)	0.010(4)

R= 18.28%

Ef= 0.75 eV

7.7 Rh(sulphos)(cod) on silica

7.7.1 EXAFS study of Rh(sulphos)(cod) on silica

The appearance of the Fourier transform of the EXAFS spectrum of this sample, shown in figure 7.8, is very similar in appearance to that of the unsupported sample. Only two shells of atoms are detectable here, which coalesce into one peak in the Fourier transform. Four equidistant carbon (cod) atoms are observable at 2.08Å, as are three phosphorus atoms at 2.28Å. Both bond lengths from the rhodium to these ligands are shortened by approximately 0.07Å. This is possibly related to the bonding of the organometallic to the surface. It is expected that the organometallic bonds to the surface via the sulphos SO_3^- group with abstraction of a proton from an OH group on the silica surface. Indeed, it is generally agreed that the hydrogen bonding of the hydrated sodium sulphonate groups to the OH groups present at the surface of silica is responsible for the immobilisation of triphenylphosphine trisulphonate complexes[17]. This idea is supported by the fact that the EXAFS of the supported system is almost identical to that of the pure organometallic, indicating little or no modification to the electronic environment of the rhodium atom.

7.7.2 Solid state NMR study of Rh(sulphos)(cod) on silica

The CP MAS ^{31}P NMR spectrum of Rh(sulphos)(cod) supported on silica consists of two signals centered at δ 23.7 and -2.1. The asymmetric profile of the latter peak indicates that different types of phosphorus may be present.

Despite the expected shift dispersion and line broadening as compared to the unsupported sample, the spectra of the unsupported and supported sample are substantially similar and thus consistent with the immobilisation of the (cod) complex on the silica through a functional group away from the coodination sphere.

Figure 7.8 Rh K-Edge EXAFS and Fourier transform for Rh(sulphos)(cod) supported on silica

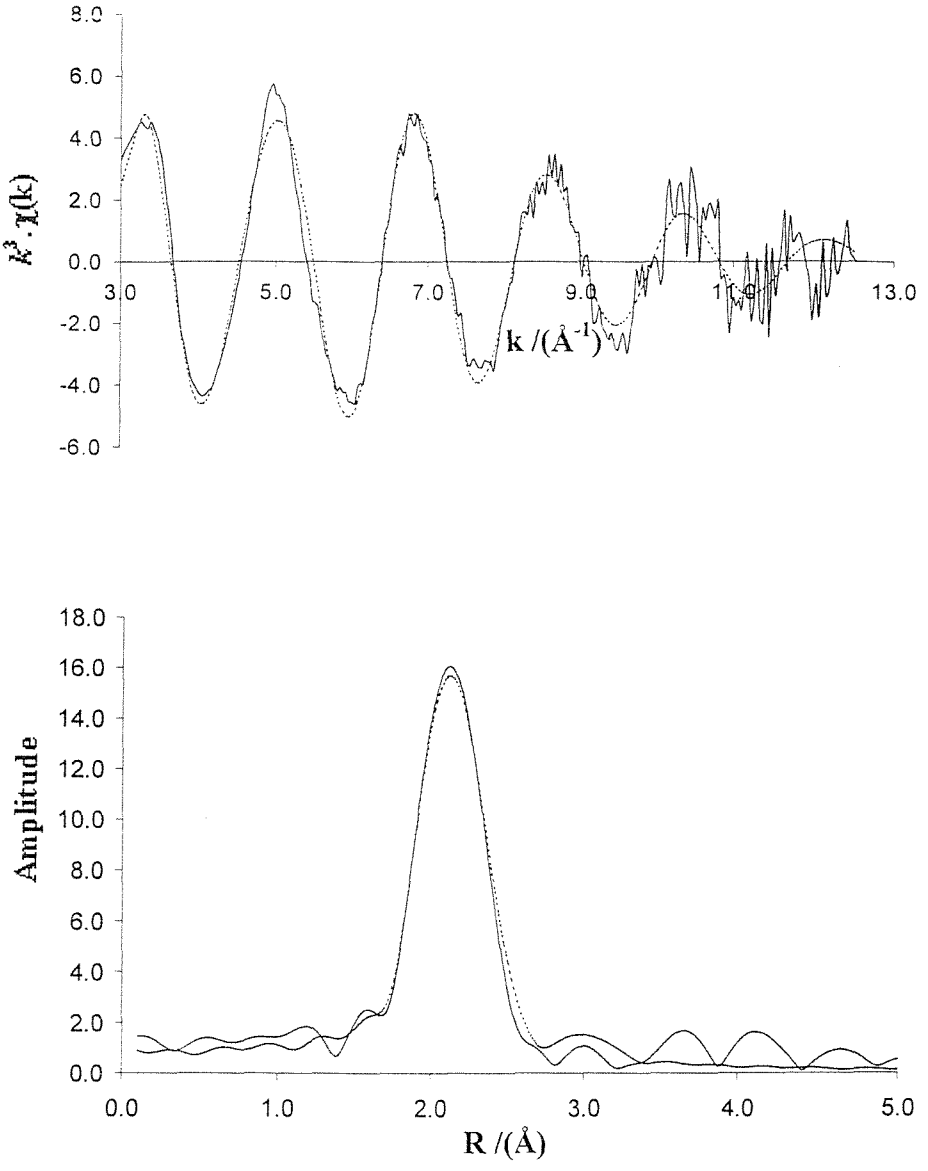

Atom	C.N.	r/Å	$2\sigma^2$ / Å^2
C	4	2.077(5)	0.009(8)
P	3	2.278(5)	0.019(1)

R= 23.06%

Ef= 5.42 eV

7.8 Rh(sulphos)(cod) on silica after reduction in H_2 at 120°C

It was anticipated that exposure of the silica supported Rh(sulphos)(cod) to one atmosphere of hydrogen at 120°C for one hour may cause substitution of the cod ligand for two monohydride ligands, and a single dihydrogen ligand. This should lead to a noticeable change in the shape of the EXAFS spectrum, as there would be a significant change in the nature of the backscattering atoms present. However, the spectrum here, shown in figure 7.9 is almost identical to the previous unreduced sample. Various fits to the data were attempted, resulting in the conclusion that the sample was unchanged after being exposed to hydrogen for an hour at 120°C.

7.9 Rh(sulphos)(cod) on silica after reaction with C_2H_4:CO: H_2

A sample of Rh(sulphos)(cod) reduced in hydrogen at 120°C, was exposed to a 1:1:1 mixture of C_2H_4, CO and H_2 at room temperature, each gas having a partial pressure of 1 bar. It was hoped that the reduced supported organometallic would catalyse the insertion of CO into C_2H_4 to produce the aldehyde, propanal, C_3H_6O. However, the EXAFS spectra and Fourier transform, shown in figure 7.10, show no change from the initial supported organometallic. The assigned structure to the spectrum acquired was that of the supported organometallic, Rh(sulphos)(cod). It was anticipated that the hydrogen exposure at 120°C would result in substitution with the (cod) ligand. The resulting hydride was hoped to catalyse the insertion reaction, to produce the aldehyde. It seems that the failure of the reduction step resulted in an unchanged and unreactive organometallic.

Figure 7.9 Rh K-Edge EXAFS and Fourier transform for Rh(sulphos)(cod) supported on silica after reduction in hydrogen at 120°C

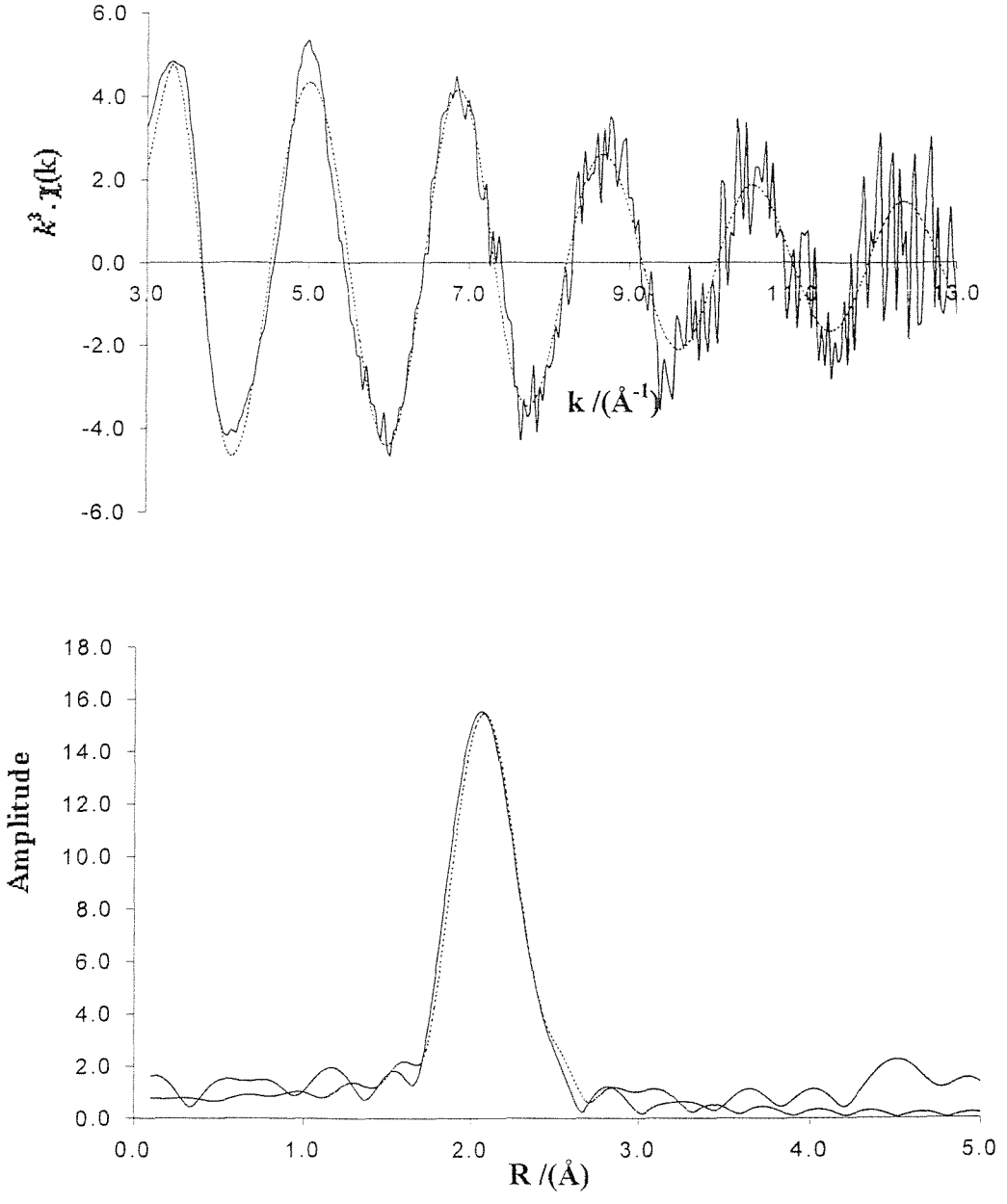

Atom	C.N.	r/Å	$2\sigma^2$ / Å^2
C	4	2.067(3)	0.005(2)
P	3	2.275(9)	0.029(5)

R= 30.99%

Ef= 5.50 eV

Figure 7.10 Rh K-Edge EXAFS and Fourier transform for Rh(sulphos)(cod) supported on silica after reaction with C_2H_4: CO and H_2

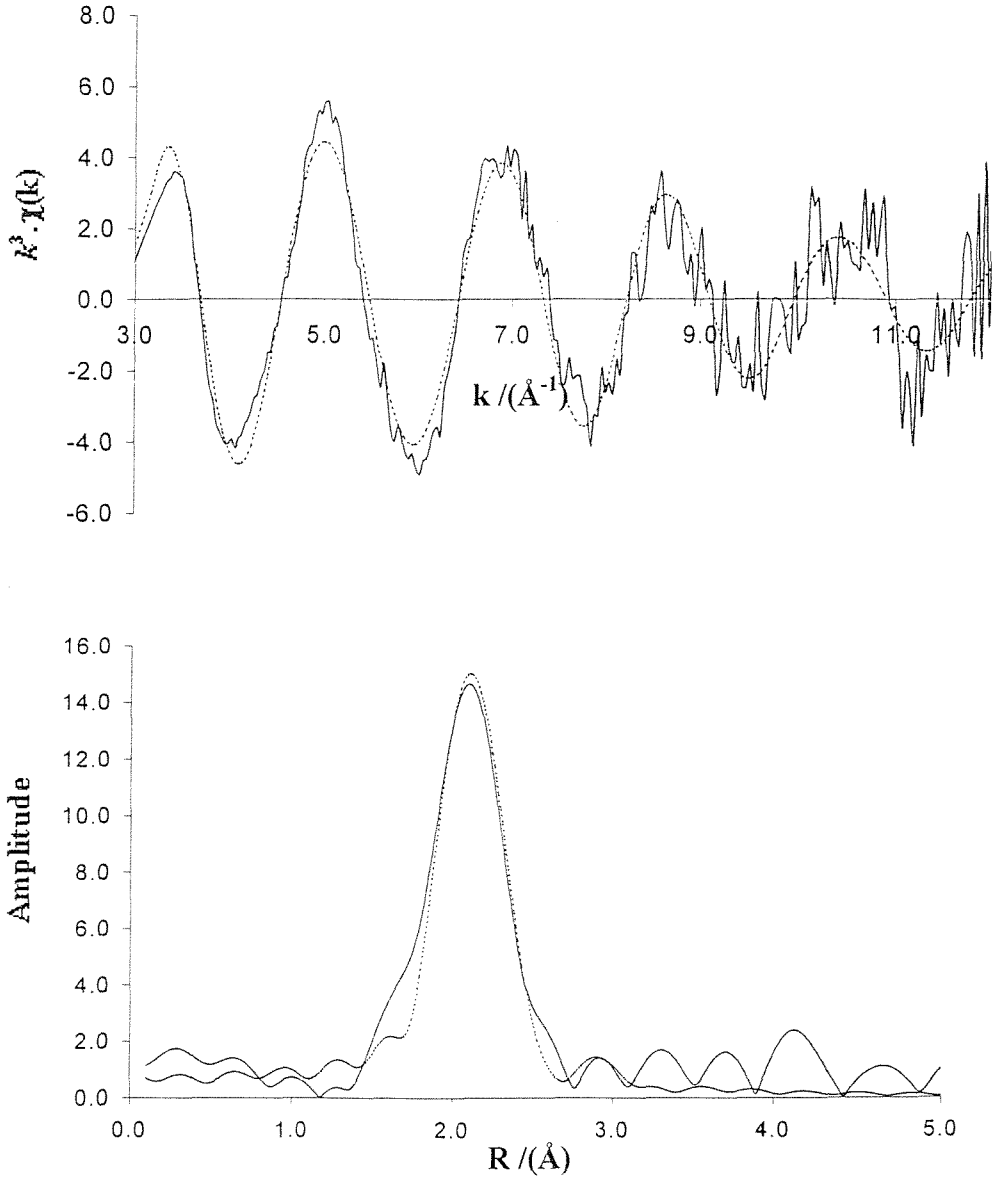

Atom	C.N.	r/Å	$2\sigma^2$ / Å^2
C	4	2.081(5)	0.006(1)
P	3	2.258(9)	0.028(3)

R= 37.59%

Ef= 5.40 eV

7.10 Rh(sulphos)(cod) on silica after reaction with CO

This sample was reduced in a hydrogen atmosphere at 120°C before being exposed to CO at room temperature for one hour. Exposure to hydrogen for one hour at 120°C was expected to result in substitution of the cod ligands for two monohydride ligands. It was anticipated that exposure to CO would result in substitution of the monohydride ligands for two carbonyl ligands. Again, as in the previous case, the EXAFS spectrum and Fourier transform, shown in figure 7.11, indicates that the silica supported Rh(sulphos)(cod) remains unchanged. The failure of any reaction with CO is probably due to the failure of the reduction under hydrogen step of the reaction.

7.11 Rh(sulphos)(cod) on silica- sample 2

A spectrum of a second sample of Rh(sulphos)(cod) was acquired prior to a series of reactions, to confirm the nature of the surface supported species. The EXAFS spectrum and Fourier transform shown in figure 7.12, agrees well with the first sample of silica supported Rh(sulphos)(cod). Again only two shells of atoms are detectable, which coalesce into one peak in the Fourier transform. Four equidistant carbon atoms from the (cod) group are observable at 2.08Å, as are three phosphorus atoms at 2.28Å. Both bond lengths from the rhodium to these ligands are shortened by approximately 0.07Å. This is probably related to the bonding of the organometallic to the surface, which is discussed in section 7.7.1.

7.12 Rh(sulphos)(cod) on silica after reduction in H_2

Contrary to the previous hydrogen reduction experiment, the Fourier transform of the EXAFS spectrum (figure 7.13) shows a very different shape to that of the supported organometallic prior to reduction. The (cod) ligand appears to have disappeared and has probably been replaced by a hydride species. Other spectroscopic

Figure 7.11 Rh K-Edge EXAFS and Fourier transform for Rh(sulphos)(cod) supported on silica after reduction and exposure to CO at room temperature

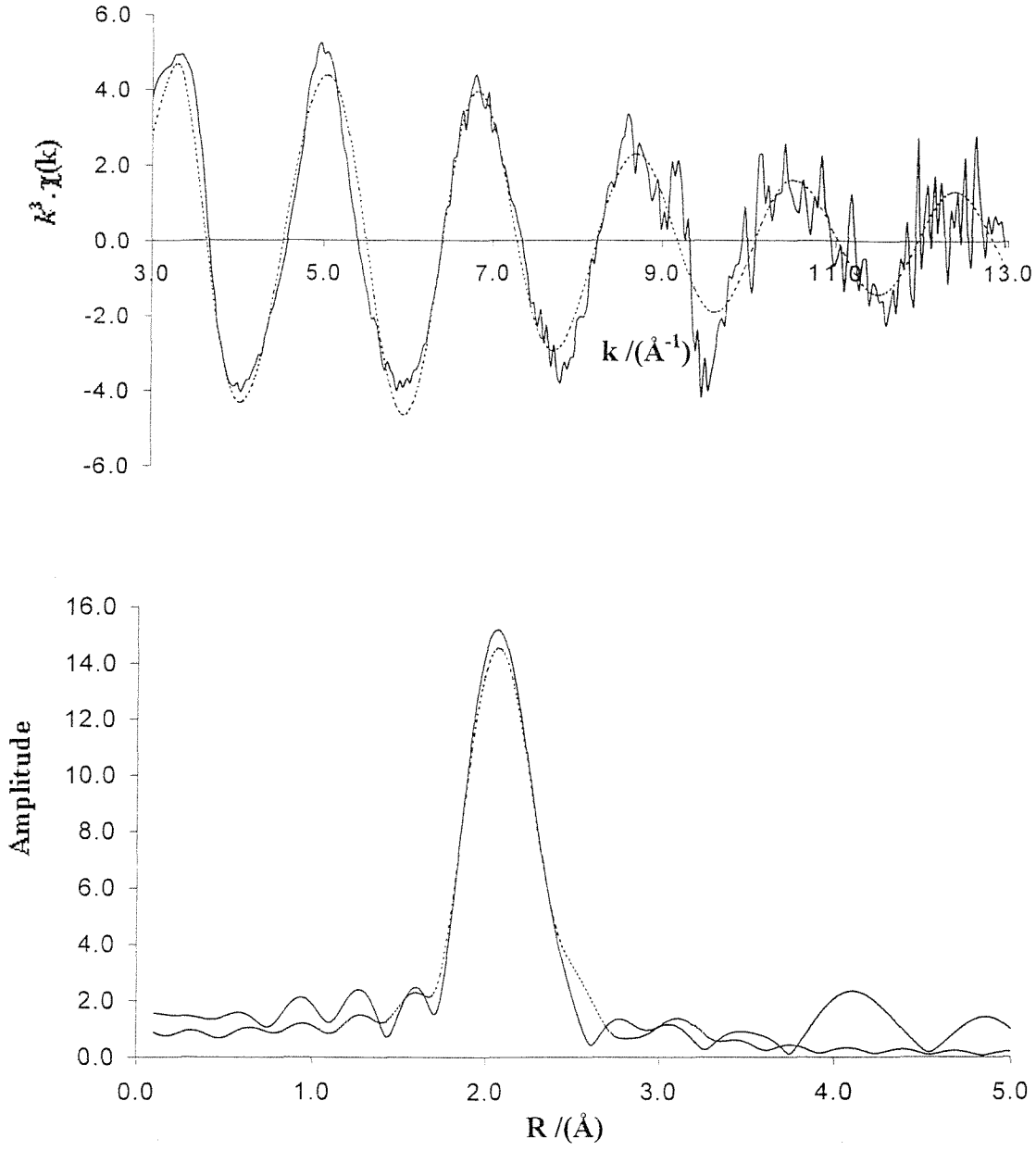

Atom	C.N.	r/A	$2\sigma^2$ / A^2
C	4	2.064(3)	0.006(5)
P	3	2.287(8)	0.030(2)

R= 29.04%

Ef= 5.65 eV

Figure 7.12 Rh K-Edge EXAFS and Fourier transform for Rh(sulphos)(cod) supported on silica

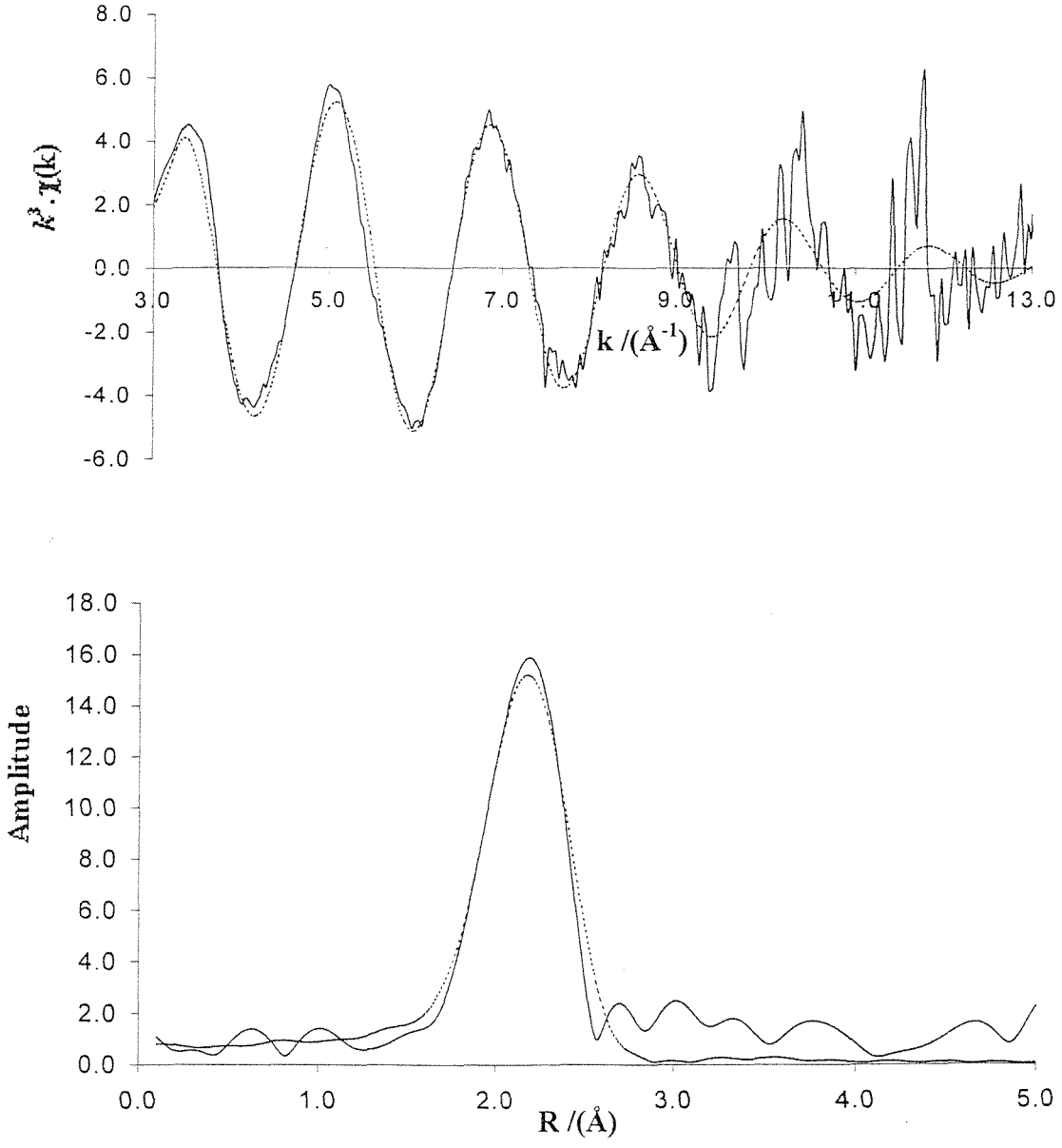

Atom	C.N.	r/A	$2\sigma^2$ / A^2
C	4	2.059(1)	0.017(1)
P	3	2.265(6)	0.014(3)

R= 31.26%

Ef= 7.23 eV

Figure 7.13 Rh K-Edge EXAFS and Fourier transform for Rh(sulphos)(cod) supported on silica after reduction in hydrogen

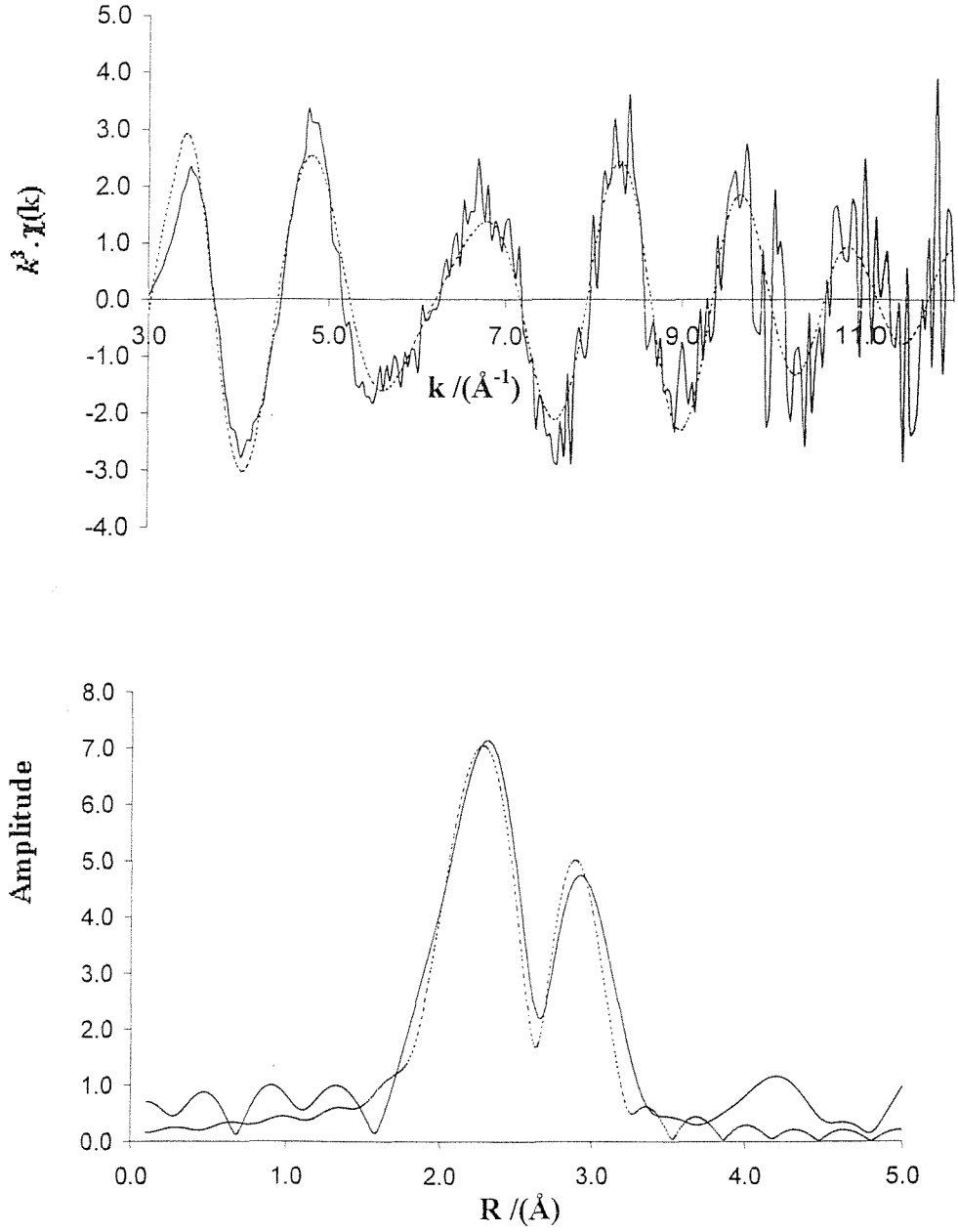

Atom	C.N.	r/Å	$2\sigma^2$ / Å^2
P	3	2.343(5)	0.021(1)
C	4	2.907(5)	0.007(2)

R= 47.15%

Ef= -5.21 eV

techniques would be required to clarify this as EXAFS is incapable of identifying hydrogen due to its low electron density. The three phosphorus atoms are clearly evident at a slightly greater radius than previously, which may be due to the substitution of the (cod) ligand for groups with greater *trans* influence such as hydride ligands. The other peak in the spectrum has been attributed to carbon from the phenyl groups adjacent to the phosphorus atoms.

7.13 Rh(sulphos)(cod) on silica after reaction with C_2H_4: H_2

A sample of Rh(sulphos)(cod) reduced in hydrogen at 120°C, was exposed to a 1:1 mixture of C_2H_4 and H_2 at room temperature, each gas having a partial pressure of 1 bar. It was hoped that the reduced supported organometallic would catalyse the hydrogenation of C_2H_4 to produce ethane, C_2H_6. The XAS was recorded after the reaction had proceeded, and the EXAFS and Fourier transform, shown in figure 7.14, indicates that a variety of C_nH_n ligands are bound to the rhodium atom, while the phosphorus atoms from the sulphos ligand remain unchanged. On the basis of their distances to rhodium, the carbon atoms are tentatively assigned to both alkyl and alkene species. There was no indication of the formation of contiguous Rh-Rh sites, indicating that the catalytic active sites are isolated Rh atoms. This is an interesting observation, as site-site isolation is not guaranteed by immobilisation of a metal complex on silica[18].

7.14 Rh(sulphos)$(CO)_2$ on silica

The EXAFS spectrum and Fourier transform for the silica supported Rh(sulphos)$(CO)_2$ is very different from that of the unsupported sample. Figure 7.15 shows only one main peak in the Fourier transform, which corresponds to two shells of three phosphorus atoms at 2.25Å, and two carbonyl oxygen atoms at 2.63Å respectively. There is a small peak at 1.79Å, which corresponds to the two carbonyl carbon atoms. Multiple scattering was employed to improve the fit at a carbonyl bond angle of 180°. The nature of bonding of the organometallic to the

Figure 7.14 Rh K-Edge EXAFS and Fourier transform for Rh(sulphos)(cod) after reduction in hydrogen and reaction with C_2H_4 and H_2

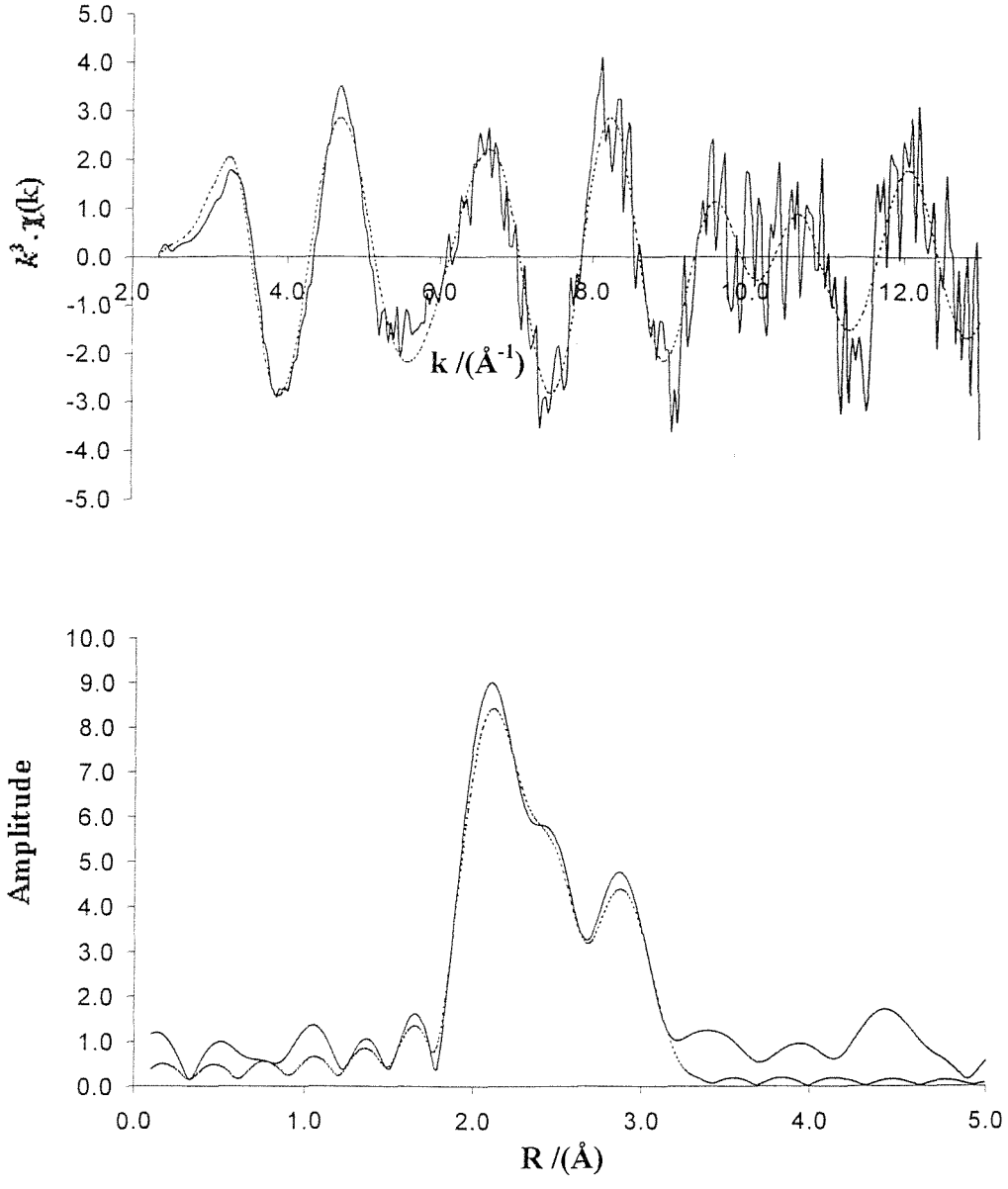

Atom	C.N.	r/Å	$2\sigma^2$ / Å^2
C	1	2.111(7)	0.001(1)
P	3	2.330(1)	0.026(2)
C	1	2.585(9)	0.002(1)
C	2	2.885(7)	0.001(1)

R= 53.12%

Ef= -1.33 eV

Figure 7.15 Rh K-Edge EXAFS and Fourier transform for Rh(sulphos)$(CO)_2$ supported on silica

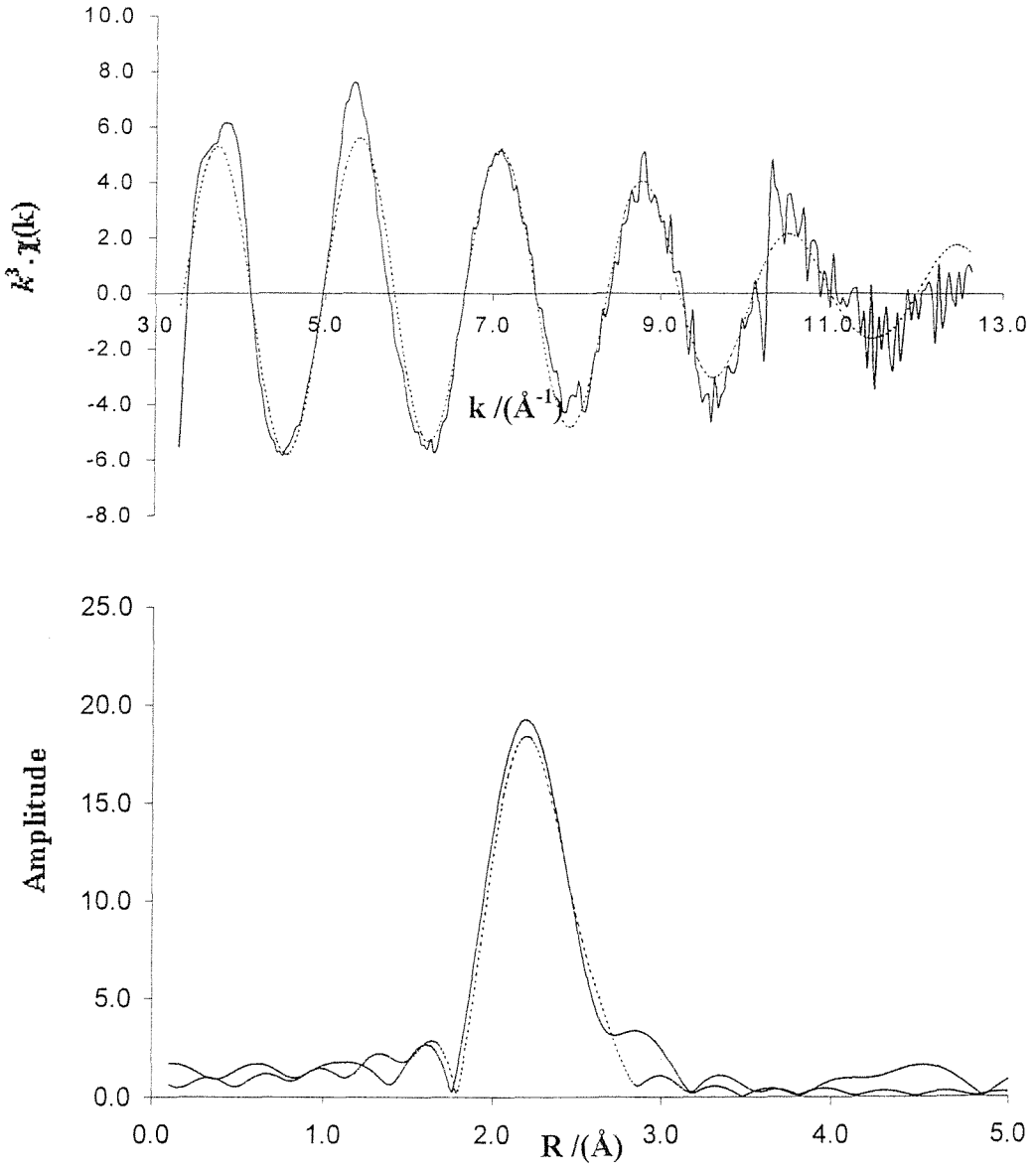

Atom	C.N.	r/Å	$2\sigma^2$ / Å^2
C	2	1.790(3)	0.0020(5)
P	3	2.250(4)	0.0105(6)
O	2	2.630(2)	0.0224(5)

R= 25.28%

Ef= 8.41eV

surface is again believed to proceed via the sulphos SO_3^- group with abstraction of a proton from an OH group on the silica surface. The authenticity of the sample was successfully verified (by L. Sordelli at the Istituto Nazionale di Coordinamento sulle Metodologie e Tecnologie Chimiche Innovative, in Italy) in light of the differing natures of the EXAFS of the supported and unsupported samples. These results are to be treated with some scepticism, as the carbonyl distances are unrealistic, and the effect of multiple scattering is not nearly as significant as for the unsupported organometallic. It is more likely that the sample has been oxidised, removing most of the carbonyls from the rhodium. The results of this experiment and subsequent reactions upon this sample are included for completeness.

7.15 Rh(sulphos)$(CO)_2$ on silica after one hour in O_2 at 120°C

Rh(sulphos)$(CO)_2$ supported on silica was reacted in a stream of oxygen gas for an hour at 120°C. The subsequent EXAFS spectrum and Fourier transform, shown in figure 7.16 shows that there is no apparent change in the local structure of the species around the rhodium atom. The local environment around the rhodium atom is, however, the same as for the unsupported organometallic (fits to other atoms were attempted). Once again, the different shape of the spectrum can only be assigned to the fact that Rh(sulphos)$(CO)_2$ is now supported on silica, or more realistically, that the rhodium environment has changed through oxidation. The bond distances of the carbon atoms of the carbonyl group have increased by 0.1Å from the previous spectrum. The rhodium- phosphorus distance is much the same as in the unsupported sample. The conclusion drawn is that the species is unchanged structurally upon bonding to the silica (though oxidation appears to have removed most of the carbonyl groups), and bonding has again occurred via the oxygen groups of the sulphonate tail, away from the metal coordination sphere. Reaction with oxygen at 120°C leaves the species unchanged

Figure 7.16 Rh K-Edge EXAFS and Fourier transform for Rh(sulphos)$(CO)_2$ supported on silica after reaction in O_2 at 120°C

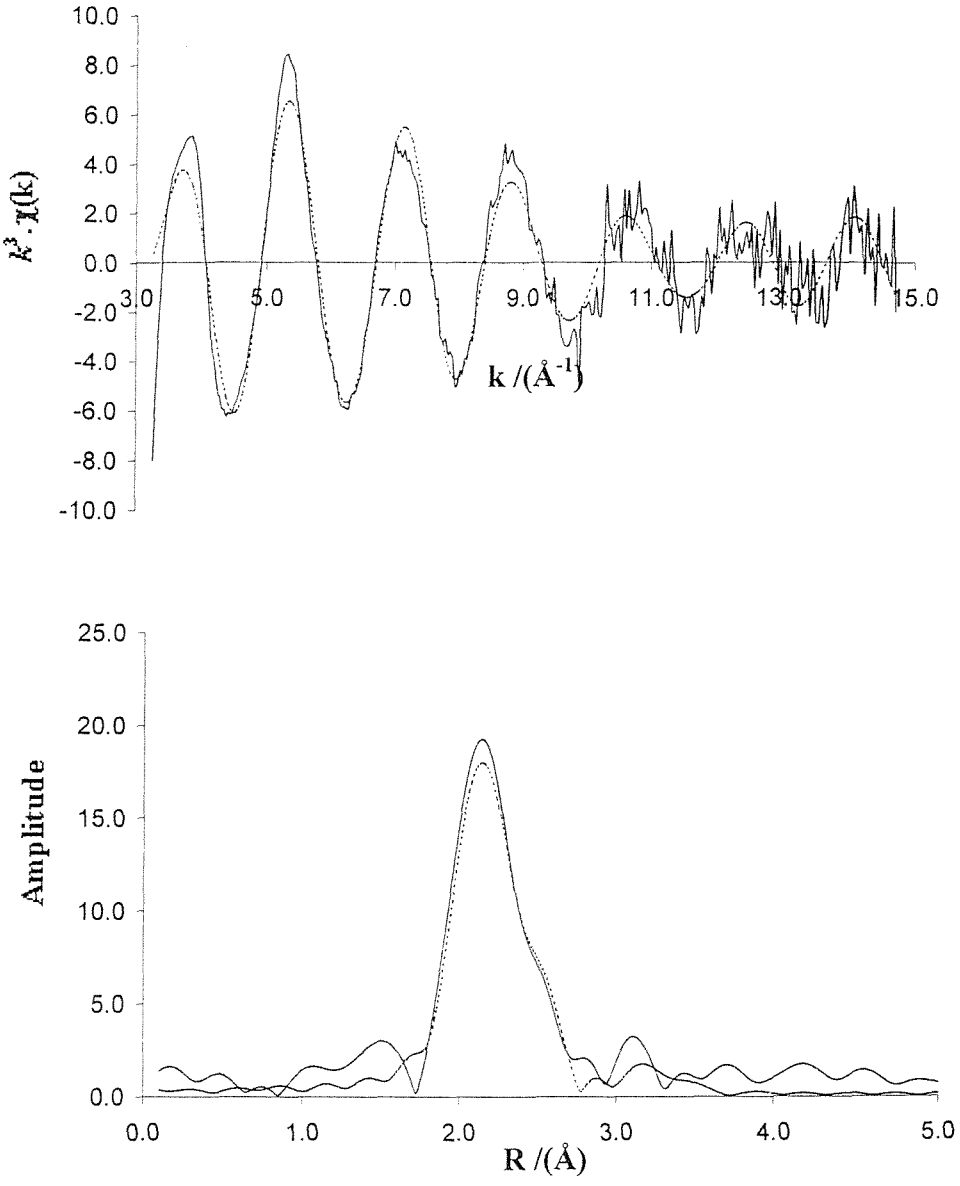

Atom	C.N.	r/Å	$2\sigma^2$ / Å^2
C	2	1.890(4)	0.000(6)
P	3	2.228(5)	0.0136(7)
O	2	2.62(2)	0.021(4)

R= 30.61%

Ef= 8.57 eV

7.16 Rh(sulphos)$(CO)_2$ on silica after one hour in N_2 at 120°C

Rh(sulphos)$(CO)_2$ supported on silica was reacted in a stream of nitrogen gas for an hour at 120°C. The subsequent EXAFS spectrum and Fourier transform, shown in figure 7.17 shows that there is no apparent change in the local structure of the species around the rhodium atom. The spectrum is almost identical to that of Rh(sulphos)$(CO)_2$ heated in a stream of oxygen gas at the same temperature. Again, it is most likely that oxidation of the sample has resulted in loss of most of the carbonyl groups. The bond distances of the carbonyl group and phosphorus groups are unchanged from before. It can again be concluded that the silica supported Rh(sulphos)$(CO)_2$ has not reacted with nitrogen at 120°C.

7.17 Conclusions and further work

This study has shown that heterogeneous, immobilised polyphosphine metal catalysts have been produced. These are denoted surface hydrogen bonded (SHB) catalysts. The organometallics, Rh(sulphos)(cod) and Rh(sulphos)$(CO)_2$ are believed to be hydrogen bonded to the silanol groups of the surface via the sulphonate groups far away from the phosphorus donor atoms of the ligands. In this way, all the metal centres are potential reagents dispersed on a very high interfacial area. There has been no evidence of the formation of contiguous Rh-Rh sites, indicating that the catalytic active sites are isolated Rh atoms.

These surface hydrogen bonded complexes have been shown to be versatile and thermally robust despite the $-SO_3\cdots HOSi-$ interaction not being as chemically robust as the covalent bonding commonly employed to immobilise organometallic complexes of wide use in heterogeneous catalysis. Rh(sulphos)(cod) supported on silica has been shown to catalyse the hydrogenation of ethene. More recent studies have shown that silica supported Rh(sulphos)(cod), suspended in a hydrocarbon solvent, is an easily recyclable hydrogenation and hydroformylation catalyst[19].

Figure 7.17 Rh K-Edge EXAFS and Fourier transform for Rh(sulphos)$(CO)_2$ supported on silica after reaction with N_2 at 120°C

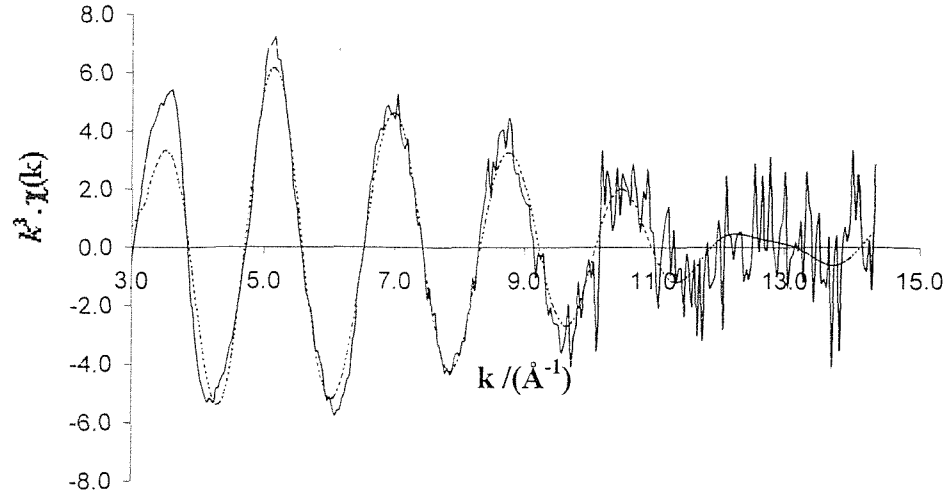

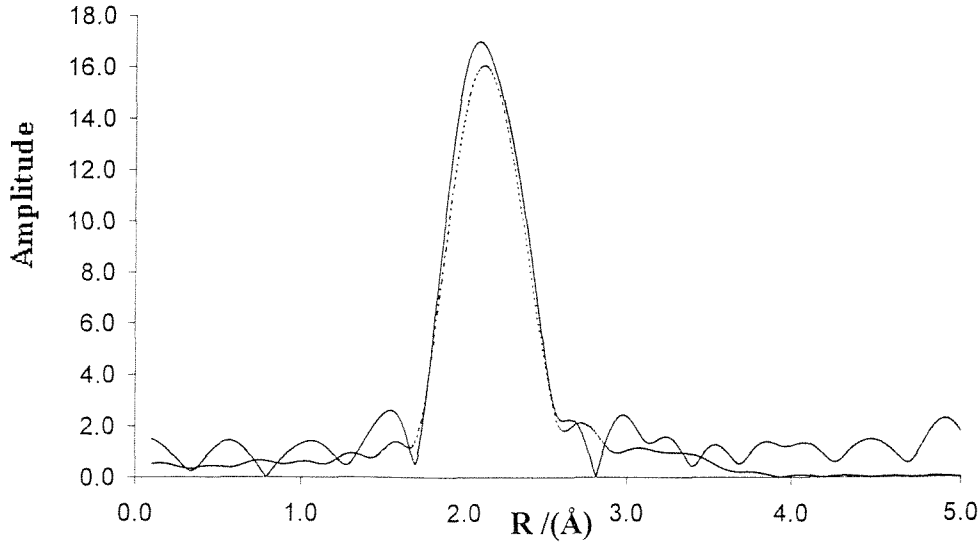

Atom	C.N.	r/Å	$2\sigma^2$ / Å^2
C	2	1.890(3)	0.0020(5)
P	3	2.250(4)	0.0105(6)
O	2	2.630(2)	0.0224(5)

R= 30.61%

Ei=8.57eV

Solid state NMR studies have indicated that the metal centre has a near square pyramidal geometry, and that there is little structural change in the vicinity of the metal upon tethering to the silica surface. The latter finding supports the belief that surface hydrogen bonding occurs via the sulphos group of the organometallic complex.

Further work on the silica-supported organometallics would involve attempting the hydroformylation reaction again. The crucial step is the reduction in hydrogen, which may permit the hydroformylation reaction to proceed. The hydroformylation of 1-hexene has been successfully demonstrated for silica supported Rh(sulphos)(cod) in a hydrocarbon solvent[19]. Hydrogenation and hydroformylation reactions of silica supported Rh(sulphos)$(CO)_2$ require investigation, as these reactions have been successfully demonstrated in liquid biphase conditions[19].

7.18 Experimental

All the samples used in this study were prepared by a research group at the Istituto Nazionale di Coordinamento sulle Metodologie e Tecnologie Chimiche Innovative, in Italy. All the pure organometallic compounds and surface supported organometallics were treated as air sensitive, and manipulations were therefore performed under an inert atmosphere using standard Schlenk techniques.

Samples were loaded into the EXAFS cell in a glove box at Daresbury laboratory, and maintaned under an inert atmosphere during the XAS experiment.

7.19 References

1. A. Theolier, A. K. Smith, J. M. Basset, G. M. Zanderighi, R. Psaro, R. Ugo, *J. Organomet. Chem.*, 1980, **191**, 415.
2. H. F. J. van't Bilk, J. B. A. D. van Zon, T. Huizinga, J.C. Vis, D. C. Koningsberger and R. Prins, *J. Am. Chem. Soc.*, 1985, **107**, 3139.
3. C. Bianchini, P. Frediani and V. Sernau, *Organometallics*, 1995, **14**, 5458.
4. C. Bianchini, A. Meli, V. Patinec, V. Sernau and F. Vizza, *J. Am. Chem. Soc*, 1997, **119**, 4945.
5. P. Van Der Voot, K. Possemiers and E. F. Vansant, *J. Chem Soc., Faraday Trans*, 1996, **843**, references within.
6. J. P. Arhancet, M. E. Davis, J. S. Morola and B. E. Hansen, *J. Catal*, 1990, **121**, 327.
7. P. B. Hitchcock, M. McPartlin and R. Mason, *J. Chem. Soc. D*, 1969, 1367.
8. M. J. Bennett and P. B. Donaldson, *Inorg. Chem.*, 1977, **16**, 655.
9. D. J. A. De Ridder and P. Imhoff, *Acta Crystallogr.*, 1994, **50**, 1569.
11. V. G. Albano, P. Bellon and M. Sansoni, *J. Chem. Soc. A*, 1971, 2420.
12. J. A. Ibers, R. G. Snyder, *Acta. Crystallogr.*, 1962, **15**, 923.
13. J. C. A. Boeyens, L. Denner, S. W. Orchard, I. Rencken, B. G. Rose, *S. Afr. J. Chem.*, 1986, **39**, 229.
14. J. Scherer, G. Huttner, O. Walter B. C. Janssen and L. Zsolnai, *L. Chem. Ber*, 1996, **129**, 1603.
15. C. Bianchini, A. Meli, M. Peruzzini, A. Vacca and F. Vizza, *Organometallics*, 1991, **10**, 645.
16. C. Bianchini *et al.*, X-Ray crystal structure of Ir(sulphos)(cod), manuscript in preparation.
17. E. Fache, C. Mercier, N. Pagnier, B. Despeyroux and P. Panster, *J. Mol. Catal.*, 1993, **79**, 117.
18. J. P Collman, L. S. Hegedus, J. R. Norton and R. G. Finke, *Principles and Applications of Organotransition Metal Chemitry*, University Science Books, 1987, 523.
19. C. Bianchini, D. Burnaby, J. Evans, P. Frediani, A. Meli, W. Oberhauser, R. Psaro, L.Sordelli and F. Vizza, *J. Am. Chem. Soc.*, 1999, **121**, 5961.

Conclusion

This study has investigated the surface chemistry of rhodium and palladium organometallics supported on high area inorganic oxides. The organometallic precursors have been sublimed (by MOCVD) under reduced pressure onto partially dehydroxylated oxide surfaces. The chemistry of the supported species has been investigated using EXAFS, EDE, DRIFTS and TPD techniques. EXAFS allows the coordination of the metal atom under investigation to be elucidated. EDE additionally enables the kinetics of reactions of the supported organometallics to be investigated. DRIFTS enables investigation of the metal ligands of supported organometallics. TPD allows analysis of gaseous species produced during reactions of surface supported species.

$[Rh(CO)_2Cl]_2$ is supported on Al_2O_3 and TiO_2 as a chemisorbed $[O]Rh(CO)_2(Cl)$ unit. Thermolysis under a helium and hydrogen atmosphere results in removal of the *gem*-dicarbonyl ligands via a linear carbonyl species, and the formation of rhodium metal clusters on the oxide surface. Reduction occurs at 90°C under a hydrogen atmosphere, whilst proceeding at over 200°C under an inert atmosphere. Re-generation of the *gem*-dicarbonyl species occurs after exposure of the thermolysed species to CO at room temperature for 1 hour.

Reaction of $[Rh(CO)_2Cl]_2$ supported on Al_2O_3 and TiO_2 with NO results in the formation of a rhodium carbonyl-nitrosyl species: $[O]_2Rh(NO)^-(Cl)$ and a mixed $[O]Rh(CO)(NO)(Cl)$ species. The rhodium *gem*-dicarbonyl species can be regenerated by exposure to CO for 2 hours. This reaction does not proceed to completion at room temperature, and is fully achieved by exposing to CO at 65°C. The rhodium nitrosyl species is more thermally stable than the corresponding *gem*-dicarbonyl species. Temperatures of 300°C are required under an inert atmosphere, to fully remove the ligands, and cause clustering of the rhodium on the alumina surface. Greater reduction of the surfaces of titania and alumina prior to MOCVD (by heating at greater temperatures and under a hydrogen atmosphere), results a strengthening in the intensity of the Rh(NO)(CO) species formed, and the appearance of a $Rh\text{-}NO^+$ band at $1920cm^{-1}$. These results bear greater resemblance to analogous experiments

performed in UHV systems, in which the surfaces are highly reduced prior to MOCVD.

Reaction of $Rh(CO)_2(acac)$ with partially dehydroxylated titania and alumina, results in the physisorption of the intact organometallic to the surface, with the consumption of surface hydroxyl groups. It is possible that hydrogen bonds are formed between the surface hydroxyl groups and the acac ligand. Thermolysis under a helium and hydrogen atmosphere results in removal of firstly the carbonyl, and then the acac ligands, resulting in the formation of small rhodium clusters on the oxide surface. Again, reduction occurs at significantly lower temperatures under a hydrogen atmosphere than under an inert helium atmosphere. Post thermolysis exposure to CO at room temperature results in the generation of rhodium *gem*-dicarbonyl species. The reaction with NO at room temperature resulted in substitution of the carbonyl ligands to form a $Rh(NO)^{\cdot}$ species. It is uncertain whether the acac ligand is retained during this reaction. Exposure to CO for 30 minutes at room temperature resulted in regeneration of the *gem*-dicarbonyl species. There is, however, no attenuation of the $NO^{\cdot}$ ligand, or change in the acac region during this reaction.

Reaction of $Pd(acac)_2$ with partially dehydroxylated titania and alumina, results in the physisorption of the intact organometallic onto the surface, with the consumption of surface hydroxyl groups. It is possible that hydrogen bonds are formed between the surface hydroxyl groups and the acac ligand(s). Thermolysis under a helium and hydrogen atmosphere, results in removal of the acac ligands, resulting in the formation of small palladium clusters on the oxide surface. Again, reduction occurs at significantly lower temperatures under a hydrogen atmosphere than under an inert helium atmosphere. Post thermolysis exposure to CO at room temperature results in generation of linear and bridging carbonyl species. Exposure to NO at room temperature resulted in the formation of a $Pd(NO)^{\cdot}$ species. The coordination of the acac ligand was observed to change, though the bonding to the palladium is not understood. Re-exposure to CO results in a very small development of a bridging carbonyl species, though the NO and acac regions are hardly attenuated by the exposure to CO.

The organometallic Rh(sulphos)(cod) was shown bond to the surface of silica via the sulphos SO_3^- group, abstracting a proton from a surface hydroxyl group in the process. Exposure to H_2 at 120°C results in substitution with the (cod) ligand. The hydrogenated species has been shown to catalyse the hydrogenation of ethene. Rh(sulphos)$(CO)_2$ has also been shown to bond to the silica surface via the sulphos group in the same way as the Rh(sulphos)(cod).

Further work would involve a more accurate determination of the metal weight loading of the organometallic species upon the oxide surfaces. This may be achieved by atomic absorption spectroscopy. Further EDE studies would enable the kinetics of the reactions studied in this thesis to be determined. Near infrared studies would enable the nature of the chlorine atom in the surface supported $[Rh(CO)_2Cl]_2$ to be more precisely understood, particularly during thermolysis reactions. A study of the pressure dependence of the CO regeneration of the Rh(NO)- species, after reaction of supported $[Rh(CO)_2Cl]_2$ with NO is required. A greater understanding of the transformations of the acac ligand during the reactions of surface supported $Rh(CO)_2(acac)$ and $Pd(acac)_2$ is desired. EDE spectroscopy and TPD studies would be useful to this end. A study of the reaction of NO with supported $Rh(CO)_2(acac)$ and $Pd(acac)_2$ by EDE spectroscopy would enable the coordination of the metal atoms to be monitored during then reaction. An investigation of the catalytic reactions of the surface supported species would establish the usefulness and potential of supported organometallics as catalysts.